PONTIFÍCIA UNIVERSIDADE CATÓLICA
DO RIO DE JANEIRO

Leonardo Pedreira Pereira

An optimized method for automotive performance predictions using different mixtures of ethanol and gasoline

Dissertação de Mestrado

Dissertation presented to the Programa de Pós-graduação em Engenharia Mecânica of PUC Rio in partial fulfillment of the requirements for the degree of Mestre em Engenharia Mecânica.

Advisor: Prof. Sérgio Leal Braga

Co-Advisor: Dr. Antonio Carlos Scardini Villela

Rio de Janeiro

August 2021

PONTIFÍCIA UNIVERSIDADE CATÓLICA
DO RIO DE JANEIRO

Leonardo Pedreira Pereira

An optimized method for automotive performance predictions using different mixtures of ethanol and gasoline

Dissertation presented to the Programa de Pós-graduação em Engenharia Mecânica of PUC Rio in partial fulfillment of the requirements for the degree of Mestre em Engenharia Mecânica. Approved by the Examination Committee

Prof. Sergio Leal Braga
Advisor
Departamento de Engenharia Mecânica – PUC-Rio

Dr. Antonio Carlos Scardinni Villela
Co-Advisor
PETROBRAS

Dr. Guilherme Bastos Machado
PETROBRAS

Prof. José Alberto dos Reis Parise
Departamento de Engenharia Mecânica – PUC-Rio

Rio de Janeiro, August the 12th, 2021

Leonardo Pedreira Pereira

Leonardo Pedreira graduated in mechanical engineering (2017) at the Pontifical Catholic University of Rio de Janeiro (PUC-Rio). He participated in automotive engineering projects, such as internal combustion engine design and testing, fuel performance analysis and vehicle performance testing. He also participated in Formula SAE and Aerodesign competition teams. Currently is at CDEV and still working on automotive projects.

Bibliographic data

Pereira, Leonardo Pedreira

An optimized method for automotive performance predictions using different mixtures of ethanol and gasoline / Leonardo Pedreira Pereira ; advisor: Sérgio Leal Braga ; co-advisor: Antonio Carlos Scardini Villela. – 2021.

258 f. : il. color. ; 30 cm

Dissertação (mestrado)–Pontifícia Universidade Católica do Rio de Janeiro, Departamento de Engenharia Mecânica, 2021.

Inclui bibliografia

1. Engenharia Mecânica – Teses. 2. Motores de ignição por centelha. 3. Desempenho de veículos. 4. Dinamômetro de chassis. 5. Modelagem. 6. Análise de combustíveis. I. Braga, Sérgio Leal. II. Villela, Antonio Carlos Scardini. III. Pontifícia Universidade Católica do Rio de Janeiro. Departamento de Engenharia Mecânica. IV. Título.

CDD: 621

Aknowledgments

Firstly, I thank God and Our Lady of Vitória for the opportunity to do this work and for my family: my parents, Lucy Maria and Júlio César, my brother, Victor Alessandro and my sisters, Juliana and Raphaella, who encouraged me and gave all possible support in these years of academic studies.

To my grandmother Lucy Vinhaes, who unfortunately left us in 2019.

I thank to my advisors, Professor Sérgio Braga and Antonio Villela for all their support, ideas, advices and guidance. It's an honor having them as advisors.

To CNPq and PUC-Rio, for the aid granted, without which this work could not have been carried out.

I thank all the members of the CDEV, Fernando Zegarra, Jorge Ricardo Moura, Gerson Silvério and professor Pedro Paulo Almeida for the friendship we made during this period. I am also grateful for the availability, teachings and help in the chassis dynamometer tests with the vehicles that were carried out in Xerém.

To Professor Florian Pradelle, for his help in finding important publications that were importants to carry out this work, and also to his wife Renata Pradelle, who helped in obtaining some specific geometric parameters of the Peugeot 207 SW and the TU3 engine that were very useful to this work.

In addition to my advisor, Professor Sérgio Braga, I would like to thank the entire Mechanical Engineering Department at PUC RIO, especially Professor José Alberto dos Reis Parise for his friendship and guidance throughout the teaching internship, which was very helpful to me in learning simulation of internal combustion engines.

Finally, I thank my goddaughter Ana Clara and my friend Aldaci Menezes for the prayers and support that have always been very important to me.

This study was financed by the Coordenação de Aperfeiçoamento de Pessoal de Nível Superior – Brasil (CAPES) – Finance Code 001.

Abstract

Pereira, Leonardo Pedreira; Braga, Sérgio Leal (Advisor); Villela, Antonio Carlos Scardinni (Co-Advisor). **An optimized method for automotive performance predictions using different mixtures of ethanol and gasoline**. Rio de Janeiro, 2021. 258p. Dissertação de Mestrado – Departamento de Engenharia Mecânica, Pontifícia Universidade Católica do Rio de Janeiro.

Vehicle performance is an important feature to be evaluated when internal combustion engines and new fuels are being developed. Predicting this parameter is also of great significance, once track testing requires long periods of time to be done and high costs with equipment, rental of the track, hiring people and displacement of vehicles and fuels. In addition, their results are directly affected by track surface irregularities and variations in weather conditions such as ambient pressure, temperature, air humidity and wind speed. Thus, this work aims to use collected data in bench tests with an internal combustion engine in order to modeling an automobile speed recovery time. The proposed methodology simulates the traction force on the wheels based on the measured torque in engine dynamometer or from the pressure curves inside the combustion chamber with the aid of friction models for spark ignition engines. In order to validate the proposed model, it became necessary to perform speed recovery tests with the car on a chassis dynamometer. Also, seven different mixtures of ethanol and gasoline were used, and it was concluded that pure anhydrous ethanol promoted a higher acceleration capacity in most of the experiments but it had higher fuel consumption. Hydrated fuels reduced performance but improved global efficiency. The simulations demonstrated a high precision in relation to the experiment, with a speed recovery time diference average of 0.51 seconds and standard deviation of 0.078. Also, the acceleration performance simulations had errors smaller than 5.25%. In addition, doing these tests in laboratory has the advantage of a greater control of the room ambient conditions and the engine operating parameters.

Keywords

Spark ignition engines; Vehicle Performance; Chassis dynamometer; Modeling; Fuel Analysis

Resumo

Pereira, Leonardo Pedreira; Braga, Sérgio Leal (Orientador); Villela, Antonio Carlos Scardinni (Coorientador). **Metodologia otimizada para previsão de desempenho automotivo utilizando diferentes misturas de etanol e gasolina.** Rio de Janeiro, 2021. 258p. Dissertação de Mestrado – Departamento de Engenharia Mecânica, Pontifícia Universidade Católica do Rio de Janeiro.

O desempenho de veículos automotivos é um importante atributo a ser avaliado quando motores de combustão interna e novos combustíveis estão sendo desenvolvidos. A previsão desse parâmetro também é de suma importância, uma vez que os testes de desempenho de automóveis em pista requerem prazos de realização e altos custos com equipamentos, aluguel da pista, contratação de pessoas e deslocamento de veículos e combustíveis. Além disso, seus resultados são diretamente afetados por irregularidades na superfície da pista e variações nas condições climáticas, como pressão ambiente, temperatura, umidade do ar e velocidade do vento. Assim, este trabalho tem como objetivo utilizar os dados coletados em testes de bancada com um motor de combustão interna com a finalidade de modelar os testes de retomada de velocidade de um automóvel convencional leve. A metodologia proposta simula a força de tração nas rodas a partir do torque medido no dinamômetro do motor ou a partir das curvas de pressão no interior da câmara de combustão com o auxílio de modelos de atrito para motores de ignição por centelha. Para validar o modelo proposto, foi necessário realizar testes de retomada de velocidade com o carro em um dinamômetro de chassi. Além disso, foram utilizadas sete misturas diferentes de etanol e gasolina, e concluiu-se que o etanol anidro puro promoveu maior capacidade de aceleração na maioria dos experimentos, mas apresentou maior consumo de combustível. Os combustíveis hidratados reduziram o desempenho, mas melhoraram a eficiência global. As simulações demonstraram alta precisão em relação ao experimento, com média da diferença do tempo de recuperação da velocidade de 0,51 segundos e desvio padrão de 0,078. Além disso, as simulações de desempenho de aceleração tiveram erros menores que 5,25%. Além disso, a realização desses testes em laboratório tem a vantagem de um maior controle das condições ambientais da sala e dos parâmetros de operação do motor.

Palavras-chave

Motores de ignição por centelha; Desempenho de Veículos; Dinamômetro de Chassis; Modelagem; Avaliação de combustíveis

Table of Contents

List of Figures

Figure II.0.1: Valve train settings (Kammil, 2013) 193

List of Tables

Nomenclature

a_x	Vehicle longitudinal acceleration (m/s²)
A_f	Frontal Area of the vehicle (m²)
A/F	Air/fuel ratio (-)
ANP	*Agência Nacional do Petróleo, Gás natural e Biocombustíveis*
ATDC	After top dead center
B	Bore (m)
AF	Air/fuel ratio
BMEP	Brake mean effective pressure (Pa or bar)
CA	Crank Angle (º)
CA10	Value of crank angle where 10% of the energy due to combustion has been released (°)
CA50	Value of crank angle where 50% of the energy due to combustion has been released (°)
CA10	Value of crank angle where 10% of the energy due to combustion has been released (°)
CDEV	Centro de Desenvolvimento em Energia e Veículos
CENPES	Centro de Pesquisas, Desenvolvimento e Inovação Leopoldo Américo Miguez de Mello
CV	Coefficient of Variation
EQM	Mean quadratic error
EV	Electric Vehicle
fr	Rolling resistance coefficient
F_d	Aerodynamic Drag Force (N)
F_{RR}	Rolling Resistance (N)
h_c	Convective heat transfer coefficient (W/m²K)
i_c	Gear box ratio
i_d	Final drive transmission ratio
ICE	Internal Combustion Engines
IMEP	Indicated mean effective pressure
I_A	Uncertainty of type A
I_B	Uncertainty of type B
I_C	Uncertainty of type C

I_E	Uncertainty of type E
I_{eng}	Inertia of the engine (kg.m²)
I_d	Inertia of the differencials (kg.m²)
I_w	Inertia of the wheels (kg.m²)
K_o	Correction Factor
L	Stroke (m)
L_b	Crankshaft bearing length (mm)
L_v	Valve displacement (mm)
l	Connecting rod length (m)
LHV	Lower Heating Value (kJ/kg)
m_p	Vehicle passenger massa (kg)
m_v	Vehicle mass (kg)
MATLAB	Matriz Laboratory
M_{ref}	Reference mass of the vehicle: passenger + vehicle + inertia of rotational components (kg)
$\dot{m}$	Mass flow rate (kg/h)
n	Number of measurements
n_{cs}	Number of camshaft bearings
n_v	Total number of valves
N_{eng}	Engine Speed (RPM)
N_w	Wheel Rotation (RPM)
p	Pressure (Pa or bar)
P	Power (W or kW)
PMEP	Pumping Friction mean effective pressure
Q	Heat (J)
$\dot{Q}$	Heat Energy (W or kW)
R	Gas constant (J/kg.K)
R^2	Coefficient of determination
rw	Rolling radius of the tire (m²)
rc	Compression ration
RPM	Rotations per minute
s	Distance between the crank axis and the piston pin axis (m)
SD	Standard Deviation
sfc	Specific fuel consumption (g/kWh)
SI	Spark Ignition

$\overline{Sp}$	Mean piston speed (m/s)
t_{dyno}	Speed Recovery time on chassis dynamomenter (s)
t_{sim}	Speed recovery time simulated (s)
T	Temperature (K or ºC)
T_b	Brake Torque (N.m)
TDC	Top Dead Center
TFMEP	Total Friction mean effective pressure (bar or kPa)
UR	Relative humidity (%)
v	Velocity (km/h)
V	Volume (m^3)
V_d	Displaced volume (m^3)
W	Work (J)
μ	Dynamic Viscosity (kg/(m.s))
ν	Kinematic Viscosity (mm^2/s)

Greek letters

ϒ	Polytropic coefficient – specific heats ration (-)
η_c	Combustion efficiency (%)
η_g	Global efficiency (%)
η_{mec}	Mechanical efficiency (%)
η_{th}	Thermal efficiency (%)
η_{tr}	Transmission efficiency (%)
η_v	Volumetric efficiency (%)
θ	Crankshaft Angle (º)
λ	Lambda (-)
ω	Absolute moisture content (-)

Subscript

air,d	air dry
air,w	air wet
amb	ambient
b	brake

cyl	Inside the cylinder
f	friction
ht	Heat transfer to the walls
i	indicated
p	Passenger
RL	Heat released
sat	saturation
SIM	simulated
v	vehicle

1 Introduction

1.1 Automotive Industry Challenges: Vehicle Performance, Emissions and Autonomy

The oil industry had its rise during the nineteenth century due to the need of fuel to operate the combustion engines. Its main derivatives, used in automotive vehicles, are gasoline and diesel oil. Since then, these products continue to be the main source of energy for automobiles and, according to the Ministry of Science and Technology of Brazil, in 2016, about 32.4% of CO_2 emissions in the atmosphere came from the energy sector, and road cars and trucks corresponds to 45.8% of this value (Brasil, 2020). As a result, regulations on fuel consumption and in air pollutants emission levels are increasingly around the world, leading automakers to seek alternatives that meet these laws.

Another important factor cited by Villela (2015) and Mashadi & Crolla (2011) is the automobile manufacturers also considers what costumers wants when buying a car. In addition to the good attributes with regards fuel consumption and emissions, customers also seek good performance characteristics when buying a vehicle. According to Villela (2015), when a car performs well, it promotes entertainment for the driver and raises the chance to scape of a risky situation.

To meet all these demands of emissions, autonomy and performance, the most viable solution would be the total replacement of the fleet of conventional vehicles by others that are little or non-polluting, such as hybrids and electric vehicles, respectively.

When the powertrain is composed only by an internal combustion engine, the largest portion of the power generated is lost by heat and friction which, consequently, reduces its energy efficiency. This problem does not exist in an electric vehicle since the power contained in the battery goes directly to the transmission without loss of power. In addition, EV's do not expel exhaust gases, so the emissions are zero. However, this change in the vehicle fleet becomes difficult nowadays due to some factors, such as the cost of the vehicles, safety and others economic aspects (Vonbum, 2015).

Another solution that has been proposed in recent decades is the hydrogen-powered vehicle. Some advantages, disadvantages and perspectives for the future on the use of this fuel can be found in Almeida et al (2019) and Vargas et al. (2014).

According to Vargas et al. (2014), some of the advantages of the hydrogen vehicles are: greater amount of energy per unit of mass than other fuels and lower levels of pollutant emissions, since after the combustion process, the engines produce H_2O and NOx values that are much lower than conventional engines. On the other hand, when compared to traditional fuels, H_2 has a lower storage capacity and higher costs related to production, transportation and the distribution system (Almeida et al., 2019; Vargas et al., 2014).

Mashadi & Crolla (2011) say that while there is a strong interest in developing new technologies such as electric and hybrid cars, conventional powertrains will still be the vast majority in the coming decades. According to the authors, a survey was made in 2009 in which cars and light trucks, whose propulsion system are part of the conventional category, corresponds about 99% of the total fleet worldwide and that in the same year there was a production of 61 million of cars of this group. In addition, the magazine "*Automotive Business*" published a report citing that Route 2030 encourages electrification but is not emphatic with its prohibition until the year 2030 (Imparato, 2019), which facilitates the maintenance of production by assemblers on conventionals powertrains.

Therefore, automotive engineers should opt for other alternatives for conventional vehicles, in which they can meet all the demands of low fuel consumption and low environmental impact, without compromising a good performance on the road.

1.2 Increase in Ethanol Demand in the Transportation Sector

Currently there is a great demand for alternative fuels that cause less environmental impacts, especially in the road transport sector. With the oil crisis in the 1970s, many governments around the world have chosen to create incentives to use ethanol in their countries mainly due to energy security. Some examples that can be cited from these incentive programs is the PROÁLCOOL, created in Brazil, and the CAFÉ *(Corporate Average Fuel Economy),* originated in the United States (Mashadi & Crolla, 2011; Brunetti, 2018).

A research by Antoniosi (2015) shows that Brazil and the United States together have the largest ethanol production in the world, totaling about 75

billions of liters of this fuel being produced per year. The author also states that there is a large participation of the European Union and China. Thus, it is notorious that ethanol is gaining increasing prominence in the international scenario as an energy source, including in the road transport sector.

Flex fuel vehicles were introduced in Brazil and the United States in 2002 and are currently the most manufactured car category in these countries (Brunettii, 2018; Antoniosi, 2015; EIA, 2021). The production of flex vehicles in Brazil in recent years can be seen in Figure 1.1, taken from Antoniosi (2015). These cars have, as characteristics, the acceptance of any volume fraction of the mixture of pure gasoline and anhydrous ethanol as fuel in the internal combustion engines.

Because of that, in the last two decades there has been an increase in the content of anhydrous ethanol in commercial gasoline, currently having 27% addition in volume. Using a flex fuel vehicle, consumer can also opt for the use of hydrated ethanol (H100), which is a mixture of anhydrous ethanol with around 4% water volume in the composition.

Figure 1.2 was taken from the *U.S. Energy Information Administration* (EIA, 2021) website and shows that the United States of America has also seen a large increase in ethanol demand since the early 1970s. Currently, in this country commercial gasoline has 10% anhydrous ethanol in its composition and used by any spark ignition engine. Unlike Brazil, pure ethanol (anhydrous or hydrous) is not marketed in the USA, but there is the alternative of using E85 gasoline (85% anhydrous ethanol in the mixture), once the vehicle engine is flex.

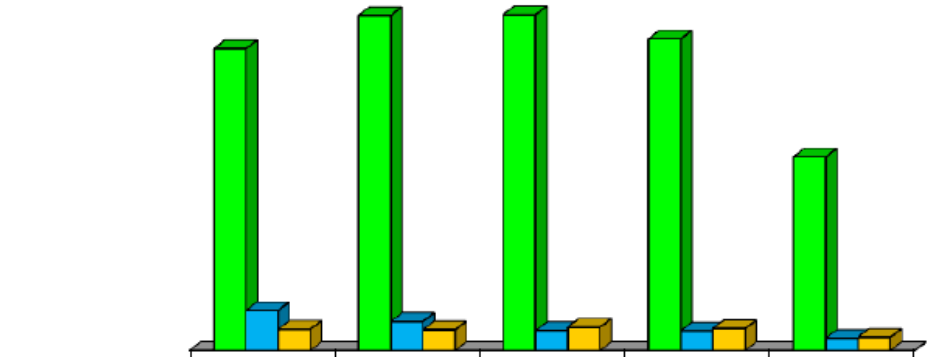

	2011	2012	2013	2014	2015
FLEX	2.848.122	3.162.874	3.169.174	2.940.508	1.828.267
GASOLINA	376.804	273.915	189.109	184.841	115.891
DIESEL	200.705	197.277	221.181	207.275	125.256

Figure 1.1: Licensed vehicles, per year and fuel type (Antoniosi, 2015)

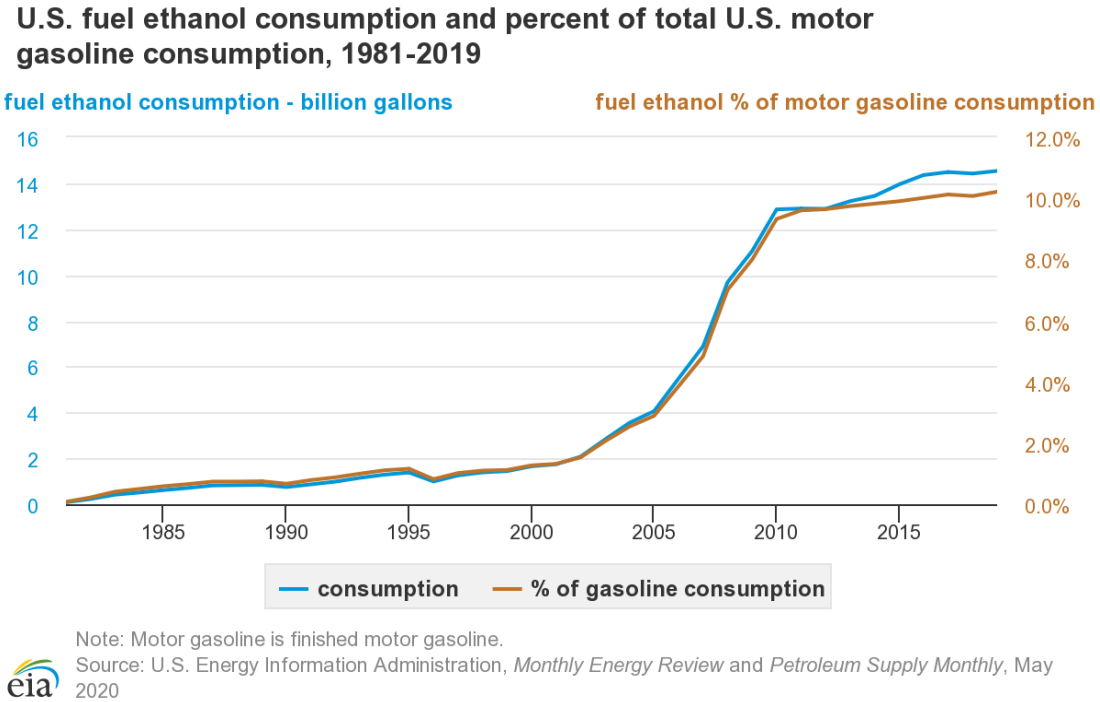

Figure 1.2: Increase in ethanol consumption over the years in the USA (EIA, 2021)

1.3 Development of New Fuels

Knowing that currently the Brazilian vehicle fleet is composed mainly of cars whose engines are flex and that there is a growing demand for ethanol as an energy source for the road transport sector, it can be concluded that a good theme of research is assessing the characteristics of a vehicle (emissions, autonomy and performance) when using different levels of this compound mixed with gasoline.

The fuel injection system of the flex vehicles accepts any content of the ethanol and gasoline mixture. However, when these fuels are produced, it is necessary to consider that some of its characteristics (e.g.: lower heating value, air-fuel ratio, octane and some thermophysical properties) vary according to the amount of each of these compounds. In addition, by changing the volumetric fraction of each component in the mixture, there is a great divergence in the chemical kinetics of combustion and in the heat transfer process. Adding all of these factors, we can see that by changing the chemical composition of a fuel to operate on the same engine, the pressure and temperature levels inside the chamber will be different and, because of that, torque and power will also be different.

As a conclusion, it can be said that it is very complex to predict the results of performance, consumption and emissions of a vehicle when using new fuels. Currently, there are mathematical methods that allow these evaluations to be done through numerical simulation and it can be found in some books such as Heywood (2018), Fergusson (2015) and Caton (2015). However, these models require chemical and thermophysical data that are very specific for each fuel and each engine operating regime, such as the burn rate, combustion duration, constant pressure-specific heat, molecular mass values for each range of the crankshaft angle, among others. Therefore, experimental evaluation with the engine in a bench becomes the best way to analyze the behavior of new fuels.

1.4 Challenges related to Automotive Track Tests

Currently, vehicle performance can be determined by speed recovery tests on track. These consist of accelerating the vehicle at full load in a pre-established speed range and measuring the time it takes. Upon reaching the minimum speed, the driver must step to the end of the accelerator, where the engine operates at full load until the final speed is reached.

Coastdown tests are also performed on a track, in which the vehicle is slowed down in neutral gearing, so that external active forces in the direction of their displacement (aerodynamic drag and rolling resistance) are quantified. The objective of this experiment is to obtain a quadratic correlation that represents these forces as a function of the speed of the automobile. Subsequently, this curve is reproduced in a chassis dynamometer where tests such as FTP 75 (*Federal Test Procedure*) can be made to evaluate the emissions and fuel consumption of the vehicle. The road loads are simulated on the dynamometer by brake forces on the rollers.

According to a study conducted by Mock (2016), there are still few tests of vehicles on track carried out by a third part, other than manufacturers. This is due to the fact that track tests has high costs and require a lot of time to be carried out. It is necessary a long and large track, such as that in Figure 1.3, and a test day with very specific weather conditions related to pressure, temperature and wind speed.

To perform on-track tests it is necessary that local winds are at very low speeds (below 5 m/s) to avoid aerodynamic interferences from aerodynamic drag and cross winds. In addition, the pressure, humidity and air temperature of the environment have also influence on the results, since they modify the engine volumetric efficiency. Experimental inaccuracies are also related to the track ground irregularities and the pilot reaction time.

Track tests must be performed repeatedly and in opposite directions to mitigate the effect of winds until they present a good accuracy in the results. Therefore, it takes a large amount of fuel to carry out the experiment. In addition to experimental inaccuracies, test tracks also require high costs, which are related to the following factors:

- Purchase of fuel and experimental equipment;
- Locomotion of people, equipment, fuel and vehicles to the test area;
- Rent of the track;
- Training and hiring people;

All this must be foreseen in order to avoid poor results and high costs losses. Taking into account all these factors, it becomes very important to have a good tool capable to predict on-track tests results.

Figure 1.3: Automotive test track.

1.5 Motivation

In the previous sections it was showed that the automotive track tests require very high costs with experimental equipment, lane rental, displacement of fuel and vehicles and hiring people. In addition, experimental inaccuracies related to atmospheric conditions may occur, directly affecting the results.

It was also mentioned that there is a great search for new fuels that promote good fuel consumption and emissions characteristics to conventional automotive vehicles, without performance loss on the road. Thus, it is necessary to create a solution capable of simplifying these experiments and reducing all expenses related to their preparation.

Therefore, this work proposes a methodology for predicting automotive performance, through simulation of the speed recovery time. This will be made from experimental tests carried out only with the internal combustion engine on a laboratory bench. This method is expected to optimize the process, as atmospheric conditions that directly affect its results can be controlled in the laboratory and eliminate costs and inaccuracies related to track tests.

For the work progress, two experiments were carried out. The first was on a bench with an internal combustion engine, in order to obtain the pressure curves, brake torque and others parameters. The second was in a chassis dynamometer with a car that had the same type of engine previously tested, to evaluate the speed recovery time and acceleration performance and compare with the simulated values. All these experiments were performed for seven different mixtures of anhydrous or hydrated ethanol with standard gasoline (alcohol-free) so that the influence of the chemical composition of the fuel with regard to its performance characteristics, fuel consumption and energy efficiency were also analyzed.

Simulations of the vehicle performance for all fuels were made from the longitudinal vehicle dynamic equation, as suggested by Mashadi & Crolla (2011), Wong (2000), Ehsani (2009), Gillespie (1992) and Brunetti (2018). This equation relates the vehicle acceleration with the longitudinal forces acting on it, which are: wheel traction force, rolling resistance and aerodynamic drag.

The summary of the present work can be seen in Figure 1.4.

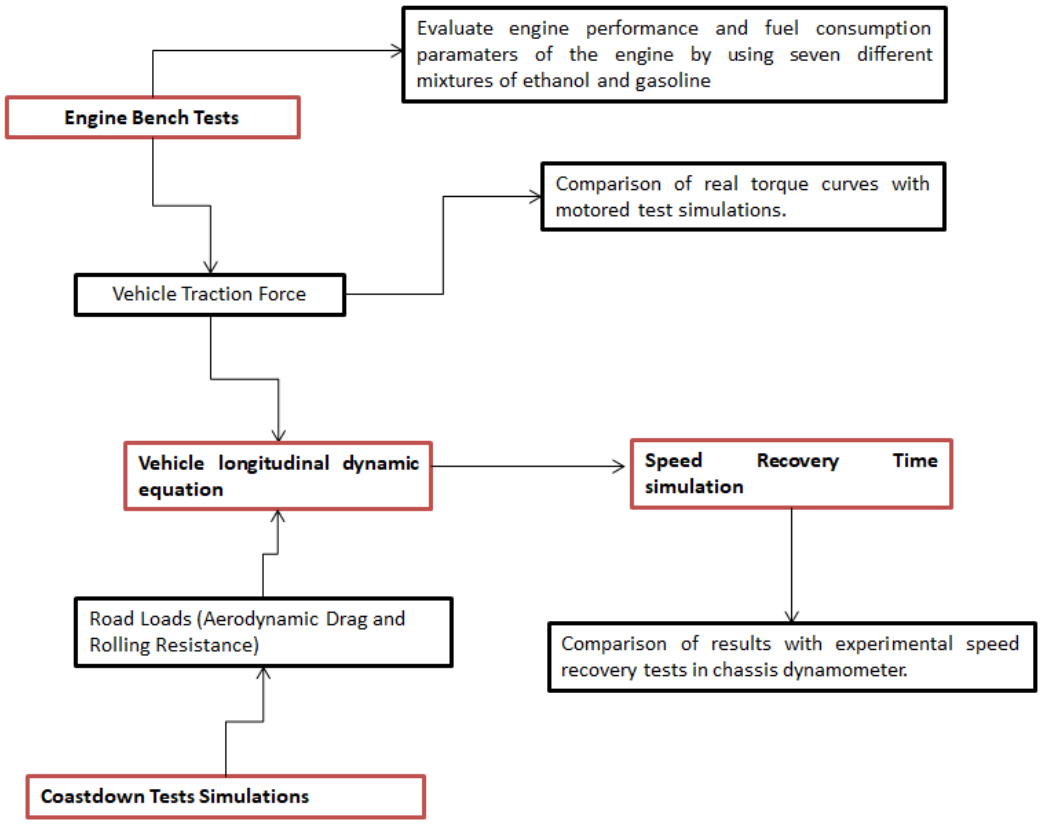

Figure 1.4: Summary of the present work.

Figure 1.5 presents the summary of the traction force calculation. The traction force on the wheels is function of the engine torque, transmission gear ratios and drivetrain losses. In this work, engine torque was found experimentally using an engine dyno or simulated. The experimental pressure curves were obtained using a transducer and were used with the aid of friction models related to spark ignition engines to calculate the simulated brake torque as a function of the vehicle speed.

Given the lack of prediction models for the drivetrain losses, this was calculated as the wheel power that was read in the chassis dynamometer roller, by the engine brake power, taken from the bench tests results. Thus, it was possible to simulate the wheel traction force.

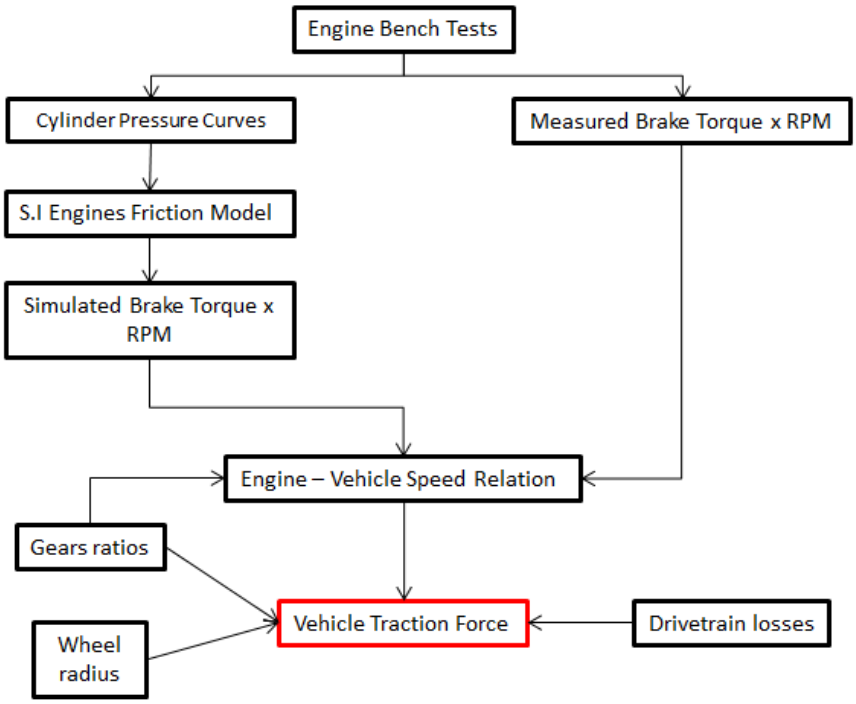

Figure 1.5: Summary of the vehicle traction force simulation.

The resistance forces to the vehicle (aerodynamic drag and rolling resistance) were calculated through correlations found in the literature and compared with experimental results published in Kadijk (2012).

In the work of Kadijk (2012) experimental results of coastdown tests for 8 different vehicles can be found. Therefore, the road load curves were plotted and a MATLAB program was created to obtain the F_0, F_1 and F_2 coefficients of all vehicles by linear regression.

From the F_2 coefficient, it was possible to calculate the value of the aerodynamic coefficient (C_d) for the calculation of the drag force (Katz, 1995). Rolling resistance was calculated by several correlations found in the literature for the rolling coefficient (f_R). Thus, it was possible to simulate the coastdown tests.

The comparison of the simulated coastdown tests with the experimental ones was made from the calculation of the coefficient of determination (R^2) and a strong approximation was observed for most of the calculated rolling resistance correlations. These results were useful for choosing the correlation used to calculate the road loads of the vehicle tested in a chassis dynamometer in the present work.

Once knowing the values of the aerodynamic drag coefficient and the frontal area of the vehicle, it is possible to calculate the value of F_{2sim}. The values

of F_{0sim} and F_{1sim} were calculated using the previously chosen correlation for rolling resistance. With this, the chassis dynamometer was programmed with these coefficients to simulate the road loads by braking force on the rollers.

A summary of these simulations can be seen in Figure 1.6.

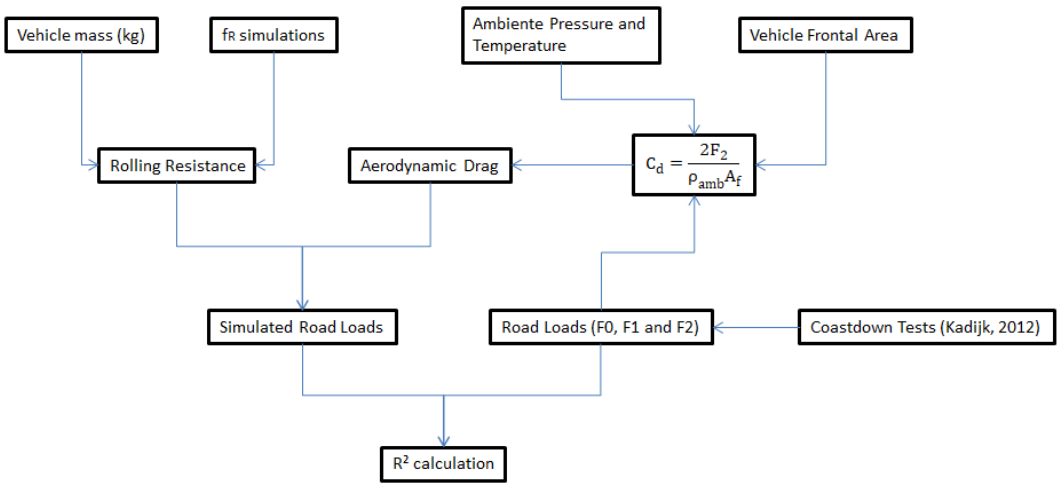

Figure 1.6: Summary of the road loads simulations.

1.6 Structure of the present work

In chapter 2, a literature review will be made in which the problems and challenges related to the present work will be addressed. Also, the modeling of the parameters of interest to obtain the speed recovery time will be shown as well as some results obtained by other publications. Chapter 3 will address all the objectives and results to be achieved throughout the work.

Chapter 4 will present all the mathematical modeling necessary for the processing of experimental data and numerical simulation of the vehicle speed recovery time. The entire experimental device and description of the experiments will also be presented in this section.

Chapter 5 will show the results obtained throughout the tests and simulations according to the methodology explained in item 4.

Finally, chapter 6 will show the conclusions of the work according to the results shown in chapter 5. Some suggestions for future work will also be cited. The appendices contain additional information for the understanding of the theory involved and complementary results to Chapter 5.

2 Literature Review

In this work, the literature review was based on evaluating lighty duty vehicle performance by calculating its speed recovery time from engine bench tests of the spark ignition engine. To do so, it was necessary to understand the entire power generation process and all sources of energy losses and their causes until it reaches the wheels. Knowing that the tests would be done for seven different mixtures of anhydrous ethanol and gasoline, the effects of these fuels on the vehicle and engine performance, fuel consumption and energy efficiency were investigated in the literature.

In addition, this work investigated mathematical models capable of predicting coastdown tests in order to quantify the power losses caused by forces acting on the vehicle (aerodynamic drag and rolling resistance). Grading resistance was desconsidered from this work, since speed recovery tests are done generally on flat tracks.

2.1 Performance of Conventional Automotive Vehicles

Villela (2015) mentions in his work that there are four main characteristics sought by consumers when buying an automotive vehicle: fuel consumption, low emissions, safety and acceleration capability. Usually a good acceleration performance is more requested in racing vehicles, as they require that the race be done in the shortest possible time. However, the author points out that conventional car consumers also expect their vehicles to perform well, as this can be a crucial factor for the driver to escape risky situations.

According to Villela (2015), a good performance is mainly related to the ignition and fuel injection systems. However, there are other aspects related to this purpose. We can cite as an example the fuel used, the presence of turbo or superchargers.

Good lubrication and cooling systems, which are related to friction and heat losses, respectively, are also important. Also, to improve performance, the vehicle mass and the resistance forces such as the aerodynamic drag and rolling on the tires can be reduced (Gillespie, 1992; Wong, 2000; Ehsani, 2009) or the intake and exhaust tunning can be improved (Heywood, 2018; Fergusson, 2015). Some of these aspects that are related to this work will be better detailed in the next items.

Mashadi & Crolla (2011) presents a brief history on the performance of conventional automotive vehicles since their invention. The authors mention that this feature has always been fundamental for the comparison between automobiles. In the first instance, it was carried out through the acceleration and grade performance or the maximum speed reached. The authors mention that around the 1970s, the main focus on the automotive design changed so that they had low fuel comsumption values. Mashadi & Crolla (2011) still point out that the main goal nowadays is low air pollutants emissions.

To evaluate the vehicle performance during a speed recovery, it is necessary to know the entire process of power and torque generation, as well as the energy losses that occur internally and externally to it.

The process that generates the traction force on the wheels occurs in the engine during the fuel combustion, occurring heat and friction losses. So, the power passes through the transmission, where occur more friction losses, reaching up to the wheels, promoting the movement of the vehicle by kinetic energy. This energy must overcome the road loads in the opposite direction of its movement, which are: the aerodynamic drag and the rolling force.

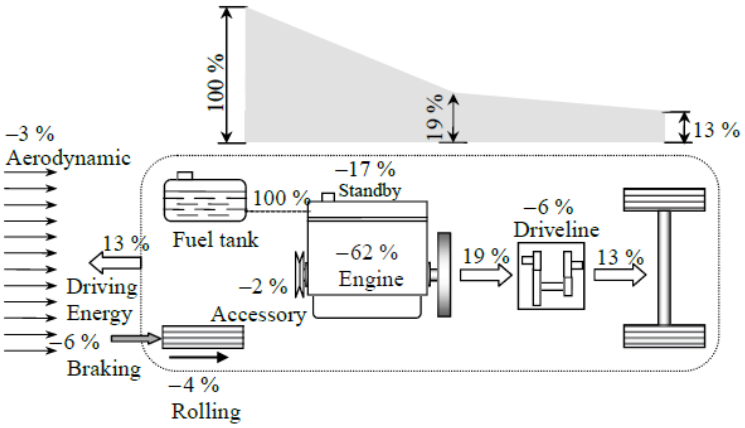

Figure 2.1: Typical example of energy losses in conventional powertrain vehicles during urban driving cycles (Mashadi & Crolla, 2011)

2.1.1 Factors Affecting Powertrain Performance

2.1.1.1 Combustion

The combustion process of conventional powertrains occurs from a mixture of air and fuel inside the cylinders, in which the two react chemically at high pressures and temperatures with the aid of a spark, in the case of spark ignited engines. This process involves several physical and chemical phenomena that are still of extensive study in the engineering field. Many aspects influence the combustion process such as air turbulence level, injection type (direct or indirect), engine geometry, fuel used, or air-fuel ratio.

Examples of engines combustion models can be found in Heywood (2018), Fergusson (2015), Taylor (1985) and Caton (2015). In general, these models present the combustion phenomenon from a burn rate defined by Wiebe (1967) or by the flame speed propagation model. In addition, it is possible to simulate combustion through more sophisticated methods, such as multidimensional, which are solved by Finite Elements, Finite Volumes and Finite Differences (Caton, 2015).

Caton (2015) presents combustion models separated by zones. When it comes to spark ignition engines, it is recommended to model combustion in two zones, referred as burned and unburned gas zones. In the remainder of the four stroke engine cycles, it is recommended to use the one zone model (the fluid is treated as a single mixture of air, fuel and residues from the previous cycle for the intake and compression, while only burned gases for the exhaust). Fergusson (2015) also recommends the same procedure. These methods are solved by ordinary differential equations created from the first law of thermodynamicste for each of the four engine strokes. Such expressions are resolved by Euler or Runge Kutta method in which the variables to be found for each variation in crankshaft angle are the pressure and temperature within the chamber.

In this work, there is no need to model the engine pressure curves by these methods, since these will be obtained experimentally in bench test cell. The combustion analysis will be done to discover some important parameters, such as the combustion duration and efficiency. To do this, Heywood (2018) provides in chapter nine of his book a methodology that must be made from the first law of thermodynamics, in which the variable to be found is the heat released in combustion.

2.1.1.2 Fuels

A history of the fuels evolution processes can be found in Brunetti (2018). According to the author, most automotive vehicles used around the world still mainly use gasoline as an energy source, although some countries, such as Brazil and USA, are adding ethanol in their mixture. Currently in Brazil two types of ethanol are used (Brunetti, 2018):

- Anhydrous ethanol (E100): added to gasoline with a maximum of 0.4% in volume of water added to the mixture.
- Hydrated Ethanol (H100): Commercial use in alcohol or flex vehicles. According to ANP Resolution No. 7 of 9.2.2011, the maximum permitted water content is 4.9%.

The nomenclature of fuels is based on the type of ethanol that is in the mixture and its respective percentage by volume:

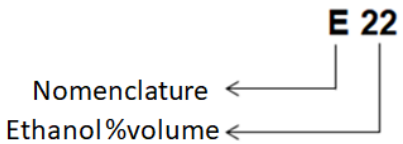

- H: Blend of hydrated ethanol with commercial gasoline.
- E: Mixture of anhydrous ethanol with standard gasoline.

The explanation of the nomenclature of ethanol and gasoline mixtures can also be seen in Villela & Carvalho (2009). In this work the fuels H30, H50 and H70 were used, which according to the authors, these fuels have in their composition the following percentages in volume of each fuel:

- E22: 78% vol. E0 + 21,9% vol. E100 + 0,1% vol. water;
- H30: 70%vol. E22 + 30% vol.H100;
- H50: 50%vol. E22 + 50% vol.H100;
- H70: 30% vol.E22 + 70% vol.H70.

The addition of alcohol in gasoline in Brazil started in low levels since 1935, but it was in 1980 that Brazilian gasoline started to have at least 20% to 22% (E20 to E22) of ethanol volume (Brunetti, 2018). However, the consolidation of its

use in the country occurred in 2002 with the introduction of flex vehicles in the Brazilian market. These cars have as main characteristic the acceptance of gasoline, ethanol or any content of the mixture as fuel (Brunetti, 2018; Melo et al, 2007).

Nowadays in Brazil, standard gasoline A (ethanol-free) must currently receive 27% (E27) in volume of anhydrous ethanol (0.4% water), which results in commercial gasoline (called C gasoline). The variation of ethanol content of the fuel results in different thermophysical properties, such as: air-fuel ratio, lower heating values and latent vaporization heat. Therefore, chemical reactions are modified when the engine operates using different mixtures of these compounds, which, consequently, generate different pressure and temperature values within the combustion chamber.

The introduction of flex fuel vehicles in the Brazilian market has actively altered the country's car fleet (Carvalho et al., 2012). As a result, several articles were published on the study of the behavior of ethanol and gasoline mixtures in automotive vehicle performance.

Carvalho et al. (2012) conducted an experimental work in which E85 and H100 fuels were compared for speed recovery, cold start, emissions and fuel consumption tests. At the end of the experiments, they concluded that E85 presented advantages over H100 in the speed recovery time, fuel consumption and emissions. On the other hand, the deposits in the intake valves were higher.

The H81 (H100 mixtured with 15% of pure gasoline) fuel was also tested for emissions and fuel consumption because it has the same percentage in gasoline volume as the E85 (15%), but with 4% more water in volume in its composition instead of gasoline.A slightly lower performance of H81 was observed in relation to E85.

Villela & Carvalho (2009) evaluated the ratio of fuel consumption between commercial fuels of that time, which were hydrated ethanol (H100) and E22 gasoline for fifteen conventional vehicles according to ABNT NBR 7024 (2010). Additionally, H30, H50 and H70 were tested. The results showed an average ratio of 32% higher fuel consumption of H100 in relation to the E22. It was also noted that fuel consumption increases by raising the content of hydrated ethanol in the mixture.

Villela & Machado (2012) also conducted comparative tests for hydrated ethanol (H100) and anhydrous ethanol (E100) on the emissions and performance of a FIAT 1.4L Flex fuel engine. Higher pressures were observed within the chamber for the E100, resulting in a torque 1.4% higher than the H100. The

volumetric efficiency of H100 was 3.9% higher, because the higher percentage of water by volume in the mixture contributes to the decrease in the temperature in the intake air, resulting in a higher density. However, the combustion efficiency of the E100 was higher resulting in 10% and 16.1% lower CO and THC emissions, respectively.

Najafi et al. (2009) used a neural data network to test the performance parameters of four ethanol-gasoline mixtures (5%, 10%, 15% and 20%). Their results showed that higher levels of ethanol in the composition decrease the specific consumption, but increases the parameters of power, torque and volumetric and thermal efficiencies. In his model, the author obtained an average error of 0.46% to 5.57% in relation to the experimental data, demonstrating a good accuracy in their results.

2.1.1.3 Heat Losses

The heat transfer to the cylinder walls and the exhaust in the engine is the main factor responsible for the power losses on conventional powertrains. A review of some existing heat transfer models is shown in Heywood (2018). A history on this topic can also be found in the work of Finol & Robinson (2006), including for HCCI engines.

According to Heywood (2018), during the engine's operating cycle, the gases transfer heat to the cylinders, mainly by forced convection. After that, heat is lost by conduction on the cylinder walls and, soon after, by convection by the coolant. There are also heat losses by radiation, but these are only relevant for compression ignition engines, since the gases are at higher temperatures.

Many studies have been conducted in the last fifty years to quantify these losses, but there is no universal correlation capable of predicting it (Finol & Robinson, 2006). What do exist are specific correlations for different types of engines. Caton (2015) and Melo et al. (2007) add a correction term f_w to the convection heat transfer equation, given by:

$$Q_{conv} = f_w h_c \, A(\theta)(T_{cyl} - T_w) \qquad (2.1)$$

where h_C is the convection coefficient, A(θ)is the heat exchange area inside the cylinder, T_{cyl} is the temperature inside the cylinder and T_w is the temperature of the cylinder wall.

In his simulations, Caton (2015) chooses arbitrary values for the correction factor f_w. However, through experiments in spark ignition engines, Melo et al. (2007) assume the correction factor for λ = 1 for ethanol and gasoline, as follows by table 2.1:

θ(°BTDC)	fw
45	1,77
36	1,67
27	1,68
18	1,45

Table2.1: Correction factors for convection losses inside the chamber of internal combustion engines (Mello et. al, 2007)

The forced convection coefficient of the gas side is modeled based on dimensional analyses, considering turbulent flow in pipes or flat plates (Heywood, 2018):

$$\mathrm{Nu} = \mathrm{aRe}^{\mathrm{b}} \tag{2.2}$$

$$\left(\frac{\mathrm{h_c B}}{\mathrm{k}}\right) = \mathrm{a}\left(\frac{\rho \mathrm{V_{ref} B}}{\mu}\right)^{\mathrm{b}} \tag{2.3}$$

where V_{ref} is the reference speed for each correlation. The Prandtl number was neglected as mentioned by Heywood (2018).

Some correlations for the convective coefficient can be found in the literature in Caton (2015), Heywood (2018) and Fergusson (2015). It can also be seen a history and evolution of them in Finol & Robinson (2006). Some of the models best known and cited by these works were done by Annand (1963), Woschni (1968), Hohenberg (1979) and Han (1997).

2.1.1.4 Friction, Pumping and Accessory Drive Losses in Spark Ignition Engines

When the power is generated inside the combustion chamber, part of it is lost by friction until it reaches the crankshaft. These energy losses occur due to friction between its mechanical components (piston, rings, bearing, valve train, camshaft and crankshaft), accessories (oil pump, fuel pump, alternator, vehicle air conditioning, etc) and intake and exhaust pumping. As a result, we can say

that the friction pressure losses, known as TFMEP, are equal to the sum of all the mentioned losses and it is described by equation 2.4.

$$\mathrm{TFMEP} = \mathrm{PMEP} + \mathrm{AMEP} + \mathrm{RFMEP} \tag{2.4}$$

where PMEP pumping friction mean effective pressure, AMEP is the engine accesory friction mean effective pressure and RFMEP is the rubbing friction mean effective pressure.

Therefore, there are several sources of friction in internal combustion engines and quantifying them mathematically is a very complex task, since there are a wide variety of engine classes on the market with regard to the geometry, design and lubricating oil.

It is possible to obtain the TFMEP in an experimental way. The indicated power, generated inside the combustion chamber, is calculated by integrating the engine pressure curves, obtained by a pressure transducer inside the chamber, as function of the cylinder volume (IMEP – Indicated Mean Effective Pressure). The power on the crankshaft is calculated using the torque read by an engine dynamometer. Subtracting the two MEP's results in the the total lost by friction. Heywood (2018) proposes a general correlation for internal combustion engines for frictional pressure losses in relation to engine speed (N), given as:

$$\mathrm{TFMEP} = \mathrm{C_2 N^2} + \mathrm{C_1 N} + \mathrm{C_0} \tag{2.5}$$

where C_0, C_1 and C_2 are constants that vary for each internal combustion engine and can be obtained by linear regression, from the TFMEP results of dynamometer tests for each rotation tested.

Another methodology capable of obtaining TFMEP is by motored engine tests. This experiment occurs without combustion, but under conditions of temperature and pressure very close to this, so that the results are as close as possible to reality. The benefit of this experiment is that the engine parts can be decoupled throughout the test, so that it is quantified how much each of these components contributes to frictional losses.

However, motored tests provide different results from real ones, since they occur without combustion. According to Heywood (2018) and Fergusson (2015), the presence of combustion is fundamental when quantifying frictional energy losses, as increasing pressure inside the chamber exerts a radial force on the

compression rings, pressing them against the cylinder wall and increasing friction.

Heywood (1988) presents a correlation that approximates values of friction losses in motored tests. In this experiment, several tests were performed with different spark ignition engines, under full load conditions and with a displacement range between 845-2000 cm³. The results are represented by the motored mean effective pressure (MMEP), given by the equation 2.6.

$$\mathrm{MMEP\ (kPa)} = 97 + 15\left(\frac{\mathrm{N}}{1000}\right) + 5\left(\frac{\mathrm{N}}{1000}\right)^2 \tag{2.6}$$

According to Heywood (2018), when motored tests are performed, piston friction with the cylinder wall contributes to most of the TFMEP (about 50%), while the valve train, bearings and accessories are approximately 25%, 10% and 15%, respectively.

In a study conducted by Brown (1973), motored tests were performed on a Diesel engine. In order to measure the losses by pumping, the engine operated in normal combustion until it was switched off, following the test procedure. After this, the intake, exhaust and the turbocharger were removed. Then, the valves and the camshaft were removed. In the end, Brown (1973) showed that about half of the frictional power losses come from the movement between the piston and the cylinder.

According to Fergusson (2015), experimental results show that friction is mainly a function of piston speed, viscosity and oil density, compression rate, piston diameter and other geometric parameters related to bearings, camshafts, valves, etc. In his book, the author makes a review of the models proposed by Bishop (1964) and Patton (1989).

These two studies were the first published studies on TFMEP predictions. These correlations consist of approaching the power decrease in all parts of the engine, considering the influence of geometric parameters and the engine rotational speed. Over the years, these models have been improved by other authors, due to the advancement of technology in engines, related to design, materials, lubricating oil and manufacturing.

Sandoval (2003) improved the Patton (1989) and Bishop (1964) models, introducing a factor for oil viscosity as a function of temperature under the terms of which lubrication regime is hydrodynamic. According to the author, this change is made because it needs a parameter that indicates the difference in friction when the engine is operating in cold or hot conditions. Shayler (2005) also uses

the same parameter, but its experiments were carried out with compression ignition engines. These models follow the scheme of the Figure 2.2, which represents the entire "path traveled" by power since it is generated in the combustion chamber until it reaches the crankshaft.

Shayler (2005) and Sandoval (2003) models showed closed simulation results in relation to the experiments, with errors around 15%. However, the correlations found in theses works use only geometric parameters of the engine and the piston mean speed, not presenting a factor relating the pressure generated in combustion and it has already been mentioned in this section the importance of it.

Moreover, Sandoval (2003) does not specify which fuel was used during the performance tests, saying only the three engines tested (V6, V10 and V8), which are larger in size and weight than that of the present study . In addition, the lubricating oil was the 10W-30, while the one of this work is a 10W-40, which alters the correction factor of the reference viscosity. These models also require knowledge of very specific characteristics of the engine, such as number of valves, number of bearings, specification of the valve train, diameter of the bearings, etc.

Given these facts and knowing that frictional losses are dependent on the combustion pressures, the correlations will be tested and compared with experimental data. However, it is expected that some results will come with divergences of the tests performed with combustion for the engine of the present work, since the pressures generated for each tested mixture tend to come different. Therefore, it is necessary to use the model of equation 2.5, obtained experimentally.

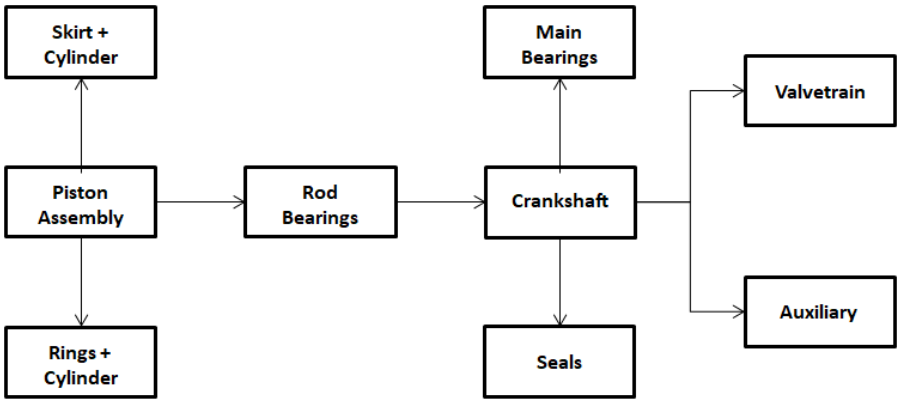

Figure 2.2: Power lost by Friction in Internal Combustion Engines.

2.1.1.5 Friction Losses on the Transmission System and the Inertia of the Rotational Components

When the torque is produced on the crankshaft, it passes through the transmission system where it is amplified or reduced depending on the gear ratio and then is routed to the wheels. A torque map in relation to the speed of the vehicle for each gear can be seen in the example in Figure 2.3, taken from Ehsani (2009).

Similar to ICE's, the contact between the mechanical parts of the transmission (gear box and differentials) generates friction. With this, we can say that this phenomenon also causes more decrease in the power generated by the engine (Ehsani, 2009; Gillespie, 1992).

Just as the vehicle needs traction to develop kinetic energy, it also takes torque so that the rotational components of the engine and the transmission overcome their inertia (Mashadi & Crolla, 2011). These elements are shown in Figure 2.4.

According to Gillespie (1992), Ehsani (2009), Mashadi & Crolla (2011) and Wong (2000), the traction force of the vehicle in a longitudinal acceleration is given according to Equation 2.5:

$$F_T = \frac{T_b i_c i_D \eta_{tr}}{r_w} - \frac{\{(I_{eng} + I_t)(i_c i_d)^2 + I_d i_d^2 + I_w\} a_x}{r_w^2} \tag{2.6}$$

where T_b is the engine torque, η_{tr} is the transmission efficiency, i_c is the gear box transmission ratio at a given gear, i_D is the transmission ratio of the differential, r_w is the radius of the wheels, I_{eng} is the rotational inertia of the engine, I_t is the rotational inertia of the transmission, I_d is rotational inertia of the axle, I_w is the rotational inertia of the wheels and a_x is the longitudinal acceleration of the vehicle.

This equation was obtained by Newton's Second Law and says that the traction force on the whells of the vehicle is equal to the torque that reaches the wheels decreased by the frictional losses and the inertia of rotational components. The equation development can be found in the books of the authors cited in this section.

Transmission efficiency is a performance parameter that quantifies how much power is lost by friction throughout the entire system, from engine output to

wheels. According to Mashadi & Crolla (2011), this value is a function of the torque and the rotational speed of the engine, but can be considered as a constant value. Gillespie (1992) states that some typical values for this parameter are between 80% and 90%.

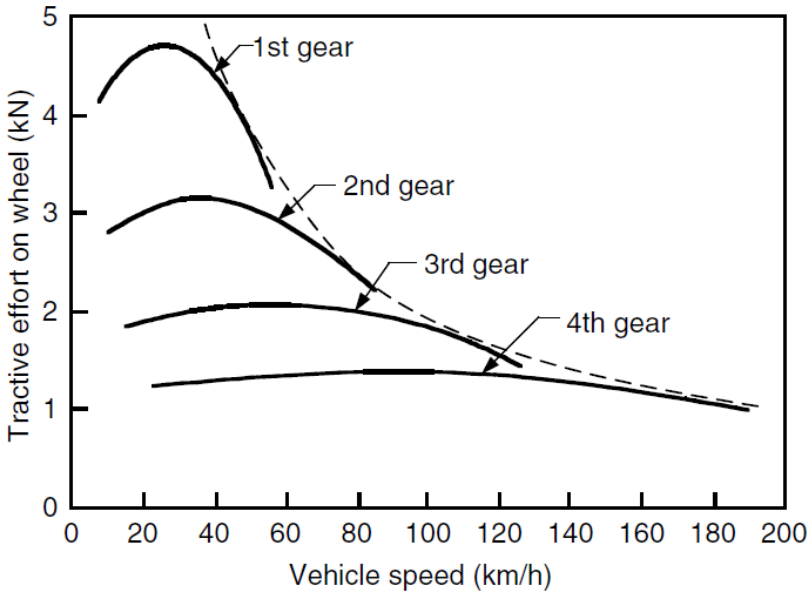

Figure 2.3: Example of a vehicle's driving force in relation to the gear (Ehsani, 2009).

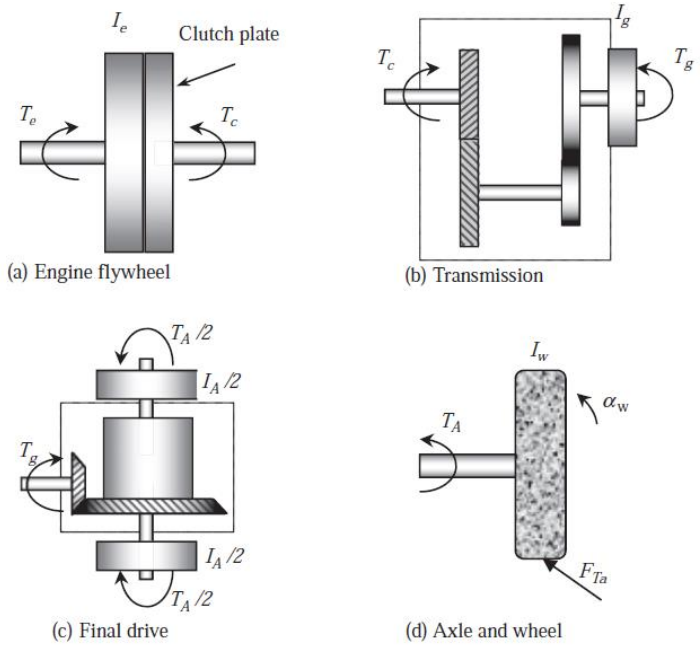

Figure 2.4: Main components of the transmission system of an automotive vehicle. (Mashadi & Crolla, 2011)

2.1.2 Factors Affecting Vehicle Performance

The vehicle's propulsion system produces mechanical energy, which, when arrives on the wheels, is converted into kinetic energy when the car is displaced. The dissipaction of this power can happen due to some factors, such as eventual braking, rolling resistance and aerodynamic drag (Guzella, 2013).

2.1.2.1 Vehicle Aerodynamics

Explanations of vehicle aerodynamics can be found in several literatures such as Ehsani (2009), Gillespie (1992), Mashadi & Crolla (2011), Guzzela (2013), Wong (2000) and, in more details in Katz (1995) and Hucho (1965). This resistance occurs due to the pressure differential between the front and rear of the vehicle when it moves or by friction, from the contact of the air with the body of the automobile. The resulting forces are divided into three components: longitudinal (drag), vertical (lift or downforce) and lateral (cross winds).

According to Guzella (2013), 65% of the aerodynamic drag in a conventional light-duty vehicle is caused by the body. Another 20% is caused in the wheel, 5% due to ventilation in the engine and the remaining 10% are divided between: rearview mirrors, antennas, among others.

The drag force is a resistive load to the longitudinal movement of the vehicle. It is a force vector component contrary to wheeldrive during acceleration. This resistance can be modified according to the body shape, ambient conditions and wind speed. Thus, it can be calculated by the following equation found in Fox et al. (2006):

$$F_D = \frac{1}{2(3.6)^2}\rho_{air,amb}A_f C_d\left(v_{v_x} + v_{w_x}\right)^2 \qquad (2.7)$$

where $\rho_{ai,amb}$ is the air ambient density (kg/m³), A_f is the vehicle front area (m²), v_v is the vehicle speed (km/h), v_w is the wind velocity (km/h) and C_d is the aerodynamic drag coefficient, that are given by manufacturers and can be obtained in wind tunnels or coastdown tests (Katz, 1995).

The higher the drag force, lower is the vehicle performance, since this component acts in the opposite direction to traction. For this reason, track tests should be done in low wind conditions, as it is necessary to mitigate its effects on the results.

According to Katz (1995), the support force, which is perpendicular to drag, known as downforce also has great relevance to the automotive performance. This promotes greater grip of the tires with the ground without having to increase the mass of the car. As a result, it is possible to make curves at higher speeds, without sliding off the track. However, this phenomenon is more explored in competition vehicles, adding some elements to the structure of the vehicle, such as diffusers and airfoils, which allow this force to be created (Katz, 1995). This effect is negligible in conventional vehicles, so it will not be studied in detail for this work. More information about this phenomenon can be found in Katz (1995) or in Murray (1998).

2.1.2.2 Rolling Resistance

Detailed explanations of rolling resistance can be found in Gillespie (1992), Wong (2000), Ehsani (2009), Brunetti (2018) and Guzella (2013). This is determined by the contact of the tires with the ground that generate deflections and deformations that dissipate the power coming from the engine. As the tire deforms, part of the energy is stored and another is dissipated in the form of heat, known as hysteresis losses.

This force is characterized by the rolling resistance mechanical drag coefficient, $f_{r,}$ wich varies with the vehicle speed, with the structure of the ground surface and some parameters related to the tires, such as filling pressure, material and temperature. The mass of the vehicle also has great influence on this force, which is described below in equation 2.8.

$$F_{RR} = m_v g f_r \cos(\alpha) \tag{2.8}$$

According to Brunetti (2018), tires internal pressure has a major influence on rolling resistance. The higher it is, the lower the rolling resistance is. However, a very large increase can lead to some disadvantages such as increased wear and stability problems, primarily in curves.

According to Guzzella (2013), the influence of tire pressure on rolling resistance is proportional to the inverse of its parameter square root. The author also mentions that wet asphalt increases rolling resistance by 20%, and that driving on sand surface can double this value.

Any variation in internal pressure can lead to errors in the measurement of the rolling resistance force. This occurs because the deformation level of the tire

and its ground contact area are modified. Therefore, in order to avoid errors in testing, it is very important to calibrate the tires and to control the filling pressure.

Another determining factor is the tire temperature. Usually track tests begin with the tires being cold. As long as the car is running on track, its temperature is increased due to friction with the ground surface and the higher the temperature of the tire, the lower is the rolling resistance. According to Gillespie (1992), after performing any test with the vehicle it is necessary to heat the tires for about 20 minutes to avoid the cold temperature interference in the results. Guzzella (2013) says that this period is around 10 minutes.

Also, according to Brunetti (2018), when the vehicle speed is increased, the tire excitation frequency is also elevated, generating more cyclic deformations during the movement. It amplifies the contact area with the ground, generating more heat energy dissipation. This effect does not have much relevance for low speeds and can be considered constant except when the filling pressure is below that the one specified by the manufacter (Brunetti, 2018; Gillespie, 1992).

2.2 Track Tests

Automotive track testing is done with the aim of evaluate some specific characteristic of the vehicle such as acceleration, speed recovery, braking, tipping and deceleration. In this work, the main focus will be on the speed recovery tests, which will be numerically modeled. Consequently, coastdown tests should also be simulated, as they are related to the contrary forces acting on the vehicle during acceleration.

2.2.1 Coastdown Tests

The coastdown tests aim to find the coefficients F_0, F_1 and F_2, which represent the resistance to longitudinal movement of the vehicle and are related to aerodynamic drag and the rolling resistance. The mass M_{REF} is the mass of the vehicle added to the inertia of the rotational components and the passenger inside the vehicle. As a result it is represented by the equation 2.9.

$$M_{REF}\frac{dv}{dt} = F_2 v^2 + F_1 v + F_0 \tag{2.9}$$

The purpose of obtaining these coefficients is to perform other tests on chassis dynamometer, such as emissions and fuel consumption driving cycles or in the case of this work, speed recovery tests. These constants are reproduced in the chassis dynamometer, which simulates the resistance acting on the vehicle by braking forces on the dyno rollers, implementing equal conditions as in the track.

Figure 2.5 represents how forces outside the vehicle act on it as the vehicle speed increases. The rolling resistance is practically constant and little depends on the speed, unlike the aerodynamic drag that varies greatly when the car is going faster.

According to the Kadijk (2012), road loads depend heavily on the rolling resistance from 0 to 40 km/h, while for values greater than 80 km/h the predominant force acting on the car is the aerodynamic drag.

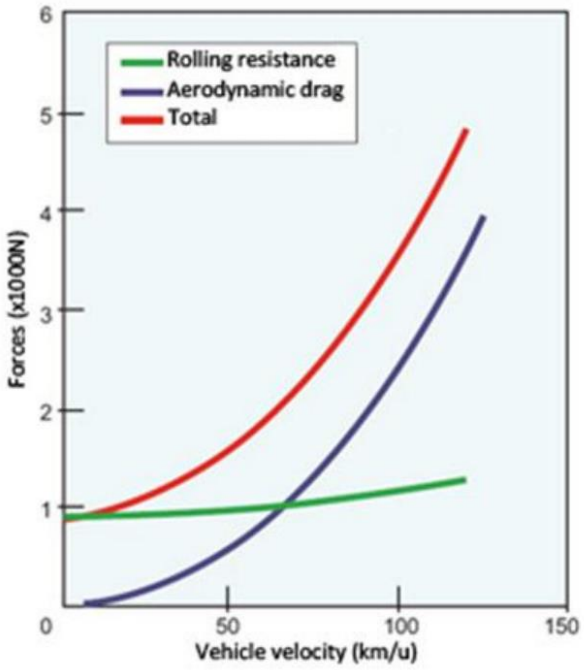

Figure 2.5: Vehicle road loads (Kadijk, 2012)

Kim (2016) shows a history of the SAE standards on coastdown tests. Studies and tests on external forces working on a vehicle began around the year 1950 (Kim, 2016). Between 1970 and 1980 SAE published the SAE J1623 (2010) standard, which standardized the methodology for performing the tests. Between 1980 and 1990, SAE published another standard, SAE J2263 (2008), with the same objective. The two standards have their particularities, but both are carried out in a similar way. In Brazil, the ABNT NBR 10312 (2014) standard is used. It's

important to note that SAE J1623 (2010) was revised in 2010 and SAE J2263 (2008) was revised in 2008.

Before quantifying these forces, the vehicle must be accelerated on a sufficiently long and straight track, as it was shown in Figure 1.3, until it reaches a certain speed. After this step, the driver must start the test by placing the vehicle in neutral gear and letting the car slow down by inertia, in order to the road loads act on it. According to Gillespie (1992), Ehsani (2009) and Guzzella (2013), applying the vehicular longitudinal dynamic equation (based on Newton's Second Law) to this condition, leads to:

$$-F_{ac} = F_D + F_{RR} \tag{2.10}$$

The experiment should be done with the aid of sensors and softwares for the acquisition of vehicle speed data as a function of the test time. With these parameters, it is possible to find the total resistance on the vehicle by the left side of Equation 2.8 and the coefficients are determined by linear regression. Tests should be repeated in both directions to mitigate the effects of wind speed, until the average values of the deceleration curve have certain accuracy, according to the standard.

The SAE J1263 (2010), originated in the 1970s, was developed in the work of White (1972), and can also be found in Chapin's work (1981). After obtaining the velocity-time curve, the following non dimensional parameters related to the time (τ) and velocity (ν) can be calculated according to White (1972):

$$\tau = \frac{t_i}{t_f} \tag{2.11}$$

$$\nu = \frac{1}{\beta}\tan[(1-\tau)\tan^{-1}\beta] \tag{2.12}$$

where t_f is the final time, t_i is the initial time and β is a constant.

It is possible to evaluate the aerodynamic drag coefficient (C_d) and the rolling resistance force (F_{RR}) using the equations 2.12 and 2.13, respectivly:

$$C_d = \frac{2M_{REF}\beta\tan^{-1}(\beta)}{v_0 t_f \rho A_f} \tag{2.13}$$

$$F_{RR} = \frac{v_0 M_{REF} \tan^{-1}(\beta)}{\beta t_f g} \tag{2.14}$$

These values are found by adjusting β in a velocity-time dimensional curve similar to Figure 2.6. As already mentioned, this method is simple because it does not need an anemometer, but is little used due to the restriction of low-speed winds and little accuracy compared to other more sophisticated methods (Kim, 2016).

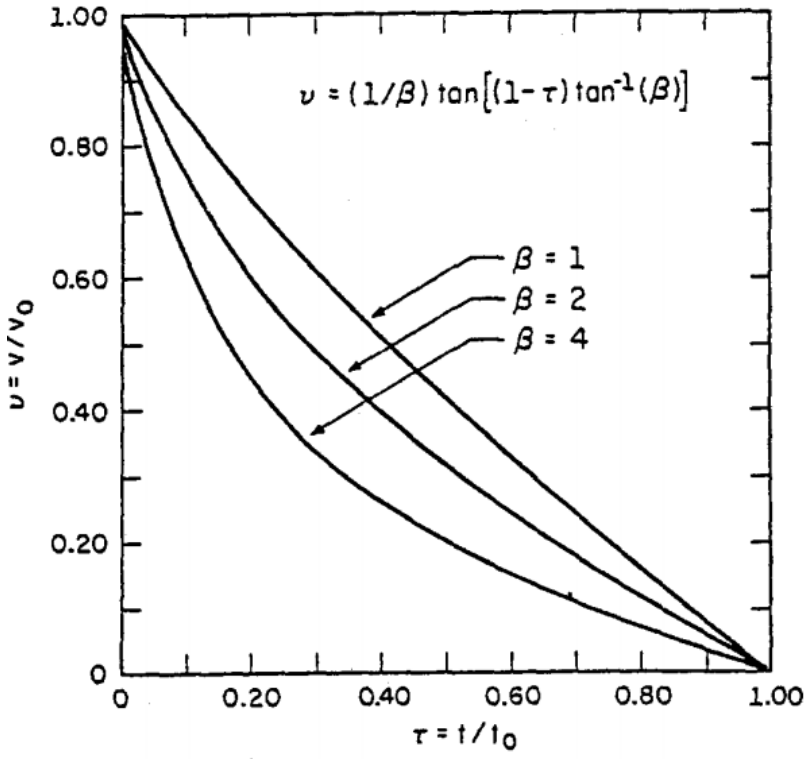

Figure 2.6: Dimensional time-to-time speed curves (White, 1972)

The SAE J2263 (2008) standard was based on an algorithm called the "ABCD Method", which was made in the mid-1980s, being first acquired by the Ford Motor Company in 1988 (published in 1995) and can be seen in Buckley (1995). This method consists of adding an anemometer installed 2 meters in front of the vehicle.

With the anemometer installed, the wind speed and the direction in wich it reaches the car in real time can be obtained. Therefore, drag forces are calculated in all directions. The disadvantage is that the presence of the anemometer causes aerodynamic interferences on the vehicle, because it changes the value of the drag coefficient (Buckley, 1995).

The calculation of the SAE J2263 (2008) is represented by Equation 2.15 and its coefficients are obtained using the least squares method:

$$-M_e\left(\frac{dv_v}{dt}\right) = F_0 + F_1 v_v + F_2 v_v^2 + \frac{1}{2}\rho_{air} A_f (v_v + v_w)^2 \left(a_0 + a_1\gamma + a_2\gamma^2 + a_3\gamma^3 + a_4\gamma^4\right) \pm m_v g\, sen(\alpha) \quad (2.15)$$

- M_e is the effective vehicle mass (kg);
- $\left(\frac{dv_v}{dt}\right)$ is the vehicle acceleration (m/s²);
- v_v is the vehicle speed (km/h);
- v_w is the wind velocity (km/h);
- ρ_{air} is the air density (kg/m³);
- A_f is the vehicle frontal area (m²);
- γ is the yaw angle of apparent wind relative to direction of vehicle travel (deg);
- $sen(\alpha)$ is the sine of the slope of the track, but when the tests are carried out on flat track, this value is equal to zero.
- $a_0,\ldots,a_n$ are the aerodynamic drag coefficients as function of the yaw angle (deg^{-n});
- F0 (N), F1 (N/km) and F2 (N/km²) are the road load coefficients in relation to the vehicle speed.

without the use of an anemometer, equation 2.15 is turned into equation 2.16:

$$-M_e\left(\frac{dv_v}{dt}\right) = F_0 + F_1 v_v + F_2 v_v^2 \quad (2.16)$$

The ABNT NBR 10312 (2014) standard specifies that the force curve by vehicle speed is given without the linear term. Therefore, the equation becomes:

$$F_{RL} = F_2' v^2 + F_0' \quad (2.17)$$

Villela (2016) evaluated the removal of the linear coefficient of the coastdown tests, as in ABNT NBR 10132. The elimination of this term implies that the rolling resistance is constant when increasing the speed of the vehicle.

However, the results obtaneid through rolling resistance tests on a chassis dynamometer clearly demonstrated that there is a variation in the rolling force in the tires with the increase in the speed of the car. Guzzela (2013) also uses this assumption, but the author states that for high speeds there is a relevant change to the rolling force.

2.2.2 Speed Recovery Tests

Speed recovery tests take place on the same track as coastdown tests and aim to assess vehicle performance. The automobile must be accelerated under full load at a pre-established gear range and the recovery time is counted until the end velocity. The standard that establishes the procedures for performing the speed recovery test is the SAE J1491 (2006).

Results of speed recovery tests using the SAE J1491 (2006) standard can be found in Villela (2015). First, an optical sensor was installed in the vehicle, and it is capable of measuring distance travel intervals and speeds. The experiment starts by accelerating the vehicle to a speed near the minimum velocity. At this point the pilot should accelerate slowly and very carefully until he hears a sound emitted by the sensor. When listening to it, the pilot must step to the bottom of the accelerator pedal, so that the internal combustion engine is in full load condition. When the vehicle reaches final speed, another sound is emitted and the test is completed.

2.2.3 Factors Influencing Track Test Results

Coastdown tests are directly related to the track's surface, tyre type and wind velocity and direction (Kim, 2016). In addition to these factors, the speed recovery tests are interconnected with the traction force of the vehicle, coming from its respective powertrain. Knowing this, we can affirm that all factors mentioned in 2.1.1 section contribute directly to the results. External sources to the car such as atmospheric conditions (air pressure, temperature and humidity) and vehicle mass can also affect results (Kim, 2016; Soares, 2002).

In higher altitude locations, there will be a shorter speed recovery time than at sea level. This is due to the lower pressure and with this the density of the intake air will be lower. Then, a smaller amount of fuel will be injected and consequently, the lower will be the power and torque developed by the engine (Baechtel, 2015).

Similarly, colder locations influence speed recovery tests in order to increase the power developed by the internal combustion engine, since the higher the temperature, the higher the air density. This parameter also directly influences aerodynamic drag, since this force is directly proportional to the ambient air specific mass.

Air humidity is also a relevant factor for the test result, since the higher this parameter, the lower the air density. In addition, water vapor molecules are unfavorable to the combustion process because they reduce the flame propagation velocity (Soares, 2002).

Soares (2002) evaluated the speed recovery time of a conventional vehicle with four-stroke spartk ignition engine and variable intake air geometry for different atmosferic conditions. The same vehicle was tested at sea level and another at 827 meters above, to evaluate the effect of the pressure difference. The experiments were performed for different temperatures. It was concluded that pressure has a greater influence than temperature with regard to the results of the experiments, with a difference of 3% in the recovery time.

In Kuhlwein (2016), coastdown tests were performed for 19 different vehicles and the results were compared to those approved by the manufacturers. The results presented divergences and the author explains some factors that may have led to these differences. Among them, we have the atmospheric conditions and a list of possibilities that the author suggests that manufacturers may have used to improved the results, decreasing the rolling resistance and aerodynamic drag.

Kadijk (2012) performed coastdown tests in 8 different vehicles in two locations (Netherlands and Belgium) and the results obtained differed from those provided by manufacturers. The results showed an average difference of 61% for 20 km/h and 18% for 120 km/h. The author states that this difference occurs mainly in the rolling resistance force of the tires since some adjustments may have been different from the manufacturers.

In addition, Kadijk (2012) evaluated the results of some vehicles varying the vehicle reference mass. The author demonstrates that by adding 201 kg in a vehicle of 1523 kg, the results of the coastdown tests road loads are increased by 6.1%.

2.3 Automotive Tests in Chassis Dynamometer

Villela (2015) describes two alternatives in which the speed recovery tests can be done in a chassis dynamometer. The first, called "Partial *Dyno*", is done in a similar way to the speed recovery tests on track. The other, called "*Total Dyno*", has a methodology that eliminates the reaction effects of the pilot and the transient stage of the engine. According to the author, the benefit of performing these experiments in the laboratory occurs because they eliminate the variability of the track such as ground surface irregularities and wind speed.

In the methodology *"Total Dyno"* proposed by Villela (2015), the driver steps to the end of the acceleration pedal, causing the engine to operate under full load. The car tries to accelerate, but the chassis dynamometer, which is at constant speed, keeps the vehicle at the same speed. With the entire system stabilized, the dynamometer operator configures it to operate under the road load conditions, starting the tests. The disadvantage of this method lies on the fact that it does not represent the real time of speed recovery, since it eliminates the time it takes to the engine to develop full load from the moment the rider steps on the pedal.

In another work, Villela (2016) presents an alternative to coastdown tests to obtain the curve coefficients of equation 2.16. The autor determined the rolling resistance by rolling tests with the vehicles on a chassis dynamometer and the aerodynamic drag was calculated by equation 2.7, in which the front area and drag coefficient were specified by the manufacturers. Five cars were used and all coefficients found showed a good accuracy (within the margin of 15%, error interval determined by ABNT NBR 103132 (2014), when compared to the experiments on the track.

The author also evaluated the removal of the linear coefficient by ABNT NBR 10312. According to the author, by eliminating the term $F_{1,}$ it implies stating that rolling resistance force is constant when speed is increased. The results of the rolling tests on the dynamometer did not confirm this fact and the elimination of this coefficient was said to be a simplification adopted by the Brazilian standard.

2.4 Performance Simulation and Track Testing

Efforts to predict automotive performance have been taking place since the time of its invention, at the end ofthe 19th century (Mashadi, 2011). Faix (1998)

states that the main obstacle for performance simulation is to make the model to be able to predict a wide variety of automobiles types (types of transmission, tires, engines, etc) and atmospheric conditions.

According to Mashadi & Crolla (2011), it was from the year 1930 that performance forecasts in automotive vehicles began to have better accuracy due to the development of effective methodologies for estimating engine performance and the forces of rolling and aerodynamic drag. However, the author states that since the 1970s, due to the oil crisis, there has been great pressure from world governments for cars to have better autonomy. As a course, the effort to search for better performance predictions was greater.

Currently, automotive performance is predicted by models based on the vehicle longitudinal dynamic equation, which is elaborated from Newton's Second Law. An image of the forces acting in the car at the moment of the acceleration can be seen in Figure 2.7. Equation 2.16, made from the balance of the forces in Figure 2.7, represents this modeling, and can be found in detais in Ehsani (2009), Gillespie (1992), Wong (2000) and Mashadi & Crolla (2011).

$$F_G = F_T - F_{RR} - F_A$$

$$m_v \varepsilon \frac{dv}{dt} = \frac{T_b i_c i_D \eta_{tf}}{r_w} - m_v g f_r \cos(\alpha) - \frac{1}{2}\rho C_d A_f V_r^2 \qquad (2.16)$$

The parameter δ, according to Gillespie (1992) and Ehsani (2009) is called mass factor and represents the inertia of the rotational components presented in 2.1.1.5.

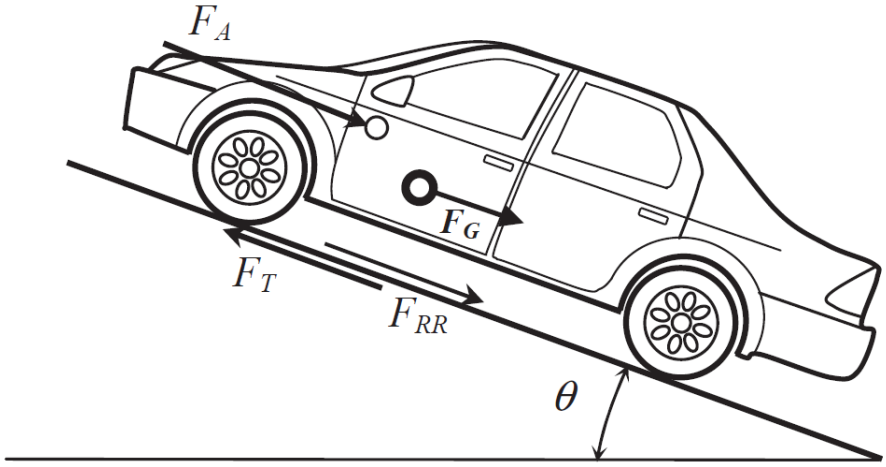

Figure 2.7: Free Body Diagram of an Automotive Vehicle

2.4.1 Speed Recovery Tests Simulation

Literature shows that vehicle performance prediction can be made through mathematical models using Newton's Second Law. This same model can be seen in the work of Ehsani (2009), Mashadi & Crolla (2011) and Gillespie (1992), and can be described according to the speed recovery time in the following integral:

$$t_f = \int_{v_i}^{v_f} \frac{m_v \varepsilon}{\frac{T_b i_c i_D \eta_{tf}}{r_w} - m_v g f_r \cos(\alpha) - \frac{1}{2}\rho C_d A_f v_v^2} dv_v \tag{2.17}$$

The engine torque (T_b) varies according to its rotational speed, which is related to the vehicle speed through equation 2.18 that can be found in Brunetti (2018), Mashadi & Crolla (2011) and Ehsani (2009). Furthermore, it was also mentioned in section 2.1.2.2 that the roll coefficient (f_R) is also a function of the car's speed.

$$N_w = \frac{N_{eng}}{i_c i_d} \tag{2.18}$$

Therefore, to solve the integral shown in equation 2.17, it is necessary to know how T_b and f_R vary according to the vehicle speed.

2.4.2 Coastdown Tests Simulations

Based on the analytical form, one can simulate the coastdown tests by the equation of the longitudinal dynamics of the vehicle considering the traction force on the wheels as equal to zero, since the car slows in neutral gearing. As a result the equation 2.18.

$$-m_v \varepsilon \frac{dv}{dt} = m_v g f_r \cos(\alpha) + \frac{1}{2}\rho C_d A_f v_r^2 \tag{2.19}$$

Villela (2017) evaluated eight different vehicles in order to obtain a correlation for the coeficientes of the ABNT NBR 10132 (2014). According to the standard, the values must be in the range within 15% of the experimental error. Of the eight vehicles tested, only one of the coefficients presented an error of 16%, validating the proposed model.

$$F_{0_{SIM}} = 0.2615\left(\frac{m_v}{p_{tire}}\right) + 22.153 \quad (2.20)$$

$$F_{2_{SIM}} = 0.0656(C_d A_f) - 0.0055 \quad (2.21)$$

2.4.3 Aerodynamic Drag and Rolling Resistance Coefficients

For the aerodynamic drag coefficient, reference values for some vehicles can be found in Wong (2000), Ehsani (2009), Katz (1995) and Gillespie (1992).

For the rolling resistance friction between the tire and the ground, we can find a model demonstrated by Ehsani (2009) and Brunetti (2018), which provides for most filling pressures and in concrete track, a linear variation with speeds of up to 128 km/h:

$$f_r = 0.01\left(1 + \frac{v_v}{100}\right) \quad (2.22)$$

Brunetti (2018) also mentions another correlation for ordinary passenger cars, which relates to speed and different types of track:

$$f_r = s(0.0116 + 0.0000142 v_v) \quad (2.23)$$

where s is the characteristic coefficient of the type of floor, equal to 1,316 for concrete or asphalt.

According to Gillespie (1992), the Stuttgart Technical Institute carried out tests on tyres with different filling pressures and reached the following correlation:

$$f_r = f_o + 3.24 f_s \left(\frac{v_v}{161}\right)^{2.5} \quad (2.24)$$

where velocity v_v is given in km/h, f_o and fs are coefficients that can be obtained in the following graph:

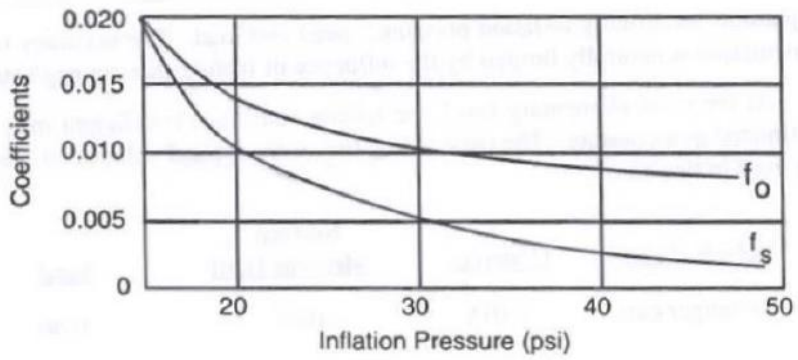

Figure 2.8: Table of coefficients for the calculation of the rolling resistance coefficient. (Gillespie, 1992)

Another correlation found on the website called Engineering Toolbox (2021) can be seen in the Equation 2.24

$$f_r = \left(0.014 \frac{2}{p_{tire}}\right)\left(1 + \left(0{,}6214 \frac{v_v}{100}\right)^2\right) \quad (2.25)$$

2.5 Comments

The literature review of this work aimed to arrive at an automotive performance model. Using the longitudinal dynamics equation, it is concluded that the parameter to be calculated depends on the traction force on the wheels, the mass, the size of the wheel and tire assembly, the inertia of its rotational components and the resistances due to mechanical friction and wind drag. It is worth mentioning that this work refers to conventional vehicles, whose propulsion is done only by an internal combustion engine, and that these vehicles make up the majority of the automotive fleet mentioned in section 1 of this work.

The traction force on the wheels comes from the powertrain system of the automobile; wich can be composed by a spark ignitition engine and the transmission. So, it was necessary to make an analysis of the entire power generation process during the operation of the engine and find models capable of predicting with good precision the heat and friction losses. At the end of the process, an engine torque curve is generated in relation to the engine speed that will be used to calculate the traction force of the automobile in the longitudinal dynamics equation.

It was seen that many authors proposed correlations that approximate the heat losses by the engine cylinder walls and also frictional losses. Researching on these subjects, it is concluded that these models are approximations of a

certain class of engines, because the results vary greatly depending on their characteristics, such as: bore, stroke, weight, displacement and operation temperatures and pressures within the combustion chamber.

To obtain the real friction of the internal combustion engine it is necessary to carry out bench tests with the aid of a pressure sensor and a dynamometer. Knowing that the engine to be tested in this work will be a spark ignition one, the most attractive friction model would be the proposed by Sandoval (2003), because in addition to the predicting of total friction, it is still able to provide how much each engine component contributes to it. However, these losses are related to the pressure and temperature inside the combustion chamber, because the variation of these parameters modifies the oil viscosity and the forces exerted on the piston and cylinder walls. Consequently, it influences engine and vehicle performance.

When using different fuels, there is no way to know if the correlation of Sandoval (2003) will be valid because the author does not mention in his work which content of the ethanol and gasoline mixture was used. This conclusion can be done once it was seen that when the composition of the fuel is changed; its thermophysical properties are also modified, directly affecting the performance and efficiency parameters of the engine.

We sought the references which the results obtained by other authors in the parameters of performance and efficiency of engines and vehicles for different mixtures of ethanol and gasoline, since in this project will be used seven different compositions of these fuels. Although the pressures inside the chamber are obtained experimentally, we sought to present some combustion models that can be found in the literature or in engine simulation softwares.

In addition to the factors related to engine and transmission, it was verified that the performance of an automotive vehicle is influenced by aspects related to its body, mass, tire pressures, wheel size and also the type of track surface, wind speed and slope with horizontal. These characteristics relate directly to the forces acting on the vehicle such as traction, rolling resistance or aerodynamic drag.

The biggest challenge of quantifying aerodynamic drag is to find its drag coefficient as it can only be obtained in wind tunnel tests or free deceleration tests. This value can be provided by the manufacturer and it have been presented sources in the literature or websites where this parameter can be found for a particular automobile or an average value for its class (Station Wagon, Hatch, Sedan, etc.).

The rolling resistance is directly related to the mass of the vehicle, the type of track surface and aspects related to tires and wheels. As well as aerodynamic drag, it has been shown that it is also dependent on the speed of the vehicle. Some authors consider that this dependence is linear and others evaluate in a parabolic way. The Brazilian standard ABNT NBR 10132 (2014), for example, simplifies the rolling resistance as a constant value for each model vehicle.

In addition to all that has been mentioned, it has also been sought that atmospheric conditions influences the performance parameters of the engine and the vehicle. Therefore, when performing tests with cars on the track it is necessary to evaluate all these aspects, because it can cause inaccuracies in the results. These imprecisions are related primarly to the wind speed and values of atmospheric pressure and temperature. In order to eliminate these experimental uncertainties, it was looked for publications in which these experiments were done in chassis dynamometer, since within the laboratory these characteristics can be controlled.

3 Objectives

Predicting the speed recovery time of a conventional automotive vehicle is a major challenge. This task requires a complete energy analysis of the car and the atmospheric conditions of the environment in which it is located. It has been noted that the performance of the car differs when the ethanol content is changed in the mixture and that the main reason for this is the modifications of the fuel thermophysical properties and engine calibration. For this reason, the pressures and temperatures inside the combustion chamber are different, directly influencing engine power and torque when using different fuels.

As a result, this work aims to bring some contributions on:

- Computational modeling of the speed recovery tests for conventional automotive vehicles from engine bench tests. Given the complexity of the combustion models mentioned in the references and the lack of data for the calculation of the thermophysical properties of all seven fuels, it was decided to obtain the engine pressure curves experimentally on a laboratory bench. The speed recovery time will be simulated from the equation of the longitudinal vehicular dynamics. The pressure curves will be used for the acquisition of the engine's power and torque parameters as a function of rotation, which are required to calculate the traction force on the vehicle wheels.
- Computational modeling of the coastdown tests. This is important to calculate the resistance forces acting on the vehicle during the acceleration. Therefore, the correlations mentioned in the previous section will be compared with the results of experiments on the track, published by Kadijk (2012) to validate the present model.
- Computational modeling of friction in engines. Once the pressure curves are obtained, there are losts due to some factors such as accessory drive, pumping and friction between the engine components. These power losses will be calculated based on the correlations of Sandoval (2003) and Heywood (1988) and compared with the real friction of the engine, obtained experimentally with the aid of a dynamometer.

- Experimental evaluation of the speed recovery time of a conventional vehicle in a chassis dynamometer, since there may be experimental inaccuracies in the track and also in order to validate the proposed computational model.
- Evaluation of the performance parameters of internal combustion engines according to the change of anhydrous ethanol and water content in the fuel composition.
- Simulation of motored tests. The Sandoval friction model (2003) provides for the contribution to the friction allocated to each engine component. With this, these values will be calculated and demonstrated how they influence the loss of power by friction. These models will be used to simulate the speed recovery time also with the pressure curves to obtain the engine torque.

4 Methodology

This section will show all the methodology and development of the present work for the analysis and modeling of the performance of a conventional automobile using different mixtures of ethanol and gasoline. The experimental tests were divided into two parts: one with the engine on a bench and the other with the complete vehicle in a chassis dynamometer. Therefore, it was chosen for testing a Peugeot 207 SW, model year 2010/11, and its respective engine, known as TU3 engine.

The main objective of the engine bench tests is to obtain the pressure curves and the brake torque, witch was necessary to simulate the speed recovery time. Also, the bench tests were useful to make an analysis of the combustion parameters of each fuel tested.

The chassis dynamometer tests were done to evaluate how the increase of the ethanol content and water addition affects the vehicle performance and to compare the speed recovery time with the numerical model. Also, the dyno tests were usefull to evaluate the drivetrain losses of the model.

The theoretical analysis for the treatment of the experimentally obtained data will also be addressed in the sections of this chapter.

4.1 Equipment

This section contains all the necessary information from the entire engine bench tests and chassis dynamometer tests that was made in order to achieve the goals of this works. First it will show the equipment related to the bench tests and than the dyno tests with the entire vehicle.

4.1.1 Fuels

For the analysis of the influence of fuel composition in internal combustion engines and in vehicle performance, seven mixtures of ethanol and standard gasoline were chosen: E22, E50, E85, E100, H36, H81 and H100.

Pure gasoline (E0), anhydrous ethanol (E100) and hydrated ethanol (H100) were used to produce the mixtures. These were in reservoirs contained in the CDEV. The blends were also produced in CDEV, with a METTLER TOLEDO digital scale, Model IND560, shown in Figure 4.2.

Table 4.1 and 4.2 shows the fuels data provided by CENPES that were used for the production of the fuels. Among these, we can mention the stochimetric air-fuel ratio and the fuels density.

Figure 4.1 : Standard Gasoline and Anhydrous Ethanol Reservoirs

Figure 4.2: METTLER TOLEDO Digital Scale, model IND 560

Description	E22	E50	E85	E100	H36	H81	H100
E0	78	50	15	0	50	15	0
E100	21,6	49,6	84,6	99,6	46	81	96
Water	0,4	0,4	0,4	0,4	4	4	4

Table 4.1: Percentage of standard gasoline, water and anydrous ethanol in the mixtures used.

Propriedade	Método	Unidade	H100	H80	E100	E85	E50	E22
Pressão de Vapor	ASTM D5191	kPa	14,1	36,7	15,9	29,8	53,6	60,6
Massa Específica	ASTM D4052	kg/m³	808,8	794,3	790,2	783,3	760,3	745,5
Água	ASTM E203	%massa	6,16	4,85	0,22	0,38	0,15	0,26
C	xxx	%massa	53,0	58,1	56,2	60,0	69,2	78,1
O	xxx	%massa	32,7	27,6	29,4	25,8	16,9	7,9
H	xxx	%massa	14,3	14,3	14,4	14,2	13,9	14,0
C	xxx	átomos	1,847	2,622	1,994	2,715	4,475	5,942
O	xxx	átomos	0,985	0,843	0,999	0,858	0,518	0,233
H	xxx	átomos	5,663	6,886	5,988	7,103	9,840	12,114
Relação H/C			3,066	2,626	3,003	2,616	2,199	2,039
Relação O/C			0,533	0,322	0,501	0,316	0,116	0,039
Relação Ar-Combustível Estequiométrica			8,716	10,375	8,935	10,425	12,740	13,928

Table 4.2: Main properties of fuels analyzed in CENPES and used in tests.

As shown in table 4.1, the pairs E50 and H36 contain the same pentage in volume of standard gasoline (E0) in their mixtures, with the difference that H36 contains 4% in water. The same is for blends: E85/H81 and E100/H100. Because of this, the presence of water in the mixture composition was also evaluated in this work.

In this work, it was choosen to fill the fuel tank with 10 liters of each blend. The volume percentage is shown in table 4.1, and the respective volume in liters (L) of each fuel was given by equation 4.1 and 4.2.

$$V_{E0} = V_{total} * \%_{E0} \tag{4.1}$$

$$V_{E100} = V_{total} * \%_{E100} \tag{4.2}$$

where V_{total} is the total volume of the mixtures (10 L), V_{E0} and V_{E100} are the volume of each fuel (E0 and E100) in the mixture and $\%_{E0}$ and $\%_{E100}$ are the volume fraction of each fuel given by table 4.1.

Once having the density of each blend given by table 4.2, provided by CENPES, and calculating the volume of each E0 and E100 in the mixture, it is possible to find each of these fuel mass (m_{fuel}), in kg, as:

$$m_{E0} = \rho_{E0} V_{E0} \tag{4.3}$$

$$m_{E100} = \rho_{E100} V_{E100} \tag{4.4}$$

where ρ_{E0} and ρ_{E100} is the fuel density (kg/m³) given by table 4.2. Once calculated m_{fuel} for E0 and E100, it is possible to produce the blends using the

Mettler Toledo mass digital scale, setting the mass values of each fuel. Some of the blends produced is shown in Figure 4.3.

Figure 4.3: Fuels H100, H81 and H36.

4.1.2 Engine Bench Tests

The IC engine tested in this experiment was a TU3 1.4L Flex Fuel (Figure 4.4), from PSA Peugeot-Citroen, the same model that makes up the vehicle chosen for this job. The maximum power, according to the manufacturer's manual is 55 kW at 5400 RPM, while the maximum torque is 118 Nm at 3300 RPM. The main focus of these tests was the capture of the pressure curves from inside the engine combustion chamber for all tested fuels. Adding this to other experimental data obtained, it was possible to evaluate all parameters of efficiency and performance of the engine.

Figure 4.4: Tested Engine - TU3 (Peugeot 207)

The test bench was equipped with an AVL START ALPHA 240 engine dynamometer, that is shown in Figure 4.5. It has maximum torque, power and rotation limit of 550 Nm, 240 kW and 7,500 RPM, respectively. Its torque uncertainty is 0.2%.

At the bottom of Figure 4.5 there is a shell and a heat exchanger tube. The dynamometer has a controller that regulates the water flow that comes from a tower to the heat exchanger to keep the engine block temperature stable at the nominal value specified by the manufacturer. When the temperature exceeds the nominal value, the controller set the thermostatic valve to open, allowing the free movement of water in the heat exchanger.

Figure 4.5: AVL START ALPHA 240

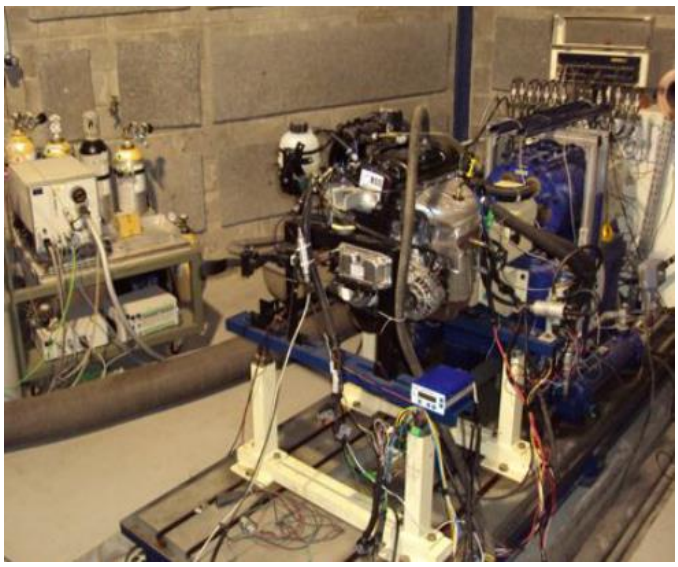

Figure 4.6: Engine Bench

The air consumption of the instake system is the MERIAM, model 50MC2-2 and can be seen in Figure 4.7. This equipment has the function of inducing air flow to the laminar regime. The equipment has inside an array of capillary tubes (Figure 4.7.B), which have a much smaller diameter than the length to maintain an almost linear relationship between the flow of the fluid and the inlet / outlet pressure difference.

Figure 4.7: Laminar type meter used in air consumption measurements.

The emission limits made it necessary to measure fuel consumption instantaneously (Brunetti, 2018). For this experiment, a gravimetric fuel balance was used. This considers the average consumption of a fuel mass during a given time interval.

The gravimetric fuel balance responsible for measuring fuel consumption that was used in this experiment is an AVL model 733 S and can be seen in Figure 4.8. Data acquisition and control software send consumption values every 0.25 seconds. When the reservoir is almost empty, the balance control interrupts the measurement and refills it with a new volume stored in the laboratory tanks.

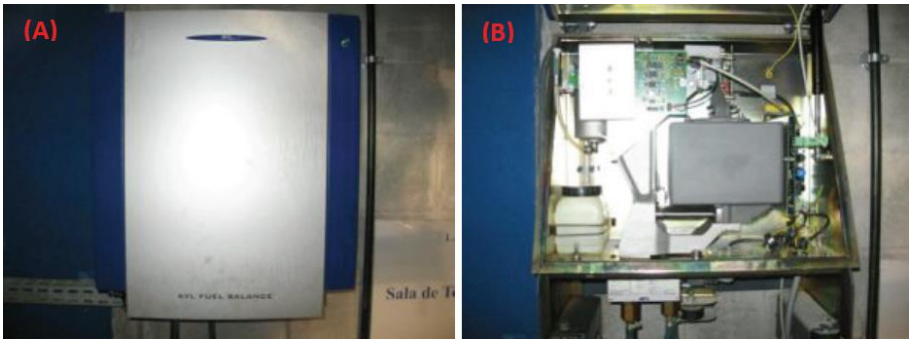

Figure.4.8: Fuel scale used in the fuel consumption measurement.

In order to obtain the pressure curves inside the engine combustion chamber, a spark plug containing a pizoelectric transducer (AVL fabrication) was installed on the cylinder number 1. The electrical charge coming out from the transducer passes through an amplifier, where it is converted into an amplified voltage signal. Soon after, it is digitized and collected by AVL's INDIMETER 619.

To obtain the angular positioning of the crankshaft, a Kistler 2614-A optical encoder, with a maximum resolution of 0.1 degree. It reproduces electrical pulses from the rotational motion of a grooved disk, which moves between a light source and a photodetector. The wheel has 60 teeth, 2 of which are vacant for synchronization purposes. This transducer is connected to INDIMETER 619 in order to obtain the exact position of the pressure values on the cylinder. Figure 4.6 shows all these equipment.

The piezoresistive transducers installed at all engine points (intake and exhaust manifold) were SENSOTEC manufacturing (FP 2000 series). However, the thermocouples and the atmospheric moisture transducer were manufactured by OMEGA.

An oxygen sensor was installed before the engine catalyst to check the quality of the intake air-fuel mixture. Through this lambda probe in conjunction with its module (ETAS, model LA4), it was possible to read the oxygen signal of the exhaust gases and, from this reading, calculate the value of λ. These equipment can be seen in Figure 4.7.

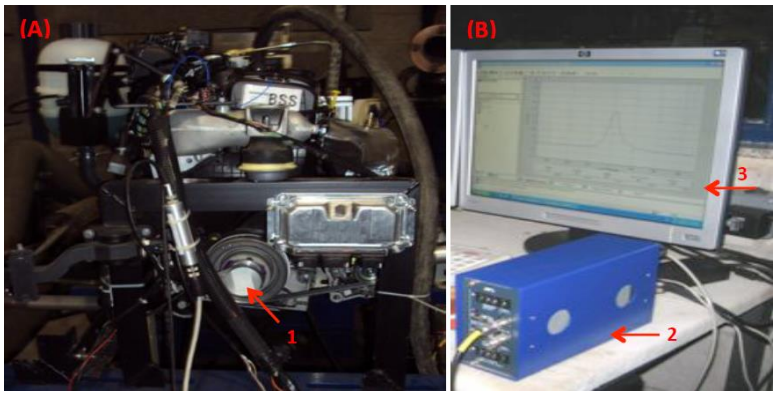

Figure 4.9: Instrumentation used to measure the pressure inside the cylinder.
1 - Encoder; 2- amplifier; 3- indicom software screen.

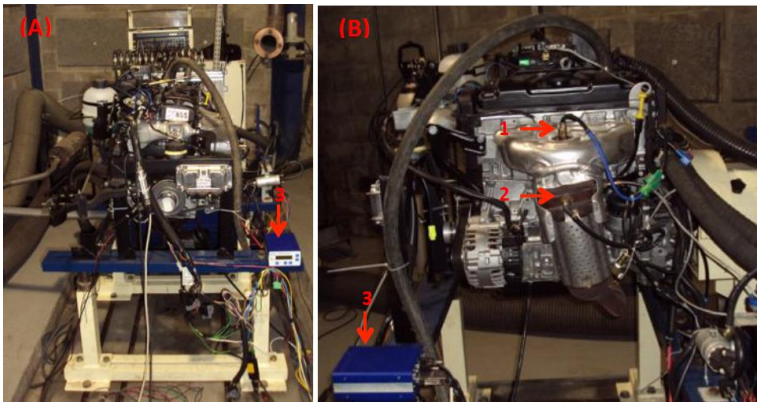

Figure 4.10: View of the installation of the oxygen sensor in the exhaust system
1 - Original Engine lambda sensor; 2 - Additional ETAS probe; 3 - Electronic Module LA4.

To communicate the test cell computer with the ECU, it was necessary to use an ETAS 590.1 interface. In view of the same percentage of anhydrous ethanol for pairs E50/H36, E85/H81 and E100/H100, it was used a programmed ECU for each of these pairs. Also, it was used another ECU for the E22 blend, totaling 4 different ECU's. These were programmed by the systemist, using the data provided by CENPES, such as the stochiometric air-fuel ratio and the hydrogen/carbon and oxygen/carbon molar relationships.

4.1.3 Speed Recovery Tests on Dyno

The vehicle used in this work was a Peugeot 207 SW of 1.4L, whose internal combustion engine is of the same model as the one tested in the engine bench. To perform the tests it was used a HORIBA chassis dynamometer VULCAN EMS CD48L 2WD. This system is designed for rear-wheel drive or front-wheel drive vehicles.

For the engine cooling during the chassis dynamometer experimets, an EVG Lufttechnikaxial fan was used, type AVHN - 56 - 1000M - GB3. This was installed at 300 mm in front of the vehicle. To ensure good cooling, the fan speed has been programmed to be equivalent to the speed of the chassis dynamometer roller. All these equipment were necessary to perform the speed recovery tests and they are shown in Figures 4.11 to 4.14.

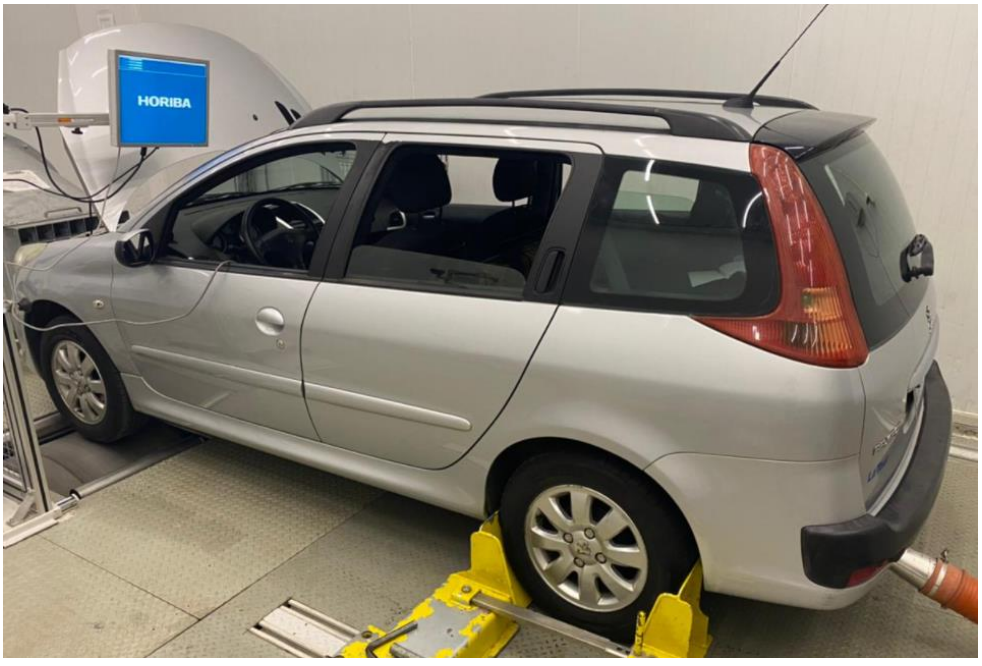

Figure 4.11: Peugeot 207 SW 1.4 FLEX on the Vulcan dyno (rear view).

Figure 4.12: Assembly of the entire Experimental Device on Vulcan

Figure 4.13: Bottom View of VULCAN EMS CD48L

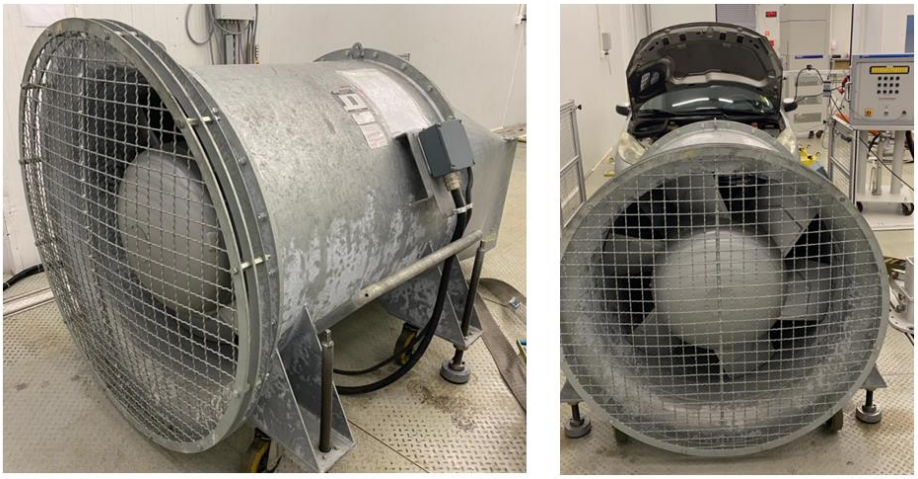

Figure 4.14: Axial Fan EVG Lufttechnik

For the calibration of the tires it was used a digital manometer PREMIUM type M1514 of resolution 1 psi and with indication range from 3 to 145 psi. It is shown in figure 4.15.

Figure 4.15: Premium Digital Manometer M1514

The software responsible for sending and receiving the data from the dynamometer is the SPARC Vehicle. Figure 4.16 shows the screen where the road load coefficients are placed. The logging function can be used to obtain the power values on the rollers and linear speed (km/h). The speed resolution is 0.1 km/h, while the time is 0.1 seconds.

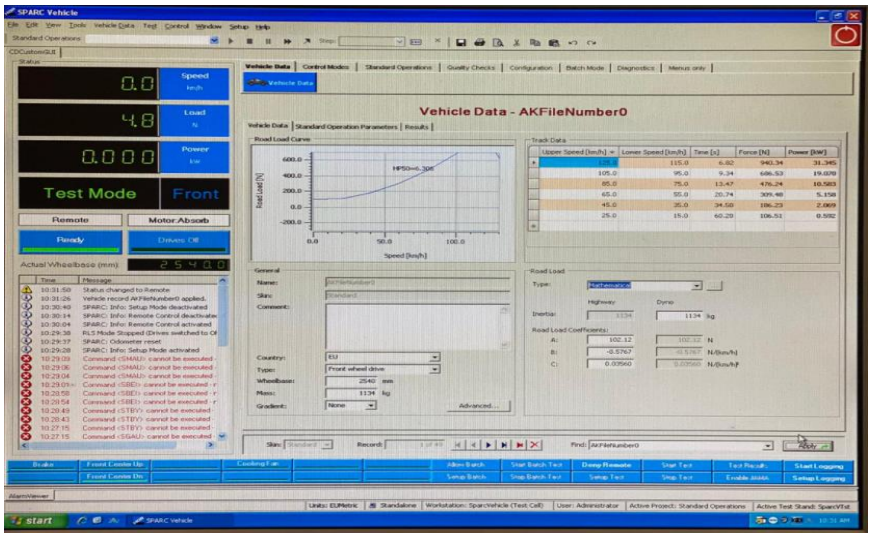

Figure 4.16: Sparc Vehicle screen image

4.2 Tests Performed

In this section it will be described the entire procedure for testing the engine on the bench and the vehicle in a chassis. All experiments in this section were conducted at the CDEV (Center for Development of Energy and Vehicles), based in Xerém and belonging to the Pontifical Catholic University of Rio de Janeiro.

4.2.1 Description of the Engine Bench Tests

Before start the experiments, the engine speed and load must be selected. The tests were performed in partial and full load regimes in three engine speeds: 1300, 2500 and 3500 RPM. All seven fuels were tested and repeated two more times for each of these combinations.

However, only the results for the full load condition were used, for two reasons that are related to the objectives of this work: the maximum performance of the fuel in the engine is given in full load operating regime and speed recovery tests are done with the driver stepping on the accelerator until the end, promoting a total opening of the butterfly valve in the air intake system (full load).

The pressure transducers and the angular measuring encoder must work together to provide the pressure inside the cylinder for each angular position of the crankshaft. In the experiments, a resolution of 1 degree was adopted in order to save computational time in the treatment of data.

As already mentioned, the programming of the four ECU's was performed by the systemist based on the data provided by CENPES. The use of multiple

ECU's is justified to avoid the error of adapting maps for different fuels. Therefore, the tests were performed with the values of ignition timing, based on their calibrations, for each mixture used.

The pressure inside the cylinder was referred to as absolute pressure with the aid of another pressure transducer installed in the intake manifold. It was considered that the pressure at the lower neutral at the end of the intake time is equal to the mean value of the intake manifold pressure. This choice was made because at that moment of the cycle the piston is practically with the exhaust valve closed and the intake valve opened.

In each condition analyzed, 200 motor cycles were acquired. The pressure curve representing the torque and speed pair was selected based on the one with the highest IMEP of all cycles. In cases where the covariance of IMEP is greater than 10%, the number of cycles is increased to 300 to reduce the data devious. However, in most situations that this occurred, this approach did not present a positive result.

Before starting the data acquisition, it was necessary to warm up the engine, untill the temperatures of the cooling water and lubricating oil reach nominal values, of 87°C and 100°C, respectively. When this condition was reached, the parameters of interest were recorded during an interval of 60 seconds. The whole process was repeated twice for each combination of fuel, engine speed and load.

4.2.2 Description of the Speed Recovery Tests on Chassis Dynamometer

The Peugeot 207 SW has front-wheel drive, so for the start of testing, the front wheels were located on top of the chassis dynamometer rollers. Soon after, the tank was filled with the first fuel to be tested. The tires were calibrated to a pressure of 33 psi, according to the manufacturer manual.

The ECU of the vehicle is different from the ones used in the engine bench tests. It is closed and it's known that it accepts any content of the mixture of ethanol and gasoline. Therefore, the FTP-75 phases 1 and 2 cycles was run, before the speed recovery tests, to make sure that electronic injection was adapted to the new mixtures inside the tank.

Due to the infeasibility of performing coastdown tests, a correlation was used from the literature to approximate the road loads coefficients (F_0 and F_2), with the greatest possible precision. These formulations were compared with

results of experiments on real tracks found in Kadijk (2012). The formulation choosed was the one published by Villela (2017).

Therefore, the SPARC Vehicle software was programmed with the road loads coefficients and with the mass of the vehicle so that the chassis dynamometer could simulate resistance forces during the speed recovery tests.

The SPARC Vehicle software also has the "logging" option which is capable of collecting some parameters of VULCAN as a function of time during the tests. For this work, the capture of the speed in the roller and the power on the wheels was chosen, the latter being necessary for the subsequent calculation of the transmission efficiency. The time interval between measurements in the software was selected as 0.1 seconds.

In order to carry out the tests in accordance with SAEJ1491 standard (2006) (which indicates the procedure for measuring a vehicle's acceleration), the range near from 40 to 80 km/h and 60 to 100 km/h for the third and fourth gears were chosen. Upon completion of the evaluation, the fuel tank was emptied and filled with another formulation. Subsequently, the first phases of the FTP 75 cycle for the adaptation of the ECU were repeated. So the speed recovery tests were done with the new mixtures.

With the values of time, speed and power on the wheels, the tests were repeated three times for each fuel, for two speed ranges and two different gears, totalizing 84 tests.

Figure 4.17: Driving the Vehicle in phases 1 and 2 of the FTP-75 cycle

Figure 4.18: Changing fuels between the tests

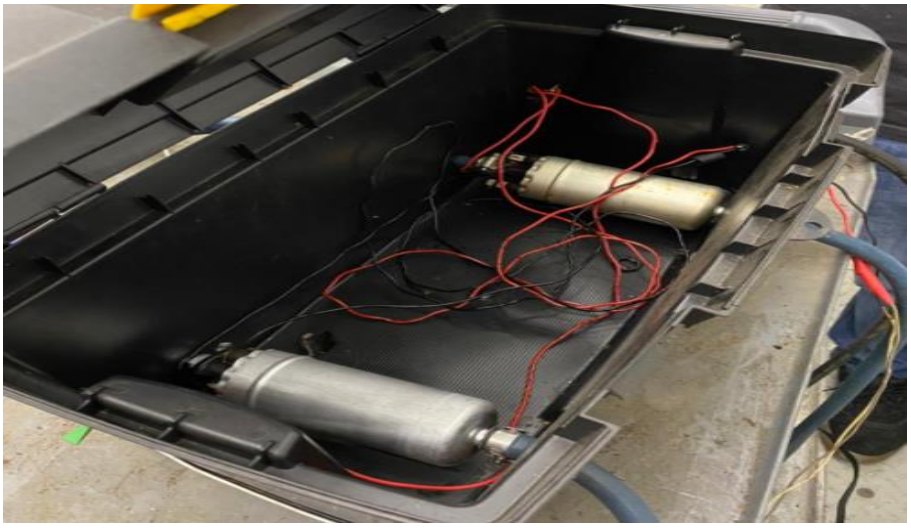

Figure 4.19: Fuel Pump.

4.3 Engine and Vehicle – INPUTS

From the experimental tests, the input parameters are the pressure inside the cylinder for each angle of the crankshaft (p_{cyl}), in bar, and the mass flow rate of the wet air ($\dot{m}_{air,w}$) and fuel ($\dot{m}_{fuel}$), in kg/h. The conditions of the testing environment such as pressure, temperature and relative humidity were also measured and were usefull to some calculations. It was also necessary the power on the wheels (P_w) during acceleration on dyno speed recovery tests to quantify the drivetrain losses. Also, some parameters provided by the manufacturer of the TU3 and from the Peugeot 207 SW can be found in Tables 4.3 and 4.4.

Principal Parameters	
Bore (mm)	75
Stroke (mm)	77
Crankshaft Rradius (mm)	38,5
Number of Cylinders	4 (In Line)
Compression Ration	10,5
Displacement (cc)	1360
Injection Type	Multipoint
Connecting Rod	
Lenght (mm)	126,8
Bearings Diameter (mm)	19,75
Bearings Width (mm)	77
Number of Bearings	4
Crankshaft	
Bearings Diameter (mm)	77
Bearings Width (mm)	17,29
Number of Bearings	5
Camshaft	
Configuration	SOHC
Type of the Follower	Roller Follower
Number of Bearing	5
Intake and Exhaust Valves	
Valves per cylinder	2
Intake Valve Diameter (mm)	35
Intake Valve Displacement (mm)	8,8
Exhaust Valve Diameter (mm)	27,5
Exhaust Valve Displacement (mm)	8,75

Table 4.3: Geometrical parameters of the TU3 engine

Peugeot 207 SW 1.4 FLEX			
Year		2011	
Traction		Frontal	
Mass		**Transmission**	
Mass (kg)	1113	Type	Manual
Permissible Mass (kg)	1490	No of Gears	5
Total Mass (kg)	2390	**Gear Ratios**	
Tires		1st	12x41
Tire Pressure (bar)	33	2nd	21x38
Tire Type	185/65 R14	3rd	32x41
Aerodynamics		4th	40x39
Frontal Area (m²)	2	5th	43x33
Cd (Aero)	0,31	Differential	14x60

Table 4.4: General Features of the Peugeot 207 SW 1.4 Flex (PEUGEOT, 2011)

4.4 Powertrain Modeling

The objective of this section is to use the input data that was obtained in the engine bench and dyno speed recovery tests to model the vehicle traction force. Than, it could be used in the longitudinal dynamic equation in order to simulate the vehicle performance. Also, the combustion parameters will be presented in order to evaluate engine performance using different blends of ethanol, gasoline and water.

To achieve these objectives, it is necessary to have a good powertrain model. As shown in figure 4.20, there are several sources of energy losses since fuel is injected inside the combustion chamber until power reaches the vehicle wheels.

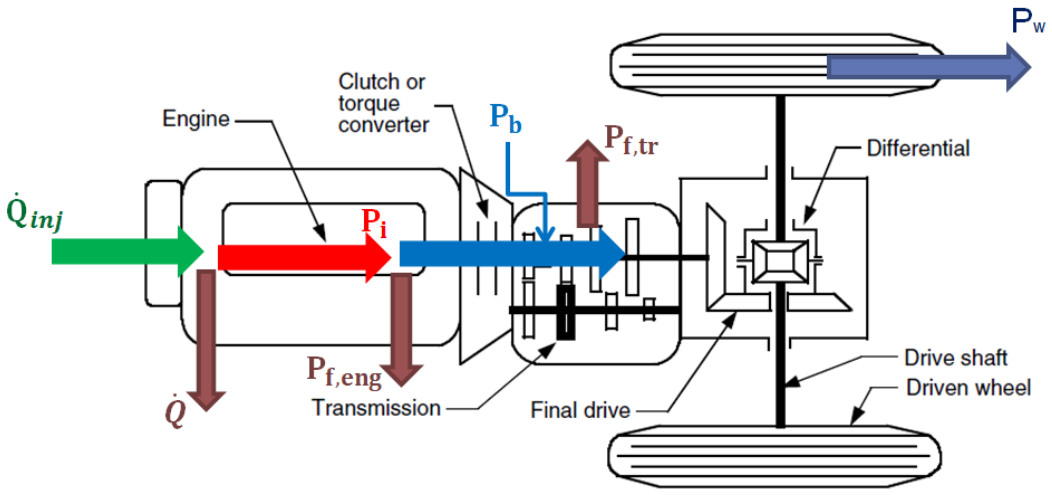

Figure 4.20: Conventional powertrain.
Figure adapted from Ehsani (2009).

When fuel is injected during the engine cycle as Q_{inj}, some of this energy is lost due to heat losses and incomplete combustion of the fuel (Q). Simultaneously, indicated power (P_i) is generated inside the chamber due to the work done by the piston during expansion. When P_i is generated, some of this energy is lost due to rubbing friction of the engine components, auxiliary accessories and to pump gases into and outside the engine. So, the power reaches the crankshaft as brake power (P_b). Until this power reaches the vehicle wheels, it has to overcome the energy loss due to the inertia of rotational components and also by the friction due to the transmission components.

4.4.1 Engine Geometry

The equations for the determination of geometric parameters and kinematics of the four-stroke internal combustion engines can be found in Heywood (2018), Caton (2015) and Fergusson (2015). Its representation can be seen in Figure 4.21. The basic parameters are: B as the cylinder Bore, *a* is the crankshaft radius, l is the connecting rod length, S is the piston stroke, s(θ) is the distance between the piston pin and the center of the crankshaft which is calculated as a function of θ, the angle of the crankshaft.

Other parameters can be obtained from these basic parameters, such as the piston stroke (S), the cross section area of the cylinder (A_{cyl}), the lateral area of the combustion chamber (A_L), the lateral area of the cylinder (A_{Lcyl}), the total surface area (A_{tot}) the volume displaced by the piston (V_d), the volume of the combustion chamber (V_c) and the compression ratio (r_c). Equations 4.6 to 4.9 show the relation between all of these parameters.

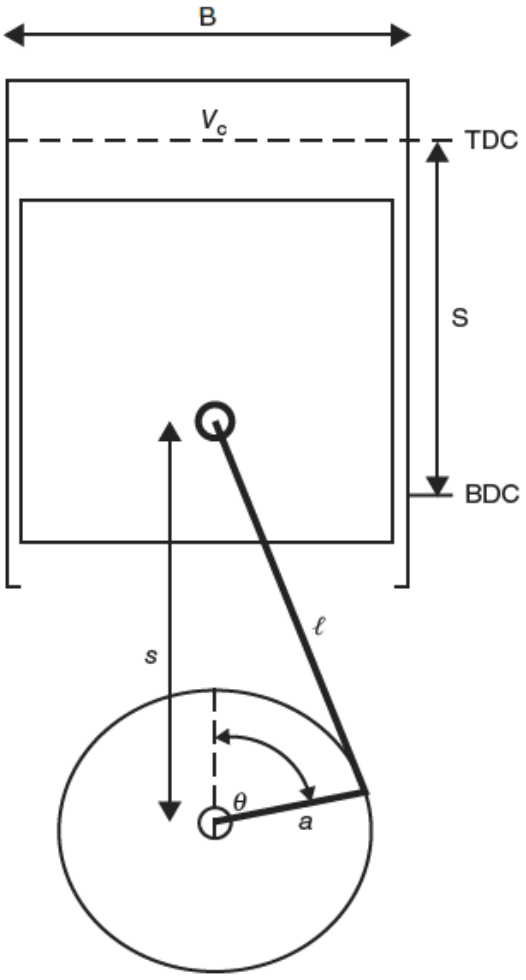

Figure 4.21: Cylinder and piston scheme. (Adapted from Caton, 2015)

$$S = 2a \tag{4.6}$$

$$A_{cyl} = \frac{\pi B^2}{4} \tag{4.7}$$

$$V_d = \frac{V_t}{n_{cyl}} \tag{4.8}$$

where V_t is the engine total displacement volume and n_{cyl} is the number of cylinders.

$$V_c = \frac{V_d}{r_c - 1} \tag{4.9}$$

By using the trigonometric relationships, for any angle value θ, it is possible to obtain s (θ), the instantaneous position of the piston. A(θ) is the surface area of instantaneous heat exchange and V(θ) is the instantaneous volume. Later it will be seen that these values are fundamental for engine performance analyses. These relations are show in equations 4.10 to 4.14.

$$s(\theta) = a\cos\theta + (l^2 - a^2\sin^2\theta)^{\frac{1}{2}} \tag{4.10}$$

$$V(\theta) = V_c + \frac{\pi B^2}{4}\left(l + a - a\cos\theta + (l^2 - a^2\sin^2\theta)^{\frac{1}{2}}\right) \tag{4.11}$$

$$\frac{dV}{d\theta} = \frac{\pi B^2}{4} a\sin\theta\left[1 + \frac{a\cos\theta}{(l^2 - a^2\sin^2\theta)^{\frac{1}{2}}}\right] \tag{4.12}$$

$$A(\theta) = 2\frac{\pi B^2}{4} + \pi B(l + a - s) \tag{4.13}$$

The mean piston speed, $\overline{S_p}$ in meters per second, is given by:

$$\overline{S_p} = \frac{2SN_{eng}}{60} \tag{4.14}$$

where N_{eng} is the engine speed in revolutions per minute and S is the stroke in meters. The piston speed as a function of the cranskshaft angle can be represented by equations 4.15 and 4.16:

$$S_p = \frac{ds}{dt} \tag{4.15}$$

$$\frac{S_p}{\overline{S_p}} = \frac{\pi}{2}\sin\theta\left(1 + \frac{a\cos\theta}{(l^2 - a^2\sin^2\theta)^{\frac{1}{2}}}\right) \tag{4.16}$$

4.4.2 Air-Fuel Ratio

The lambda value is the ratio between the real and the stoichiometric massic flow rate ratio of the dry air and the fuel, as equation 4.12. Values of the stoichometric air fuel ratio for all the blends of ethanol and gasoline tested were provided by CENPES and can be found in table 4.2.

$$\lambda = \frac{\left(\frac{\dot{m}_{air,d}}{\dot{m}_{fuel}}\right)_{real}}{\left(\frac{\dot{m}_{air,d}}{\dot{m}_{fuel}}\right)_{stoich}} \tag{4.17}$$

Note that the mass flow rate of the air measured is for the wet air. Therefore, to find real AF ratio and calculate the value of λ, it is necessary to obtain the amount of air mass that reacts with the fuel, removing the part of the water vapor. Thus, according to Sonntag et al (2003), absolute humidity is given by:

$$\omega = \frac{0{,}622\, U_r . p_{sat}}{p_{air,w} - U_r . p_{sat}} \tag{4.18}$$

where U_r(%) is the relative humidity, $p_{air,w}$ is the pressure of the wet air and p_{sat} is the saturation pressure of the water vapor, which according to Cibse (2007) is given in unit of kPa by:

$$\log(p_{sat}) = 30{,}59 - 8{,}2\log(T_{air,w}) + 0{,}0024804 T_{air,w} - \frac{3142{,}31}{T_{air,w}} \tag{4.19}$$

being $T_{air,w}$(K) is the test room air temperature.

As a result, the partial pressure of ambient water vapor and the pressure of dry air are given, respectively by:

$$P_v = U_R * \frac{p_{sat}}{100} \tag{4.20}$$

$$P_{air,d} = P_{air,w} - P_v \tag{4.21}$$

And the dry air mass flow rate is given by:

$$\dot{m}_{air,d} = \frac{\dot{m}_{air,w}}{1+\omega} \tag{4.22}$$

4.4.3 Volumetric Efficiency (η_V)

It represents the performance of the engine's intake and exhaust system, i.e. the engine's ability to admit atmospheric air to the cylinders and expel the residual gases outside the engine. It can be calculated as the ratio between the real mass flow rate and the theoretical:

$$\eta_v = \frac{120\dot{m_{air}}}{\rho_{amb} N_{eng}} \tag{4.23}$$

It is worth mentioning N_{eng} is given as rotations per minute and that with each revolution the engine fills two cylinders with air. The theoretical air density in this work was considered as the density of the environment in which the engine was tested, by means of temperature and pressure measured.

$$\rho_{air,d,amb} = \frac{p_{air,d}}{R_{air,d} T_{amb}} \tag{4.24}$$

Being $R_{air,dry}$= 287 N.m/(kg.K). The ambient pressure read by the laboratory sensor is moist air, so it was converted to dry air pressure.

4.4.4 Fuel Energy

The energy injeted inside the engine ($\dot{Q}_{inj}$) is given by Heywood (2018) and Caton (2015), as:

$$\dot{Q}_{inj} = \frac{\dot{m_{fuel}} LHV}{3600} \quad (4.25)$$

Where $\dot{m_{fuel}}$ is the mass flow rate of the fuel in kg/h and LHV is the lower heating value of the fuel in J/kg.

4.4.5 Heat Released during Combustion

Heywood (2018) uses the energy balance to model the heat released during combustion. Ignoring blowby losses, this is given by the sum of the work done by the piston with the heat losses on the cylinder walls (these will be demonstrated in item 4.1.3.9). According to Heywood (2018), compression and expansion processes undergo a polytropic process, PV^k = constant. The author states that these processes can be approximated, considering them as isentropic, that is, k= γ (ratio between specific heats of constant pressure and volume).

According to Heywood (2018), the energy balance can be seen in equation 4.23.

$$\frac{dQ_{RL}}{d\theta} = \frac{\gamma}{\gamma - 1} p_{cyl} \frac{dV_{cyl}}{d\theta} + \frac{1}{\gamma - 1} V_{cyl} \frac{dp_{cyl}}{d\theta} + \frac{dQ_{ht}}{d\theta} \quad (4.26)$$

Integrating equation 4.23 throughout the compression and expansion process, the heat released is given by equation 4.24:

$$Q_{RL} = \frac{\gamma}{\gamma - 1} \sum_{i=1}^{n-1} \left(\frac{p_{i+1} + p_i}{2} \right) (V_{i+1} - V_i) + \frac{1}{\gamma - 1} \sum_{i=1}^{n-1} \left(\frac{V_{i+1} + V_i}{2} \right) (p_{i+1} - p_i) \quad (4.27)$$

4.4.5.1 Polytropic Coefficient

It is known that γ vary with the gas temperature, tending to rise during compression and decrease during expansion. In addition, it also varies with the chemical composition of the gas (Heywood 2018; Caton, 2015).

No correlations of the polytropic exponent were found in the literature for all mixtures of ethanol and pure gasoline used in this study, so a methodology proposed by Heywood (2018) was used. The author states that the value can be approximated as the angular coefficient of the linear stretches of compression

and expansion of the log (P) x log (V) graphs and that this approximation provides very adequate results for combustion analysis.

In order not to be required to manually calculate all the values of the angular coefficient, a function in MATLAB called *"polytropic_coefficient"* was created that does this procedure automatically. This algorithm plots the line that best approximates the experimental points of compression and expansion of the log (P) x log (V) curve and gets its angular coefficient. To ensure a good estimate of the results, it was sought a coefficient of determination R^2 greater than 0.999 between the line and the experimental points.

4.4.5.2 Combustion Duration

The duration of combustion was calculated according to Heywood (2018). The author says that this parameter can be defined as the sum of the flame development period (ignition point up to 10% of the total heat released) and the rapid burning period (interval fom 10 to 90% of the total heat released).

According to the author, the duration of combustion is determined as follows:

- Flame development angle: Period between the point at which it is given the spark up to 10% of the total mass fraction burned;
- Rapid burning angle: Period between 10% and 90% of the total mass fraction burned;
- Total combustion duration: Sum of flame development and rapid burning periods.

4.4.6 Heat Transfer to Cylinder Walls

The heat losses by cylinder walls were calculated considering only convection, disregarding radiation and conduction (Heywood, 2018; Finol, 2011). With this, the convection equation is given by:

$$\dot{Q_{ht}} = f_w h_c A(\theta)(T_{cyl} - T_w) \tag{4.28}$$

Taking into account that the lambda values of the experiment for all fuels were close to 1.0, the correction factor f_w was determined according to Melo et al. (2007). It was chosen to use the Hohenberg (1979) model for the convection coefficient, which is shown in the equation 4.26:

$$h_c(\theta) = 130 p_{cyl}(\theta)^{0.8} T_{cyl}(\theta)^{-0.4} \left(\overline{S_p} + 1{,}4\right)^{0{,}8} V(\theta)^{-0{,}06} \quad (4.29)$$

being T_{cyl} and p_{cyl}, the temperature and pressure of the gas inside the cylinder in K and bar, respectively and V is the instantaneous cylinder volume in m³.

The temperature of the gas inside the cylinder was calculated by the ideal gases law:

$$T_{cyl} = \frac{p_{cyl} V_{cyl}}{(m_{air} + m_{fuel}) R} \quad (4.30)$$

The R value used was that referring to wet air (Pradelle, 2017). Wall temperature T_w in equation 4.25 was considered as the temperature of the cooling water when the thermostatic valve is opened.

4.4.7 Heat Lost due to Incomplete Combustion

At the end of the combustion process, there still an amount of fuel inside the chamber witch is not burned. It can be calculated as the difference between the injected heat and the heat released during combustion (Heywood, 2018).

$$Q_{inc} = Q_{inj} - Q_{RL} \quad (4.31)$$

Thus, according to Heywood (2018), we can define the combustion efficiency. It represents how much fuel is effectively burned throughout the engine cycle. This can be quantified by the ratio between the heat released and the injected energy:

$$\eta_c = \frac{\dot{Q_L}}{\dot{m}_{fuel} LHV} \quad (4.32)$$

4.4.8 Heat Transfer to the Exhaust System

By applying a control volume evolving the internal combustion engine and applying the First Law of Thermodynamics it is possible to get the following equation:

$$\dot{m_{fuel}} LHV = P_i + \dot{Q_{ht}} + \dot{Q_{exh}} + \dot{Q_{inc}} \quad (4.33)$$

In this equation, the left side represents the energy injected into the system, given by the mass fuel flow ($\dot{m}_{fuel}$), measured in the AVL gravimetric balance, multiplied by the lower heating value (LHV) of the fuel. On the right side we have the sum of the power lost by heat transfer to the walls ($\dot{Q}_{ht}$), heat transfer to the exhaust system ($\dot{Q}_{exh}$), indicated power inside the cylinders (P_i) and the energy lost by incomplete combustion ($\dot{Q}_{inc}$).

By isolating $\dot{Q}_{exh}$, the heat transfer to the exhaust system is given by:

$$\dot{Q}_{exh} = \dot{m}_{fuel} Q_{LHV} - P_b - P_f - \dot{Q}_{ht} - \dot{Q}_{inc} \tag{4.34}$$

4.4.9 Indicated Power (P_i)

The data processing presented in this section was based on the methodology proposed by Heywood (2018) and Caton (2015). With the data obtained by the INDIMETER 619, it was possible to plot a a pressure curve as a function of the crankshaft angle. Using equation 4.11, it was possible to obtain it as a function of the instantaneous volume of the cylinder, as indicated by Figure 4.22.

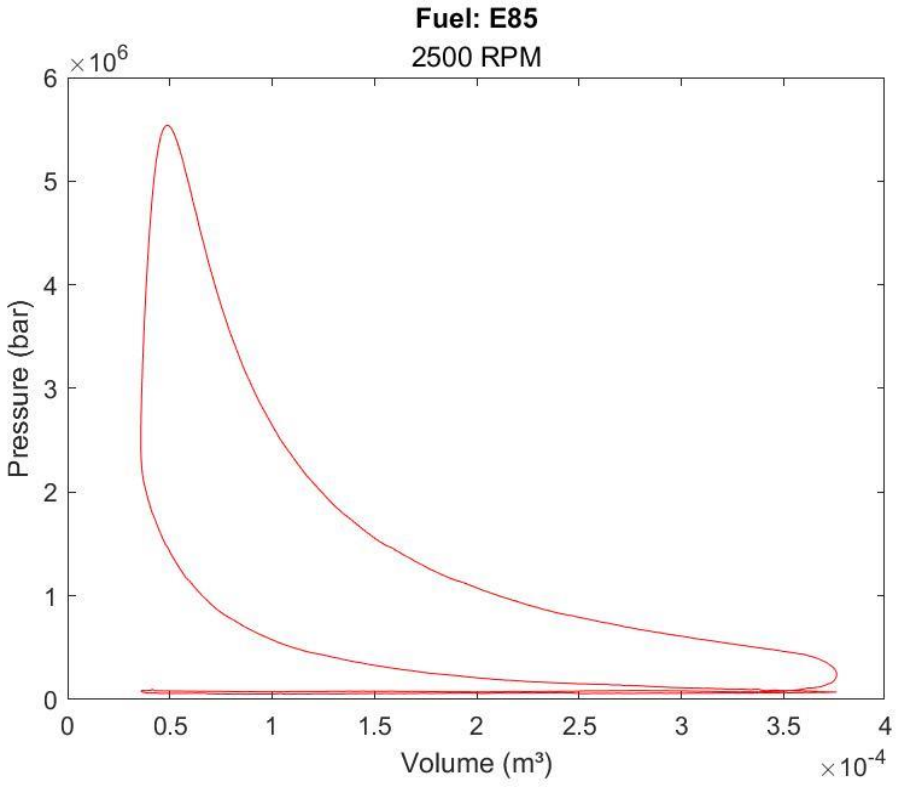

Figure 4.22: Cylinder pressure as a function of the volume for the blend E85 in 2500 RPM.

The bottom area of the curve in Figure 4.22 represents the work done to pump air into the cylinders and the residual gases out of them. The upper side represents the work performed during the cycle by gases. Being p_{cyl} the pressure inside the chamber at each instant of the cycle, the indicated work (W_i), the indicated mean effective pressure (IMEP) and the Indicated Power (Pi) are calculated by the following relation:

$$W_i = \int_{-180}^{+180} p_{cyl} dV \tag{4.35}$$

$$IMEP = \frac{W_i}{V_d} \tag{4.36}$$

$$P_i = \frac{4 V_d N_{eng} IMEP}{120} \tag{4.37}$$

The thermal efficiency represents how much energy from the fuel is transformed in work by the engine:

$$\eta_{th} = \frac{P_i}{\dot{m}_{fuel} LHV} \tag{4.38}$$

4.4.10 Engine Friction Losses

When the indicated power is generated inside the combustion chamber, some of this energy is lost before it reaches the shaft, due to rubbing friction between the engine components, pumping the gases inside and outside the cylinders and by the auxliriary accessories of the engine.

In this work, engine frictional losses were calculated in two different ways: experimentally (real friction of the TU3 engine) and by two SI engine numerical friction models, that were proposed by Sandoval (2003) and the other one by Heywood (1988). Figure 4.23 shows the fluxogram of the TFMEP calculations.

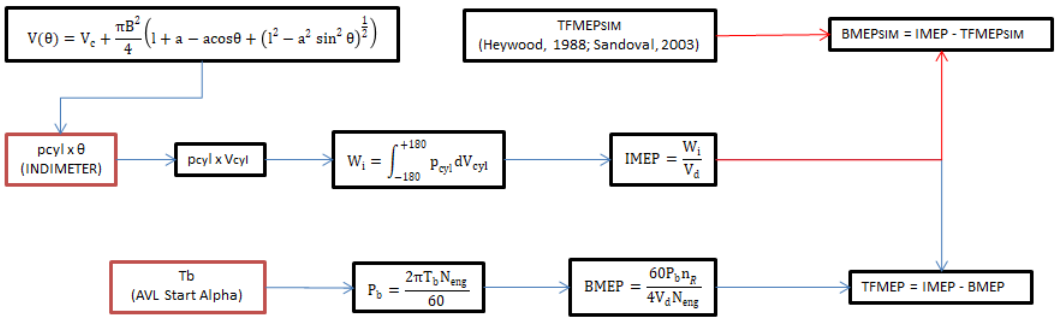

Figure 4.23: Fluxogram of the TFMEP calculations

4.4.10.1 Real Engine Friction

Friction pressure losses were calculated for each engine rotational speed (1300, 2500 and 3500 RPM), as the difference between the indicated mean effective pressure (IMEP) and the brake mean effective pressure (BMEP), as given by equation 4.39.

$$\mathrm{TFMEP} = \mathrm{IMEP} - \mathrm{BMEP} \tag{4.39}$$

Heywood (2018) indicates that TFMEP and the engine speed (N_{eng}) are related as second order polynomial as equation 4.40.

$$\mathrm{TFMEP} = C_2 N_{eng}^2 + C_1 N_{eng} + C_0 \tag{4.40}$$

where C_2, C_1 and C_0 are the friction coefficients. Using the calculated TFMEP for each engine speed, the coefficients are obtained by linear regression of these results.

4.4.10.2 Numerical Friction Models

Alternatively, in view of the non-need for the use of a dynamometer to obtain torque, these experimental results were compared with the model proposed by Sandoval (2003) and Heywood (1988), in order to validate the correlation for flex fuel engines. When getting the $TFMEP_{SIM}$ (simulated), it was taken the reverse path to get the $BMEP_{SIM}$.

The $TFMEP_{SIM}$ was calculated using two different models found in the literature. The Sandoval (2003) correlation can be seen in the Appendix I and the other model is proposed by Heywood (1988) and it is given by equation 4.39.

$$\mathrm{TFMEP_{SIM}\ (kPa)} = 97 + 15\left(\frac{\mathrm{N_{eng}}}{1000}\right) + 5\left(\frac{\mathrm{N_{eng}}}{1000}\right)^2 \quad (4.41)$$

It should be noted that the correlation proposed by Heywood (1988) was improved for more current engines and this change may be visible in the second edition in Heywood (2018). However, according to Vilanova (2015), the TU3 engine was designed in 1992 and, therefore, it was used the first edition correlation (Heywood, 1988).

4.4.11 Brake Power (P_b)

As shown in Figure 4.23, TFMEP was calculated in two different ways: one experimentally with the aid of the AVL Start Alpha engine dynamometer and the other one were from numerical friction models for SI engines. As the indicated power is lot due to friction, it can be concluded that the brake power (P_b) is the difference between the indicated power and the energy lost by friction.

4.4.11.1 Experimental Brake Mean Effective Pressure (BMEP)

The performance parameters on the crankshaft are obtained using brake torque (T_b), in Nm, read on the AVL dynamometer. Power and brake mean effective pressure (BMEP) can be calculated using Equations 4.34 and 4.35.

$$\mathrm{P_b} = \frac{2\pi \mathrm{T_b N_{eng}}}{60} \quad (4.42)$$

$$\mathrm{BMEP} = \frac{60 \mathrm{P_b} n_R}{4 \mathrm{V_d N_{eng}}} \quad (4.43)$$

Once calculating the brake power (Pb), the specific fuel consumption (g/kWh) can be also calculated by the equation

$$\mathrm{sfc} = \frac{\dot{\mathrm{m}}_{\mathrm{fuel}}}{3600 \mathrm{P_b}} \quad (4.44)$$

where $\dot{\mathrm{m}}_{\mathrm{fuel}}$ is the fuel consumption, in kg/h.

4.4.11.2 Simulated Brake Mean Effective Pressure ($BMEP_{SIM}$)

When calculating friction by Sandoval (2003) or Heywood (1988), the simulated BMEP can be calculated by the reverse path of the equation 4.39, as:

$$\mathrm{BMEP_{SIM}} = \mathrm{IMEP} - \mathrm{TFMEP_{SIM}} \tag{4.45}$$

Therefore, the simulated brake torque (T_{bSIM}) is given by equation 4.46:

$$\mathrm{T_{b_{SIM}}} = \frac{2\mathrm{V_d}\mathrm{BMEP_{SIM}}}{\pi \mathrm{n_R}} \tag{4.46}$$

Where Vd is the displaced volume of each cylinder and n_R is the number of revolutions per cycle (in this case, equal to 2).

4.4.11.3 Mechanical Efficiency

Mechanical efficiency represents the ratio of the brake power and the indicated power.

$$\eta_{\mathrm{mec}} = \frac{\mathrm{P_b}}{\mathrm{P_i}} \tag{4.47}$$

where n_R is the number of crankshaft revolutions per power cycle (for four-stroke engines n_R = 2, as there are two revolutions per cycle) and N_{eng} is the engine speed in revolutions per minute.

4.4.11.4 Correction Factor (K_O)

The power generated in internal combustion engines is influenced by air temperature, pressure and air humidity. When engines are tested in different locations, altitudes or on different days, performance parameters can have their values changed as a result of the intake air parameters modifications.

In order to standardize to a reference condition and eliminate the effects of the environment, a correction factor is used which, according to the ABNT NBR ISO 1585 (1996), is given by Equation 4.47:

$$K_o = \left(\frac{99}{p_{air,d}}\right)^{1,2} \left(\frac{273 + T_{air,amb}}{298}\right)^{0,6} \quad (4.48)$$

where $T_{air,amb}$, is the temperature at the entrance of the engine intake in Kelvin, and $p_{air,d}$ is the dry air pressure, in kPa.

4.4.12 Drivetrain Losses

As the energy reaches the drivetrain, some is lost due to friction or by the inertia of the rotational components. It was not found in the literature numerical models capable to predict drivetrain losses. Thus, it was introduce a term that quantifies these losses, called as transmission efficiency.

The transmission efficiency can be represented by how much energy comes out of the engine shaft divided by the power that actually reaches up to the wheels. Thus, it can be calculated by the equation 4.49 and Figure 4.24 indicates the fluxogram of the calculation.

$$\eta_{tr} = \frac{P_w}{P_b} \quad (4.49)$$

P_w is the vehicle wheel power read by the chassis dynamometer data acquisition system during the speed recovery test, and P_b is the power on the engine shaft, obtained in the bench test.

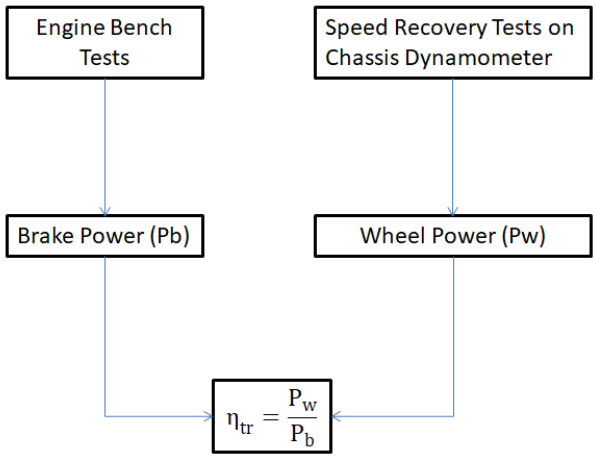

Figure 4.24: Fluxogram of the drivetrain losses calculations

According to Mashadi & Crolla (2011), transmission efficiency is a function of engine torque and speed. The authors also state that this parameter can be

considered as constant. In order to simplify the calculations and observing the proximity of the results for this parameter as a function of the speed of the vehicle, the transmission efficiency was considered as a constant in this work, as an average of the measured values in the dyno acceleration tests.

Note that P_w is the power on the wheels, so it includes all terms of the traction force of the equation 2.6. As a result, the inertia of the rotational components is also included in P_w and there was no need to calculate this paramater.

4.5 Vehicle Traction Force Model

It is important to note that one of the objectives described in section 3 is the modeling of the speed recovery time starting from the engine bench tests. Therefore, the traction force used in this model is calculated from the engine experiments and also simulated engine torque curves in function of the engine speed, which were obtained in the TU3 bench tests. In short, two ways were used to calculate the speed recovery time by the equation of longitudinal vehicular dynamics:

- Traction force from engine experimental torque;
- Traction force from the pressure curves and friction models to get the simulated torque.

According to Mashdi & Crolla (2011) and Gillespie (1992), the traction force on the wheels is given by:

$$F_T(v_v) = \frac{T_b i_c i_D \eta_{tr}}{r_w} \tag{4.50}$$

where T_b is the engine brake torque and it can be substituted for Tb_{SIM} when calculated from the simulated friction model (equation 4.46). The terms i_c and i_D are the transmission gear ratios, r_w is the rolling radius and η_{tr} is the transmission efficiency.

The brake torque is a function of the engine speed, witch changes as vehicle speed is increased. Thus, during the acceleration of the automobile in the speed recovery tests, it can be concluded that T_b is not a constant value and it is necessary to find a relation between torque and vehicle speed.

In this work, brake torque was obtained experimentally by the AVL engine dynamometer or simulated by equation 4.46. These methods were used for the three engine speeds tested in the bench that was 1300, 2500 and 3500 RPM. Figure 4.25 shows the result for the brake torque of the engine using the blend H36.

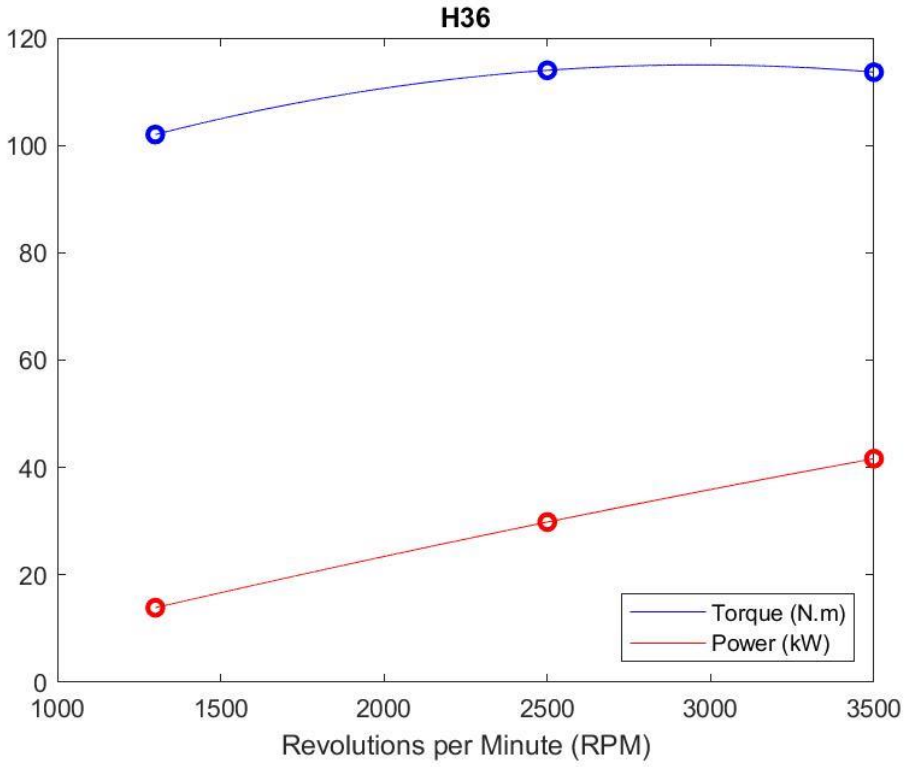

Figure 4.25: Brake torque curve obtained experimentally for the H36.

It can be noticed that the torque tends to fall from 2500 to 3500 RPM for all the results obtained by the dynamometer. Thus, to create a relation between engine speed and brake torque, it was used a parabolic curve, given as equations 4.51 and 4.52.

$$T_b = AN_{eng}^2 + BN_{eng} + C \tag{4.51}$$

$$T_{b_{SIM}} = A_{SIM}N_{eng}^2 + B_{SIM}N_{eng} + C_{SIM} \tag{4.52}$$

where A, B, C, A_{SIM}, B_{SIM} and C_{SIM} are the torque curve coefficients. Note that the relation is between torque (N) and engine speed (RPM). It is still necessary to use an engine-vehicle relation that turns engine speed into vehicle speed.

When acceleration tests, from 0 to 100 km/h, are performed, there are many experimental inaccuracies related to gear change time and tyre slippage in

relation to the ground. These sources of inaccuracy do not occur in speed recovery tests since they are done in a single gear and the slipping is negligible.

This consideration was made, disregarding the effect of the slipping of the tires in relation to the ground. Thus, the vehicle speed will be considered as equal to the wheel speed. This assumption can be found in Mashadi & Crolla (2011) and Brunetti (2018). In addition, it's known that the angular speed of the wheel is equal to the angular speed of the engine divided by the transmission gear ratios (i_c and i_d). With these assumptions we can reach the equations 4.53 and 4.54

$$v_v = \frac{2\pi N_w r_w}{60} \tag{4.53}$$

$$N_w = \frac{N_{eng}}{i_c i_d} \tag{4.54}$$

where N_w is wheel speed in RPM and r_w is the rolling radius of the wheels. By replacing equation 4.53 in 4.54, we obtain the relationship between engine rotational speed and vehicle longitudinal speed:

$$v_v = \frac{2\pi r_w}{60 i_c i_d} N_{eng} \tag{4.55}$$

Substituting this engine-vehicle speed relation given by equation 4.55 into the equations 4.51 and 4.52, the brake torque curve in function of the vehicle speed (experimental and simulated) are given by equations 4.56 and 4.57.

$$T_b = A\varphi^2 N_{eng}^2 + B\varphi N_{eng} + C \tag{4.56}$$

$$T_{b_{SIM}} = A_{SIM}\varphi^2 N_{eng}^2 + B_{SIM}\varphi N_{eng} + C_{SIM} \tag{4.57}$$

were $\varphi = \frac{60 i_c i_D}{2\pi r_w}$. When a vertical force is applied to the tyre, it is deformed and modifies the rolling radius (r_w). According to Brunetti (2018), it can be calculated by equation 4.47.

$$r_w = (a_r + L_b s_b)\frac{C_p}{\pi} \tag{4.58}$$

where a_r is the measure of the wheel bead (m), L_b is the tread width, s_b is the relationship between tire height and tread width (%) and C_p is the dimensional

coefficient and is characteristic of each type of tire. According to Brunetti (2018), the value for C_p to be used is 3.05 since the Peugeot 207 SW has radial tires.

4.6 Road Loads

As it was not possible to coastdown the vehicle of the present work in a track, it became necessary to find a numerical model to determine road loads. Appendix II shows some additional results that were done to evaluate the aerodynamic drag and rolling resistance models that was found in the literature review. The Horiba chassis dynamometer used in this work receives the road load coefficients F0' and F2' as ABNT NBR 10132 (2014), given by equation 4.57.

$$F_{dyno} = F_0' + F_2' v_v^2 \tag{4.59}$$

Based on the results of Appendix II, the road loads coefficients will be determined through Villela (2017), witch numerical model predicts the values of F0' and F2', as shown in equations 4.58 and 4.59. This model was choosen also because it is in accordance with the Brazilian standard ABNT NBR 10132 (2014).

$$F_{0_{SIM}}' = 0.2615\left(\frac{m_v}{p_{tire}}\right) + 22.153 \tag{4.60}$$

$$F_{2_{SIM}}' = 0.0656(C_d A_f) - 0.0055 \tag{4.61}$$

where C_d is the drag coefficient given by the manufacturer, p_{tire} is the filling pressure of the tires (bar), A_f is the front area of the vehicle (m^2) and m_v is its mass (kg), obtained by the technical information of the vehicle in table 4.4.

Substituting the values of the table 4.4 in equations 4.58 and 4.59, the road load coefficients of the Peugeot 207 SW are given as:

$$\mathbf{F_{0_{SIM}}' = 150.07\ N}$$

$$\mathbf{F_{2_{SIM}}' = 0.03540\ \frac{N}{\left(\frac{km}{h}\right)^2}}$$

By setting these values into the SPARC Vehicle software, it makes an iterative process that generates a new curve that inserts the linear term to simulate the road loads adapting to the dynamometer, as equation 4.60.

$$F_{dyno} = F_0 + F_1 v_v + F_2 v_v^2 \tag{4.62}$$

The road load coefficients given by SPARC Vehicle are given as:

$$F_0 = 102.12\ \mathrm{N}$$

$$F_1 = -0.5767 \frac{\mathrm{N}}{\frac{\mathrm{km}}{\mathrm{h}}}$$

$$F_2 = 0.03562 \frac{\mathrm{N}}{\left(\frac{\mathrm{km}}{\mathrm{h}}\right)^2}$$

Figure 4.26 presents the road load curve, calculated by equation 4.60.

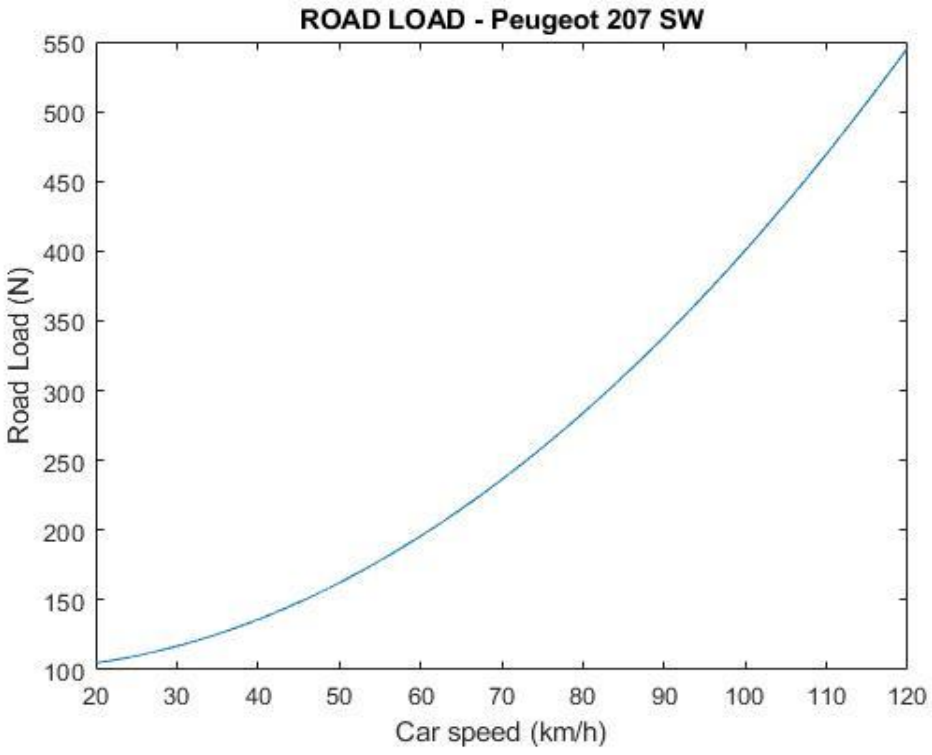

Figure 4.26: Simulated curve of road load on the Peugeot 207 SW as function of the vehicle speed, according to Villela (2017) model.

4.7 Vehicle Performance Modeling

The main objective of the theoretical modeling is to use the experimental data inputs of the engine bench tests and dyno tests, in order to simulate the vehicle performance for all tested blends of ethanol and gasoline. To achieve this goal, it was used the longitudinal dynamic equation during acceleration (Guzzela, 2013; Mashadi & Crolla, 2011; Wong, 2000; Gillespie, 1992), given by:

$$\left(m_v + m_p\right)\frac{dv_v}{dt} = F_T(v_v) - F_2 v_v^2 - F_1 v_v - F_0 \tag{4.63}$$

where dv_v/dt is the vehicle acceleration (m/s²), m_p and m_v is the passenger and vehicle mass (kg), respectively, F_T is the wheel traction force as function of vehicle speed and F_2 (N/km²), F_1 (N/km) and F_0 (N) are the road loads coefficients that represents the rolling resistance and aerodynamic drag force.

The traction force was calculated started from the experimental pressure curves of the engine, that was obtained by the pressure transducer or from the brake torque measured in the engine dynamometer and than, all the powertrain losses were simulated until power reach the wheels to calculated the vehicle traction force.

The chassis dynamometer needs the values of the vehicle road loads coefficients (F_0, F_1 and F_2) to simulate these forces as brake force on the dyno rollers. As it was not possible to do coastdown tests with the vehicle, it was also necessary to model the road loads to get these coefficients.

Once having the traction force calculated starting from the inputs of the bench tests and also having calculated the road loads, it was possible to use the longitudinal dynamic equation to simulate vehicle performance.

After all these assumptions, equation 4.63 it's turned into equation 4.64. The brake torque in function of the vehicle speed was calculated by equations 4.56 or 4.57 (depending if the calculations were from the simulated or experimental brake torque) and the road loads were calculated as equation 4.62 with the coefficients F_2, F_1 and F_0 given by the SPARC Vehicle.

$$t_f = \int_{v_i}^{v_f} \frac{m_v + m_p}{\frac{T_b i_c i_D \eta_{tr}}{r_w} - F_{2_{SIM}} v_v^2 - F_{1_{SIM}} v_v - F_0}\, dv_v \tag{4.64}$$

η_{tr} is the transmission efficiency given by equation 4.49 and r_w is the rolling radius given by equation 4.58.

It's important to note that the transmission efficiency is calculated from the power measured on the wheels by the SPARC Vehicle. Thus, the drivetrain losses of the inertia of the rotational components are also included in this term.

4.8 Model Errors and Adjustments

The coefficient of determination (R^2) is calculated according to equation 4.70 and is used in statistics to explain, as a percentage, the proximity of the values of the model in relation to those observed. The closer it is to 1, the closer the simulated values are to the real ones. This value serves to verify whether the simulations reflecting the experimental data. The farther away the value from 1, the worse the adjustment is.

$$R^2 = \frac{\sum_{i=1}^{n}(\hat{y}_i - \bar{y})^2}{\sum_{i=1}^{n}(y_i - \bar{y})^2} \tag{4.65}$$

In equation 4.70, $\hat{y}_i$ is the predicted value, $\overline{y}$ is the average of the observations and y_i is the observed value. In this work, the coefficient of determination was classified according to Hinkle (2013).

R^2	Classification
$0,9 < R^2 < 1,0$	Very Strong
$0,7 < R^2 < 0,9$	Strong
$0,5 < R^2 < 0,7$	Moderated
$0,3 < R^2 < 0,5$	Week
$R^2 < 0,3$	Very Week

Table 4.5: Adjustment classification according to the determination coefficient.

It is known that a low value of R^2 means that the model is not well adjusted, but a high value does not mean that it is close to the experiment (Figueiredo). Therefore, the coefficient of determination is used in the first instance to detect bad models.

This allows other complementary models to estimate the model fit. To have an average on the amount of samples, it was utilized the mean quadratic error (EQM to estimate an average of how far the values are from the parameter to be estimated. This is calculated using Equation 4.71:

$$EQM = \sqrt{\frac{1}{n}\sum\left(y_{exp} - y_{sim}\right)^2} \tag{4.66}$$

n being the total number of points of the sample and y_{exp} and y_{sim} the experimental and simulated values of the variable, respectively. Knowing that the measured values may vary, the EQM was divided by the mean of the experimental values, in order to obtain a parameter to compare the errors under different operating conditions. Thus, the EQM% can be seen in equation 4.72:

$$EQM\% = \frac{\sqrt{\frac{1}{n}\sum\left(y_{exp} - y_{sim}\right)^2}}{\bar{y}_{exp}} * 100\% \tag{4.67}$$

The final parameter to be compared in this work with the experimental values is the speed recovery time. The tests on each gear and range of speeds were performed three times for seven different fuels. As a result, to ascertain how simulations differ from the experimental tests, the mean between these differences t_{sim}-t_{dyno} was calculated. Soon after, the standard deviation (SD) was determined, which indicates the dispersion of the experimental data set for all simulations.

$$\Delta t_{dyno-sim_{med}} = \sum\left(\frac{\left(t_{dyno} - t_{sim}\right)}{n}\right) \tag{4.68}$$

$$SD = \sqrt{\sum_{i=1}^{n}\frac{\left(\Delta t_{dyno-sim_i} - \Delta t_{dyno-sim_{med}}\right)^2}{n}} \tag{4.69}$$

In order to exclude the order of magnitude of the variable to detect how homogeneous the simulated time data are, the coefficient of variation (CV) was used, calculated using equation 4.75:

$$CV = \frac{SD}{\Delta t_{dyno-sim_{med}}} \tag{4.70}$$

According to the experimental results, the simulated recovery time is shorter than the experimental one. With this the relationship between both can be given by equation 4.76.

$$t_{dyno} = t_{sim} + \Delta t_{dyno-sim} \tag{4.71}$$

4.9 Experimental Uncertainties

The uncertainties were calculated according with the Guide to Measurement Uncertainties by ABNT & INMETRO (2003) and can be seen in Machado (2012), which followed the guidelines of Melo (2006). Type A uncertainty (I_a) was obtained according to the standard deviation (SD) of the measured values, while type B (I_b) refers to equipment uncertainties.

The type B uncertainties were determined by multiplying the uncertainty of the instrument by the mean values measured for each parameter. The variables of interest, which were calculated according to the data obtained from the equipment readings, had the I_b determined by the uncertainty combination methodology, according to equation 4.78 by Kline & McClintock (1953). When equipment uncertainty is not available, this was obtained by dividing its respective resolution by the root of 3 (Machado, 2012; Melo, 2006).

$$\delta z = \sqrt{\left(\frac{\partial z}{\partial x_1}\delta x_1\right)^2 + \left(\frac{\partial z}{\partial x_2}\delta x_2\right)^2 + \cdots + \left(\frac{\partial z}{\partial x_n}\delta x_n\right)^2} \tag{4.72}$$

δz Is the type B uncertainty of the dependent variable of interest, z=z(x1, x2… xn), and δx_n are the type B uncertainties of the independent variables.

The combined uncertainty I_c was calculated as the square root of the sum of squares of I_b and I_a, according to equation 4.79:

$$I_c = \sqrt{I_a^2 + I_b^2} \tag{4.73}$$

The expanded uncertainty I_e was obtained by multiplying I_c by the coverage factor k. The value of k was assumed equal to 2 since this consists of a 95% confidence level for the mean of the calculated variables.

$$I_e = kI_c \tag{4.74}$$

5 Results

In this section it will be presented all the results obtained by the model described in section 4. The main objective is to simulate the vehicle's performance from the pressure curves and the torque obtained by the engine bench tests. Additionally, there are some contributions of this research, such as the analysis of the influence of fuel composition on engine combustion, vehicle performance parameters and simulations of motored and coastdown tests.

First, all the data acquisition that was experimentally obtained in the bench test will be shown. Then, these will be used to calculate the parameters of energy distribution, such as power (indicated and effective), heat injected, heat released, heat loss, frictional losses and amount of unburned fuel. As a result, it is possible to obtain the engine performance indicators and make analyses and comparations of the behavior of the different fuels.

The next step was the calculation of mechanical efficiency, which quantifies how much power is delivered to the shaft in relation to the energy generated in the engine operating cycle. The determination of this parameter will also be performed by motored test simulations and the results will be compared with the real friction of the engine, obtained experimentally. In addition, one of the numerical models used provides the contribution of each component of the internal combustion engine in the frictional power losses.

The car's performance model will use the longitudinal dynamics equation for automotive vehicles. The experimental and simulated torque results and the combustion performance parameters (obtained in the previous analysis) will be used to calculate the traction force of the vehicle. Technical information of the Peugeot 207 SW, which was obtained in the manual of the vehicle, will be used for the calculation of aerodynamic drag and rolling resistance.

5.1 Kinematics and Geometry of the SI Engine

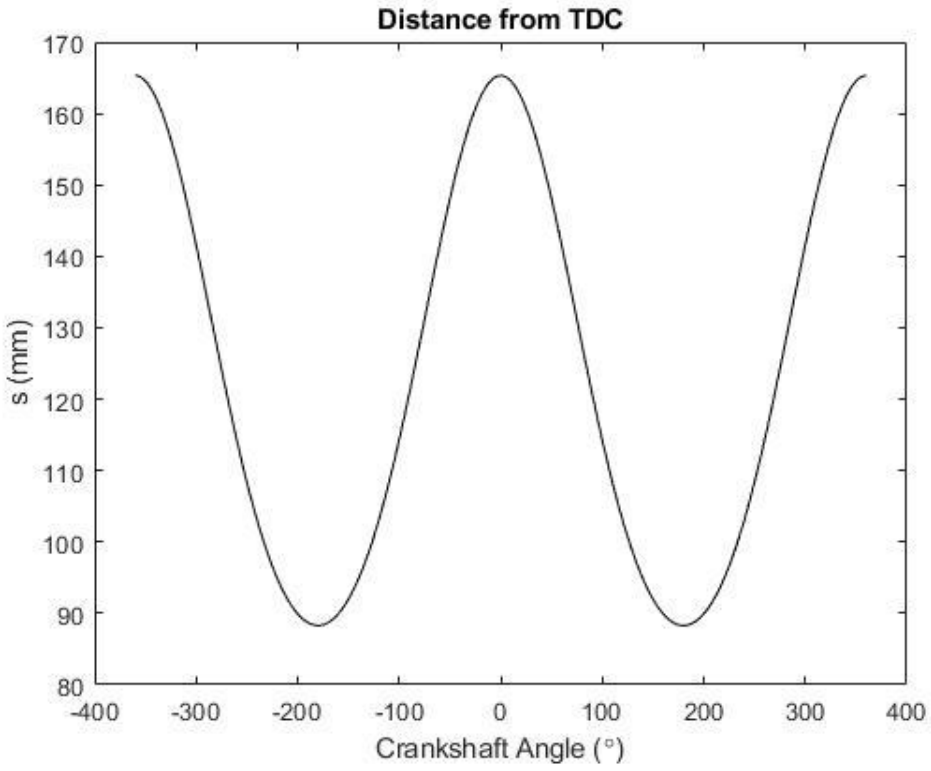

Figure 5.1: Distance of the top of the piston from TDC in fuction of the crankshaft angle.

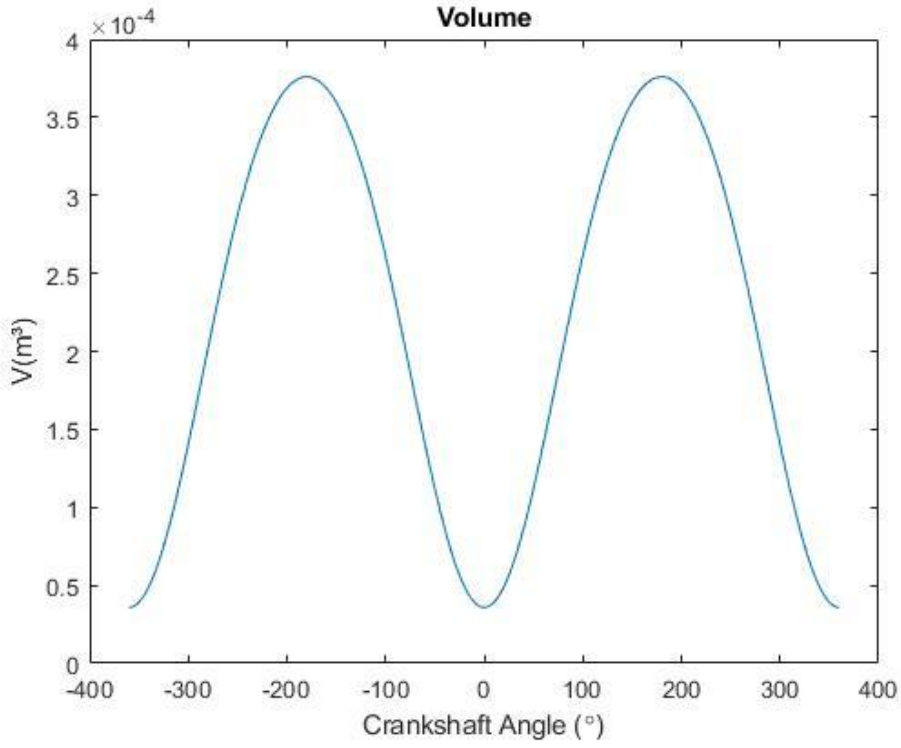

Figure 5.2: Volume inside the engine chamber in function of the crankshaft angle.

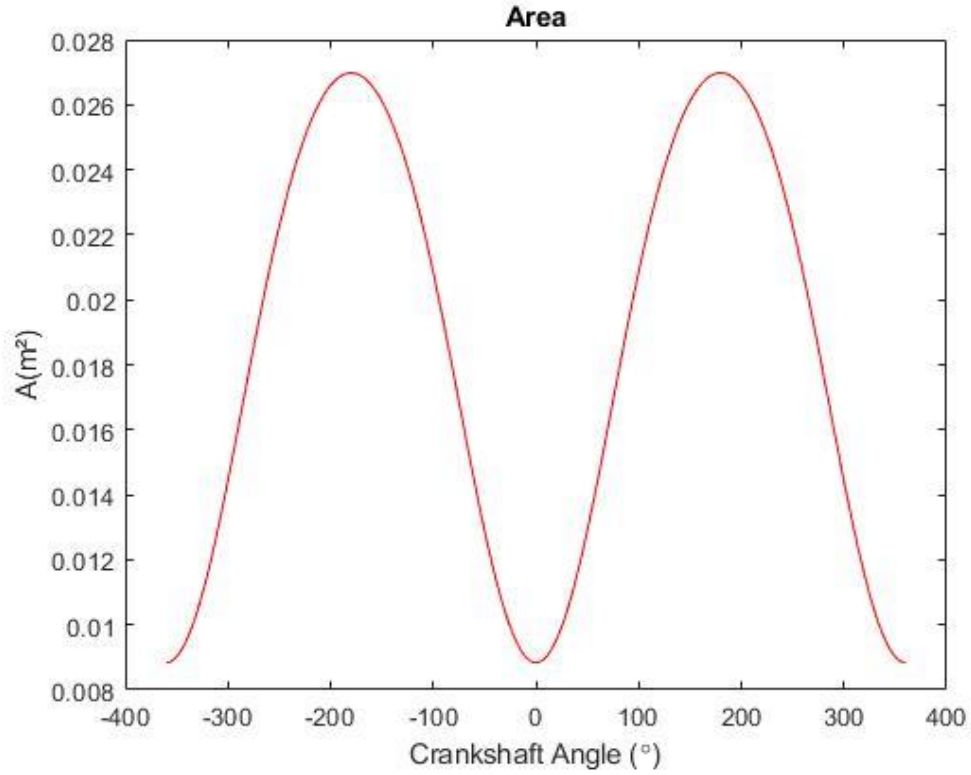

Figure 5.3: Engine chamber area in function of the crankshaft angle.

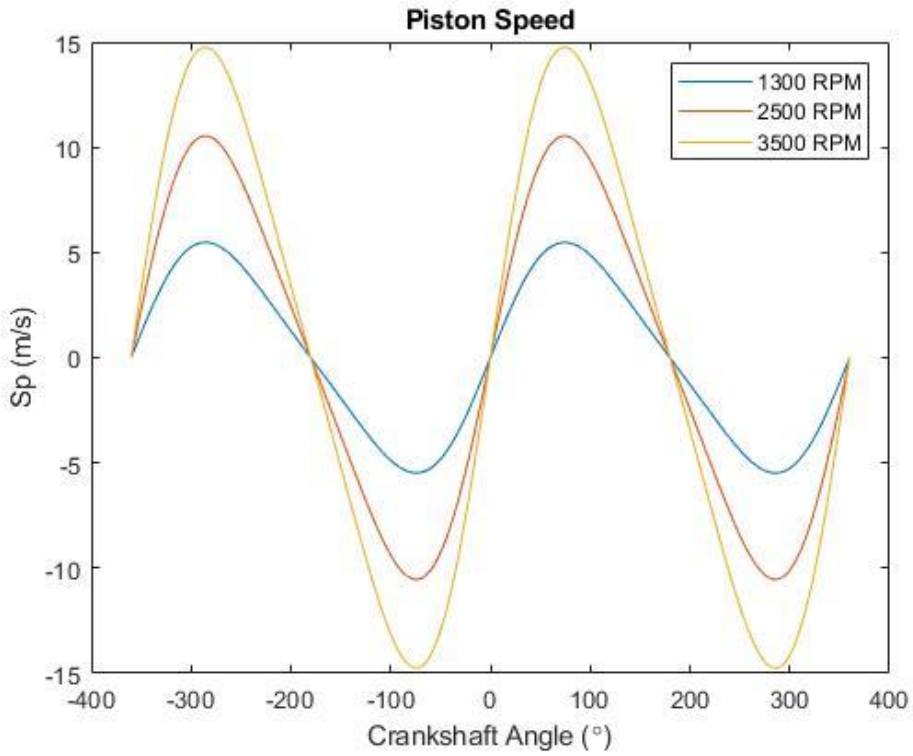

Figure 5.4: Piston speeds reached for the three rotationsas a function of the crankshaft angle

5.2 Pressure x Crankshaft Angle

Figures 5.5 to 5.7 show the pressure curves as a function of the crankshaft angle of all fuels plotted together for the same engine rotational speed. Table 5.1 and Figure 5.8 show the values of the maximum pressures of each test for the seven fuels. These were captured by the MATLAB *max* function. The first observation is that the E22 generates lower pressures than other fuels when tested at 1300 and 2500 RPM. Nevertheless, it will be shown in the following sections that this does not mean that the IMEP will be smaller than the rest of the fuels.

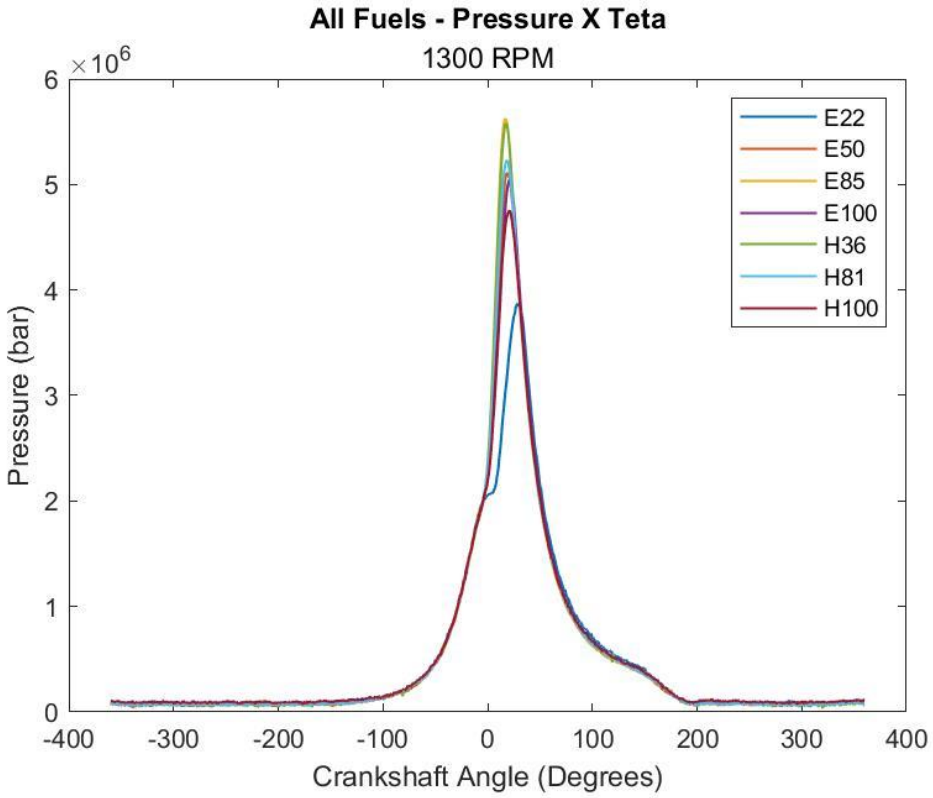

Figure 5.5: Fuels pressure curves at 1300 RPM.

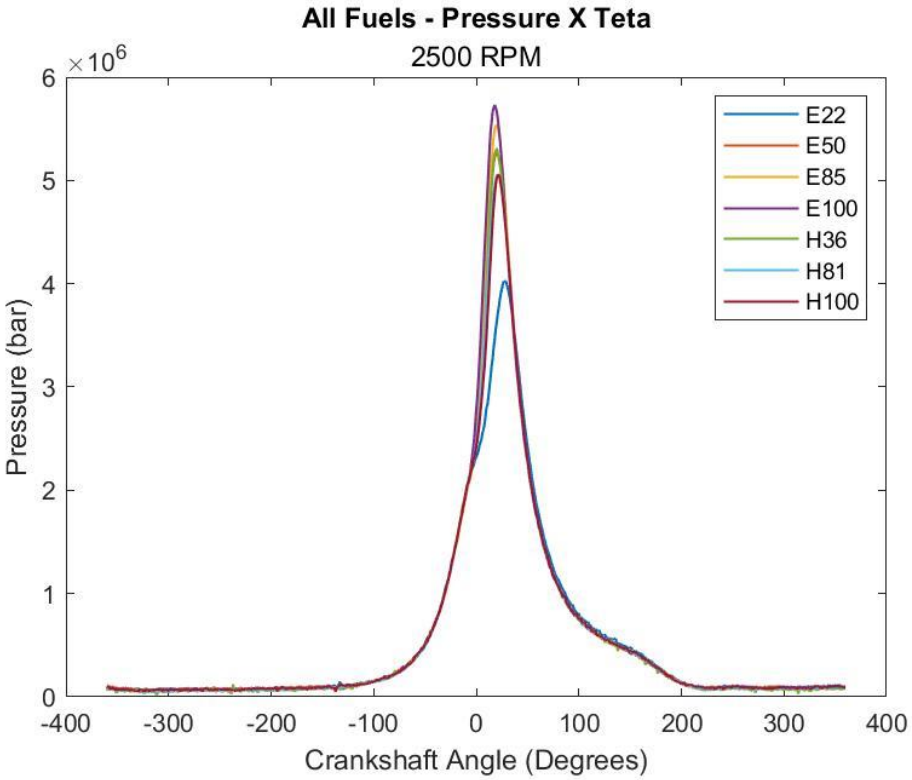

Figure 5.6: Fuels pressure curves at 2500 RPM

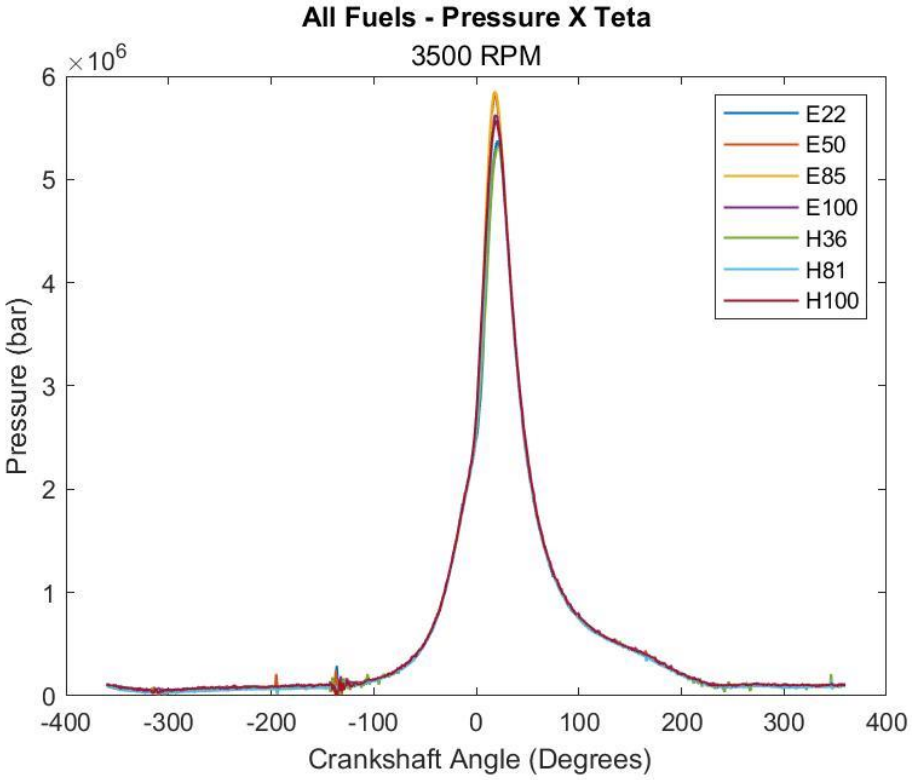

Figure 5.7: Fuels pressure curves at 3500 RPM.

Fuel	1300 RPM		2500 RPM		3500 RPM	
	Máx. Pressure (bar)	Crankshaft Angle (º)	Máx. Pressure (bar)	Crankshaft Angle (º)	Máx. Pressure (bar)	Crankshaft Angle (º)
E22	38,732	30	40,231	28	53,759	22
E50	51,143	20	52,579	20	58,158	19
E85	56,267	18	55,396	21	58,508	19
E100	50,511	22	57,317	19	56,209	19
H36	55,77	18	53,115	21	53,185	23
H81	52,297	19	50,581	22	55,545	20
H100	47,577	22	50,528	22	55,657	20

Table 5.1: Maximum pressures inside the combustion chamber for each tested fuel and engine speed.

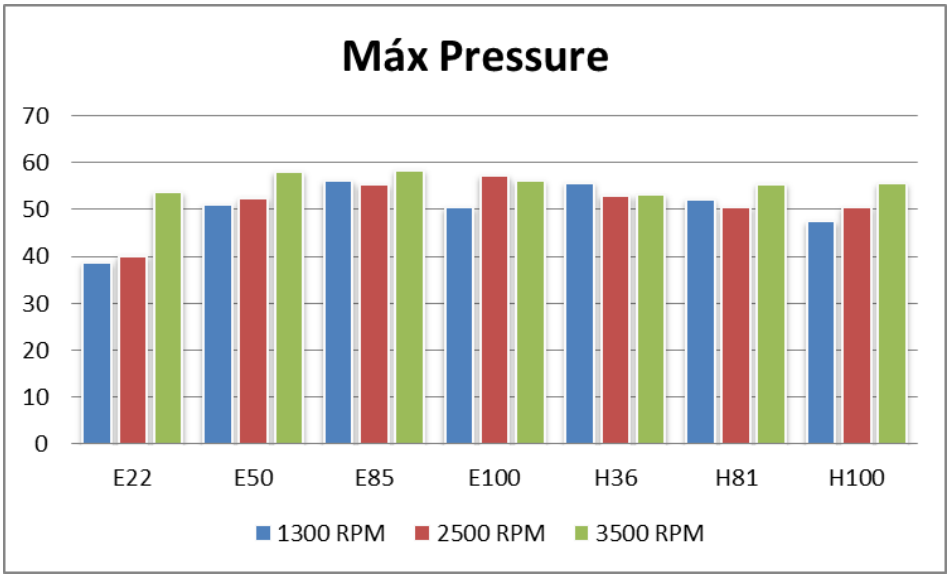

Figure 5.8: Maximum pressures during combustion.

5.3 Air-Fuel Ratio

Table 5.2 shows the values of lambda that was given by the ECU's. It is noticed that, in general, the values close to the stochiometric. However, some values provided showed a slightly rich mixture with $\lambda < 1$.

It is important to note that the E85 and E100 at 3500 RPM tests provided λ values lower than 0,9, characterizing an enriched mixture and this may affect the comparison of the results of the engine performance parameters in relation to other fuels.

The λ values for E85 and H81 gave different values for all tests. Therefore, it is expected that the combustion evaluation parameters are divergent, which will make it difficult to analyze the addition of water in the E85 mixture. Note that the tests with these two fuels had the same ECU, as H36 and E50 also used the

same. It can provide different values of lambda since the ECU is not optimized for each of these fuels.

It can be also noticed a strange behavior of the E85 blend because the mixture was rich in all engine speeds tested. This behavior is due to the ECU programming module witch was not optimized for some fuels giving the lambda values far from 1.0.

λ			
Fuel	**1300 RPM**	**2500 RPM**	**3500 RPM**
E22	1	0,97	0,92
E50	1,01	1,01	0,94
E85	0,91	0,92	0,85
E100	0,97	0,98	0,88
H36	1,01	1,01	0,94
H81	1	1	0,93
H100	1,01	0,99	0,93

Table 5.2: Values of lambda for all tested fuels and engine speeds.

5.4 Torque

In this work, engine brake torque was obtained in two ways: experimentally and numerically (from engine friction models and the experimental pressure curves). The data in this section are referred to the torque measured on the axis of the AVL dynamometer, while the error with the model is calculated in the section referring to the mechanical efficiency.

From the literature review, it is expected that the blends with more ethanol content presents higher torque values, once the velocity of the flame propagation is higher for the ethanol than gasoline. Also, higher water content is expected to reduce the torque values.

Some results presented in Figure 5.9 do not correspond to the expectated results. It can be observed from Figure 5.9 that the addition of water in the mixture caused an increase in the torque of H36 in relation to the E50. Also, E50 presented lower values of torque than E22. It can be noticed that the engine calibrations for each fuel are not optimized and it can be seen this in the results of lambda in Table 5.2.

Also analyzing table 5.9, it can be observed that for most fuels, the torque value increases from 1300 to 2500 RPM, but decreaces when turning to 3500 RPM. With these results, it was chosen to approach the results by a parabolic curve, according to equation 5.1. Coefficients A, B and C were obtained by linear

regression of the results in figure 5.9. So, in order to do it, the *polyfit* function of MATLAB was used.

$$T_{eng} = AN_{eng}^2 + BN_{eng} + C \tag{5.1}$$

The values contained in table 5.3 will be used in the subsequent results to calculate the speed recovery time of the Peugeot 207 SW.

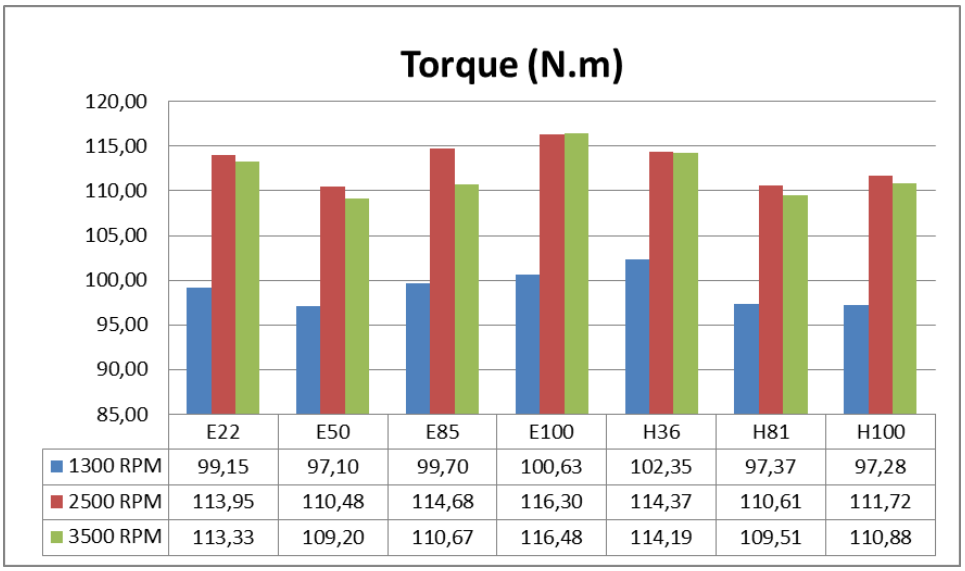

	E22	E50	E85	E100	H36	H81	H100
1300 RPM	99,15	97,10	99,70	100,63	102,35	97,37	97,28
2500 RPM	113,95	110,48	114,68	116,30	114,37	110,61	111,72
3500 RPM	113,33	109,20	110,67	116,48	114,19	109,51	110,88

Figure 5.9: Corrected Torque read by AVL dynamometer.

Fuel	Torque Coefficients		
	A (N.m/(RPM²)	B (N.m/RPM)	C (N.m)
E22	-5,90E-06	0,0347	63,946
E50	-5,65E-06	0,0326	64,245
E85	-7,49E-06	0,0409	59,130
E100	-5,85E-06	0,0353	64,618
H36	-4,63E-06	0,0276	74,288
H81	-5,52E-06	0,0320	65,095
H100	-5,85E-06	0,0343	62,628

Table 5.3: Coefficients of the experimental torque curves for each fuel.

5.5 Combustion Parameters

This item will show all engine combustion parameters obtained from processing the data set presented in section 5.1. The parameters are the temperature inside the chamber, the polytropic coefficient, the IMEP, fuel consumption and the injected, lost and released combustion heats, and the combustion, thermal and volumetric efficiencies of the engine.

5.5.1 Temperatures inside the Chamber

The temperatures inside the chamber were obtained using equation 4.32, (ideal gases law). The results of this parameter for each fuel at 1300, 2500 and 3500 RPM are shown in Figures 5.10, 5.11 and 5.12, respectively.

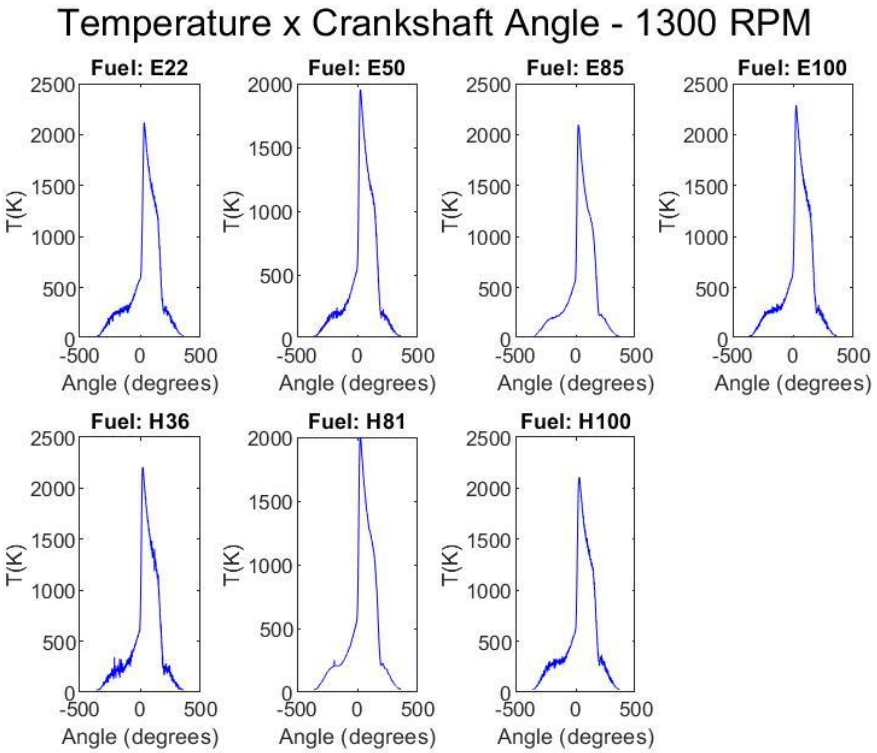

Figure 5.10: Temperature inside the combustion chamber at 1300 RPM for all tested fuels.

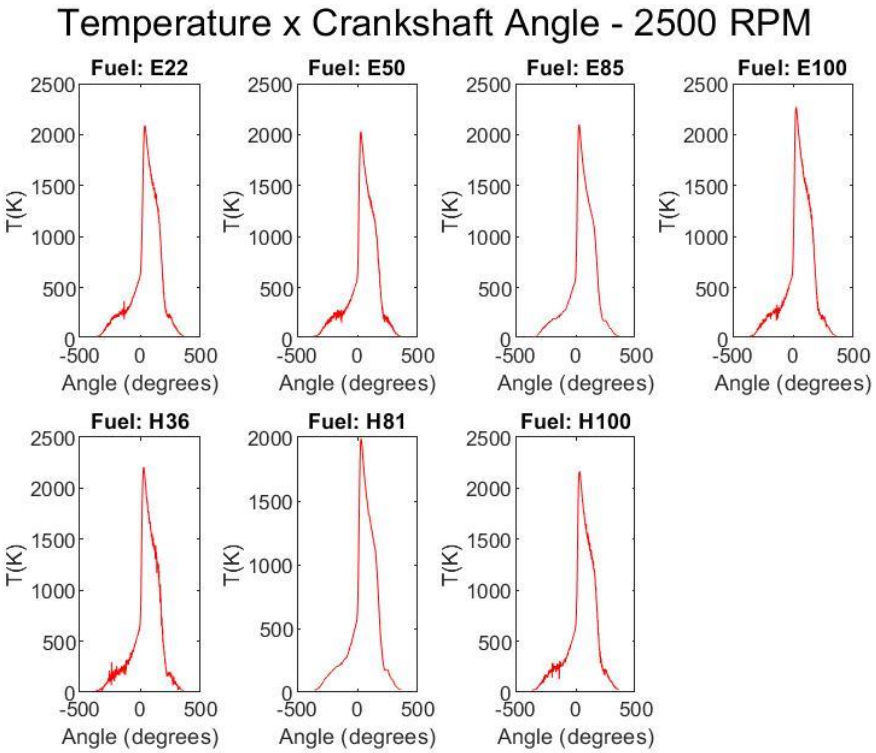

Figure 5.11: Temperature inside the combustion chamber at 2500 RPM for all tested fuels.

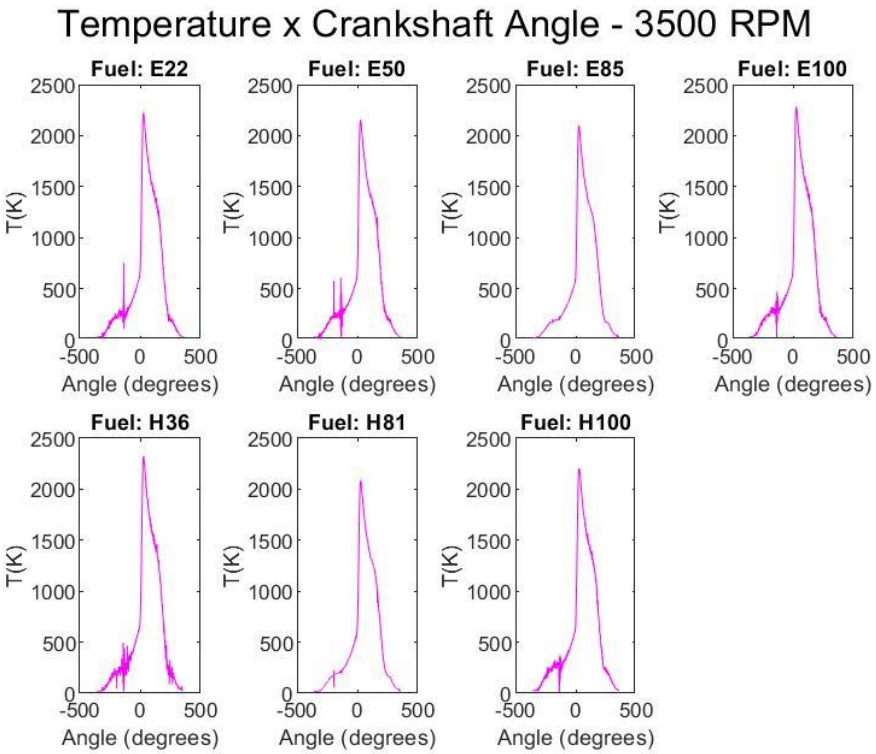

Figure 5.12: Temperature ofthe combustion chamber at 3500 RPM for all tested fuels.

5.5.2 Determination of the Polytropic Coefficient

As already mentioned, the polytropic coefficient was calculated as constant through the engine cycles, as indicated by Heywood (2018). It was created a function in MATLAB called *polytropic coeficient* function that searches for line values that best approximates the compression and expansion points. Table 5.4 represents these obtained values and an example for the mixture H81 at 2500 RPM can be seen in Figure 5.13.

It was observed a greater difficulty in obtaining accurately the points of the beginning of compression for lower engine speeds. Therefore, it became necessary to decrease the accuracy of the compression line to a coefficient of determination (R^2) of 0.9984, while the expansion coefficient remained 0.999.

It is noted that all the values of the polytropic coefficient are within the range mentioned by Heywood of 1,3 ± 0,05 with the exception of E85 and H81 that were slightly higher than expected (1,36). Nevertheless, the lines showed a good accuracy in relation to the experimental points by the value of the coefficient of determination (R^2).

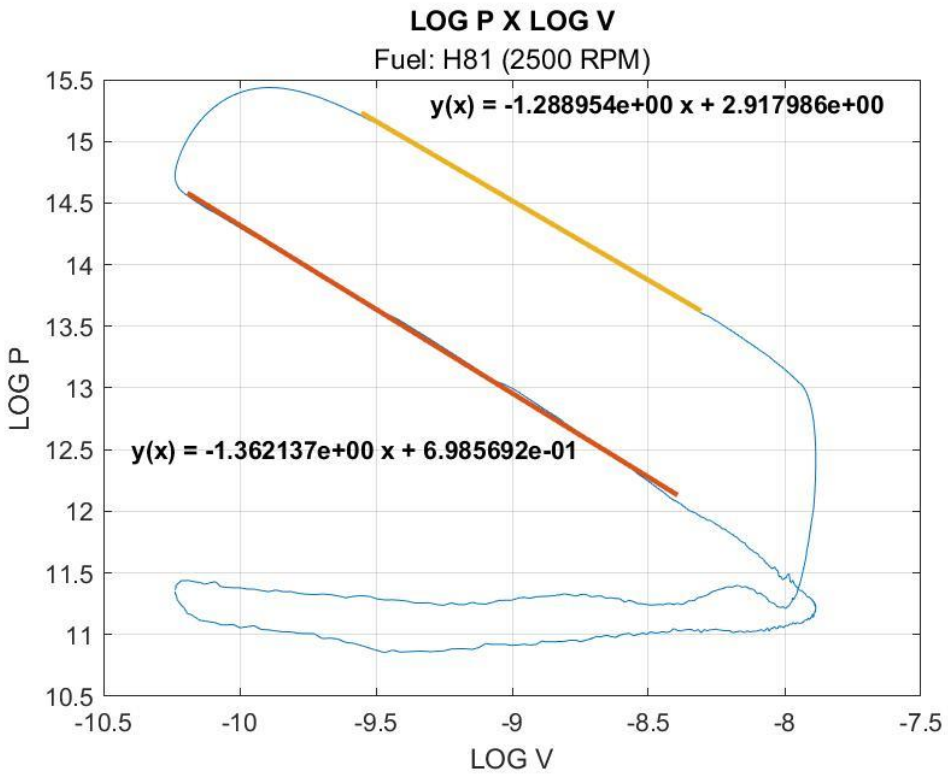

Figure 5.13: Log p X Log V diagram at 2500 RPM of the H81.

Fuel	1300 RPM				2500 RPM				3500 RPM			
	Υ_{comp}	R^2	Υ_{exp}	R^2	Υ_{comp}	R^2	Υ_{exp}	R^2	Υ_{comp}	R^2	Υ_{exp}	R^2
E22	1,3176	**0,9984**	1,3117	**0,9994**	1,3292	**0,9987**	1,2808	**0,9994**	1,3339	**0,9989**	1,2888	**0,9996**
E50	1,3443	**0,9989**	1,3153	**0,9997**	1,3149	**0,9990**	1,2822	**0,9997**	1,3049	**0,9994**	1,2795	**0,9998**
E85	1,3203	**0,9995**	1,3219	**0,9998**	1,3643	**0,9986**	1,3002	**0,9998**	1,3254	**0,9994**	1,2906	**0,9999**
E100	1,3227	**0,9986**	1,3128	**0,9995**	1,3257	**0,9985**	1,2768	**0,9996**	1,2949	**0,9990**	1,2777	**0,9997**
H36	1,2871	**0,9991**	1,3006	**0,9993**	1,3310	**0,9984**	1,2816	**0,9995**	1,3160	**0,9990**	1,2908	**0,9995**
H81	1,3210	**0,9996**	1,3090	**0,9998**	1,3621	**0,9989**	1,2890	**0,9996**	1,3424	**0,9995**	1,2916	**0,9999**
H100	1,2989	**0,9987**	1,2902	**0,9995**	1,3357	**0,9987**	1,2850	**0,9996**	1,3047	**0,9987**	1,2831	**0,9997**

Table 5.4: Polytropic coefficients and the respective R^2 of all tested fuels.

5.5.3 Convective Heat Transfer Coefficient Simulation

The convective heat transfer coefficient was calculated according to the model proposed by Hohenberg (1979) and the results for 1300, 2500 and 3500 rpm are shown in Figures 5.14, 5.15 and 5.16. The results shown were used to quantify the heat loss by the walls, which are demonstrated in Appendix IV.

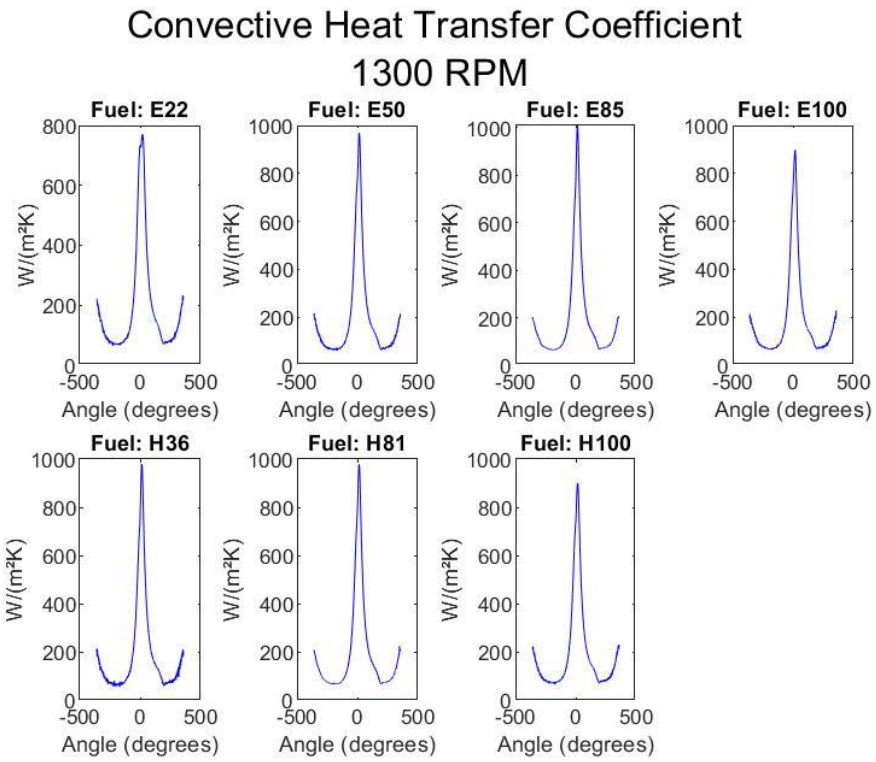

Figure 5.14: Convective heat transfer coefficient calculated by Hohenberg (1979) for 1300 RPM.

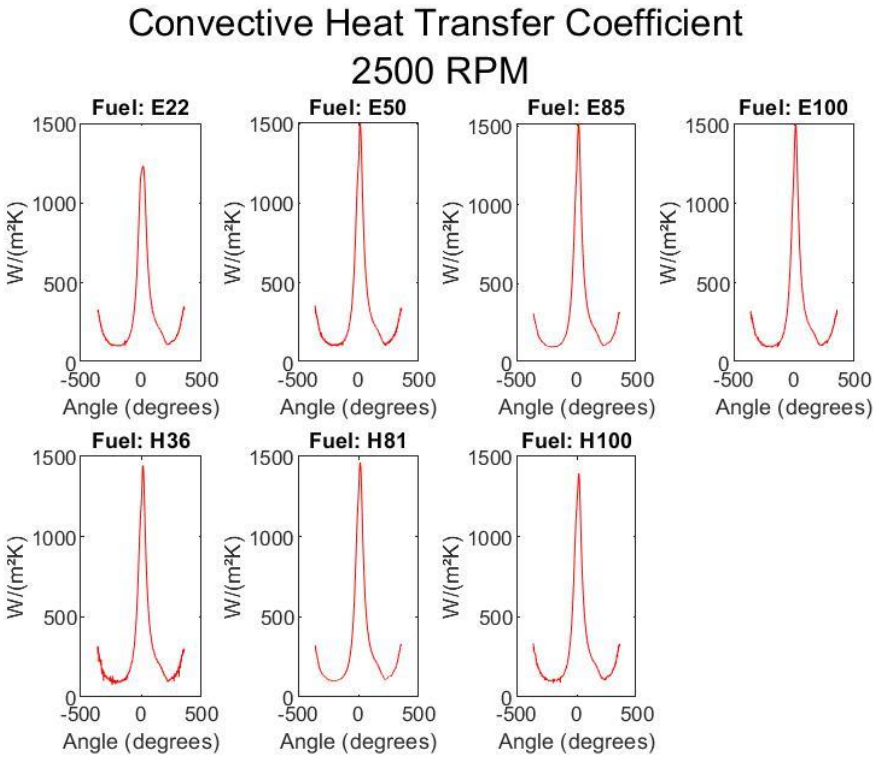

Figure 5.15: Convective heat transfer coefficient calculated by Hohenberg (1979) for 2500 RPM.

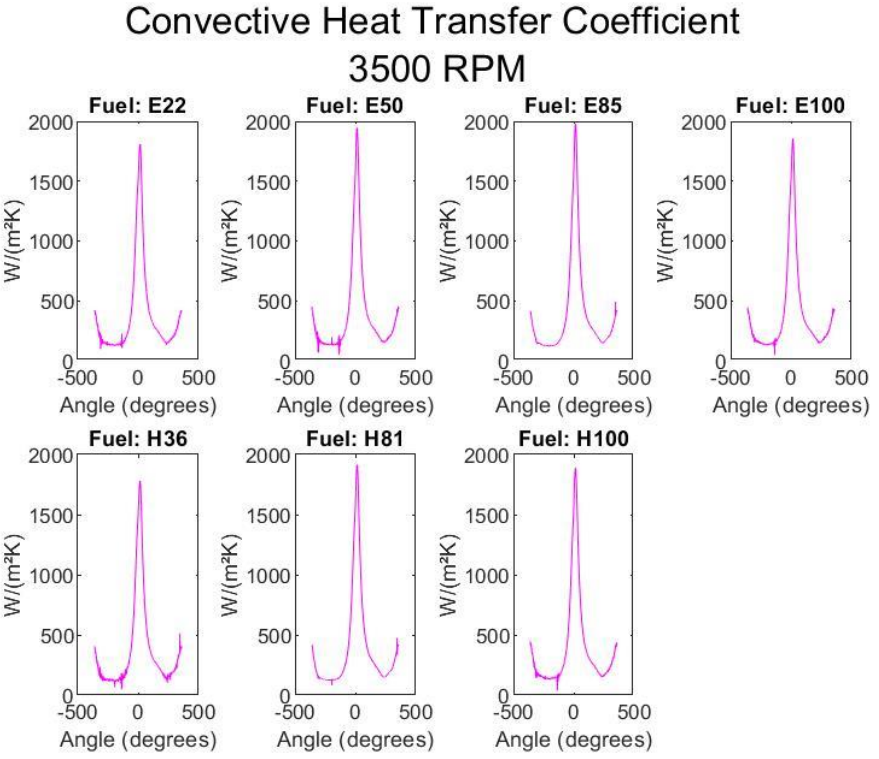

Figure 5.16: Convective heat transfer coefficient calculated by Hohenberg (1979) for 3500 RPM.

5.5.4 Combustion Efficiency

Figures 5.17, 5.18 and 5.19 represent the experimental graphs for all fuels in all engine speeds, which match the first law of thermodynamics for the combustion period. The injected heat was calculated by the mass flow rate of the fuel, which was supplied by the gravimetric scale, multiplied by LHV of each fuel. The heat lost by the walls was calculated by Hohenberg (1979). Looking at the figures, it can be seen which fuels have good combustion efficiency. The closer the heat released is to the injected, it means that there is more fuel being burned.

In this work, combustion efficiency was calculated according to chapter 9 of Heywood (2018) and the results are shown in Figure 5.20. According to the author, this parameter is calculated by the ratio between the heat released and heat injected. Another alternative to find this parameter is through the correlation proposed by Melo et al. (2007), however, it considers the same model for all mixtures and the author used only H100 and E22.

Table 5.5 shows the results of combustion efficiency using these two models, while Figure 5.21 graphically shows the difference between both for all speeds. The model found in Melo et al. (2007) proposes that the maximum combustion efficiency for gasoline-powered engines is 90%. It is observed that when calculating this parameter according to Heywood (2018) this condition is met.

Increasing the ethanol content in the mixtures in most of the cases the combustion efficiency decreased. However, when testing the H100 and E100, which do not have standard gasoline in its composition, a high performance is noted for all speeds.

For 2500 and 3500 RPM, a low combustion efficiency of the E85 is noted, since the injected heat is far from that released in combustion, indicating that there is a lot of energy lost by incomplete fuel burning. On the other hand, mixtures without the presence of gasoline in their composition have higher combustion efficiency.

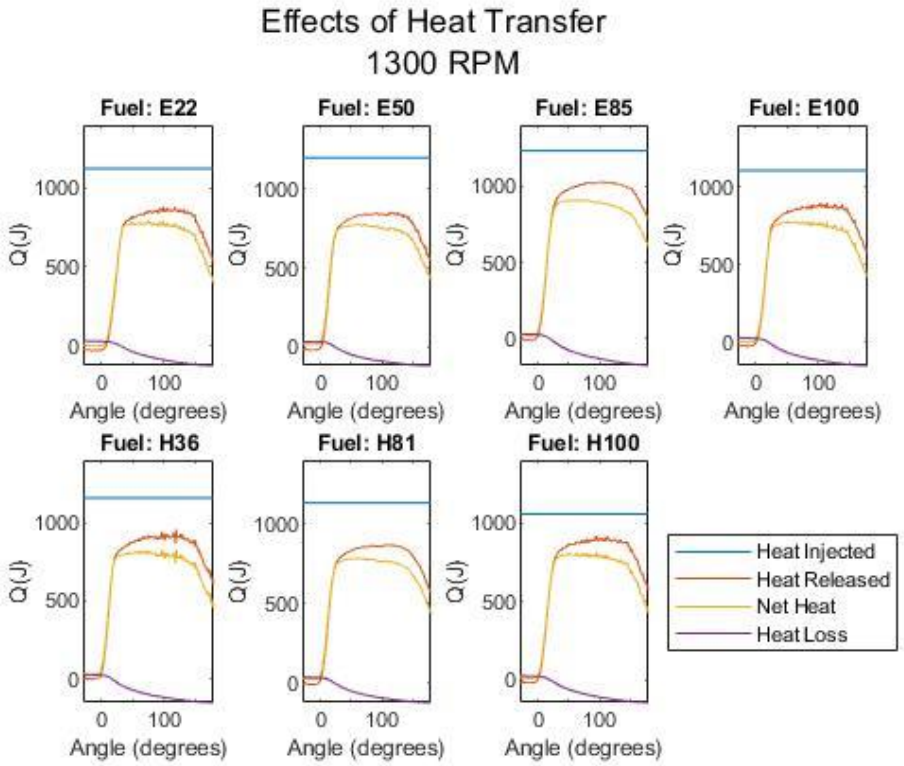

Figure 5.17: Heat released, net heat and heat lost by the walls at 1300 RPM

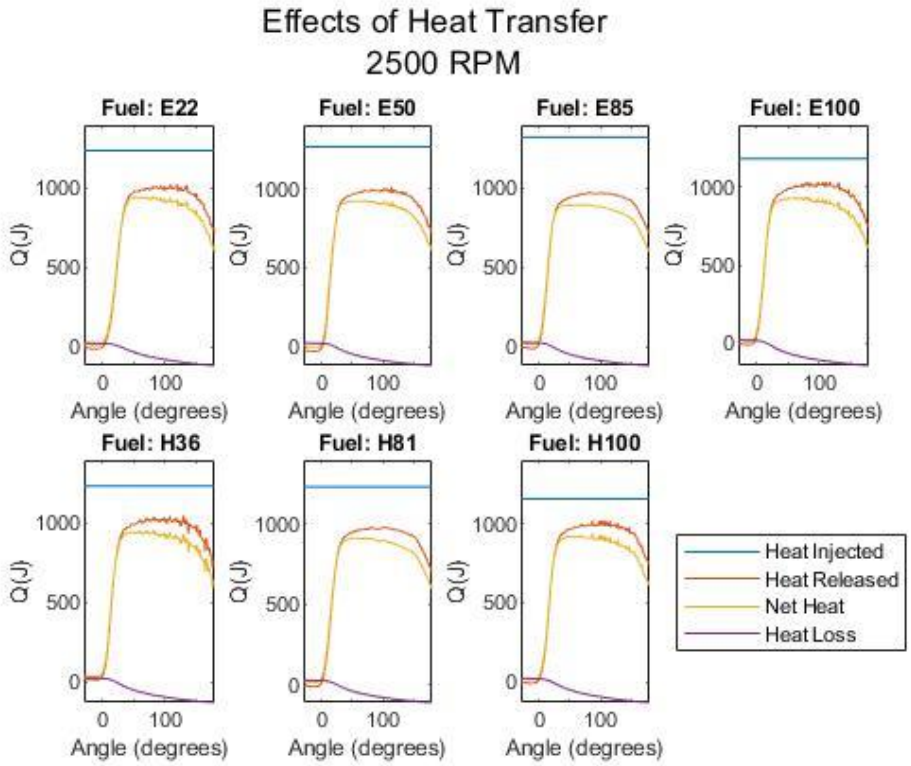

Figure 5.18: Heat released, net heat and heat lost by the walls at 2500 RPM

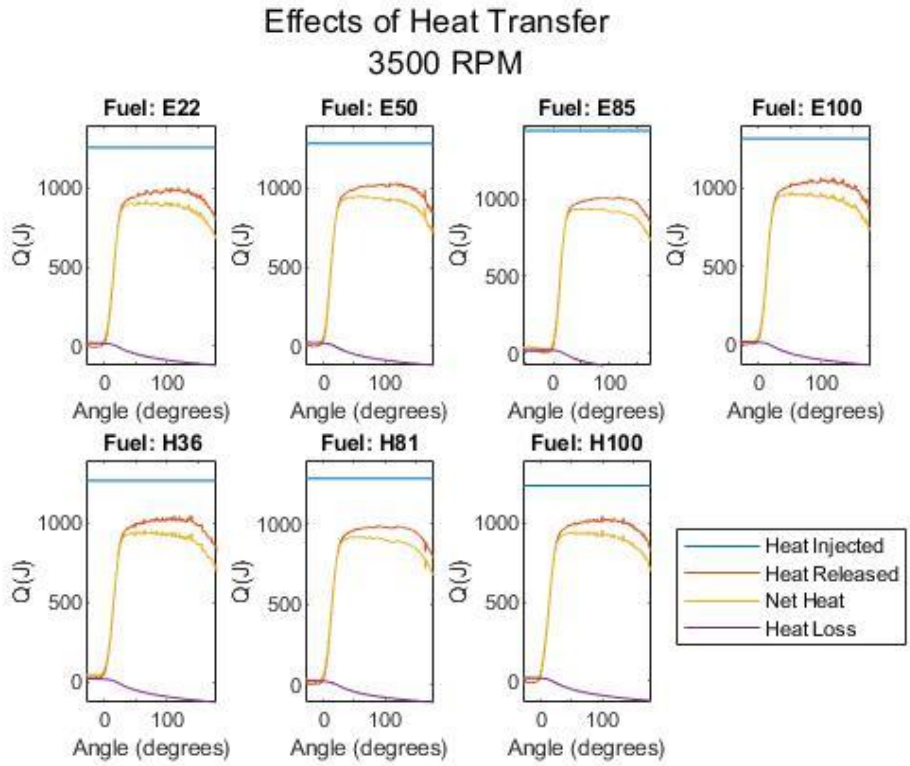

Figure 5.19: Heat released, net heat and heat lost by the walls at 3500 RPM

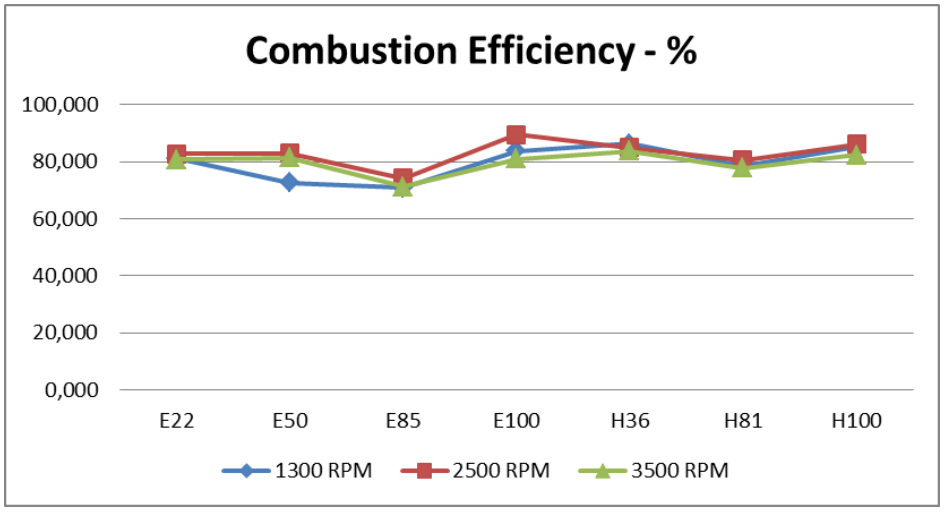

Figure 5.20: Efficiency of combustion of bench tests, according to Heywood (2018).

Combustion Efficiency (%)						
Fuels	Heywood (2018)			Melo et. al (2007)		
	1300 RPM	2500 RPM	3500 RPM	1300 RPM	2500 RPM	3500 RPM
E22	81,040	82,728	80,812	86,967	85,454	82,185
E50	72,600	82,840	81,383	87,397	87,397	83,605
E85	70,740	74,285	71,148	81,419	82,185	76,038
E100	83,690	89,370	80,861	85,454	85,996	78,897
H36	86,240	84,897	83,634	87,397	87,397	83,605
H81	78,646	80,443	77,703	86,967	86,967	82,913
H100	85,055	85,991	82,340	87,397	86,500	82,913

Table 5.5: Comparison between the models to obtain combustion efficiency.

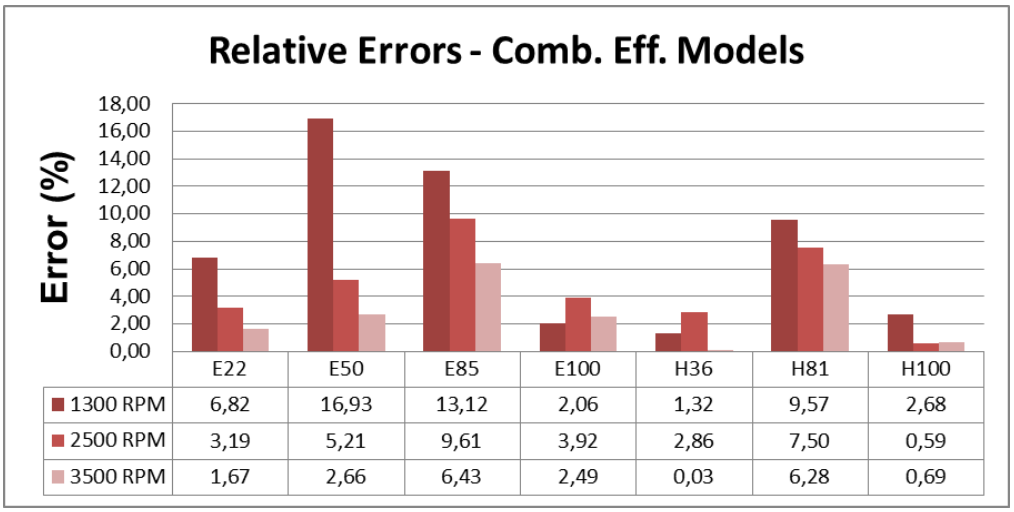

Figure 5.21: Relative error of the model of obtaining the combustion efficiency proposed by Heywood (2018) in relation to the correlation found in Melo et al. (2007)

5.5.5 Volumetric Efficiency

From figure 5.22 it can be noted that all fuels have an increase in volumetric efficiency of 1300 to 2500 RPM. When the speed is increased to 3500 RPM, there is a decrease of this parameter (with the exception of the H100 and E100, which are mixtures without the presence of standard gasoline A). This is related to intake air dynamics and time available to fill the engine cylinders.

An increase in the volumetric efficiency of the H100 compared to the E100, as well as the H81 to E85, confirming one of the conclusions of Villela & Machado (2012) in which the addition of water to the mixture increases the value of this parameter. However, this does not occur between compounds E50 and H36 and this can be explained due to the pressure, humidity and temperature conditions of the test room (see these values in Appendix IV). The E50 test presented a higher density of the engine intake air in relation to all fuels.

The decrease in volumetric efficiency of ethanol when compared to E22 is in accordance with the results of Candido (2016). The author explains that this fact occurs as a result of higher mass fuel consumption when using ethanol. Therefore, the air parcial pressure inside the cylinders is lower, causing a density decrease and, consequently, the volumetric efficiency is reduced.

However, the increase in ethanol content in some cases showed an improvement in volumetric efficiency. An example of this is the H81 that presented this parameter higher than H36 at all engine speeds. In addition, the E85 had also larger volumetric efficiency than the E50 at 2500 RPM.

According to the results shown in Appendix IV, although the E50 has a higher amount of dry air mass within the cylinders at 2500 RPM, the ambient air density of the E85 test is relatively lower than that of the E50 (approximately 1,11 and 1,16 kg/m³). Because of this, the volumetric efficiency of the E85 is higher in this speed.

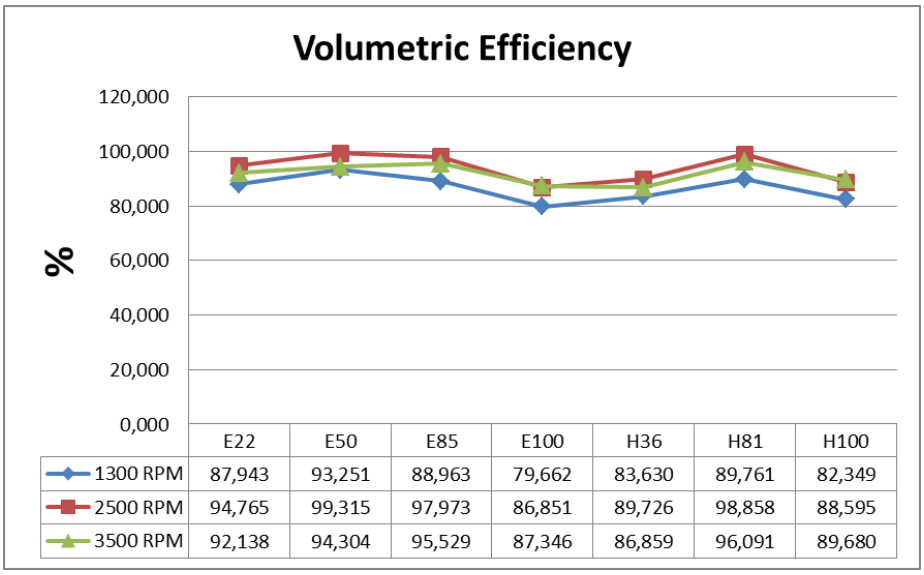

	E22	E50	E85	E100	H36	H81	H100
1300 RPM	87,943	93,251	88,963	79,662	83,630	89,761	82,349
2500 RPM	94,765	99,315	97,973	86,851	89,726	98,858	88,595
3500 RPM	92,138	94,304	95,529	87,346	86,859	96,091	89,680

Figure 5.22: Volumetric efficiency of the tested fuels.

Fuels	% Volumetric Efficiency		
	1300 RPM	2500 RPM	3500 RPM
E50/H36	11,504	10,687	8,572
E85/H81	0,889	0,895	0,585
E100/H100	3,263	1,969	2,602

Table 5.6: Percentual difference in volumetric efficiency due to the addition of water in the mixtures of ethanol and standard gasoline.

5.5.6 Duration of Combustion

The definition for the combustion duration can be found in section 4.4.5.2. First, it becomes necessary to obtain the ignition advance value for each fuel. This parameter was obtained by the ECU interface.

It was define as CA the crankshaft angle of the engine reffered to the percentage of mass burn. Table 5.7 shows the ignition timing advance given by the ECU in ETAS program, Table 5.8 shows the CA10, CA50 and CA90 reffered as the percentage of 10%, 50% and 90% of mass burn for each fuel and Table 5.9 shows the duration of combustion.

At low speeds the ignition advance of the H100, E100 and E22 are lower than other fuels. As engine speed increase, ignition timing is advanced. This is necessary because there is less time available for the combustion process.

Fuel	Ignition Timing Advance (°BTDC)		
	1300 RPM	2500 RPM	3500 RPM
E22	5	13	16
E50	12	16	17
E85	13	16	16
E100	8	17	16
H36	12	16	17
H81	13	16	17
H100	9	17	16

Table 5.7: Ignition advance of the tests for all the fuels.

Fuel	CA10			CA50			CA90		
	1300 RPM	2500 RPM	3500 RPM	1300 RPM	2500 RPM	3500 RPM	1300 RPM	2500 RPM	3500 RPM
E22	12	7	5	24	18	16	43	34	32
E50	6	6	3	15	16	13	33	32	28
E85	3	5	2	12	15	13	31	29	27
E100	6	2	4	16	13	15	39	30	31
H36	2	5	3	12	16	16	41	33	34
H81	4	5	3	14	17	14	31	32	28
H100	5	6	3	16	17	14	37	35	33

Table 5.8: Crankangles corresponding to 10, 50 and 90% of mass fraction burned.

Fuel	ΔΘd Flame Development Angle (°)			ΔΘr Rapid Burning Angle (°)			ΔΘo Overal Burning Angle (°)		
	1300 RPM	2500 RPM	3500 RPM	1300 RPM	2500 RPM	3500 RPM	1300 RPM	2500 RPM	3500 RPM
E22	17,25	19,55	21,19	31,00	27,00	27,00	48,25	46,55	48,19
E50	18,00	21,75	19,94	27,00	26,00	25,00	45,00	47,75	44,94
E85	15,76	20,76	18,10	28,00	24,00	25,00	43,76	44,76	43,10
E100	14,05	18,50	20,10	33,00	28,00	27,00	47,05	46,50	47,10
H36	13,97	20,75	20,02	39,00	28,00	31,00	52,97	48,75	51,02
H81	16,75	20,75	19,50	27,00	27,00	25,00	43,75	47,75	44,50
H100	14,36	22,50	19,19	32,00	29,00	30,00	46,36	51,50	49,19

Table 5.9: Flame development, rapid burning and overall burning angle of the fuels.

5.5.7 Mass of Fuel Burned and Unburned

The results found here represent the amounts of fuels that are burned and not burned after the combustion process. It was calculated as the injected mass of fuel inside the cylinder multiplied by the combustion efficiency, as equation 5.1:

$$m_{burned} = \eta_c m_{fuel} \tag{5.1}$$

Analyzing the results (Figures 5.23, 5.24 and 5.25), it can be noticed that by increasing the ethanol content in the mixtures the fuel consumption per cycle increases. In such cases, there are also larger quantities of fuel mass that are not burned, except in cases where ethanol is without the presence of gasoline (E100 and H100).

Higher volumes of gasoline in the mixtures results in better energy efficiency. In Figures 5.23, 5.24 and 5.25 it can be noted lower mass values of unburned fuels when the ethanol fraction is reduced.

The increase in ethanol content in the mixtures promotes an increase in the burned and unburned masses after the combustion process while the pressures inside the chamber also increases. This means that fuel mass consumption increases, while the power developed by the engine is also higher as will be seen in the following sections.

However, when using mixtures that do not have standard gasoline in its composition (E100 and H100), there is an improvement in combustion efficiency. Although these follow the same pattern of increased mass consumption when raising the ethanol content in the mixture, it is noted that there are smaller amounts of unburned fuel at the end of the combustion process.

According to Brunetti (2018), when engine is operating with a optimized calibrated ECU, the hydrated mixtures allows for greater mass of burned fuel, because the intake air is cooled by water and, consequently, becomes denser. As a result, the ECU introduces larger amounts of fuel into the cylinders. The addition of water also decreases the fuel mass consumption, except in the particular case between the H100 and the E100. However, despite this increase, the H100 still burns larger amounts of its mixture in the combustion process when compared to the E100.

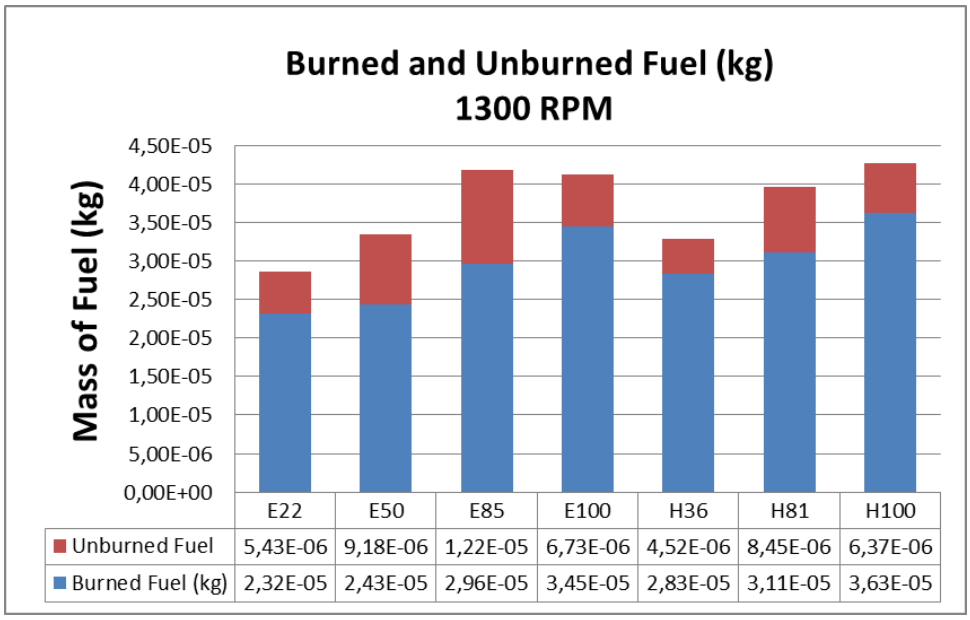

Figure 5.23: Burned and unburned fuel mass for testing at 1300 RPM.

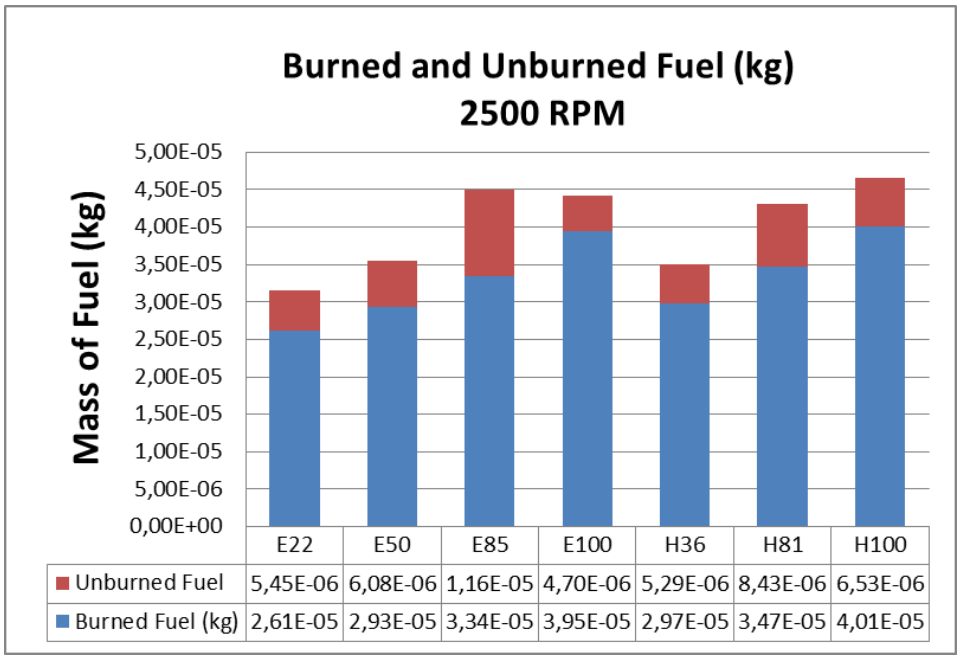

Figure 5.24: Burned and unburned fuel mass for testing at 2500 RPM.

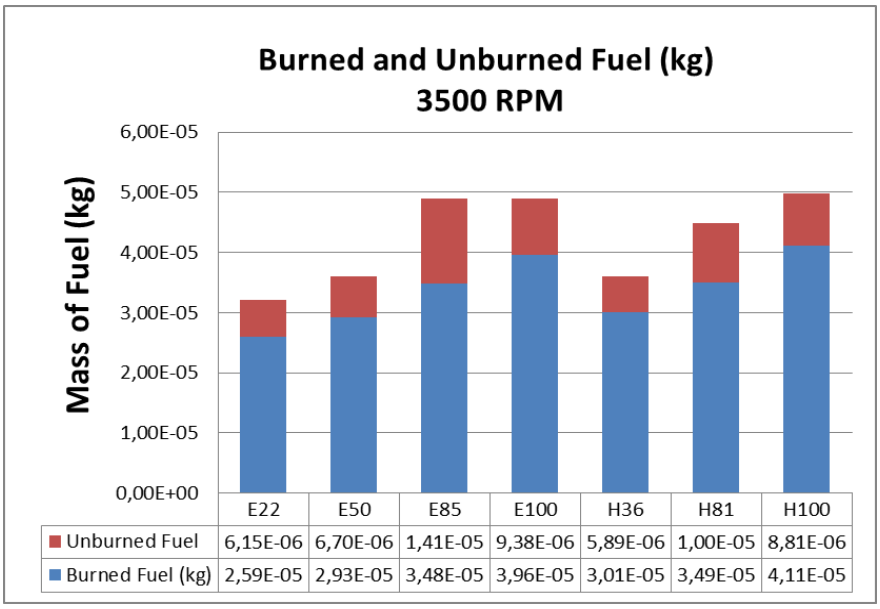

Figure 5.25: Burned and unburned fuel mass for testing at 3500 RPM

5.5.8 Specific Fuel Consumption

Figure 5.26 shows the specific fuel consumption values for each test. For non-hydrated mixtures, there is an increase in specific fuel consumption for higher levels of anhydrous ethanol in the mixture, with the exception of E100 in which this parameter showed a fall in relation to E85, but with very close values. Hydrated compounds behaved similarly, but H100 had a significant increase in relation to H81.

It is noted that the addition of water in the mixtures reduced the specific fuel consumption, with the exception of the H100 which was increased in relation to the E100.

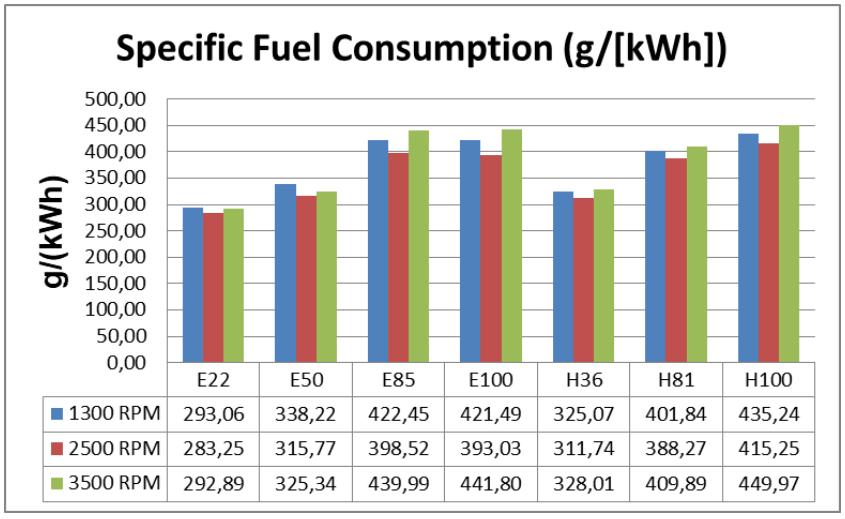

Figure 5.26: Specific fuel consumption of the fuels tested in each engine speed.

5.5.9 Indicated Mean Effective Pressure (IMEP)

Figure 5.27 shows the IMEP values for all tests. The increase in IMEP is notorious when engine speed is higher. The difference is less significant between 2500 and 3500 RPM, indicating that when passing through the maximum torque speed, the power rises when the engine speed gets higher.

In most cases, the addition of water promotes a reduction of IMEP with the exception of H36 and E50 at 1300 RPM, in which the hydrated compound has the highest IMEP. This occurs because there are higher pressures within the chamber, resulting in higher indicated work values.

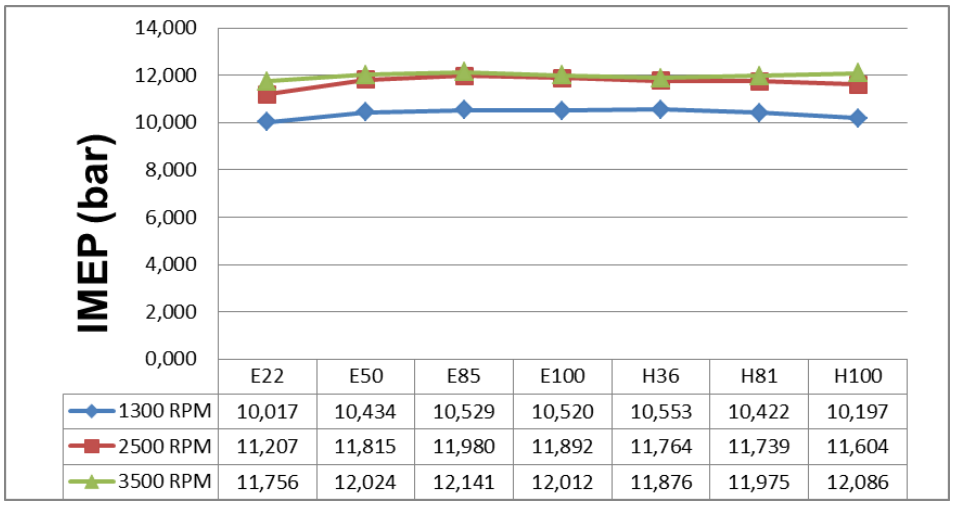

	E22	E50	E85	E100	H36	H81	H100
1300 RPM	10,017	10,434	10,529	10,520	10,553	10,422	10,197
2500 RPM	11,207	11,815	11,980	11,892	11,764	11,739	11,604
3500 RPM	11,756	12,024	12,141	12,012	11,876	11,975	12,086

Figure 5.27: IMEP of the tested fuels in each engine speed.

5.5.10 Thermal Efficiency

The thermal efficiency values can be seen in Figure 5.28. This parameter determines the how much power is generated inside the combustion chamber due to the amount of energy that is supplied by fuel injection. The thermal yield is mainly dependent on the pressures generated inside the chamber and the fuel burned mass fraction.

By increasing engine speed up to 2500 RPM, a small increase in thermal efficiency for all fuels is achieved. However, at 3500 RPM this parameter was reduced due to the higher λ values of the mixtures that are richer than at the smaller engine speeds. As a result, there is a greater amount of unburned fuel as a percentage in the engine residual gases, which reduces the combustion and thermal efficiency, also.

It is noted that hydrated ethanol (H100) has higher thermal efficiency than E22 gasoline in all rotations. Thus, it can be affirmed that the results found in this study for this parameter are similar to those obtained by Candido (2016).

Nevertheless, it can be seen that the increase in ethanol content by volume in the compounds decreases the thermal efficiency with the exception of mixtures E100 and H100, which has its value increased in relation to E85 and H81, respectively. Similar to combustion efficiency, the thermal efficiency rises when the compounds are without the presence of standard gasoline (anhydrous or hydrated ethanol). It is also possible that by adding water to the mixtures there is an increase compared to pure compounds (H36 better than E50 and H81 better than E85), due to higher pressures inside the chamber during combustion.

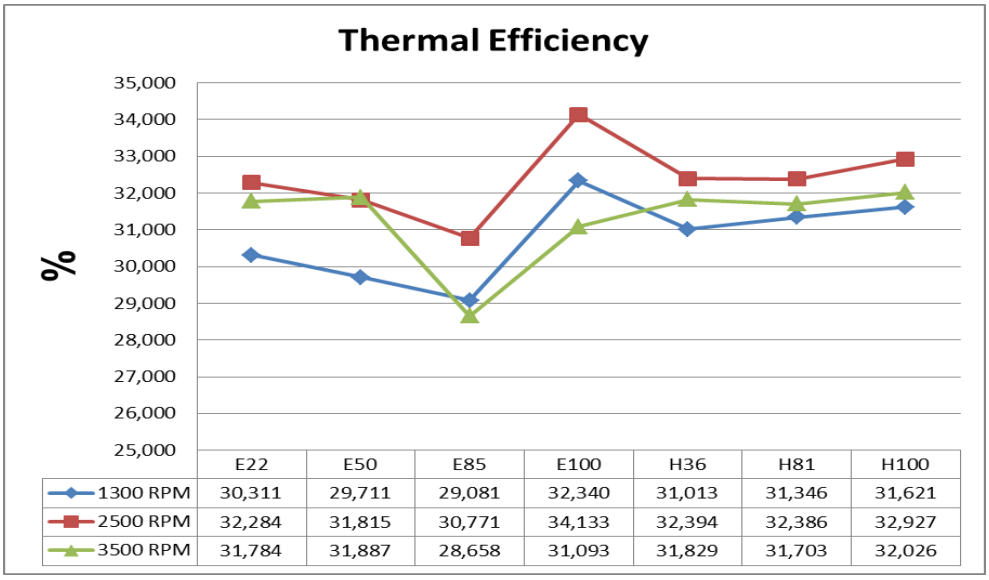

	E22	E50	E85	E100	H36	H81	H100
1300 RPM	30,311	29,711	29,081	32,340	31,013	31,346	31,621
2500 RPM	32,284	31,815	30,771	34,133	32,394	32,386	32,927
3500 RPM	31,784	31,887	28,658	31,093	31,829	31,703	32,026

Figure 5.28: Thermal efficiency of the fuels in all engine speed tested.

5.6 Frictional Losses in the Engine

Once the indicated power is generated, part is lost by pumping the gases, auxiliary accessories and by the friction between the internal parts of the engine. In this section the real friction of the engine was obtained for each test with the aid of torque measured in dynamometer. Another form was through a correlation proposed by Sandoval (2003) and another from Heywood (1988) for friction pressure losses in spark ignition engines.

The Correlation of Sandoval (2003) predicts frictional pressure losses due to its geometric parameters and the average piston speed. This model can be used to evaluate friction losses in each engine component separately, as well as losses from the drive of accessories and pumping losses. Heywood (1988)

predicts total engine friction for motored testing conditions, whose operating conditions are close to real.

5.6.1 Experimental TFMEP

With the aid of a dynamometer it was possible to obtain torque on the shaft. Thus, equations 4.25 and 4.26 were used to obtain the brake mean effective pressure (BMEP). Thus, it is possible to calculate the pressure lost by friction (TFMEP) by decreasing the IMEP of BMEP, as demonstrated in section 4.4.11.

Once with the TFMEP values for the three test rotational speeds, a linear regression was made with the aid of the *polyfit function* of MATLAB, in order to find the second order polynomial that best approximates its values (Heywood, 2018):

$$\mathrm{TFMEP} = \mathrm{C_2 N_{eng}^2} + \mathrm{C_1 N_{eng}} + \mathrm{C_0} \tag{5.2}$$

The results of the coefficients for each fuel are shown in Table 5.10 and the TFMEP values calculated from the experiment can be seen in Appendix IV.

Fuel	TFMEP Coefficients		
	C2 (kPa/(RPM²))	C1 (kPa/RPM)	C0 (kPa)
E22	-1,07762E-05	0,082460749	26,1639427
E50	9,06216E-06	-0,018699293	153,8441271
E85	6,62346E-06	-0,008893029	155,5877477
E100	9,77486E-06	-0,032824447	189,7130229
H36	9,31099E-06	-0,020667856	150,3140654
H81	1,01316E-05	-0,024212869	163,5044624
H100	2,30173E-05	-0,077901304	193,5983268

Table 5.10: Coefficients of frictional pressure loss curves in the engine.

5.6.2 TFMEP Simulation

In this section, the pressure loss by engine friction curves will be simulated by Heywood (1988) and Sandoval (2003) and compared with the torque curves obtained experimentally by the dynamometer. The objective of this simulation is to be able to obtain these losses without the need of an engine dynamometer to measure the torque on the shaft.

The correlation proposed by Heywood (1988) is simpler, whereas it is function only of engine rotation. The model proposed by Sandoval (2003) is more

sophisticated and dependent on many specific geometric parameters such as bearing geometry, number of bearings, camshaft shape and valves. In contrast, this is able to provide how each component contributes separately to engine friction. In the following section these values are presented for TU3 engine.

5.6.2.1 TFMEP simulation as a function of Engine Speed

The correlation proposed by Heywood (1988) considers that friction is the same for all fuels, since it is a function only of engine rotational speed. The results of the $TFMEP_{SIM}$ curves and the errors related to the calculated from Equation 5.2 are shown in Figures 5.29 and 5.33.

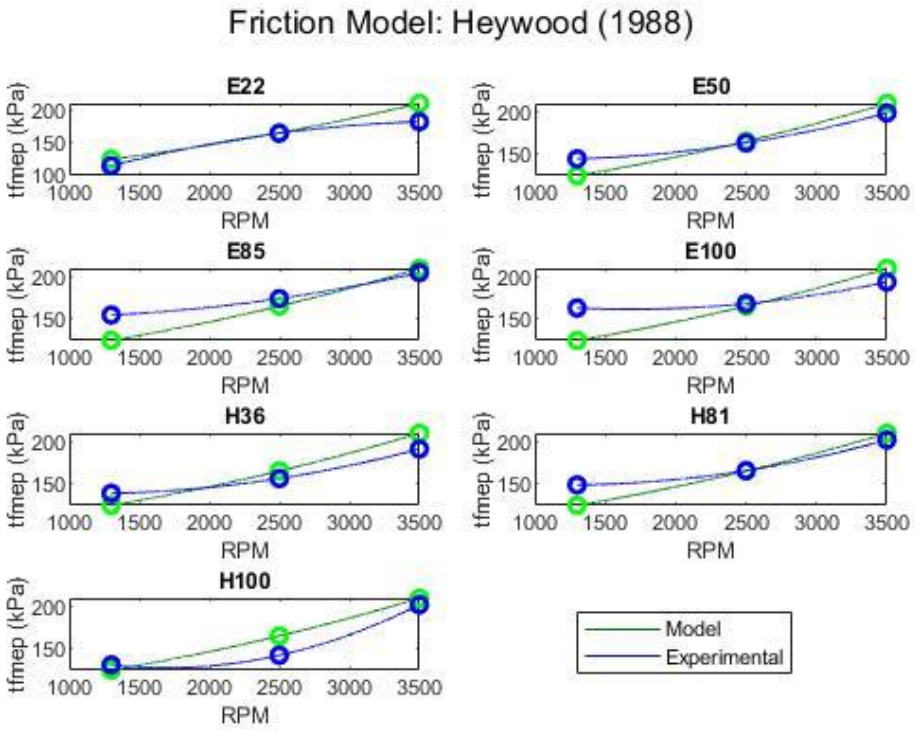

Figure 5.29: Real TFMEP and simulated by Heywood (1988) for all fuels tested.

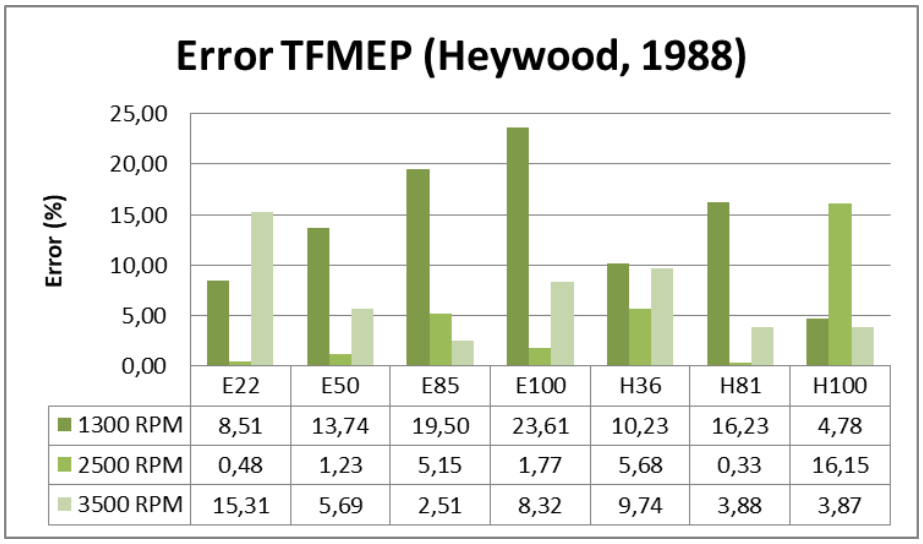

	E22	E50	E85	E100	H36	H81	H100
1300 RPM	8,51	13,74	19,50	23,61	10,23	16,23	4,78
2500 RPM	0,48	1,23	5,15	1,77	5,68	0,33	16,15
3500 RPM	15,31	5,69	2,51	8,32	9,74	3,88	3,87

Figure 5.30: Heywood correlation error (2018) in relation to experimental friction.

When the engine operates at 1300 RPM, there is a higher percentage error in relation to the experiment as the ethanol content increases in the compounds, with the exception of H100. This difference is from 4.78% to 23.61%.

At 2500 RPM, errors related to all fuels tended to decline, between 0.33 and 16.15%. It can be observed that the H100 has a higher associated error than the other mixtures.

At 3500 RPM rotation, errors are between 3.87 and 15.31%. It is noticed that the associated errors are less than 10%, with the exception of E22, which has higher errors in relation to the experiment for this rotation.

5.6.3 TFMEP simulation as a function of Engine Geometric Parameters and Average Piston Speed

This correlation proposed by Sandoval (2003) simulates the friction coming from each engine components. Once calculated and summed up, the $TFMEP_{SIM}$ can be calculated. This section will present the total friction of the engine calculated by this model. Further details on friction in each component will be demonstrated in section 5.7.

It can be noted that, with the exception of E22 and H100, the errors to the experiments are higher at low rotations and tend to rise as it gets higher. Like the correlation proposed by Heywood (1988), the error raises as the volume of ethanol in the mixtures increases, with the exception of the H100 in which it is reduced.

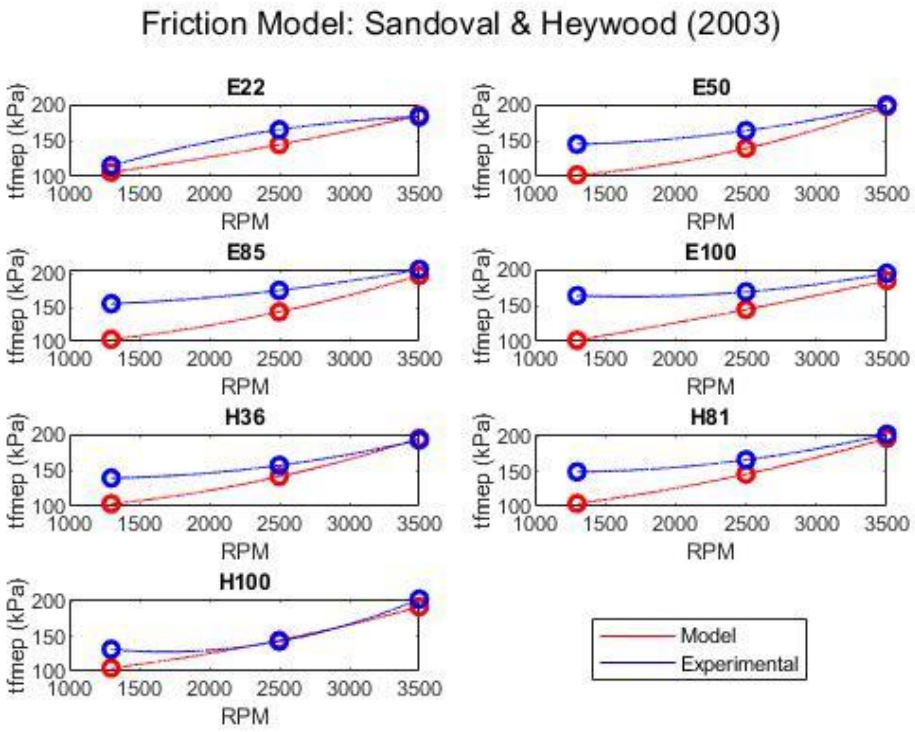

Figure 5.31: Real TFMEP and simulated by Sandoval (2003) for all tested fuels.

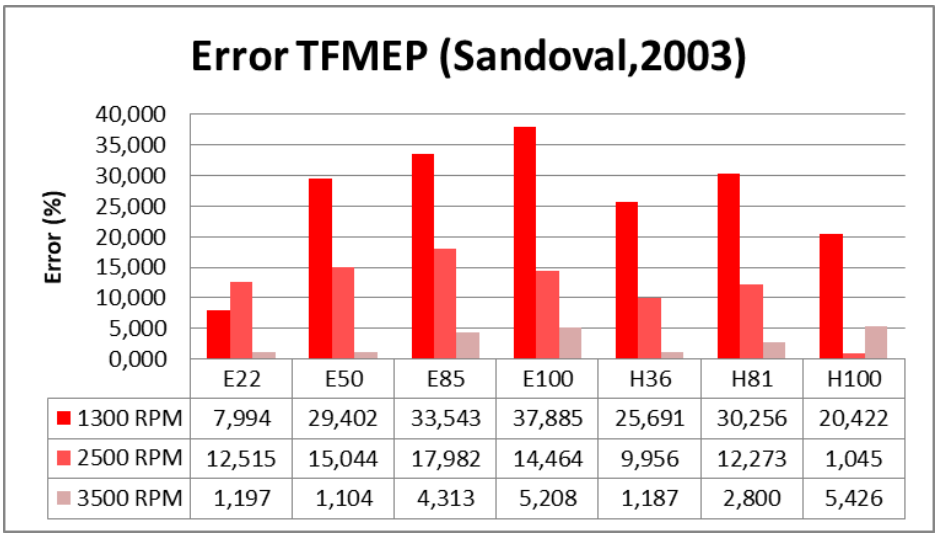

	E22	E50	E85	E100	H36	H81	H100
1300 RPM	7,994	29,402	33,543	37,885	25,691	30,256	20,422
2500 RPM	12,515	15,044	17,982	14,464	9,956	12,273	1,045
3500 RPM	1,197	1,104	4,313	5,208	1,187	2,800	5,426

Figure 5.32: Error of the Correlation of Sandoval (2003) in relation to experimental friction.

Figure 5.33 shows the EQM values for simulated TFMEP according to the proposed models. We can clearly see that the Heywood model (1988) provides better results of friction prediction than Sandoval (2003), with the exception of experiments conducted for E22.

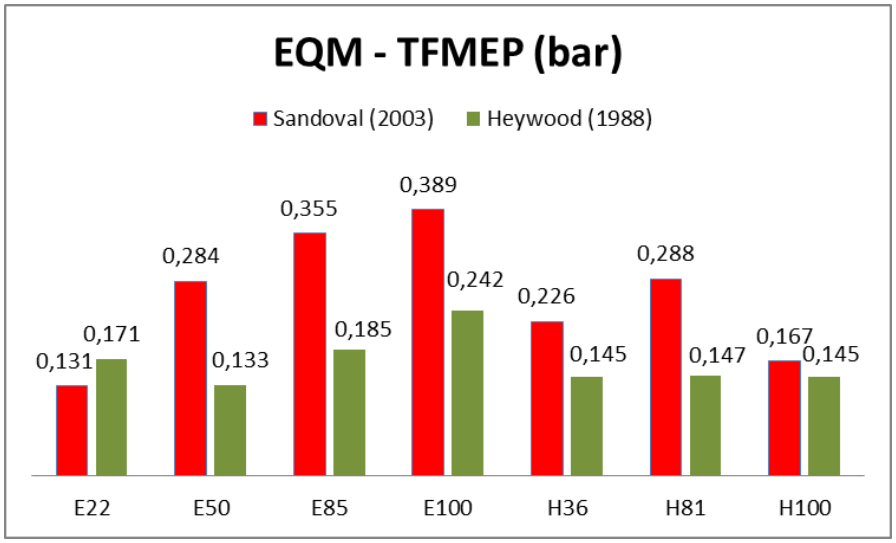

Figure 5.33: EQM of simulated TFMEP`(bar)

Fuel	EQM% - TFMEP		EQM% - η_m	
	Sandoval (2003)	Heywood (1988)	Sandoval (2003)	Heywood (1988)
E22	0,0850	0,1110	0,01331	0,01722
E50	0,1679	0,0784	0,03107	0,01446
E85	0,1988	0,1035	0,03853	0,02049
E100	0,2215	0,1380	0,04291	0,02671
H36	0,1387	0,0892	0,02453	0,01486
H81	0,1666	0,0851	0,03191	0,01642
H100	0,1054	0,0913	0,01869	0,01462

Table 5.11: EQM% of the simulated TFMEP and mechanical efficiency.

5.6.4 Torque x RPM

From the results of IMEP and $TFMEP_{SIM}$, Equation 4.29 is used to obtain the $BMEP_{SIM}$ and, from it, the torque is found by Equations 4.25 and 4.26. Figures 5.34 and 5.35 represent these curves obtained by the correlations of Sandoval (2003) and Heywood (1988), respectively, together with the experimental results whose coefficients can be found in table 5.10.

When the torque is calculated from Heywood (1988) friction model, a good proximity to low rotations is noted, despite the distance of TFMEP and $TFMEP_{SIM}$. With the exception of the H100 and E22, it can be seen that the simulated torque is higher up to 2500 RPM, tending to be smaller and closer to the real for the higher rotations.

The simulated torque for the E22 fuel is very close to the experimental between 1300 and 2500 RPM. However, it tends to move away for higher

rotations. The H100 has proximity at 1300 and 3500 RPM, with a clearance at 2500 RPM.

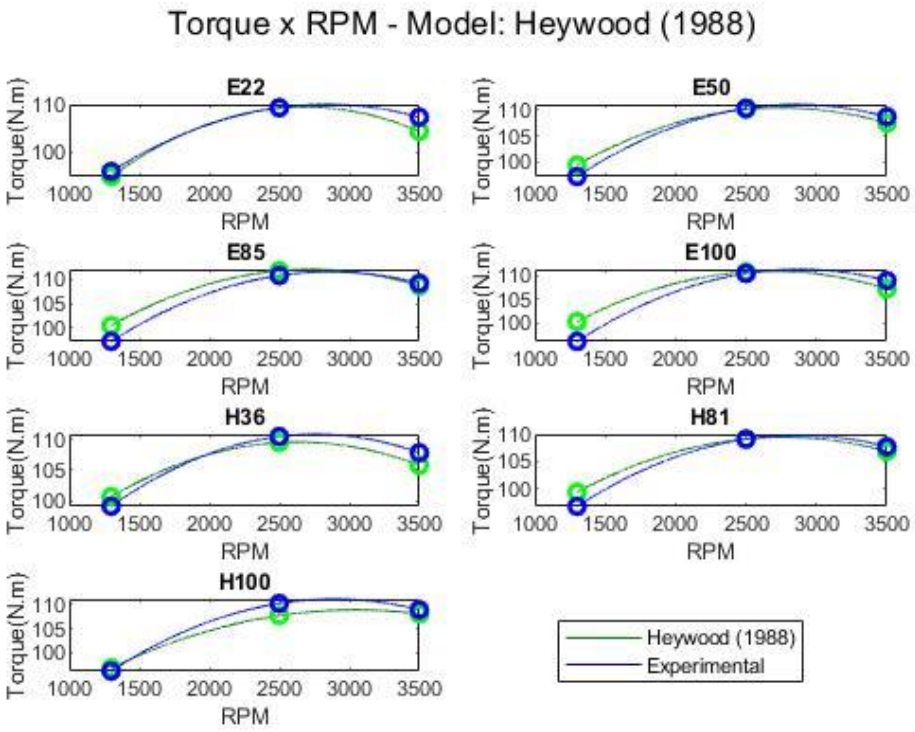

Figure 5.34: Real torque and simulated by Heywood (1988) for all fuels tested.

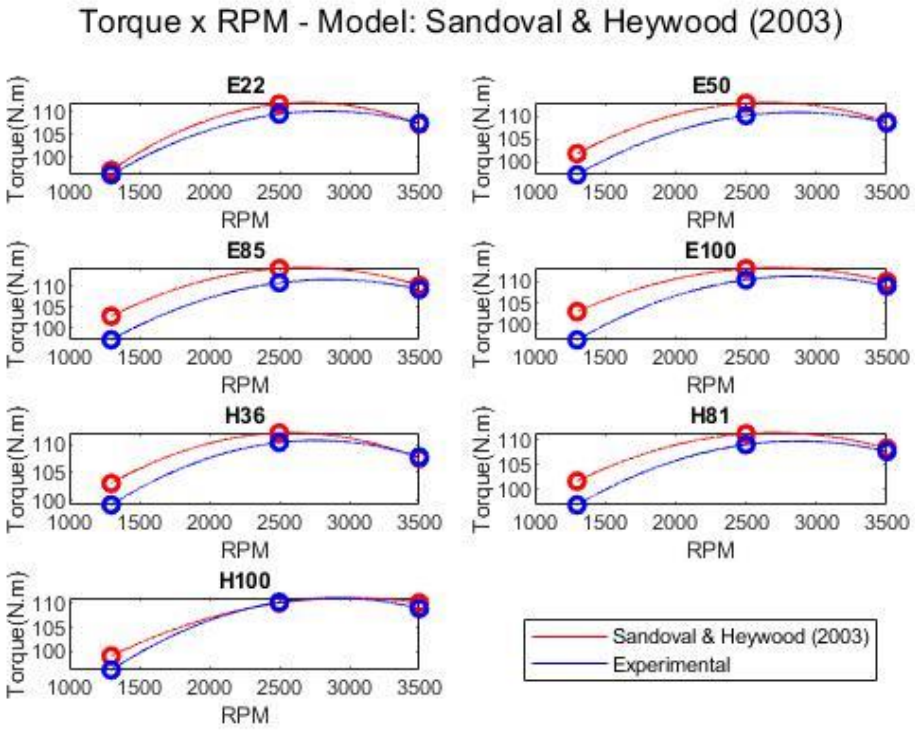

Figure 5.35: Real torque and simulated by Sandoval (2003) for all fuels tested.

For the torque simulated using the Sandoval (2003) friction model, there is a greater distance for low rotations of all fuels, except for E22. As the rotation is raised, the curve is getting closer to the real one.

5.6.5 Mechanical Efficiency: Experimental vs Simulation

The values for experimental and simulated TFMEP, as well as mechanical efficiencies can be found in Appendix IV. Figures 5.36, 5.37 and 5.38 are referred to the mechanical efficiencies calculated by the real friction of the engine and the friction correlations in the literature for 1300, 2500 and 3500 RPM, respectively. The columns of the images demonstrate the relative error between the simulated mechanical efficiency in relation to the experimental.

Figure 5.39 represents the average relative error of the mechanical efficiency of all fuels in relation to the friction models. It can be noted that the biggest errors are for lower speed, tending to decrease when increasing the engine speed. It can also be noted that, even with errors greater than 30% of $TFMEP_{SIM}$ in relation TFMEP, mechanical efficiency had errors of no more than 6.97% and 4.35% for the models proposed by Sandoval (2003) and Heywood (1988), respectively.

Figure 5.40 represents the EQM calculated using the two models for each fuel. The Heywood model (1988) showed greater accuracy in the results, which was already expected by the results of the EQM% for the $TFMEP_{SIM}$.

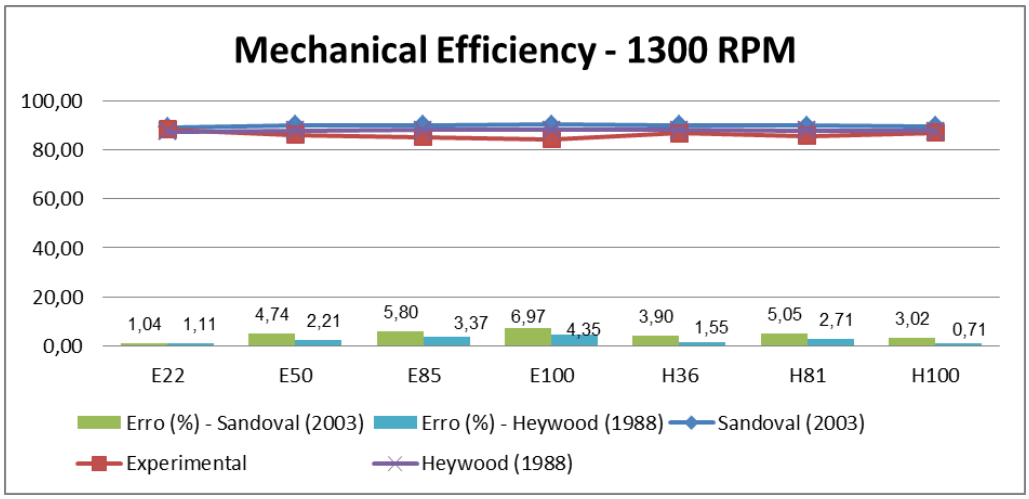

Figure 5.36: Experimental and Simulated Mechanical Efficiency at 1300 RPM.

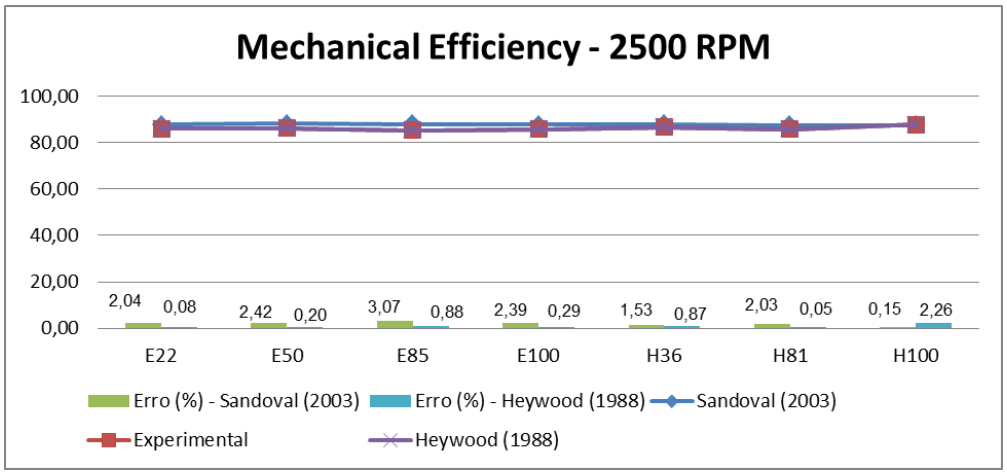

Figure 5.37: Experimental and Simulated Mechanical Efficiency at 2500 RPM.

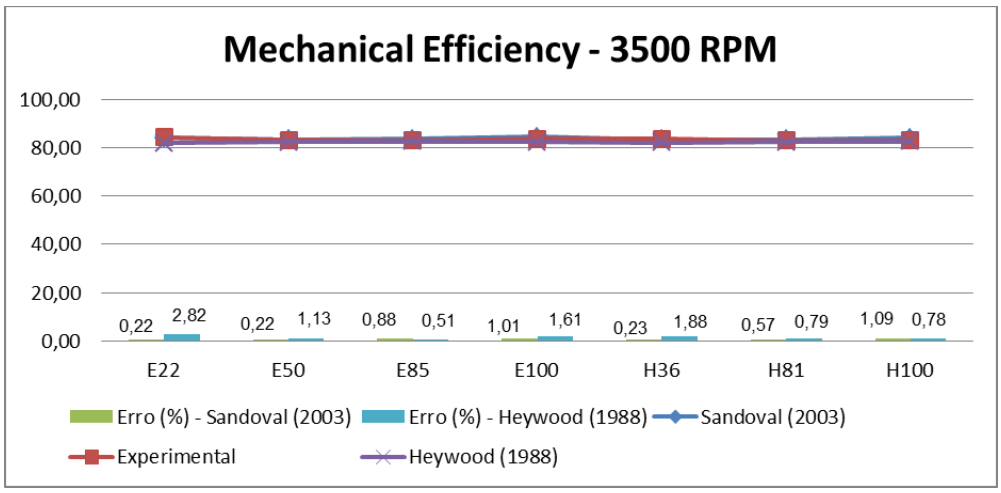

Figure 5.38: Experimental and Simulated Mechanical Efficiency at 3500 RPM.

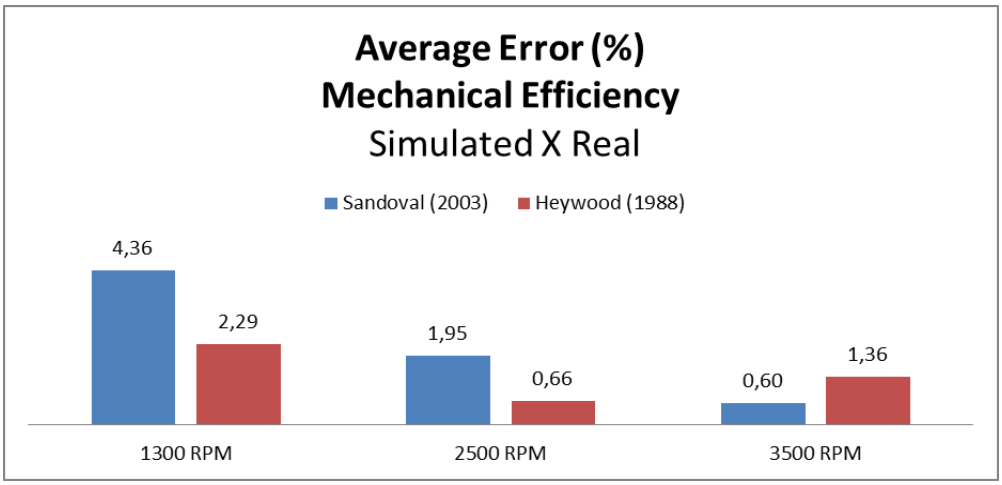

Figure 5.39: Average relative error of all fuels of friction prediction models for all rotations.

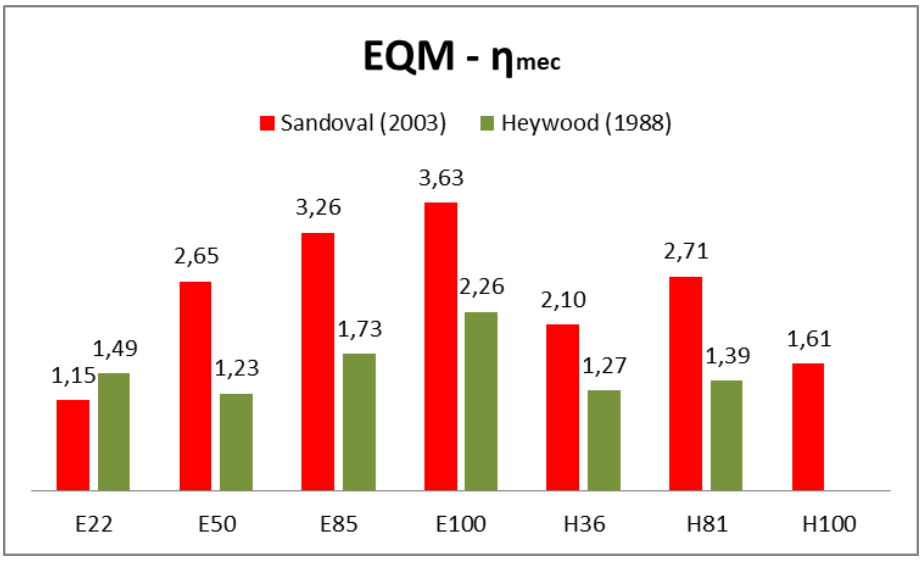

Figure 5.40: EQM of mechanical efficiency in relation to the bench tests according to the results of friction models for engines.

5.7 Motored Tests Simulation

As already mentioned, the model proposed by Sandoval (2003) is able to simulate the friction coming from each engine component. This correlation takes into account the geometric parameters of the engine, the pressures at the intake manifold and the mean piston speed. In Figures 5.41 to 5.44 we see the results for the TU3 engine.

5.7.1 Total Engine Friction

The largest total friction path in the engine for all speeds comes from the piston assembly. This grows with increased speed, but in smaller proportions than the increase in the parts of the crankshaft. The image of the friction results in each group is seen in figure 5.41.

We see that the crankshaft has low values of friction losses to 1300 RPM and that it has the highest growth rate among all groups. It will be seen in the next sections that this increase occurs due to friction in the bearings and, mainly, by turbulence dissipations for pumping lubricating oil.

The losses from the activation of the auxiliary components also grow jointly with the engine speed. Despite being one of the lowest for all speeds, these have their value increased due to the greater amount of energy needed for the operation of the fuel pump, water pump, fan, among others.

Valve train friction is practically constant when increasing the engine speed, with its value in percentage reduced as other friction allocated losses increase with engine speed.Table 5.12 shows de results for each component.

Components	Friction Pressure Losses (bar)			Piston Assembly Friction Losses (bar)			
	1300 RPM	2500 RPM	3500 RPM	Eng. Speed:	1300 RPM	2500 RPM	3500 RPM
Piston Ass.	0,510	0,570	0,640	Skirt	0,0916	0,1761	0,2465
Crankshaft	0,134	0,238	0,346	Rings	0,1277	0,1010	0,0928
Valve Tain	0,191	0,186	0,191	Gas Loading	0,2330	0,1825	0,1459
Auxiliary	0,120	0,176	0,240	C. Rod Bearings	0,0574	0,1104	0,1545
Crankshaft Friction Losses (bar)				Valve Train Friction Losses (bar)			
Eng. Speed:	1300 RPM	2500 RPM	3500 RPM	Eng. Speed:	1300 RPM	2500 RPM	3500 RPM
Bearings	0,0628	0,1208	0,1691	Bearings	0,0476	0,0535	0,0585
Seals	0,0542	0,0542	0,0542	Int. Valve	0,0718	0,0664	0,0666
Turb. Dissip.	0,0169	0,0625	0,1226	Ex. Valve	0,0714	0,0660	0,0663

Table 5.12: Simulated Friction Losses of each component of the engine.

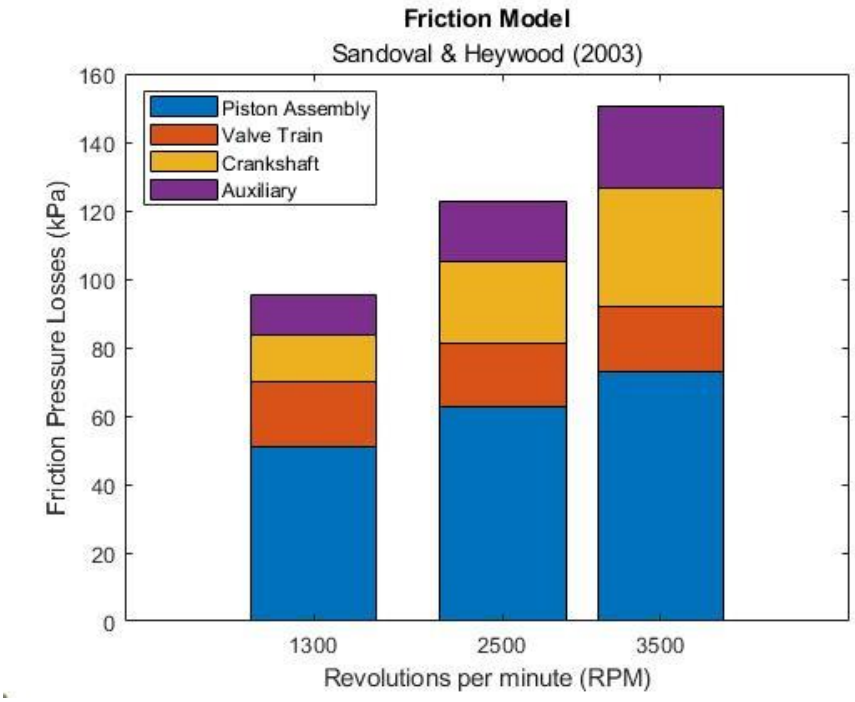

Figure 5.41: Engine components simulated friction losses.

5.7.2 Piston Assembly Friction

The piston assembly friction is separated into three components: the rod bearings in contact with the crankshaft and the friction between the cylinders with the piston shirt and its rings. These losses as a function of engine speed are shown in Figure 5.42.

The contact of the rings with the cylinder represents most of the friction, although this is reduced with increased rotations. It is noted that the increase in

friction of this component comes mainly from the contact between the piston walls with the block and also from the rod bearings.

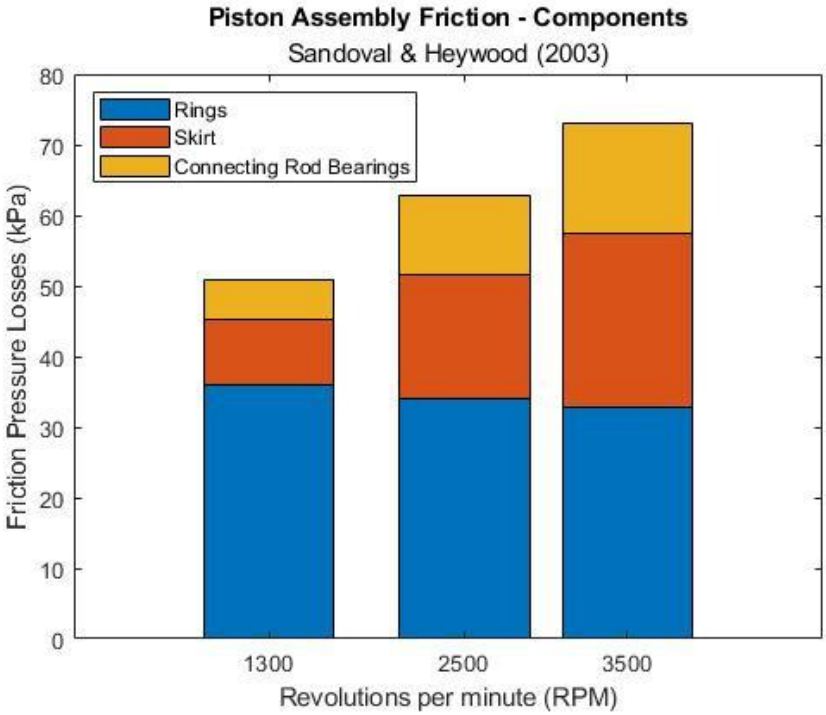

Figure 5.42: Piston Assembly simulated friction losses.

5.7.3 Crankshaft Assembly Friction

Figure 5.43 shows a large increase in friction in the crankshaft assembly when the engine speed is raised. There are no significant changes in losses by the seals, staying around 0,05 bar. On the other hand, there is an increase in turbulent oil dissipation and main bearings.

According to Heywood (2018), oil turbulence dissipations are directly proportional to N^2. It can be seen a great increase in figure 5.43, since for 1300 RPM this group represents 13% of the total losses and rises to 26% and 35% to 2500 and 3500 rpm, respectively.

On percentage issues, the main bearings of the crankshaft make up most of the frictional losses along all engine speeds. It is noted that the friction in this component increases at higher speeds, but in smaller proportions than turbulence dissipation.

It was seen that the components of the crankshaft assembly have the greatest increases in friction losses from the engine when increasing their rotation speed. As a result, it can be said that one of the main causes of the increase in TFMEP is due to dissipations due to oil turbulence.

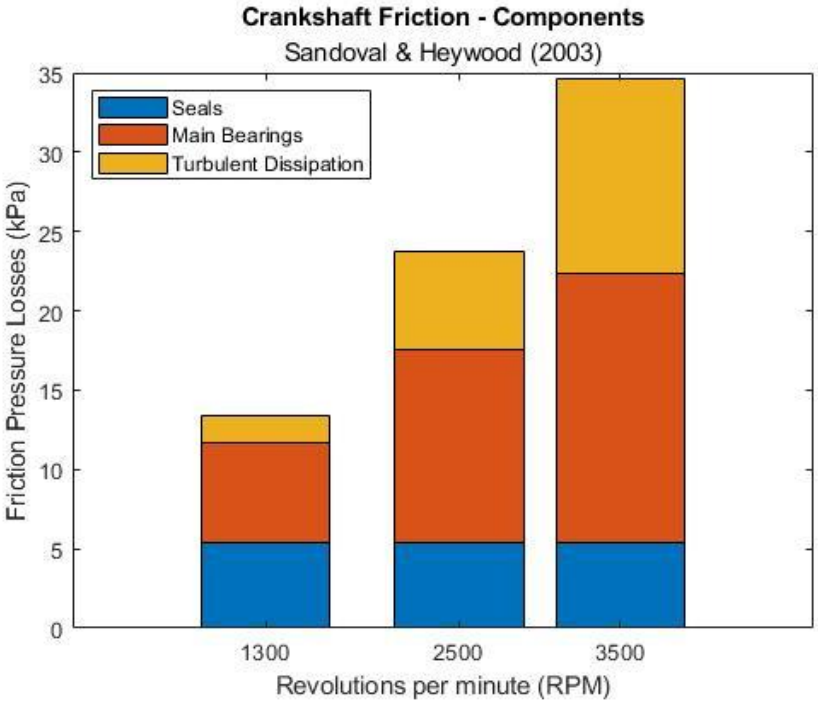

Figure 5.43: Crankshaft assembly simulated friction losses.

5.7.4 Valve Train Friction

Figure 5.44 shows that friction in the valve train does not have many changes as engine speed is increased. There is a small increase in friction in camshaft bearings, while losses by intake and exhaust valves have their value reduced.

The reduction in frictional losses in the valves occurs mainly due to increased lubrication between its parts. The intake valve has a larger diameter than the exhaust valve and, once its mass is larger, a small amount of greater power supply is required for its activation.

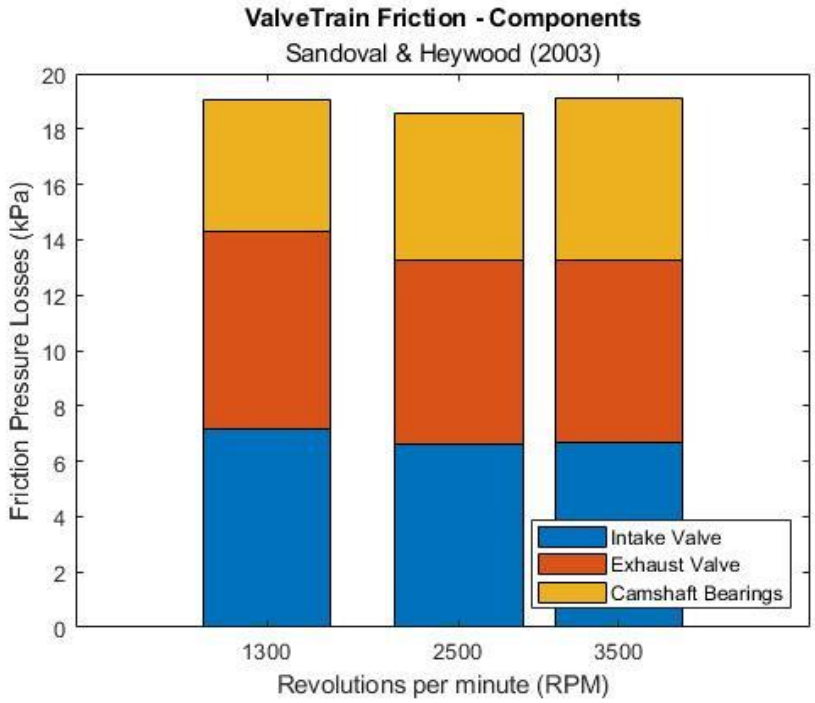

Figure 5.44: Valve train components simulated friction losses.

5.8 Automotive Vehicle Performance

This section shows the results obtained in the chassis dynamometer tests with the Peugeot 207 SW, which are addressed to its performance. First, the experimental results will be demonstrated, comparing the acceleration performance of the vehicle when submitted to the use of each of the seven fuels. Then, the mathematical model used to predict the results of these tests will be shown and compared to the experimwnts. Before applying the model, it is necessary to determine the transmission efficiency in each test.

5.8.1 Transmission Efficiency

When performing the experiment, the SPARC Vehicle provided the values of the measured power in the dynamometer roller, which is the same as the wheel of the vehicle. From these speeds values, we can find the engine speed by the engine-vehicle relation (equation 4.46). The tests were conducted in four groups of vehicle speeds and gears:

- Third gear from 40 to 80 km/h;
- Third gear from 60 to 100 km/h;
- Fourth gear from 40 to 80 km/h;

- Fourth gear from 60 to 100 km/h.

Using equation 4.46, that represents the relation between engine and vehicle speeds, the engine rotation speed interval for each test has been calculated and can be seen in table 5.13:

Engine RPM	40 km/h	60 km/h	80 km/h	100 km/h
3rd Gear	2013,5	3020	4026	5034
4th Gear	1532,2	2298	3064,41	3830

Table 5.13: Relationship between vehicle speed and engine RPM for the intervals tested with the vehicle at each gear.

From these values, it can be noted that the engine torque curves are expected to have a good approach for the tests, except for the fourth gear between 40 and 80 km/h, since the maximum engine speed tested by the engine was 3500 RPM. Therefore, the engine speed interval is outside the calculated curve for most of the test time.

As a result, transmission efficiency was calculated using equation 4.49 based on the ratio between the engine power and the wheel power. According to Mashadi & Crolla (2011), this parameter is a function of engine torque and its speed. Therefore, it is noted from Figures 4.45 to 4.48 that this value is not constant.

For simplification of calculations and, according to Mashadi & Crolla (2011), it is possible to consider the transmission efficiency as a constant value. Therefore, in this work, the mean values were used throughout each experiment. The results can be seen in Tables 5.14 and 5.15 and these indicate proximity between the mean values calculated for the three tests.

It is noted for the E85 fuel in third gear in the range between 40 and 80 km/h that there is a relevant difference in the power from the engine compared to that measured on the wheels. This can be attributed to the fact that this combination of gear and speed intervals are most of the time outside the torque curve range tested with the internal combustion engine on the bench. For these curves to be adjusted it is necessary to test the engine at higher RPM's.

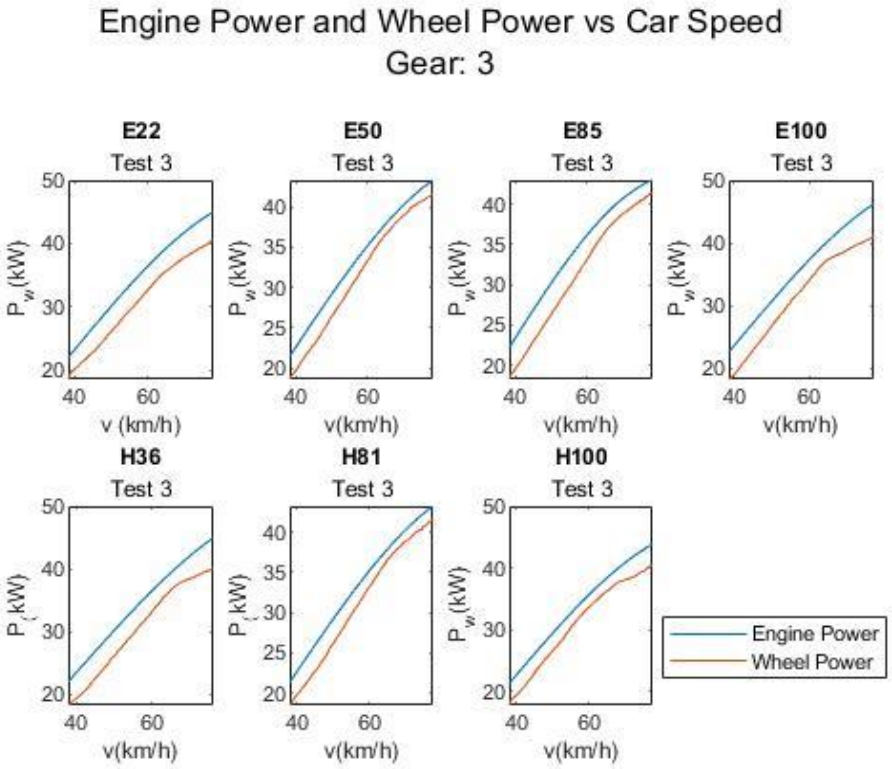

Figure 5.45: Engine shaft power vs wheel power during 3rd gear speed recovery test between 40 and 80 km/h.

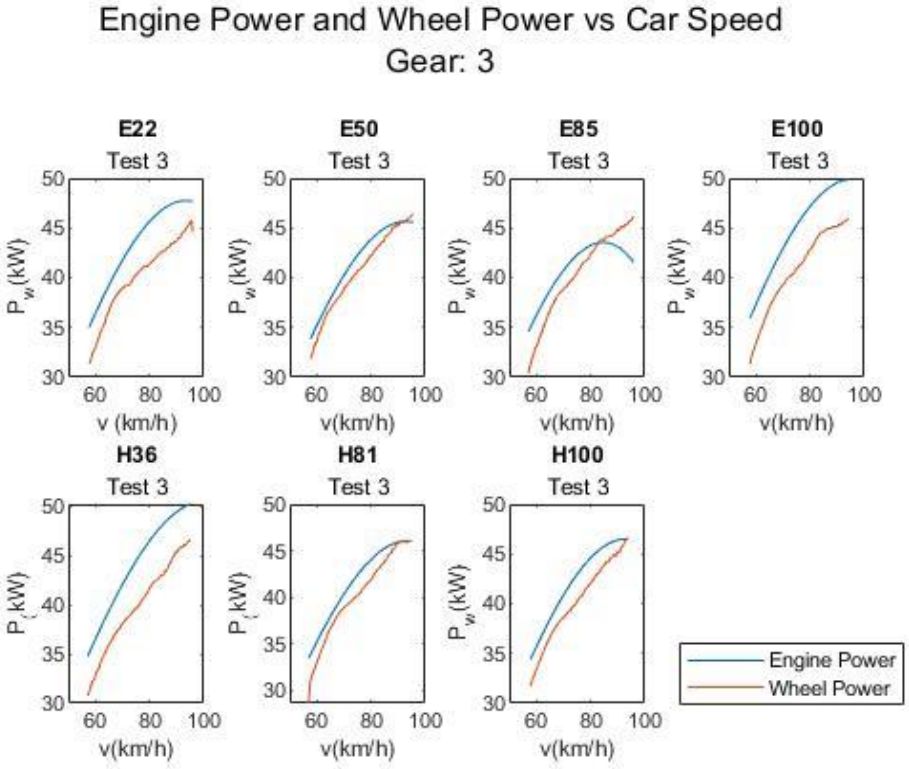

Figure 5.46: Engine shaft power vs wheel power during 3rd gear speed recovery test between 60 to 100 km/h.

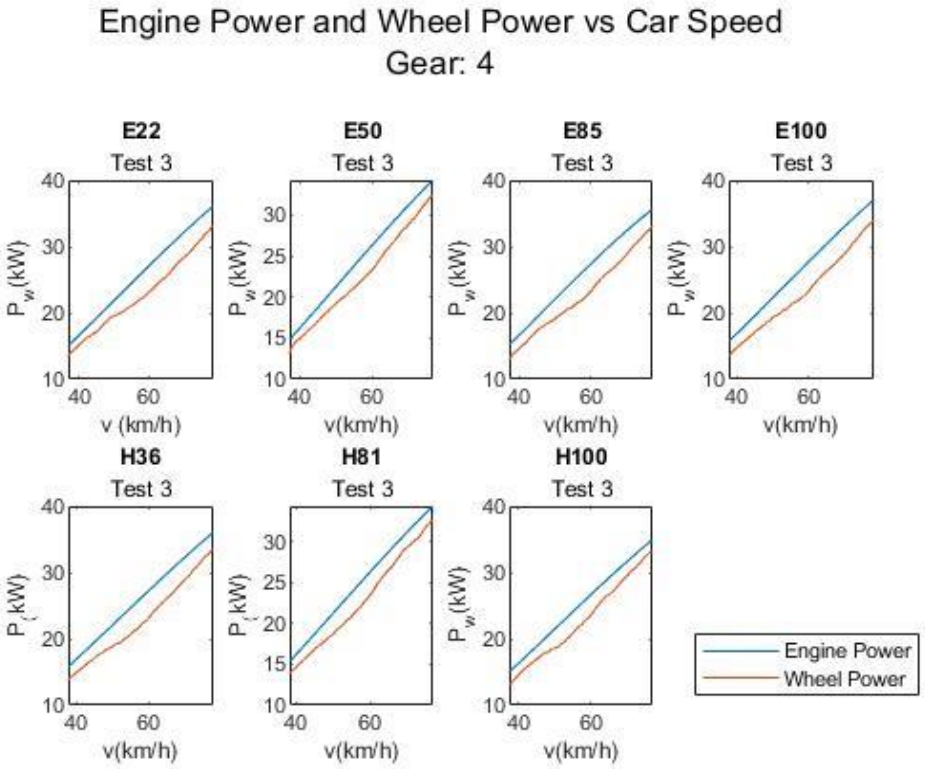

Figure 5.47: Potência on the engine axle vs wheel power during the 4th gear speed recovery test between 40 and 80 km/h.

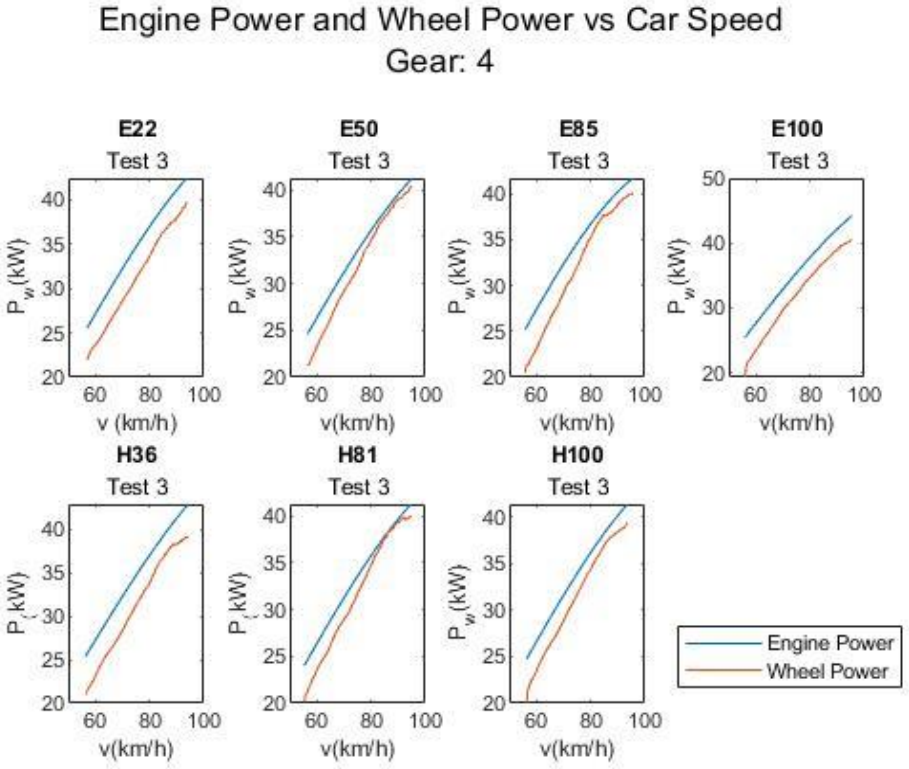

Figure 5.48: Engine shaft power vs wheel power during 4th gear resume test between 60 and 100 km/h.

Average Transmission Efficiency						
3rd Gear	40 to 80 km/h			60 to 100 km/h		
Fuel	Test 1	Test 2	Test 3	Test 1	Test 2	Test 3
E22	0,895	0,902	0,890	0,863	0,869	0,862
E50	0,931	0,932	0,935	0,907	0,911	0,911
E85	0,910	0,908	0,913	0,893	0,893	0,890
E100	0,873	0,881	0,885	0,856	0,857	0,863
H36	0,882	0,880	0,887	0,862	0,856	0,863
H81	0,919	0,929	0,930	0,909	0,902	0,908
H100	0,911	0,919	0,919	0,903	0,901	0,898

Table 5.14: Transmission efficiency mean values for third-gear tests.

Average Transmission Efficiency						
4th Gear	40 to 80 km/h			60 to 100 km/h		
Fuel	Test 1	Test 2	Test 3	Test 1	Test 2	Test 3
E22	0,892	0,895	0,901	0,913	0,915	0,913
E50	0,922	0,923	0,925	0,954	0,956	0,957
E85	0,896	0,896	0,900	0,934	0,936	0,937
E100	0,875	0,877	0,876	0,904	0,905	0,907
H36	0,881	0,882	0,880	0,910	0,908	0,905
H81	0,918	0,919	0,918	0,947	0,953	0,955
H100	0,910	0,911	0,917	0,943	0,947	0,940

Table 5.15: Transmission efficiency mean values for fourth-gear tests.

5.8.2 Acceleration Performance in Chassis Dynamomenter

The speed recovery tests on a chassis dynamometer were performed in the third and fourth gears. The speed range tested was between 40 to 80 km/h and 60 to 100 km/h. However, the vehicle speed values are not precisely these, since there are experimental inaccuracies related to the speed difference in the car speedometer and that obtained by the Sparc Vehicle.

All the results can be seen in Appendix V of this work, which shows the table with the respective initial, and final speeds, as well as the speed recovery time. The numbering of the tests can be explained according to Table 5.16, where the lower and higher speed ranges correspond to approximately 40-80 km/h and 60-100 km/h, respectively.

Test no.	Velocity Range	Gear
Test 1	Lower Speed Range (≈40 to 80 km/h)	3rd Gear
Test 2		
Test 3		
Test 4	Higher Speed Range (≈60 to 100 km/h)	
Test 5		
Test 6		
Test 7	Lower Speed Range (≈40 to 80 km/h)	4th Gear
Test 8		
Test 9		
Test 10	Higher Speed Range (≈60 to 100 km/h)	
Test 11		
Test 12		

Table 5.16: Organization of speed recovery tests on chassis dynamometer.

After finishing the vehicle tests on the chassis dynamometer, the SPARC Vehicle software captured the power and the speed in the dynamometer rollers. An example of the result provided by the software can be seen in Figure 5.49 for the E50 fuel tested in third gear.

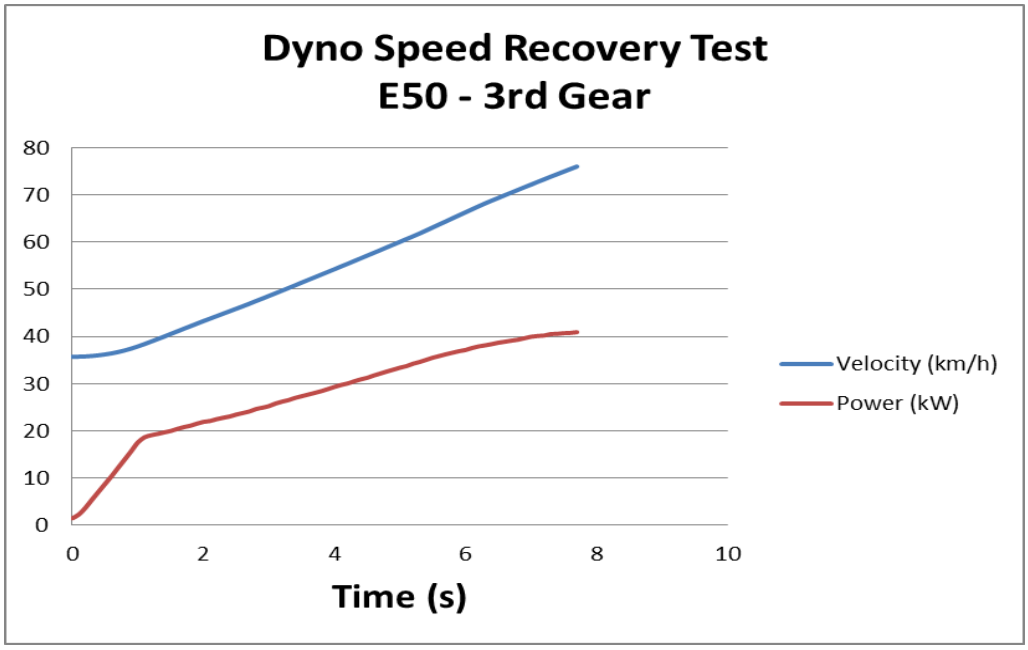

Figure 5.49: Result for the third-gear E50 speed recovery tests.

Figure 5.49 show that there is a period from the moment that the driver steps on the accelerator until the engine develops full load. When it is reached, it is noted that the speed profile grows linearly overtime. As a result, the acceleration of the vehicle was considered as constant during speed recovery tests, as the inclination of the straight line.

Experiments for each speed range and gear configuration was repeated three times for each fuel tested. Using the MATLAB *polyfit* function, it was possible to obtain the straight line that best approximates all these experimental points, as show in figure 5.50 for the E22 fuel.

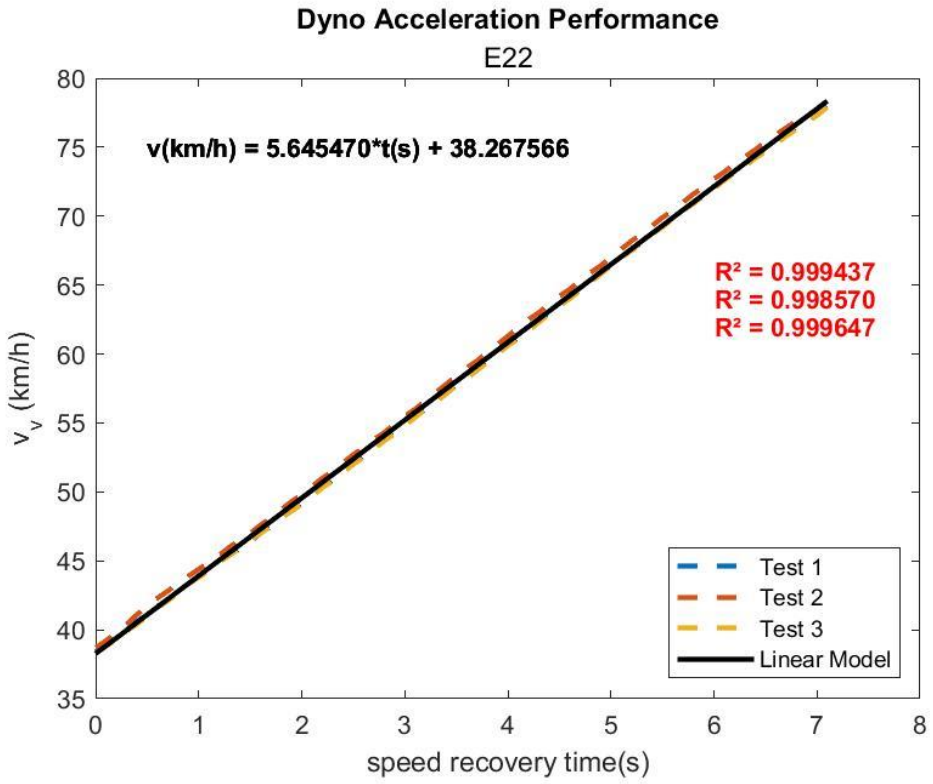

Figure 5.50: Acceleration performance of the E22 fuel in chassis dynamometer

The coefficient of determination (R^2) that approximates each tests straight line from the average straight line is shown in figure 5.51. The average accelerations for all tested fuels in all vehicle configurations are shown in Figures 5.52 and 5.53.

To ensure a good approximation of the first order polynomial with the experimental results, the MATLAB algorithm also provided the EQM and EQM% values of each test for all v_v x t plots. These showed root mean square errors less than 0.17 km/h and low dispersion, giving a very good tendency by approaching with a straight line. The results for all fuels in all test configurations can be found in Appendix VI with the respective coefficient of determination, average acceleration values and standard deviation. A summary is shown in figures 5.51 to 5.53 and Table 5.17.

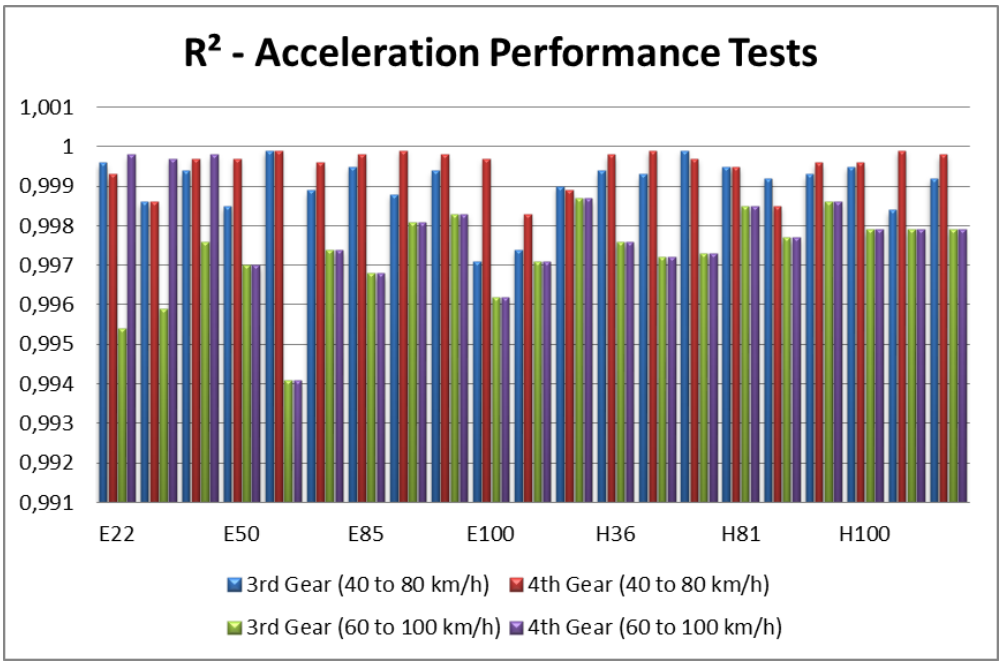

Figure 5.51: R² of all accelerations in relation to the average acceleration

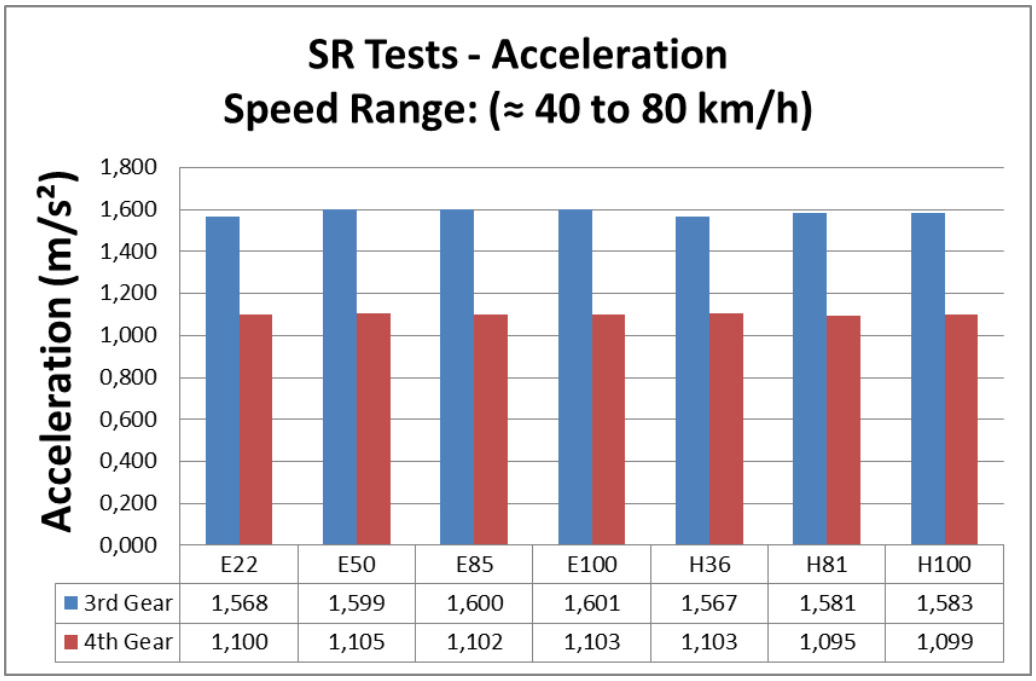

	E22	E50	E85	E100	H36	H81	H100
3rd Gear	1,568	1,599	1,600	1,601	1,567	1,581	1,583
4th Gear	1,100	1,105	1,102	1,103	1,103	1,095	1,099

Figure 5.52: Average acceleration between approximately 40 and 80 km/h in third and fourth gear of the Peugeot 207 SW for different fuels.

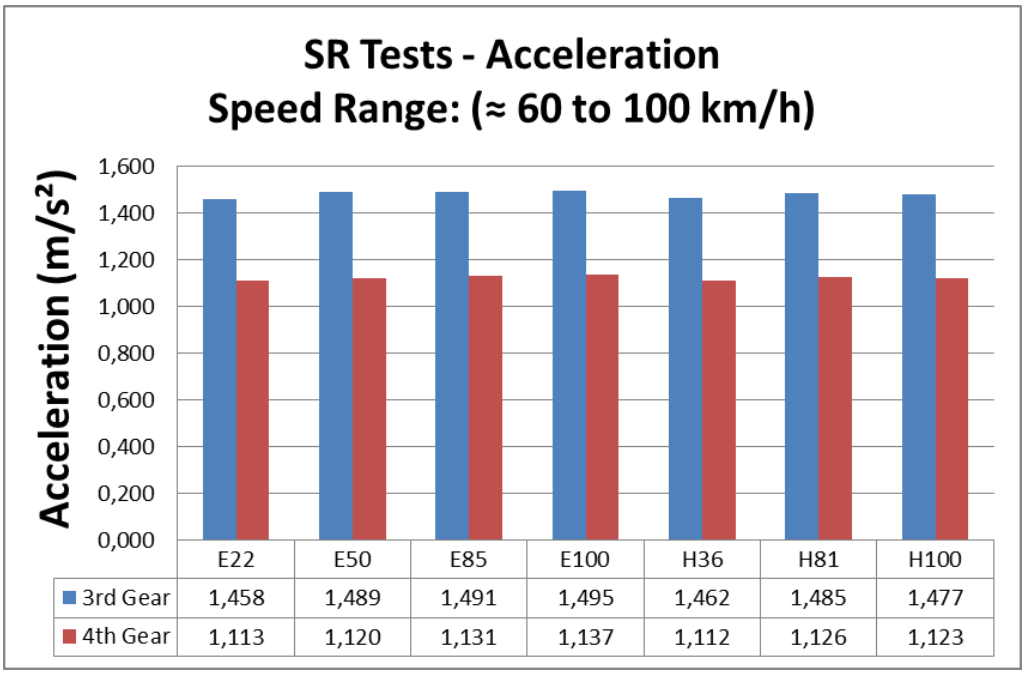

Figure 5.53: Average acceleration between 60 and 100 km/h in third and quart gear of the Peugeot 207 SW for different fuels.

Acceleration Performance Ranking				
	3rd Gear		4th Gear	
	40 to 80 km/h	60 to 100 km/h	40 to 80 km/h	60 to 100 km/h
1st	E100	E100	E50	E100
2nd	E85	E85	E100	E85
3rd	E50	E50	H36	H81
4th	H100	H81	E85	H100
5th	H81	H100	E22	E50
6th	E22	H36	H100	E22
7th	H36	E22	H81	H36

Table 5.17: Acceleration Performance Ranking of the Fuels in Chassis Dynamometer.

As it can be seen in Figure 5.51, all tests carried out on a chassis dynamometer presented excellent approximation of the straight line acceleration with the calculated average of the accelerations, presenting coefficients of determination greater than 0.994 in all tested vehicle gears and speed range configurations.

Accelerations are higher for third gear because the transmission gear ratios amplify the torque coming from the engine on the wheels, while for the fourth gear this parameter is reduced.

For the third gear, it can be seen that the acceleration is greater between 40-80 km/h, because this interval is closer to the maximum torque range than between 60 to 100 km/h.

We can note that the increase in the ethanol content in the mixture increases the acceleration of the vehicle in all cases except the H100 compared to the H81 in which it is reduced. However, near between 40 and 80 km/h the E85 and E100 had the same acceleration capacity in both gears. It's important to note that for low speed ranges at fourth gear, the E50 presented the best acceleration performance, even better than E100.

Another important observation is that the addition of water in the mixtures reduces the vehicle's acceleration performance in all tests. Therefore, among all fuels, the one that has the best performance in most of the speed recovery tests was the E100.

5.8.3 Acceleration Performance Simulation from Engine Bench Tests Results

This section shows the results of the experimental and simulated speed recovery time for each test according to the proposed model. These were calculated in two ways. The first was by the experimental torque curves obtained by the test in the bench with the engine, whose coefficients are in Table 5.3 and the second was by the pressure curves with friction models of Sandoval (2003) and Heywood (1988).

It is noteworthy that the intervals of the tests in chassis dynamometer do not have start and end speeds exactly equal to 40-80 and 60-100 km/h, because there are related inaccuracies between the driver and the speedometer view. Therefore, the purpose of this section is to show the simulation results and compare them to the experimental results between the same initial and final speed range provided by the SPARC Vehicle software. The comparison of the acceleration capacity between the fuels for the Peugeot 207 SW was made in the previous section (5.8.2).

5.8.3.1 Experimental Brake Torque Curve X Dyno Results

The Figures 5.54 too 5.67 are the experimental graphs with the simulated graphs witch was calculated using longitudinal vehicular dynamics equation, witch the traction force was calculated as function of the torque measure on the engine AVL dynamometer. The torque was calculated by equation The speed interval and the gear witch the vehicle was tested is the same as Table 5.16.

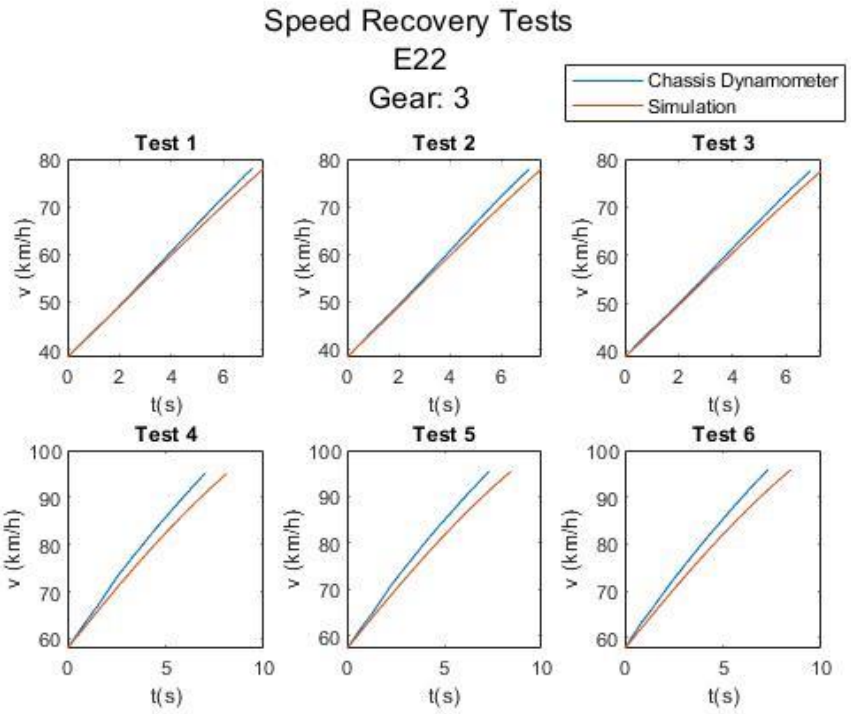

Figure 5.54: Experimental and simulated speed recovery tests for the E22 in third gear.

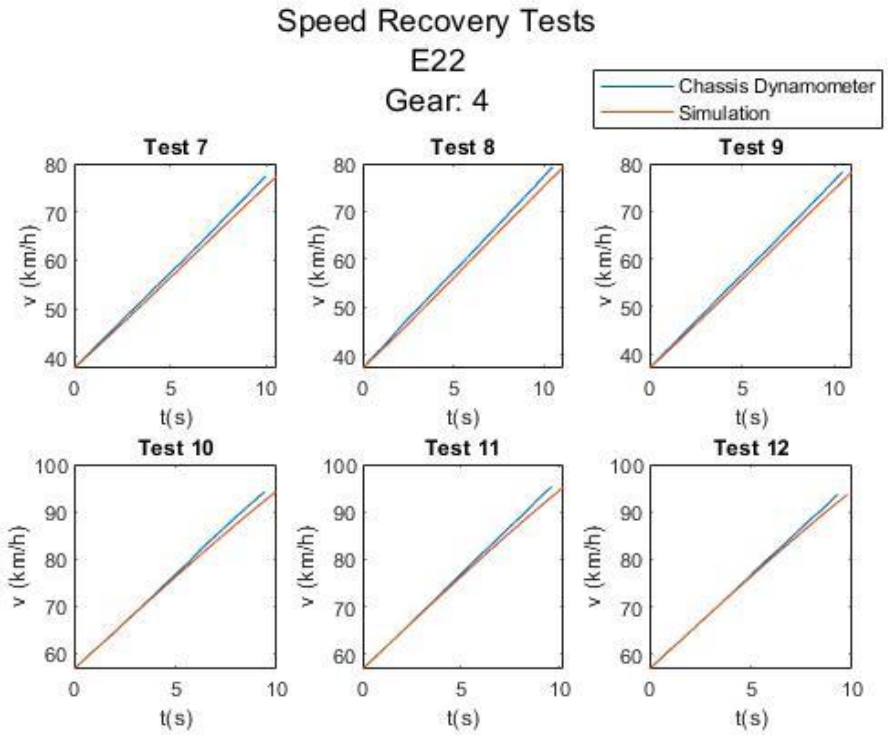

Figure 5.55: Experimental and simulated speed recovery tests for the E22 in fourth gear.

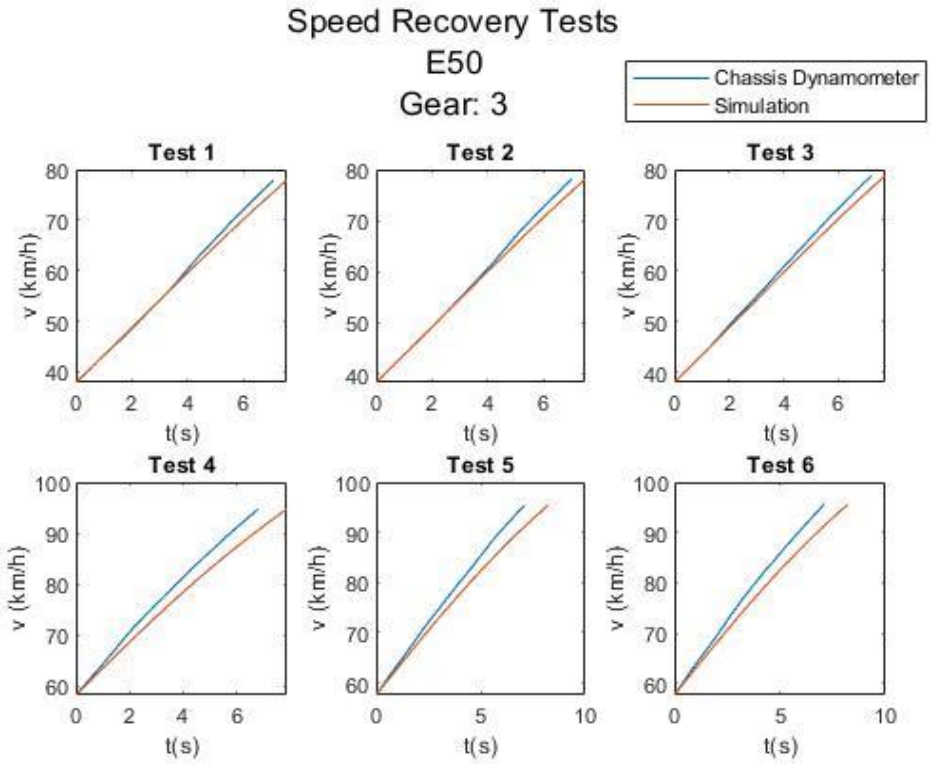

Figure 5.56: Experimental and simulated speed recovery tests for the E50 in third gear.

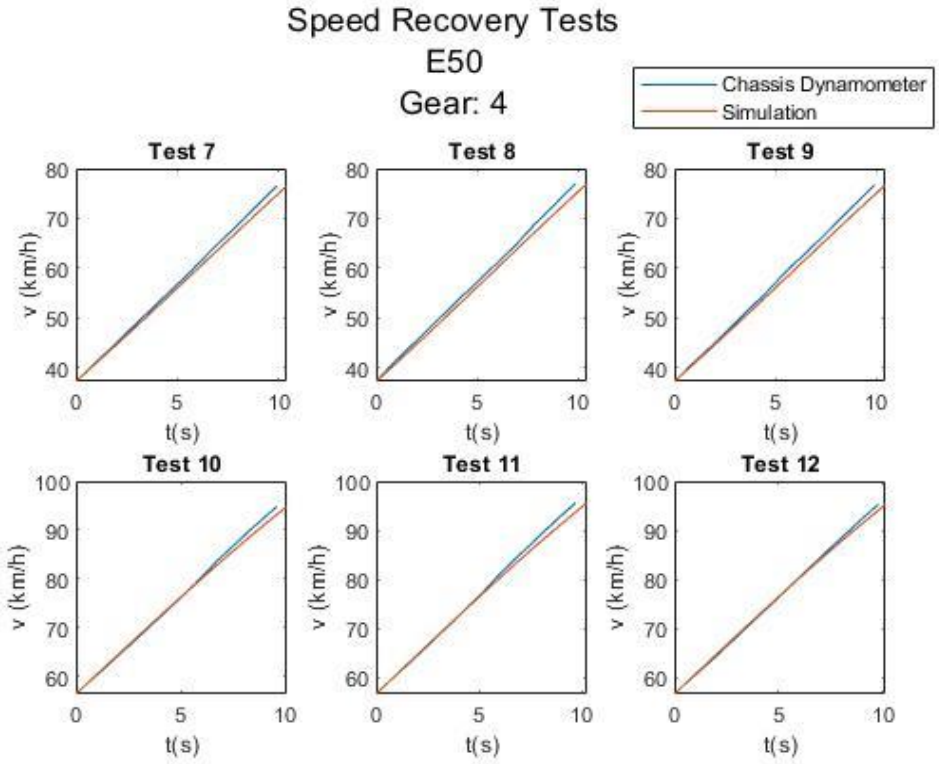

Figure 5.57: Experimental and simulated speed recovery tests for the E50 in fourth gear.

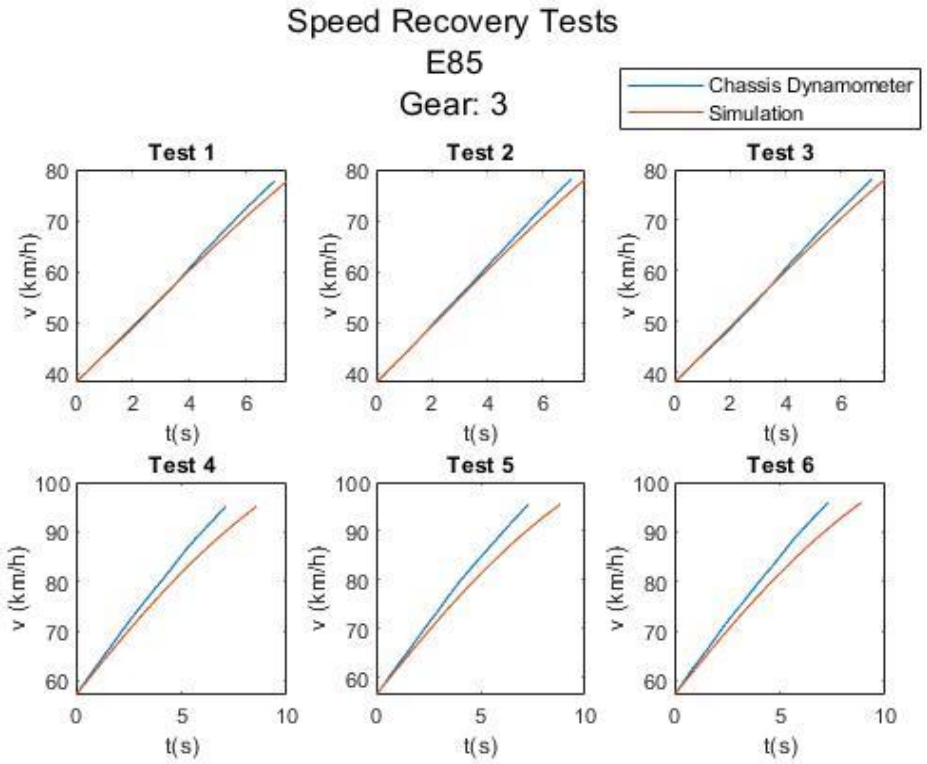

Figure 5.58: Experimental and simulated speed recovery tests for the E85 in third gear.

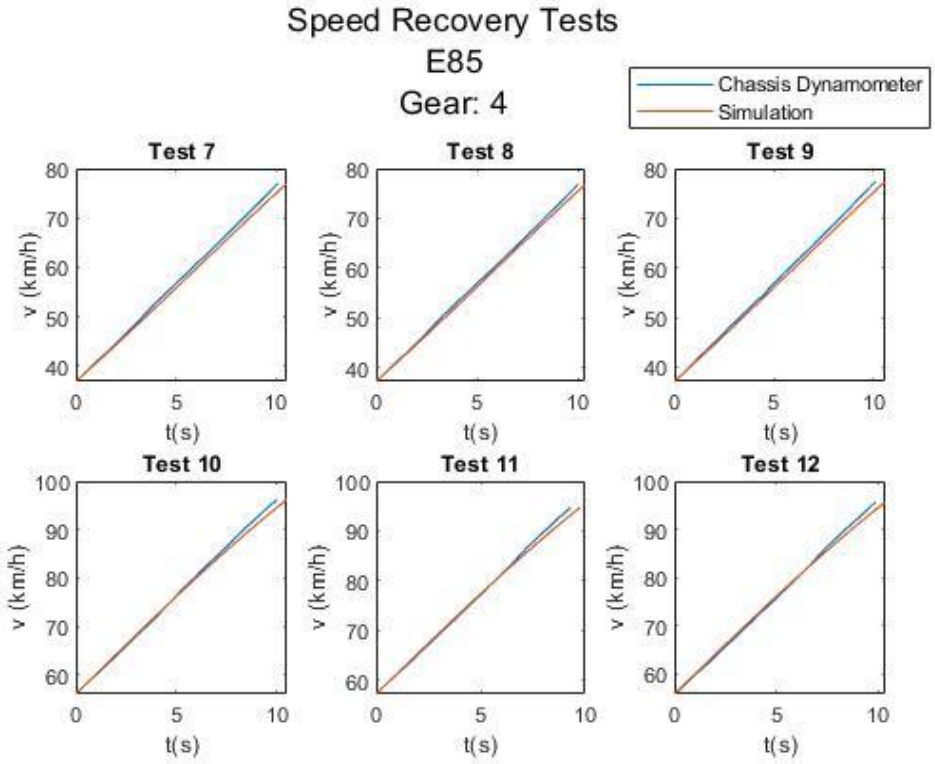

Figure 5.59: Experimental and simulated speed recovery tests for the E85 in fourth gear.

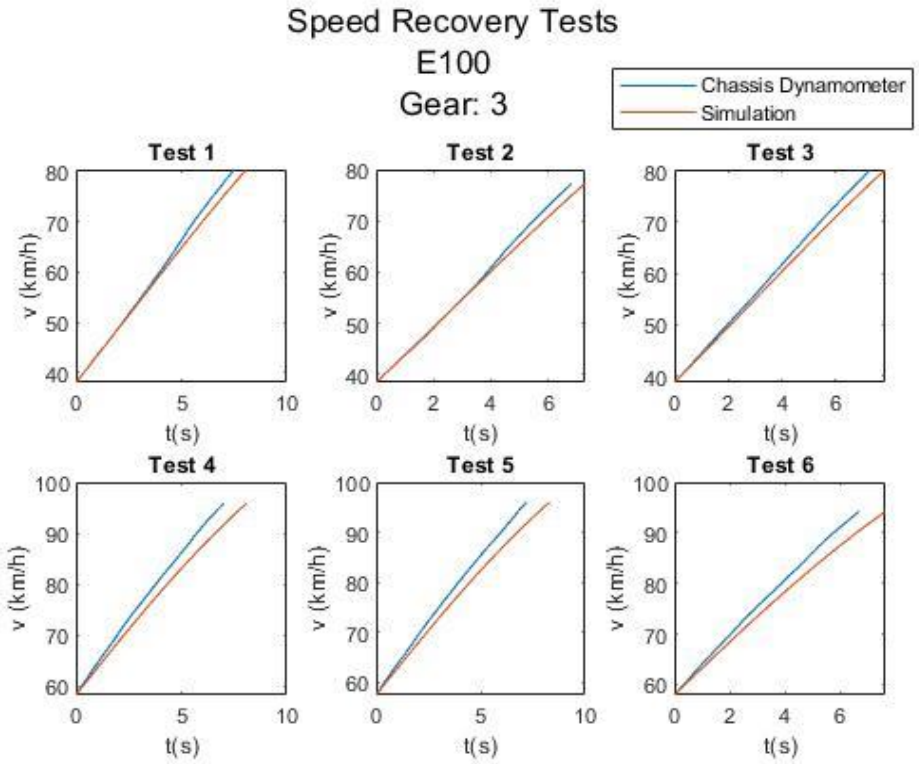

Figure 5.60: Experimental and simulated speed recovery tests for the E100 in third gear.

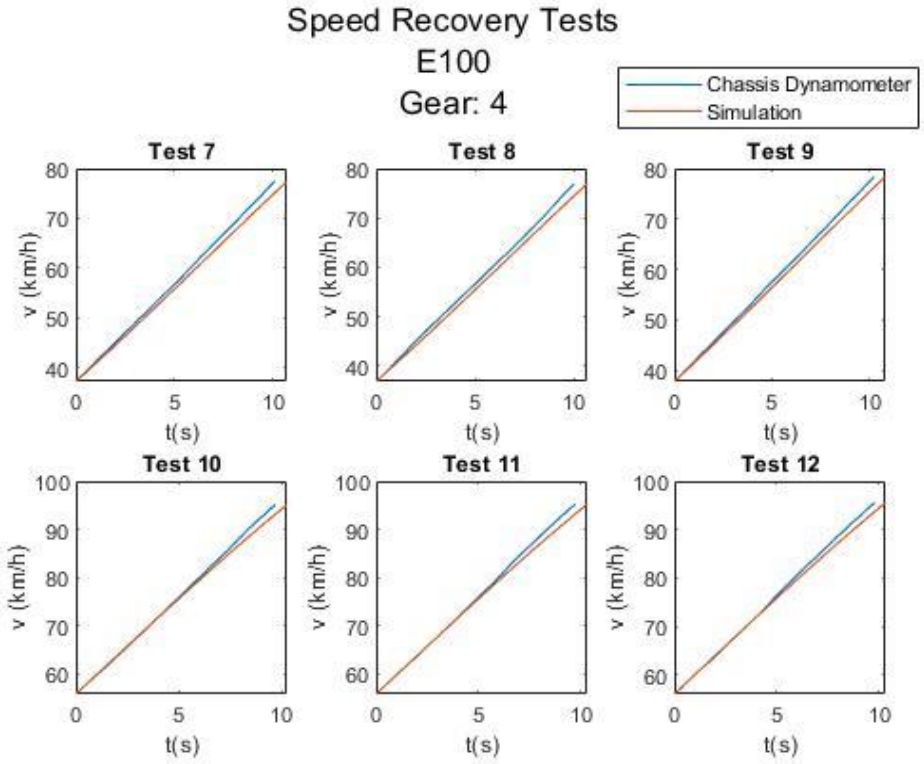

Figure 5.61: Experimental and simulated speed recovery tests for the E100 in fourth gear.

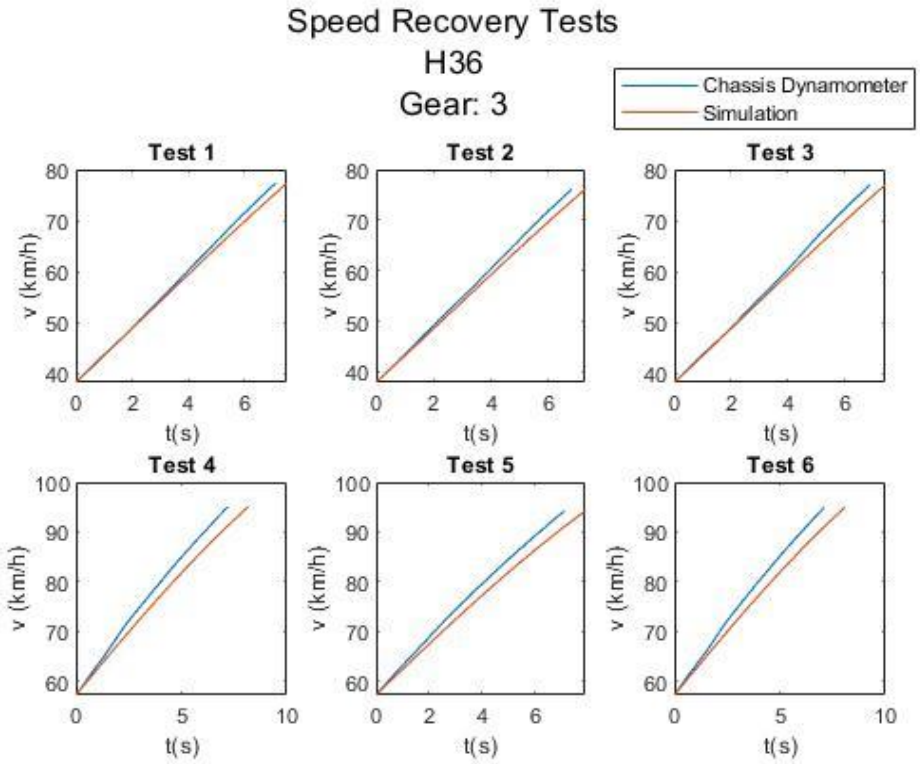

Figure 5.62: Experimental and simulated speed recovery tests for the H36 in third gear.

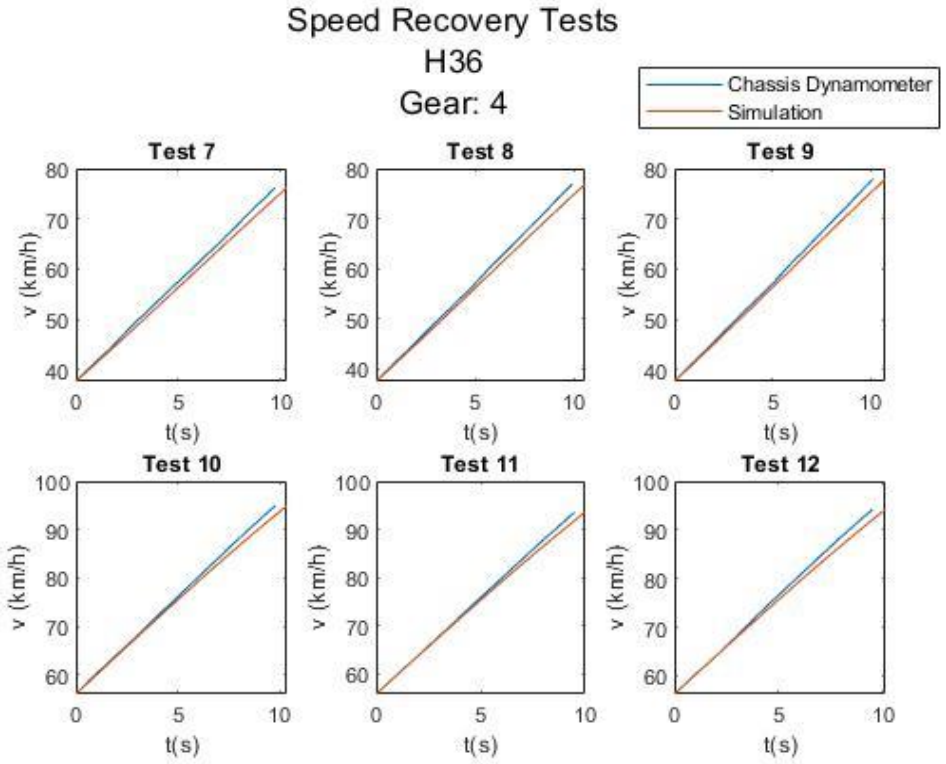

Figure 5.63: Experimental and simulated speed recovery tests for the H36 in fourth gear.

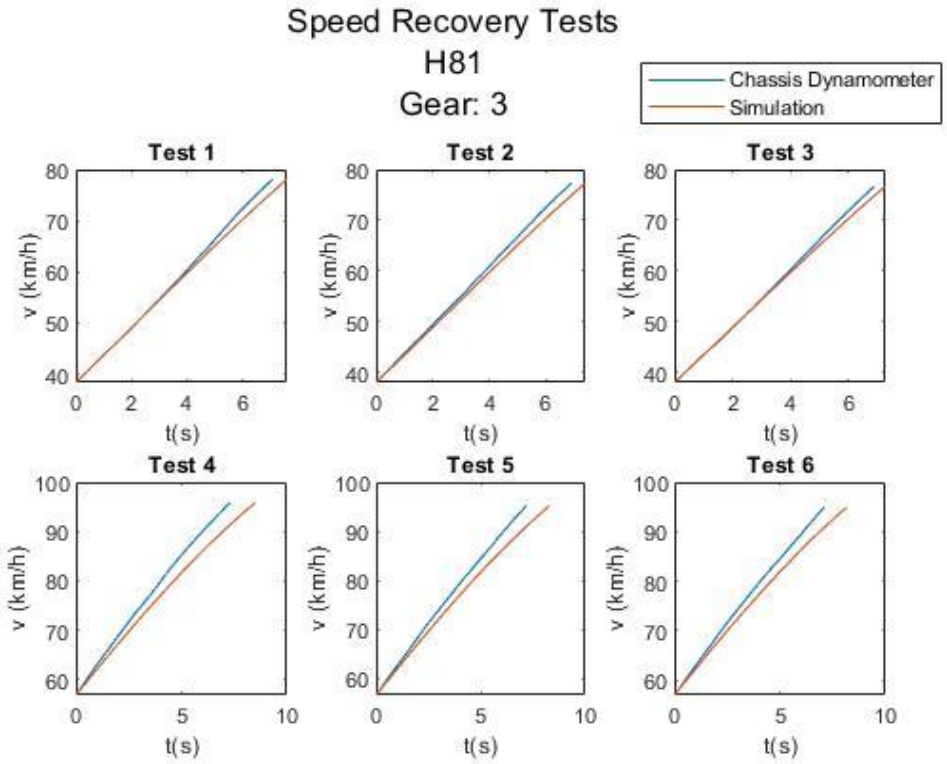

Figure 5.64: Experimental and simulated speed recovery tests for the H81 in third gear.

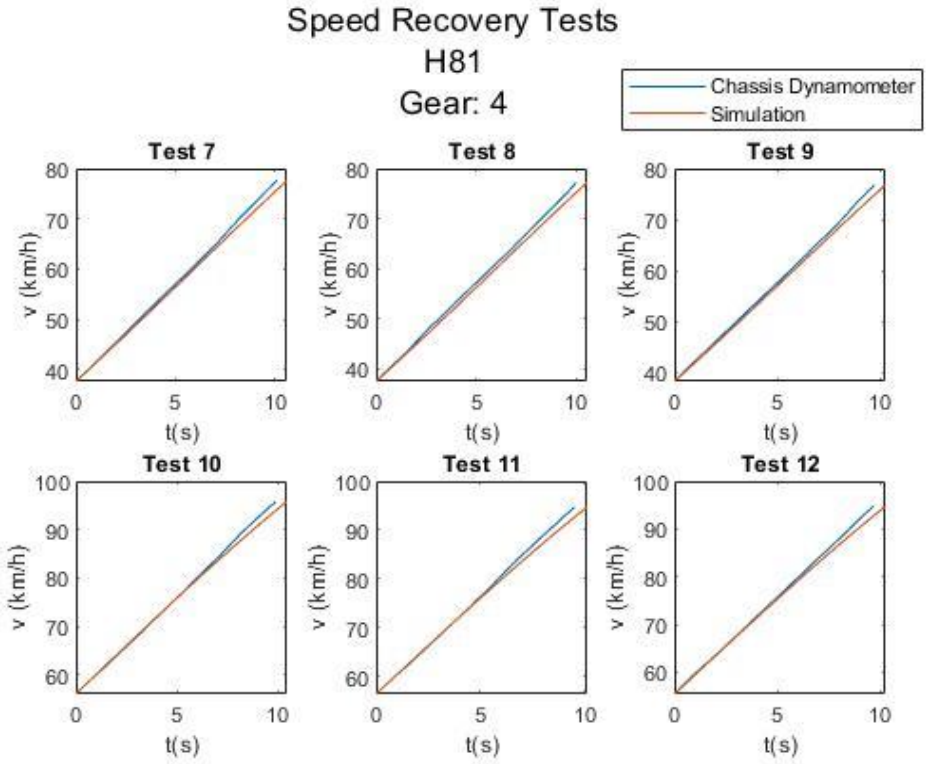

Figure 5.65: Experimental and simulated speed recovery tests for the H81 in fourth gear.

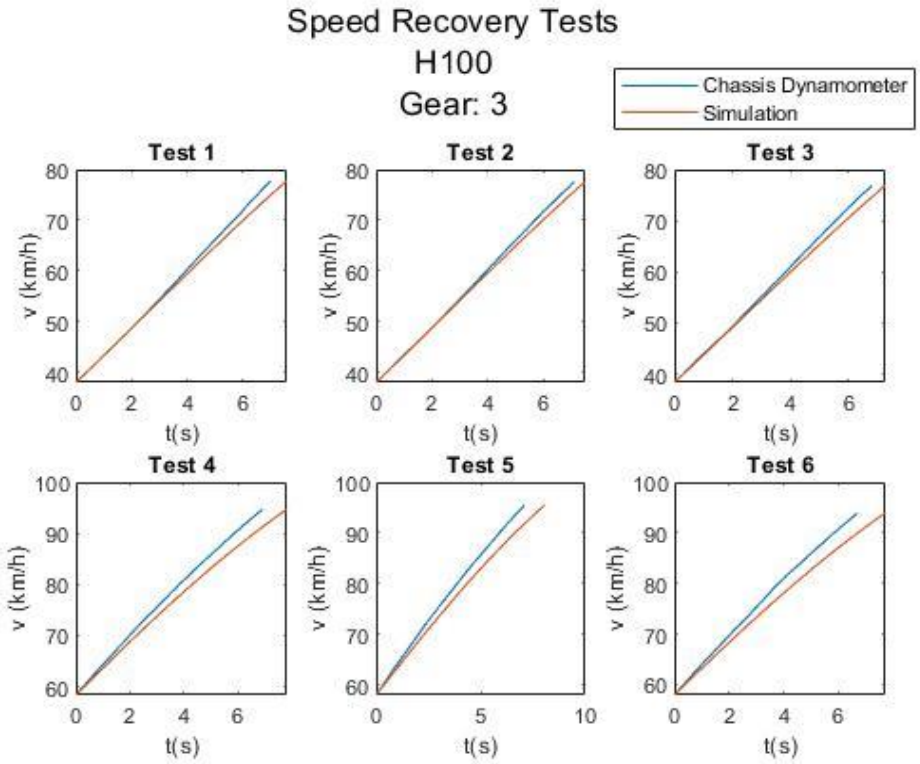

Figure 5.66: Experimental and simulated speed recovery tests for the H100 in third gear.

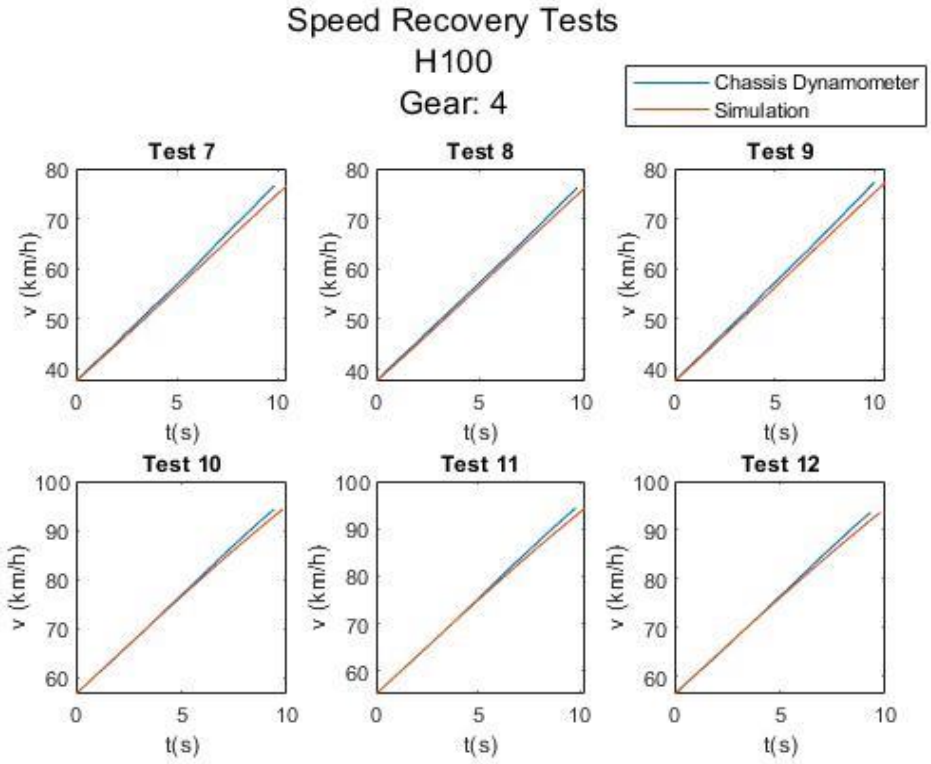

Figure 5.67: Experimental and simulated speed recovery tests for the H100 in fourth gear.

From the speed values provided by the SPARC Vehicle software, it was possible to determine the speed recovery time of each interval from the equation 4.64. So, it was calculated the error between the simulation and the experiment by the coefficient of determination (R^2). The speed recovery time of the experiment was also compared with the numerical model through the mean quadratic error (EQM) between both. All results can be found in Appendix V, being the minimum quadratic error of 0,192 seconds and the maximum of 0,738 seconds.

Figure 5.68 shows the R^2 that represents the approximation for all the numerical simulations in relation to each test done in chassis dynamometer. Figure 5.69 represents the EQM for the same.

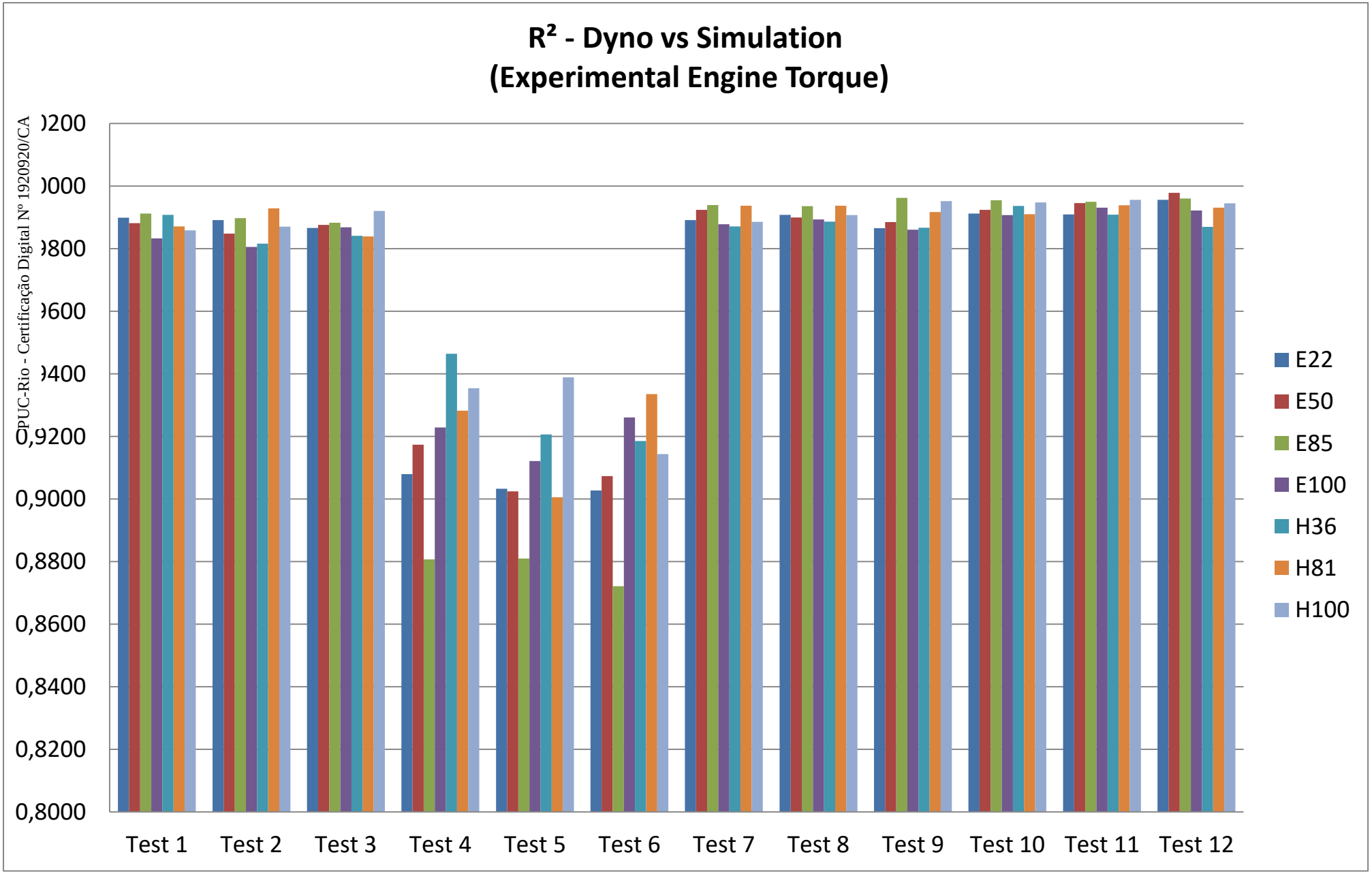

Figure 5.68: Coefficient of determination of the simulated results in relation to the experiments in dyno.

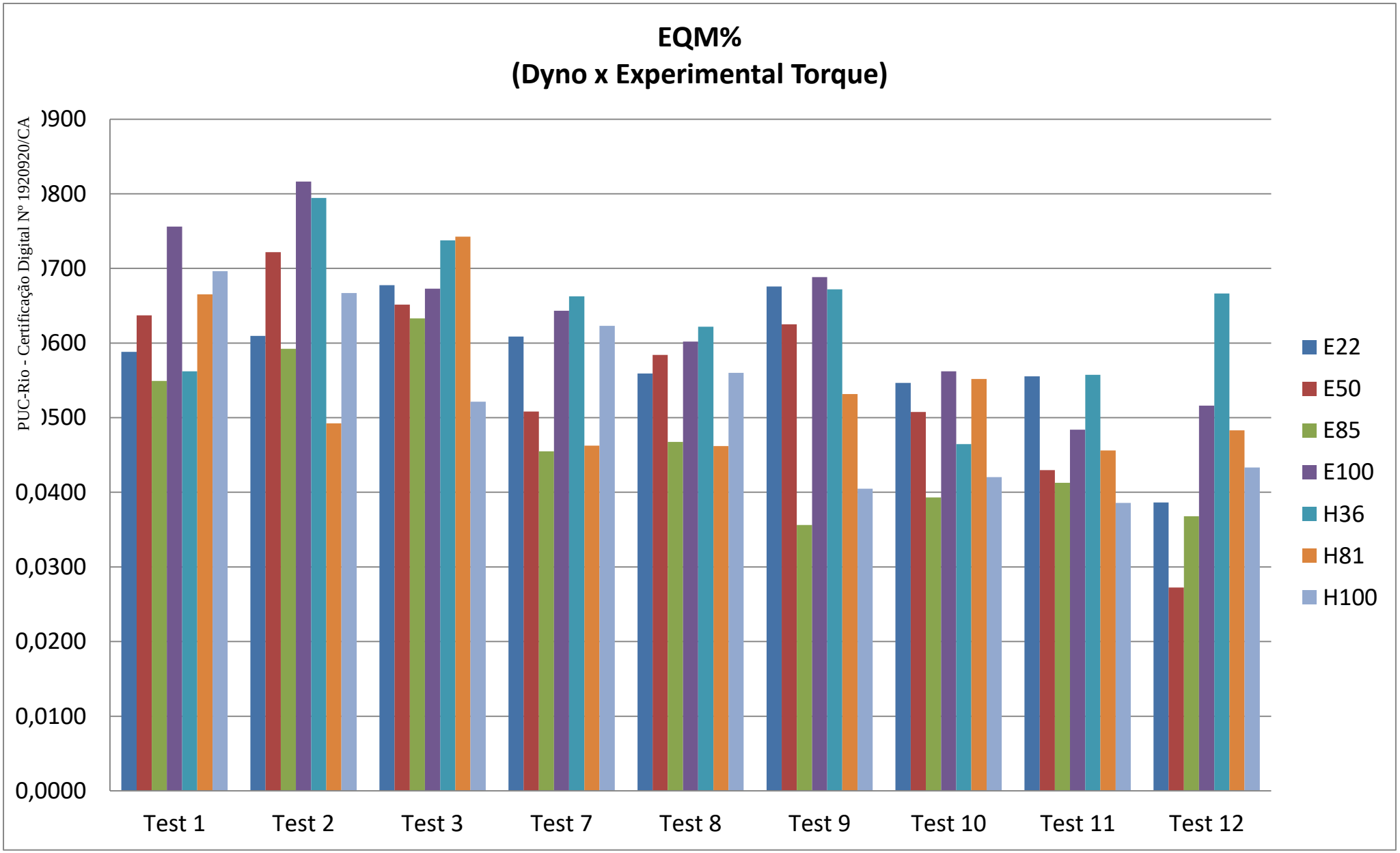

Figure 5.69: EQM% of the simulations by experimental torque of the bench engine for the speed recovery tests.

When the automobile is in a certain speed during the acceleration in chassis dynamometer, sometimes the engine is in higher revolutions than those tested with the ICE in the bench (3500 RPM). As a result, the torque calculated by polynomins is not the same as the TU3 engine torque during the speed recovery experiment. This occurred mainly for tests 4, 5 and 6. This can be perceived by the low values of R^2 in relation to the rest of the experiments. Therefore, these tests were excluded from the calculation of the EQM%, because it was already known that they provide the farthest results from the experimental ones in relation to all other tests.

The only tests on chassis dynamometer that has the engine speed interval between the final and initial velocity within the measured range of the bench tests are those of fourth gear between of approximately 40 to 80 km/h (tests 7, 8 and 9), equivalent to 1532.5 and 3064.4 RPM, respectively (see table 5.13). Those close to the range of 60 to 100 km/h, for the same gear, (tests 10, 11 and 12) have a small interval outside this margin, reaching almost 3830 RPM. However, this small overtaking did not generate significant mean quadratic errors.

From the analyzed results, we can conclude that it is necessary to do more tests with the TU3 engine in higher rotational speeds, so that the results will have greater precisions in situations where the vehicle can be at higher speeds.

In addition to the errors associated with torque, it is possible to identify other sources of inaccuracies in the calculations. As already seen, the transmission efficiency is not a constant value and this was estimated in the model. Therefore, this is a source of error that should be considered, as it was seen for the fourth gear tests between 60 and 100 km/h that this tends to grow above 90% as the speed rises.

In addition, the torque curves used in the simulation come from tests with the internal combustion engine in a bench and its electronic injection module is opened. Thus, there is greater control of the engine operating conditions. On the other hand, the vehicle used a closed ECU.

Therefore, it is not possible to know whether the conditions during the test of the mixture and ignition timing are similar to those tested with the engine on the bench. However, the transmission efficiency curves (figures 5.45 to 5.48) were satisfactory for the approximation of this parameter, except for the speed recovery tests referring to the third gear between 60 and 100 km/h, whose engine speeds intervals exceeded most of the time the 3500 RPM, maximum speed tested in the bench with the TU3 engine.

5.8.3.2 Comparison with Pressure Curves and Friction Models

For comparison with the experimental torque of the engine and validation of the SI friction models for the calculation of the vehicle's acceleration performance, the same procedure of section 5.8.3.1 was used, but using the torque curves obtained in section 5.6.4, related to the friction models for SI engines. Figure 5.70 represent the speed recovery tests calculated using the Sandoval (2003) and Heywood (1988) friction models and the pressure curves of the engine that was obtained in the bench. Knowing that the chassis dynamometer tests that are within the torque range measured by the bench are those of fourth gear whose speeds are approximately between 40 to 80 km/h, it was decided to use these experiments for the purpose of comparation and also because the better values of R^2 and EQM%.

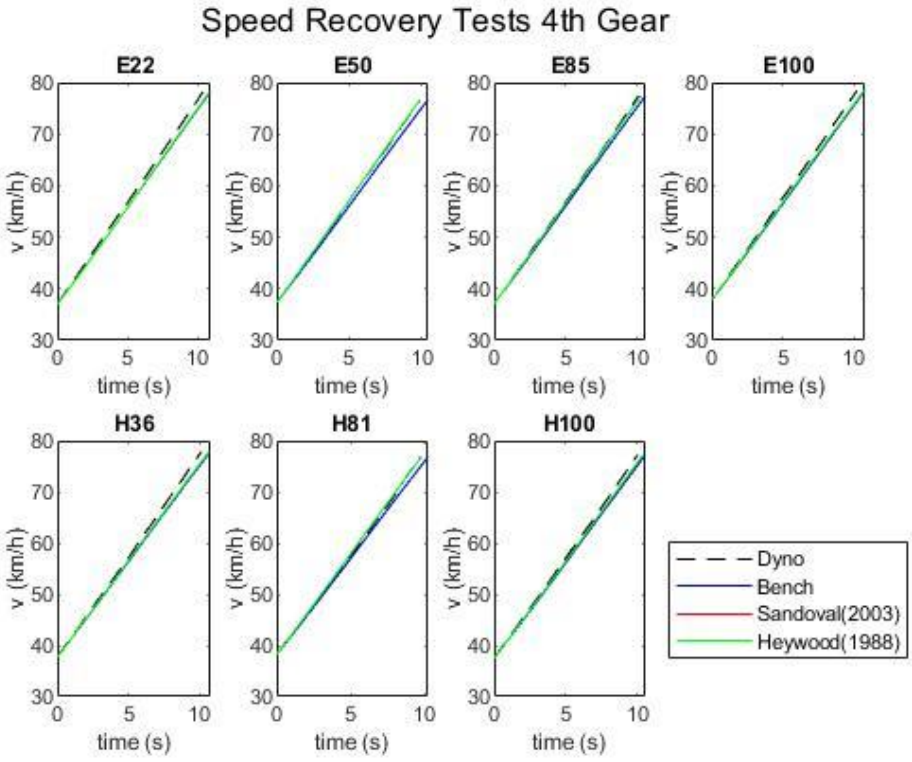

Figure 5.70: Experimental speed recovery tests and simulated by friction models for the all fuels in fourth gear.

In Appendix V it can be observed low values of EQM and EQM% referring to the approximation of v_v x t graphs obtained by a first order polynomial in all bench simulation (including with friction models). All were smaller than 0.08 km/h and with low dispersion of the results, demonstrating a good accuracy of the the results.

The comparison of these results in conjunction with those of the experimental torque of the engine in relation to the vehicle speed recovery tests performed in a chassis dynamometer can be found in figures 5.71 to 5.77 and tables that show the R^2 values:

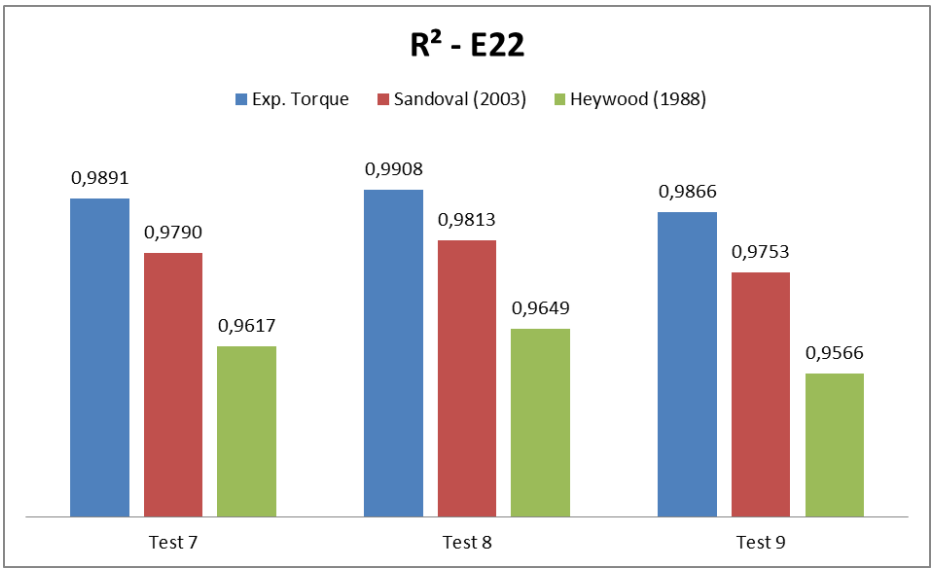

Figure 5.71: Comparison of the R^2 for the E22 fuel.

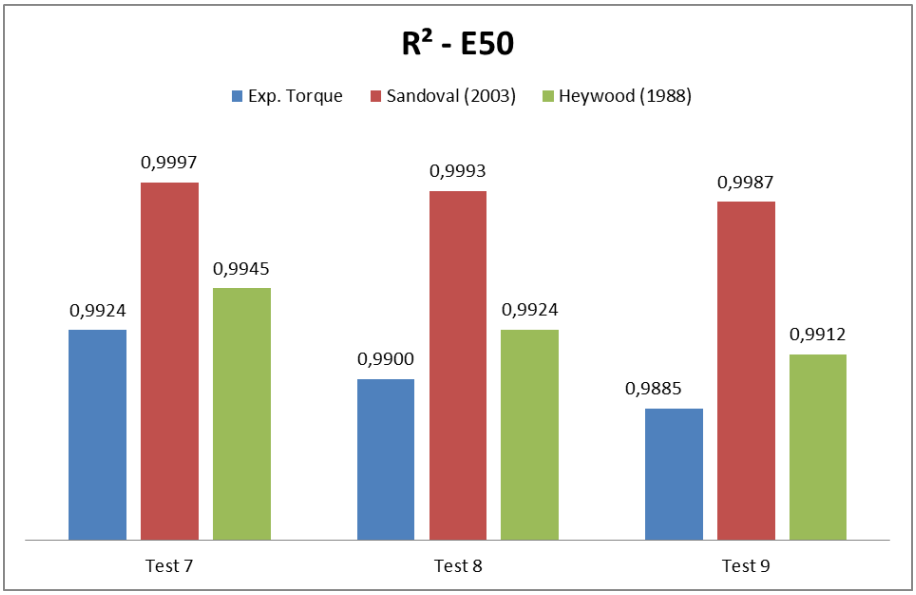

Figure 5.72: Comparison of the R^2 for fuel E50.

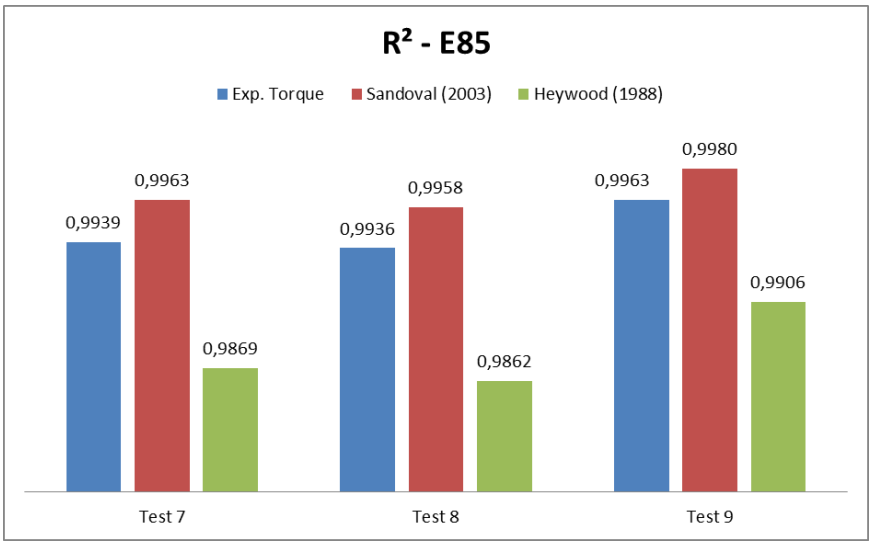

Figure 5.73: Comparison of the R² for fuel E85.

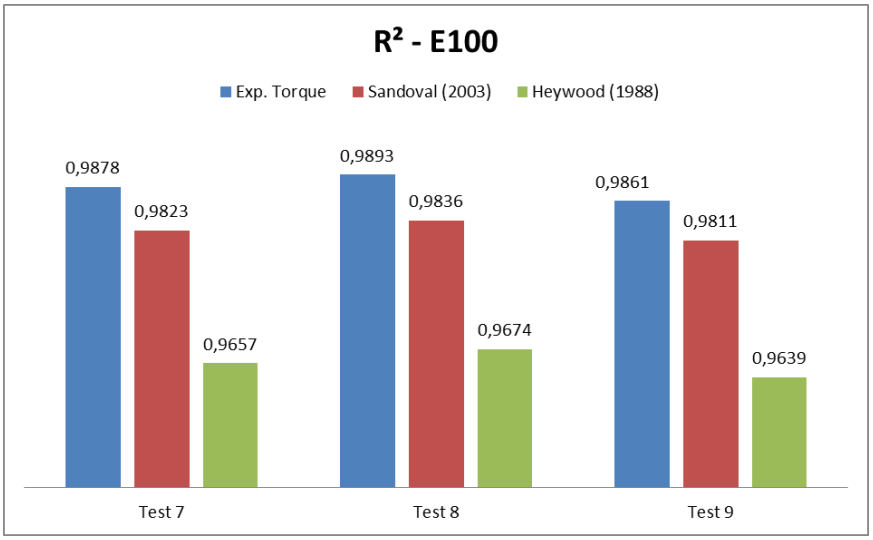

Figure 5.74: Comparison of R² for fuel E100.

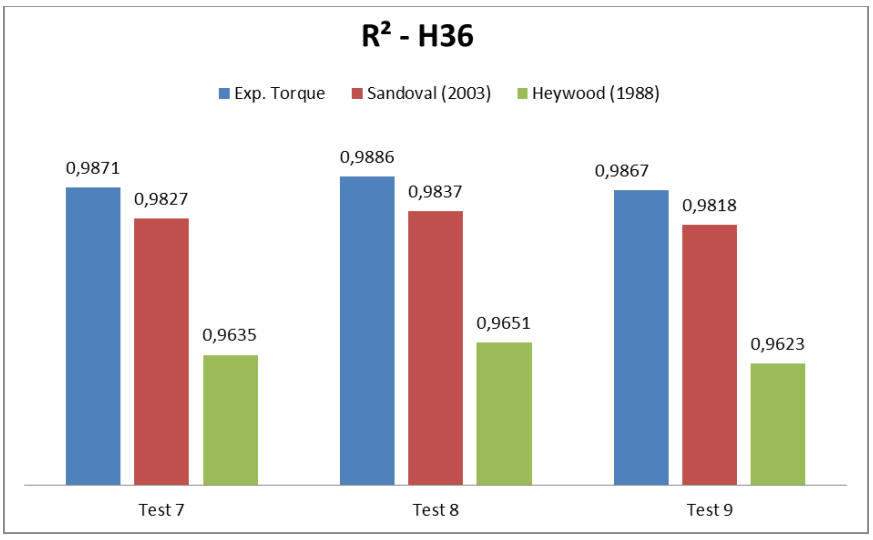

Figure 5.75: Comparison of R² for H36 fuel.

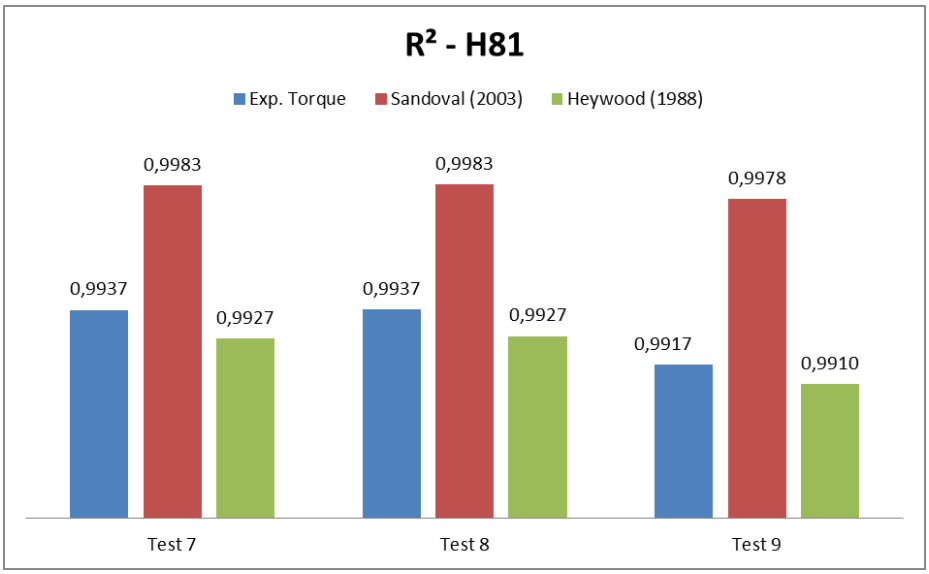

Figure 5.76: Comparison of R² for H81 fuel.

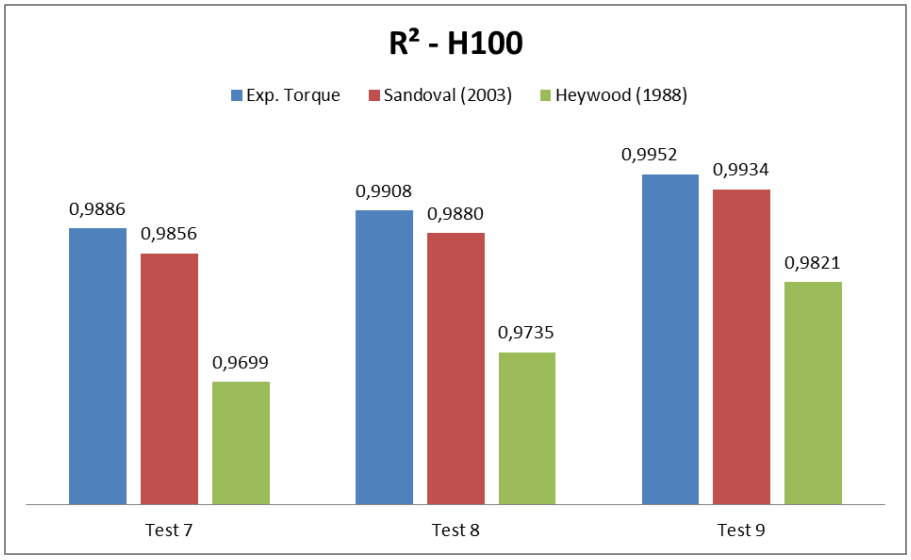

Figure 5.77: Comparison of the R² for the H100 fuel.

It can be noted that among all the models, the one proposed by Heywood (1988) presented R² values more distant from the dyno experiments in all tested fuels. Nevertheless, the results were satisfactory since the minimum values are above 0.96 and the maximum exceeds 0.99. The lowest Values of R² come from H100, E22 and H36. According to Figure 5.34, the torque values calculated by the model are lower than those experimental in some engine speed ranges throughout the acceleration test. Consequently, according to equation 4.64, the recovery time will be longer because of the lower traction force on the wheels.

In appendix VI the average accelerations obtained for these tests can be found according to all the models mentioned, including the experimental on the dyno. As already mentioned, this parameter was obtained by the inclination of the straight line of the vehicle speed x speed recovery time diagram.

As tests 8 and 9 are repetitions of test 7, it was decided to take an average of the Appendix VI values and these can be seen in Table 5.18 and the error to the experimental acceleration is in Figure 5.79.

Acceleration Performance (m/s²)					
Fuel		Dyno	Bench	Sandoval (2003)	Heywood (1988)
E22	Average	1,1001	1,0549	1,0334	1,0088
	SD	0,0051	0,0047	0,0043	0,0042
E50	Average	1,1052	1,0568	1,0915	1,0588
	SD	0,0032	0,0022	0,0021	0,0021
E85	Average	1,1023	1,0671	1,0701	1,0430
	SD	0,0035	0,0025	0,0025	0,0025
E100	Average	1,1027	1,0504	1,0304	1,0056
	SD	0,0027	0,0016	0,0009	0,0009
H36	Average	1,1029	1,0450	1,0300	1,0015
	SD	0,0040	0,0013	0,0011	0,0011
H81	Average	1,0949	1,0524	1,0694	1,0528
	SD	0,0024	0,0010	0,0010	0,0115
H100	Average	1,0989	1,0544	1,0428	1,0168
	SD	0,0085	0,0044	0,0044	0,0043

Table 5.18: Average values of the accelerations for tests 7, 8 e 9.

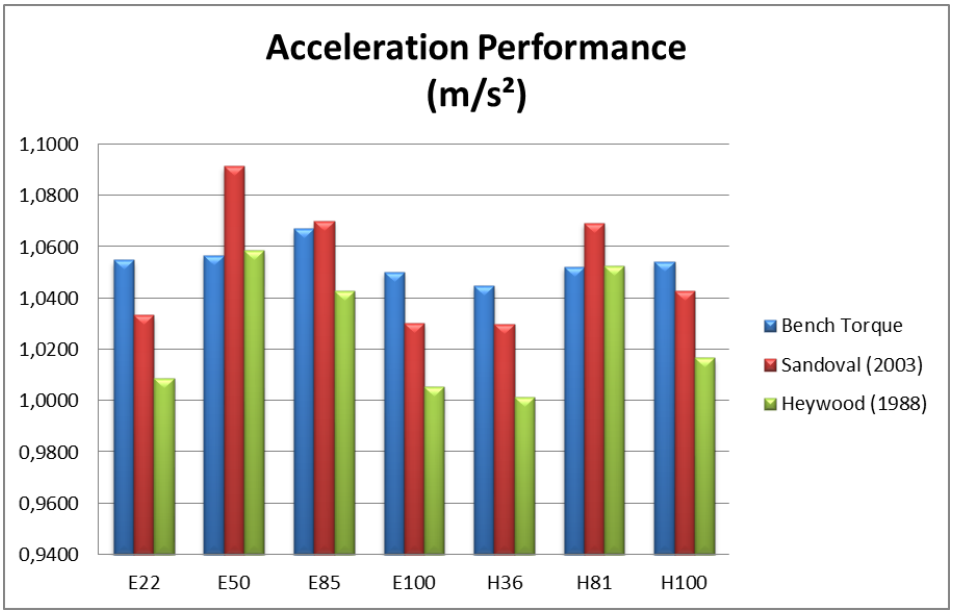

Figure 5.78: Acceleration performance according to each proposed model for all fuels tested.

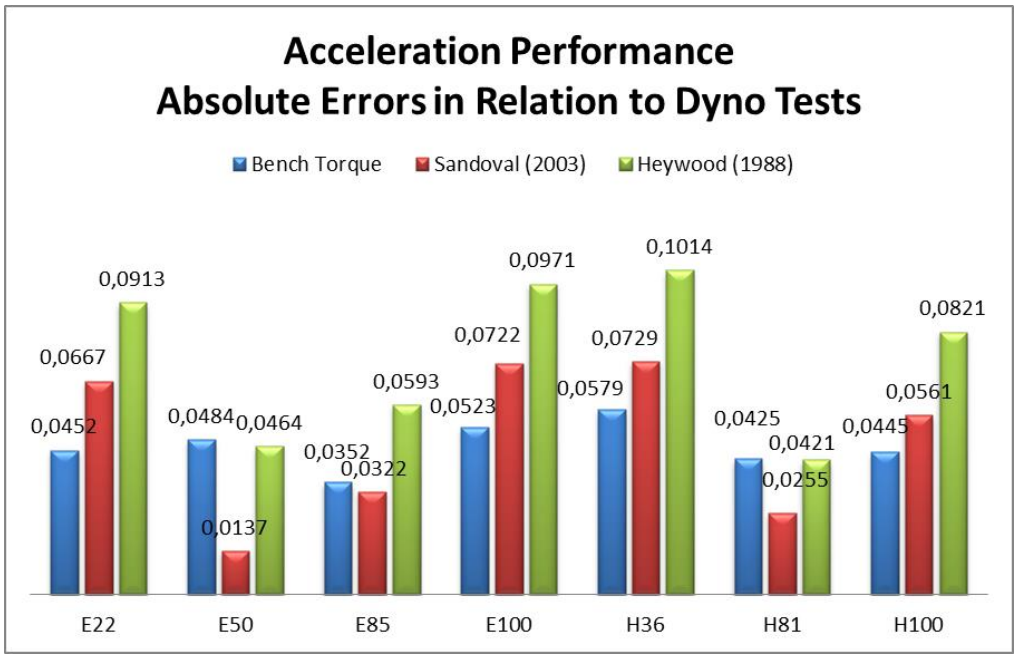

Figure 5.79: Acceleration performance absolute errors of the proposed models in relation to the experimental results on dyno.

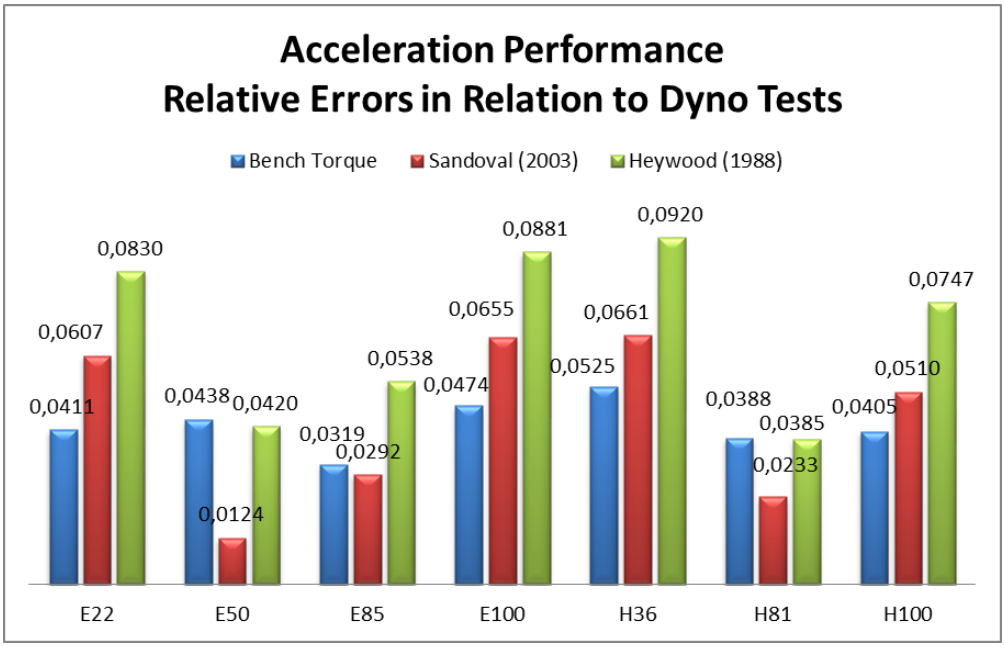

Figure 5.80: Acceleration performance relative errors of the proposed models in relation to the experimental results on dyno.

The proposed performance simulation models presented good proximity with the chassis dynamometer experiments. Note that the largest associated errors are given by the Heywood correlation (1988), but they are no more than 9.2% representing 0,1014 m/s² of absolute difference.

, This model that used the real torque obtained with the engine on the bench has greater precision for most cases, which was expected since it cancels out the errors associated with engine mechanical efficiency models. On the other

hand, in some cases, Sandoval's (2003) correlation showed better results because of its higher torque curve, which is a result of smaller friction than the real one, thus increasing the vehicle's performance. From this analysis, it can be concluded that a small difference in engine mechanical efficiency generates a very relevant influence in vehicle performance.

With regard to the simulations performed by the engine torque, it can be noted that the fuel with the greatest acceleration capacity was E85 and not E50, as seen in the chassis dynamometer tests. This difference can be attributed to the central electronics module, which provided λ values that characterized rich mixtures for all three engine speeds that were tested with the E85. As a result, greater fuel burn provides greater power and, consequently, greater vehicle acceleration capacity.

Figure 5.72, referring to the R^2 of the models proposed for the E50 fuel, shows the only case in which the simulation made from the real torque of the engine on the bench has a greater distance from the experiments in relation to those of Sandoval (2003) and Heywood (1988). Furthermore, it can be noted from the simulations that the E100 was also lower in its acceleration capacity in relation to the rest of the other fuels, contradicting the Peugeot vehicle speed recovery tests, in which this was one of the best performances.

Figure 5.81 shows the TU3 torque map for the speed range of this analysis. It can be noted that the E100 has the largest torque curve, which is in accordance with what was expected from the vehicle tests, as the greater the torque, the better the acceleration capacity. Therefore, it can be concluded that the source of inaccuracy is the transmission efficiency.

The transmission efficiency for the E100 was lower than for other fuels, according to Tables 5.14 and 5.15. This decrease in this parameter contributed to a lower acceleration capacity in relation to the E22 and E50. Note in Table 5.18 that the average accelerations are very close. Thus, a lower value in transmission efficiency contributes to a decrease in vehicle acceleration.

According to Figure 5.82, it can be see that H36, among the hydrated fuels, had the largest torque curve, which would favor higher performance. However, Table 5.17 showed that, among these blends, the H36 is one with the lowest average acceleration for most of the tests. On the other hand, Figure 5.53 is in agreement with Figure 5.82, which leads to the conclusion that the source of the error is the transmission efficiency, since this is lower for the H36 than for the H81 and H100.

It can be concluded that there are still improvements to be made in the transmission efficiency, which was considered as constant in this work, based on the average of the values obtained in the tests.

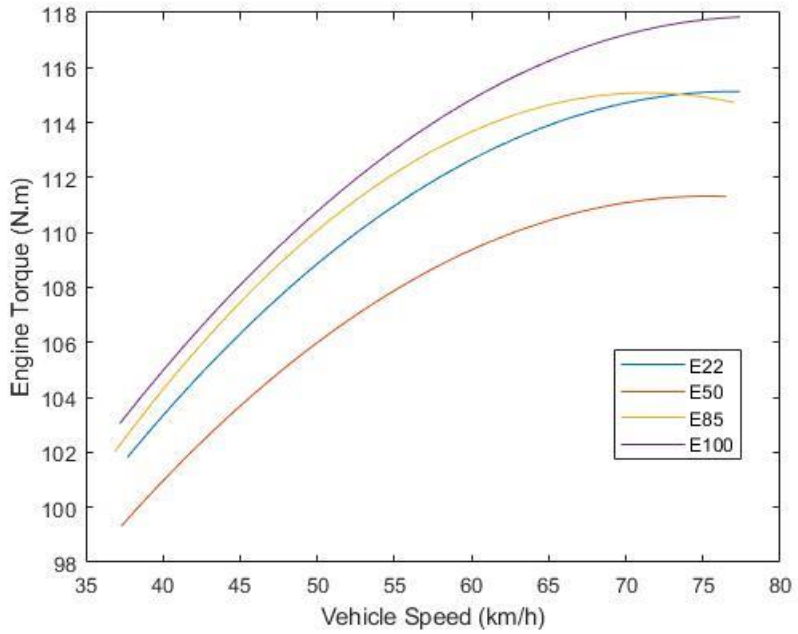

Figure 5.81: Torque vs Vehicle Speed for the 4th gear low speed range using mixtures of anhydrous ethanol and gasoline.

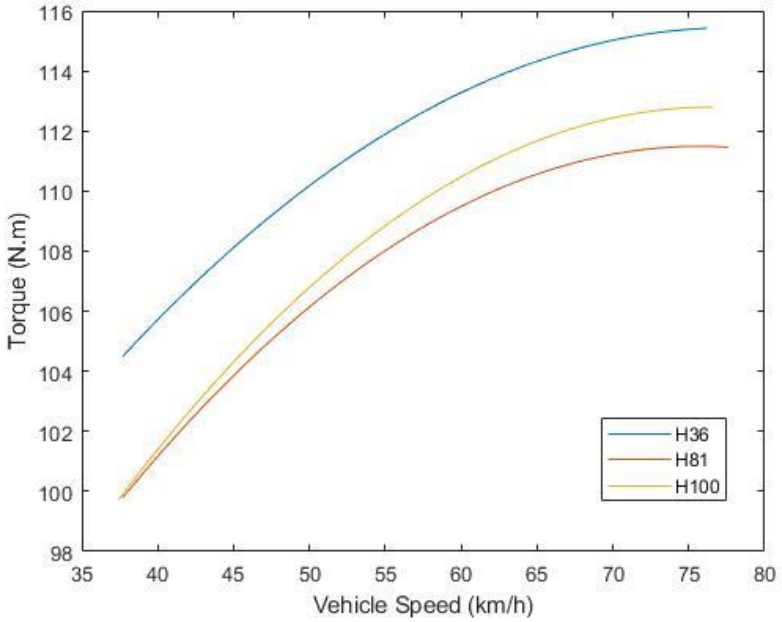

Figure 5.82: Torque vs Vehicle Speed for the 4th gear low speed range using mixtures of hydrated ethanol and gasoline.

5.8.4 Speed Recovery Time Errors

. Table 5.19 and figure 5.83 show the experimental and simulated results of the speed rescovery time for the fourth-gear tests in the near range between 40 and 80 km/h. The values for the CV (Coefficient of Variation), SD (Standard Deviation) for the mean Δt (absolute difference between the experimental and the simulated times) can be seen.

Fuel	tdyno (s)	tsim (s)	Δt(s)	Dif. (%)	Average Δt (s)	SD	CV
E22	10	10,57	0,57	5,65	0,5411	0,0804	0,14857072
	10,4	10,94	0,54	5,16			
	10,5	11,10	0,60	5,67			
E50	9,9	10,39	0,49	4,91			
	9,9	10,42	0,52	5,30			
	9,9	10,47	0,57	5,75			
E85	10,1	10,54	0,44	4,31			
	10,1	10,58	0,48	4,80			
	10	10,35	0,35	3,48			
E100	10,1	10,71	0,61	6,05			
	10,2	10,78	0,58	5,69			
	10	10,65	0,65	6,50			
H36	9,7	10,28	0,58	5,98			
	10,1	10,73	0,63	6,20			
	9,9	10,54	0,64	6,50			
H81	10,1	10,60	0,50	4,97			
	9,7	10,23	0,53	5,48			
	10	10,55	0,55	5,47			
H100	9,8	10,43	0,63	6,38			
	10	10,55	0,55	5,50			
	9,8	10,17	0,37	3,76			

Table 5.19: Peugeot 207 SW speed recovery tests comparison between simulation and dyno tests in the fourth-gear between approximately 40 to 80 km/h.

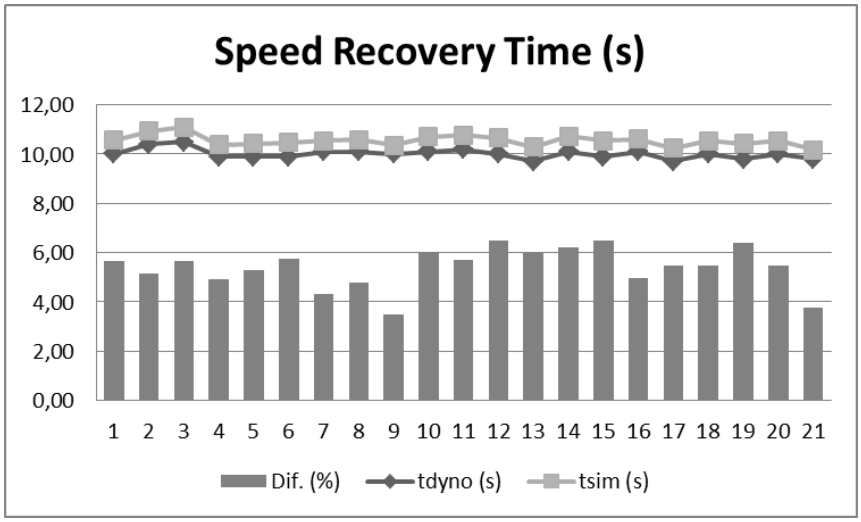

Figure 5.83: Simulated and experimental results of the speed recovery time for all fourth-gear tests at the interval 40 to 80 km/h.

The results of the simulated speed recovery time for this configuration did not exceed 6.38% in relation to the experimental one. Table 5.20 and Figure 5.84 correspond to fourth-gear tests between approximately 60 and 100 km/h.

Fuel	tdyno (s)	tsim (s)	Δt(s)	Dif. (%)	Average Δt (s)	SD	CV
E22	9,6	10,21	0,61	6,32	0,5124	0,0729	0,14219476
	9,4	9,96	0,56	5,96			
	9,3	9,77	0,47	5,09			
E50	9,7	10,25	0,55	5,71			
	9,6	10,07	0,47	4,91			
	9,8	10,12	0,32	3,27			
E85	9,3	9,75	0,45	4,86			
	10	10,50	0,50	5,01			
	9,9	10,36	0,46	4,60			
E100	9,7	10,29	0,59	6,07			
	9,7	10,25	0,55	5,70			
	9,8	10,32	0,52	5,26			
H36	9,5	9,98	0,48	5,03			
	9,8	10,36	0,56	5,76			
	9,5	10,12	0,62	6,49			
H81	9,5	10,10	0,60	6,31			
	9,9	10,45	0,55	5,57			
	9,7	10,27	0,57	5,91			
H100	9,8	10,25	0,45	4,64			
	9,4	9,81	0,41	4,35			
	9,3	9,76	0,46	4,97			

Table 5.20: Peugeot 207 SW speed recovery tests comparison between simulation and dyno tests in the fourth-gear between approximately 60 to 100 km/h.

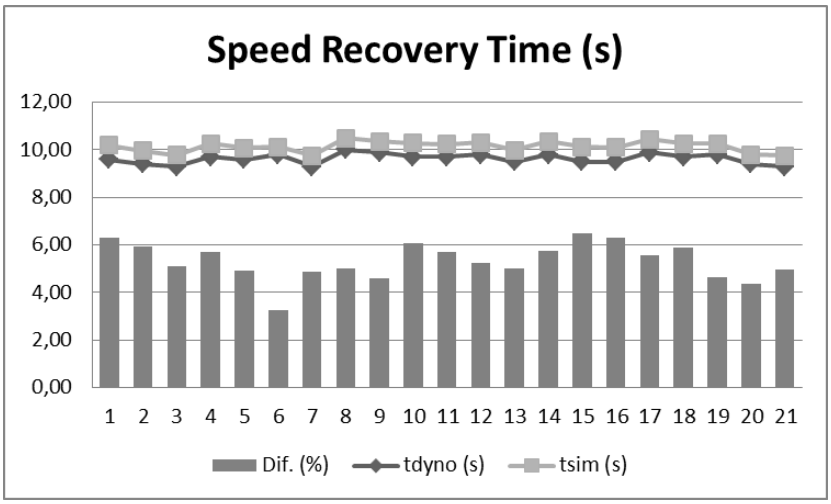

Figure 5.84: Simulated and experimental results of the speed recovery time for all fourth-gear tests at the interval 60 to 100 km/h

The maximum difference obtained in this configuration was 6.49%. It is noted that the overtaking of the 3500 RPM, maximum tested engine speed in the bench did not generate relevant differences with regard to model errors. The mean value of the time variation between the experiment and the simulation was lower than in the interval 40 to 80 km/h. This configuration also presented a lower

value of the coefficient of variation and in the standard deviation. However, there are aproximations in these values.

Table 5.21 and Figure 5.85 show the values for third gear between 40 and 80 km/h.

Fuel	tdyno (s)	tsim (s)	Δt(s)	Dif. (%)	Average Δt (s)	SD	CV
E22	7,1	7,53	0,43	6,12	0,4765	0,0568	0,119136
	6,9	7,31	0,41	6,00			
	7,1	7,58	0,48	6,83			
E50	7,1	7,57	0,47	6,57			
	7,2	7,72	0,52	7,23			
	7	7,48	0,48	6,82			
E85	7	7,43	0,43	6,12			
	7,1	7,59	0,49	6,89			
	7	7,50	0,50	7,21			
E100	7,5	8,08	0,58	7,73			
	7,3	7,85	0,55	7,48			
	6,8	7,27	0,47	6,96			
H36	7,1	7,50	0,40	5,59			
	6,9	7,44	0,54	7,79			
	6,8	7,26	0,46	6,77			
H81	7,1	7,60	0,50	7,07			
	6,9	7,28	0,38	5,46			
	6,9	7,39	0,49	7,13			
H100	7	7,58	0,58	8,28			
	6,8	7,26	0,46	6,78			
	7,1	7,48	0,38	5,36			

Table 5.21: Peugeot 207 SW speed recovery tests comparison between simulation and dyno tests in the third-gear between approximately 40 to 80 km/h.

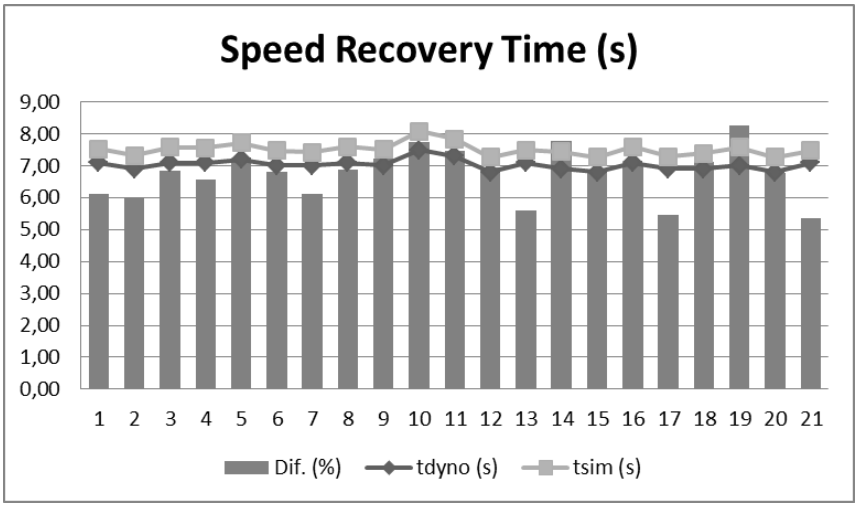

Figure 5.85: Simulated and experimental results of the time of recovery of velocity for all tests in third gear at the interval 40 to 80 km/h.

It was noted that the maximum difference of the design of the experiment was 8.38%. It can be seen that the error values in general were higher than those in the fourth gear in the same speed ranges. Nevertheless, mean differences between the experiment and the simulation were lower, with a lower dispersion and lower coefficient of variation.

It was seen in this part of the work that the values of $\Delta t_{dyno\text{-}sim,\ med}$, and their respective SD and CV indicate close results to the experiments. In addition, it was noted in the previous sections that the simulations conducted in third gear in the range close to 60 to 100 km/h are very far from the experiment because the rotational engine speed range in the experiment is mostly higher than that tested in the bench. Therefore, these tests were discarded from this section.

The results referring to the third gear for the higher speed intervals can be seen in Figure 5.86 that shows these error measures for all settings.

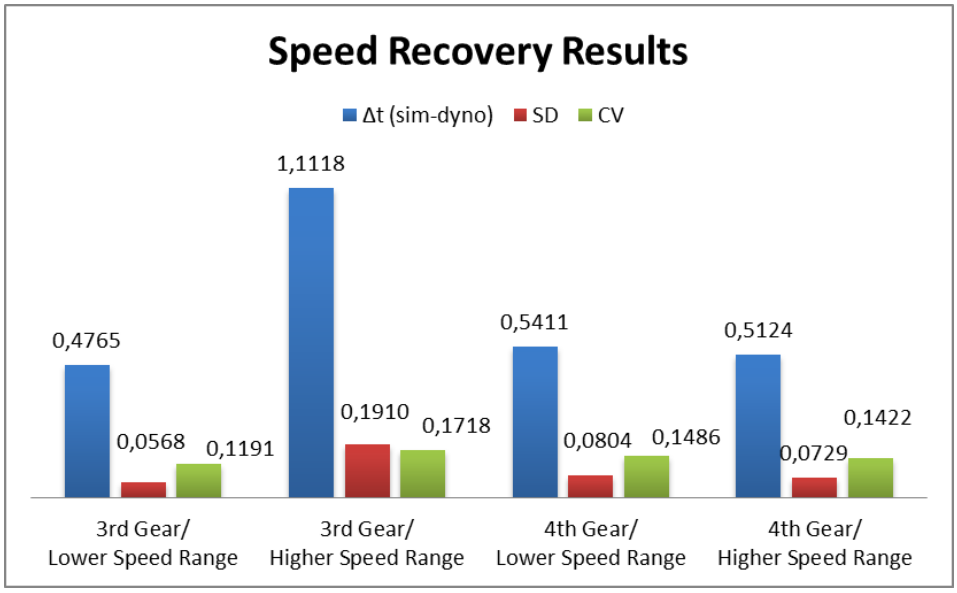

Figure 5.86: Coefficient of variation, standard deviation and absolute differences between experimental and simulated recovery time.

It is noticed that the average error for the tests whose engine speeds comprise the interval tested with the engine in the bench have very close values (between 0.4765 and 0.5411 s). In addition, all results for these experiments provided CV values lower than 15%, indicating a low dispersion of the results.

Due to the results of figure 5.86, the results indicated values close to the mean difference between the experimental and simulated speed recovery times and low dispersion, the CV and SD were also calculated in relation to all these tests together, except for those performed in the third gear for speeds close to the range of 60 to 100 km/h due to the greatest errors.

Thus, an average was obtained in the difference of experimental and simulated speed recovery time of 0.51 seconds with a standard deviation of 0.005696 seconds and a CV of 0.1479 that indicates a low dispersion of the data.

The following analysis is for the speed recovery time calculated by pressure curves and friction models proposed by Heywood (1988) and Sandoval (2003):

Fuel	tdyno (s)	tsim (s)	Δt(s)	Dif. (%)	Average Δt (s)	SD	CV
E22	10	10,80	0,80	8,00	0,5659	0,2404	0,42474868
	10,4	11,18	0,78	7,53			
	10,5	11,35	0,85	8,10			
E50	9,9	10,06	0,16	1,57			
	9,9	10,09	0,19	1,96			
	9,9	10,14	0,24	2,41			
E85	10,1	10,49	0,39	3,90			
	10,1	10,55	0,45	4,41			
	10	10,31	0,31	3,09			
E100	10,1	10,91	0,81	8,05			
	10,2	11,00	0,80	7,84			
	10	10,84	0,84	8,44			
H36	9,7	10,43	0,73	7,56			
	10,1	10,90	0,80	7,91			
	9,9	10,70	0,80	8,12			
H81	10,1	10,43	0,33	3,28			
	9,7	10,07	0,37	3,78			
	10	10,37	0,37	3,75			
H100	9,8	10,53	0,73	7,41			
	10	10,65	0,65	6,54			
	9,8	10,27	0,47	4,77			

Table 5.22: Peugeot 207 SW speed recovery tests comparison between simulation and dyno tests in the third-gear between approximately 40 to 80 km/h, according to Sandoval (2003).

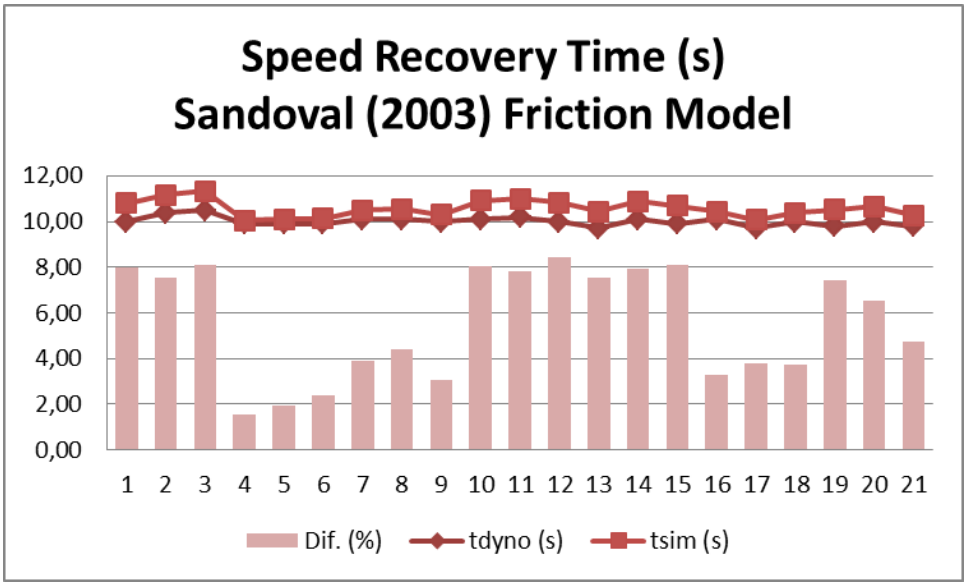

Figure 5.87: Speed recovery for all third-gear tests close to 40 to 80 km/h, according to Sandoval (2003).

Fuel	tdyno (s)	tsim (s)	Δt(s)	Dif. (%)	Average Δt (s)	SD	CV
E22	10	11,06	1,06	10,65	0,8429	0,2419	0,28697671
	10,4	11,46	1,06	10,18			
	10,5	11,63	1,13	10,77			
E50	9,9	10,36	0,46	4,66			
	9,9	10,40	0,50	5,06			
	9,9	10,45	0,55	5,52			
E85	10,1	10,77	0,67	6,58			
	10,1	10,82	0,72	7,11			
	10	10,57	0,57	5,75			
E100	10,1	11,19	1,09	10,77			
	10,2	11,28	1,08	10,55			
	10	11,12	1,12	11,17			
H36	9,7	10,73	1,03	10,59			
	10,1	11,21	1,11	10,96			
	9,9	11,01	1,11	11,17			
H81	10,1	10,68	0,58	5,73			
	9,7	10,31	0,61	6,25			
	10	10,62	0,62	6,21			
H100	9,8	10,80	1,00	10,16			
	10	10,93	0,93	9,27			
	9,8	10,53	0,73	7,44			

Table 5.23: Peugeot 207 SW speed recovery tests comparation between simulation and dyno tests in the third-gear between approximately 40 to 80 km/h, according to Heywood (1988).

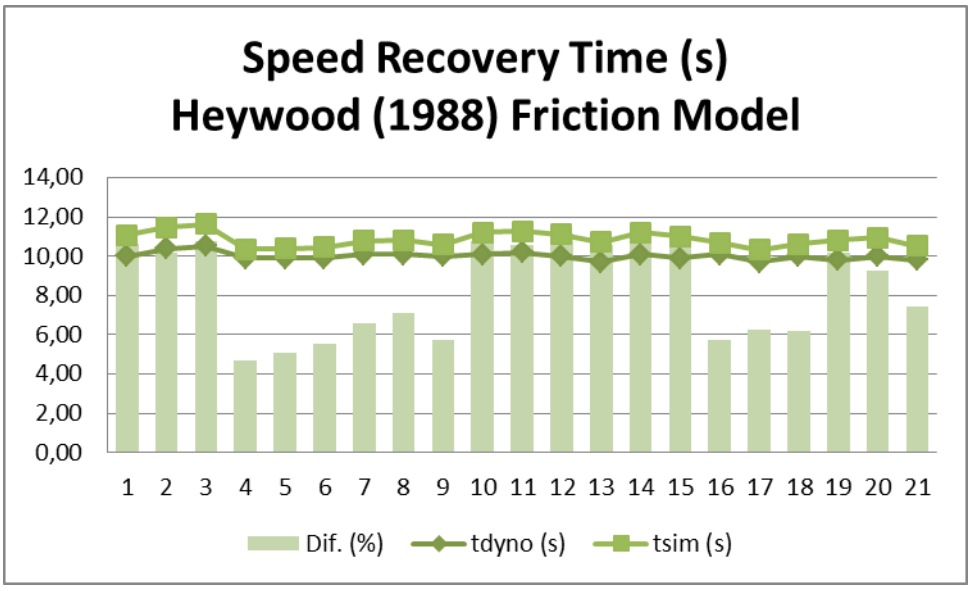

Figure 5.88: Simulated and experimental results of the velocity recovery time for all third-gear tests close to 40 to 80 km/h, according to Heywood (1988).

The results for the experimental torque obtained with the AVL engine dynamometer proved to be the most accurate, except for fuels E50, E85 and H81 in which the Sandoval model (2003) was closer. As has already been seen, over the interval measured with the engine in the bench, the simulated torque curves tend to be larger than the experimental ones and approach as the engine speed increases. Higher torque values generate lower speed recovery time. As a result, the correlation of Sandoval (2003) demonstrated a good approximation.

The CV values were high, which indicates a great variation of the results in relation to the mean. But this doesn't mean poor results since the maximum differences between the speed recovery times for the Sandoval (2003) and Heywood (1988) model were 8.44% and 10.77%, while the average differences of the results were 0.565 and 0.843 seconds, respectively.

Given the results of performance simulations, it can be said that the best model is the one that uses the torque measured on the bench, because it reduces errors related to mechanical efficiency. In the absence of an engine dynamometer, it is recommended to use the Sandoval correlation (2003). However, this requires very specific geometric parameters of the engines. If these characteristics are not known, the Heywood model (1988) should be used.

6 Conclusions

In this section, the conclusions obtained in chapter 5 will be shown, referring to the objectives of chapter 3. First, the results obtained from the vehicle performance simulations and the errors related to the speed recovery time will be mentioned. Soon after, the results obtained in the tests with the engine on the bench and with the vehicle in chassis dynamometer will be mentioned, in order to evaluate the performance parameters of both. Subsequently, the complementary results that were obtained for the development of the work will be mentioned, which refer to the simulations of coastdown and motored tests.

Finally, some suggestions for future work will be provided as a complement to the current one.

6.1 Vehicle Performance Simulation

It was seen that there is currently a great need in the development of new fuels that allow automobiles good performance characteristics. In order to eliminate the difficulties mentioned in section 1.4 for carrying out speed recovery tests on the track, this work proposed a vehicle performance simulation model based on laboratory tests only with the internal combustion engine.

The proposed model uses the vehicular longitudinal dynamics equation, where the vehicle traction force was calculated in two different ways. The first was through the real engine torque, obtained with the aid of a dynamometer on the engine bench. The second was based on pressure curves, collected by a transducer installed inside the engine combustion chamber.

However, the data processing of the pressure curves only allows obtaining the energy generated inside the combustion chamber, and it is not possible to obtain the power and torque on the crankshaft. Thus, the need for the evaluation of models of friction loss in engines arose. In this work, the correlations proposed by Sandoval (2003) and Heywood (1988) were used.

All tests were carried out with seven different blends of ethanol and gasoline and the validation of the proposed model was carried out from speed recovery tests with the vehicle in a chassis dynamometer. The internal combustion engine was tested in a range between 1300 and 3500 RPM, while the vehicle was accelerated on the third and fourth gear in a chassis dynamometer for speed recovery intervals from 40 to 80 km/h and 60 to 100 km/h.

It was seen that the only tests with the vehicle in a chassis dynamometer that comprise the range of revolutions measured with the engine on the bench were the fourth gear between 40 and 80 km/h. Thus, the simulated average accelerations were compared using these experiments.

The proposed models showed good accuracy with the experiment. The simulations performed with the experimental torque presented better results for most of the tests, where the maximum error in the average acceleration was of 5.25% and 0.06 m/s² of difference in relation to the experiments in chassis dynamometer.

The test simulations based on pressure curves and friction correlations, on the other hand, showed greater errors, which were expected since there are additional errors related to the engine mechanical efficiency. Sandoval's (2003) model presented better results than Heywood (1988) and, in a few cases, better than the model from the experimental torque.

However, despite the greater distance from the model that used the experimental torque, the simulations performed from the pressure curves and friction correlations also showed good tendency and approximation with the chassis dynamometer tests, as the maximum error in acceleration was 9.20%. Furthermore, these results showed R^2 values greater than 0.99, indicating good correlation.

6.1.1 Performance simulation using engine experimental torque

According to the simulations that used the experimental engine torque, it was possible to reach the following conclusions for each test configuration:

Third gear in the lower speed range (≈40 to 80 km/h): It has most of the engine speed interval within the range measured with the engine in the bench. Only the end of the interval is outside, staying around 4000 RPM. The results obtained had a high coefficient of determination (all greater than 0.98 and in

some cases higher than 0.99), with standard deviation of 0.0568 and low dispersion.

Third gear in the higher speed range (≈60 to 100 km/h): These had the biggest errors of all tested configurations. The coefficient of determination was lower than the other tests, while the mean difference in the speed recovery time was greater than one second. However, according to the equation describing the engine-vehicle relationship, the speeds at which the engine is subjected during acceleration in the dyno tests is outside of the measurement range in which the TU3 engine was tested on bench. As a result, there are errors related to the traction force of the vehicle by torque calculation.

Fourth gear in the lower speed range (≈40 to 80 km/h): In this configuration, engine speeds are within the measuring range of bench tests with the TU3. As a result, a high coefficient of determination was obtained, generally greater than 0.9880. The mean difference between the experimental speed recovery time for the simulated was 0.5411 seconds with a standard deviation of 0.0804 and low dispersion of the results.

Fourth gear in the higher speed range (≈60 to 100 km/h): Similarly to the configuration of third-gear with speed interval of 40 to 80 km/h, at a given time during vehicle acceleration the engine speed exceeds the range measured in the engine bench tests (3500 RPM). However, this occurs at the end of the test and this value does not represent a large portion. This can be noticed because the difference between the experimental and simulated speed recovery time was on average 0.5124 seconds with a standard deviation of 0.0729 and low dispersion. A high coefficient of determination can also be noted.

6.1.2 Performance simulation using engine pressure curves and engine friction models

In this work, engine friction was calculated experimentally and through two correlations found in the literature that was proposed by Sandoval (2003) and Heywood (1988).

It was seen that by increasing engine speed, the relative error of mechanical efficiency is reduced, indicating a greater proximity of the simulated results to the real one. The fuels with greater distance from the real friction with

the proposed models are those whose torque curve is bigger, that is, the E85 and the E100, where they had EQM% of 0.1988 and 0.2215, respectively. Nevertheless, both presented good accuracy, with an average relative error between fuels lower than 5% in relation to the experimental results of mechanical efficiency and EQM% of 0.038 and 0.043, indicating a good proximity to the calculation of engine torque from the pressure curves.

The Heywood model (1988) presented a greater distance with the tests performed in chassis dynamometer, with an average error of 0.84 seconds in relation to the experiment while the Sandoval (2003) tested it had 0.56. The standard deviation of both was close to 0.24. Despite the high coefficient of variation, that indicates high dispersion of the results, this did not influence the validation of the models since the maximum percentage difference was 10.77% and all R^2 were greater than 0.99 indicating a good tedency.

6.2 Coastdown Tests Simulations

In addition to being able to test the vehicle on the chassis dynamometer and simulate its recovery time, it became necessary to find the coefficients that represent the road loads. It has been seen that for this purpose it is necessary to do coastdown tests on the track with the car. However, it was not possible to perform them in this work. Thus, the option to find the coefficients was through correlations found in the literature.

Having the necessary parameters for the calculation of aerodynamic drag, correlations for the rolling force were searched in the literature. A total of four equations were found based on experimental results and these were tested and compared with track test results made available in Kadijk's (2012) work. All showed good results, except for one model, described by equation 5.2, which was very far from almost all experiments. Nevertheless, all the correlations showed very strong results according to the coefficient of determination (R^2).

6.3 Fuel Performance Assessment – Experimental Results

In this work, the chassis dynamometer and engine bench experiments were also done to calculate and evaluate the performance and the combustion parameters of the tested fuels. By doing a general analysis, we can conclude that fuels with higher ethanol contents promote better acceleration performances to the vehicle. On the other hand, they consume larger amounts of fuel. It was also

possible to note that adding water, formulating hydrated mixtures, reduces its acceleration capacity and improves the efficiency of the vehicle.

6.3.1 Fuel E22

It has been seen that this fuel has lower pressures generated within the combustion chamber for low speeds (1300 and 2500 RPM). Nevertheless, the results of the IMEP were not far from the other fuels.

In relation to specific and mass fuel consumption, this was the one that presented the lowest; indicating that these parameters tend to be lower when reducing the ethanol content in the compounds. On the other hand, it was noted that it has the lowest acceleration capacity among all tested mixtures.

6.3.2 Fuel E50

Increasing the ethanol content to 50% by volume in the mixture, there was an increase in IMEP and, consequently, an improvement in acceleration capacity in relation to E22, since the torque values in the measured intervals were higher. On the other hand, there was an increase in consumption parameters.

It was noticed that increasing the ethanol content produced higher torque values at the same time that the duration of the burn was reduced in all engine speeds. However, the thermal efficiency was lower due to the higher fuel consumption and the higher amount of unburned mixture.

6.3.3 Fuel E85

There is an increase in the power of the vehicle by further increasing the ethanol content in the mixture, resulting in the vehicle's increased acceleration capacity. In addition, this formulation has lower combustion efficiency than other mixtures, which results in higher amounts of unburned fuel. It is noted that the total duration of combustion is shorter than the E50, even with the largest amount of burned mixture. It was expected since usually when you shorten the combustion duration, the efficiency increases.

By conclusion, the E85 is a good fuel when a good recovery time is required, as it promotes good accelerations in the vehicle. On the other hand, there is a large amount of the unburned compound in relation to the other mixtures, generating losses for the consumer who wants to save money.

6.3.4 Fuel E100

Better combustion efficiency is perceived in relation to E85, resulting in smaller amounts of unburned mixture. It is also perceived that the total duration of combustion grows again.

Regarding the acceleration capacity of the vehicle, the E85 and E100 presented very similar values, and pure anhydrous ethanol is better in this regard in most tests. We can also attribute this fact to the combustion efficiency that is higher, making the amount of fuel burned higher than the E85, indicating a better energy efficiency.

By conclusion, the E100 presented better results of consumption and similar acceleration performance in relation to the E85, indicating that it is a better option to be used. However, the consumption parameters are still higher than the mixtures that have lower ethanol contents, such as E22 and E50. With this, pure anhydrous ethanol is the best option when the consumer wants his vehicle to have a good performance, but is not indicated for low consumption values, unless compared to the E85.

6.3.5 Addition of Water in Mixtures (Fuels H36, H81 and H100)

It is noted that the fuels with higher water contents in the mixture had longer combustion durations. This result is aligned with what was mentioned by Gülder (1984), since the amount of water present in the fuel reduces its flame propagation speed, thus increasing the flame durability time inside the cylinders.

According to Brunetti (2018), the addition of water in the mixtures promotes better volumetric fuel efficiency. This is notorious in this work, with the exception of the E50 that obtained this parameter greater than H36. This is because the higher the air density in the test environment, the larger the cylinder air filling.

Another improvement promoted by the addition of water was in combustion efficiency. The most hydrated mixtures showed higher amounts of burned fuel in the mixtures, presenting better energy efficiency. As a result, thermal efficiency has also been improved. The only case in which the hydrated mixture presented higher values in specific consumption was H100 in relation to E100.

The acceleration capacity of the vehicle has been reduced by hydrating the mixtures. According to bench tests with the internal combustion engine, this

behavior was expected since the IMEP results were lower for these compositions.

6.4 General Conclusions

From the results found in this work, it was possible to reach the following conclusions:

- A performance prediction model based on bench tests with the engine was proposed. This one presented good accuracy with the vehicle speed recovery tests in a chassis dynamometer, which validated the proposed model.

- Performance simulations made from the engine experimental torque presented better results than when made using pressure curves. This can be explained by additional errors related to engine mechanical efficiency models used in the simulated torque curves.

- The performance and combustion parameters of the vehicle and engine were evaluated using different blends of ethanol and gasoline, where the E100 had the highest acceleration capabilities, while the E22 had the lowest fuel consumption values.

- Adding water to the mixture reduces the vehicle's ability to accelerate but promotes improvements in fuel efficiency parameters.

- The engine friction prediction models of Heywood (1988) and Sandoval (2003) were validated based on experimental results on engine test bench, showing low errors related to the mechanical efficiency of the engine. The friction models showed good tendency with the experiments.

- Several correlations for rolling force found in the literature for rolling resistance were evaluated. These analyses were based on published experimental results of coastdown tests and all showed good correlation.

- There are still some improvements to do in the vehicle transmission efficiency predictions.

6.5 Suggestions for Future Work

For the improvement of the results and the model, the following future works are proposed:

- Track coastdown tests with the Peugeot 207 SW so that it is possible to pick up the experimental values of the parameters that indicate the road loads. Compare the results with the correlations mentioned in this work for the coefficient of rolling force and aerodynamic drag.

- Testing the TU3 engine at higher speeds so that it is expected to have better precisions in the results for higher vehicle speeds in the recovery time simulations.

- Study the effects of transmission efficiency on vehicle speed recovery so that it is possible to obtain a correlation for this parameter as function of the torque and engine speed.

- Conducting motored tests with the TU3 engine for the validation of the Sandoval (2003) model for friction from each engine component.

- Improve test procedure in order to always start the vehicle speed recovery at the same velocity.

7 References

ABNT – ASSOCIAÇÃO BRASILEIRA DE NORMAIS TÉCNICAS. **NBR ISO 1585**: Veículos rodoviários – Código de ensaio de motores – Potência líquida efetiva. Rio de Janeiro, 1996.

ABNT – ASSOCIAÇÃO BRASILEIRA DE NORMAS TÉCNICAS. **NBR 10132**: Veículos rodoviários automotores leves – Determinação da resistência ao deslocamento por desaceleração livre em pista de rolamento e simulação em dinamômetro. Rio de Janeiro, 2014.

ABNT – ASSOCIAÇÃO BRASILEIRA DE NORMAS TÉCNICAS. **NBR 7024**. Veículos rodoviários automotores leves – Medição do consumo de combustível – Método de ensaio. Rio de Janeiro, 2010.

ABNT- ASSOCIAÇÃO BRASILEIRA DE NORMAS TÉCNICAS; INMETRO - INSTITUTO NACIONAL DE METROLOGIA, NORMALIZAÇÃO E QUALIDADE INDUSTRIAL. **Guia para a Expressão da Incerteza de Medição (ISO GUM)**. Terceira edição brasileira em língua portuguesa. Rio de Janeiro: ABNT, INMETRO, 2003. 120 p.

ALMEIDA, A.S.; DE SOUZA, J.G.; MADEIRO, L.C.N.; DA COSTA, M.L.A; CUNHA, A.L.; RODRIGUES, M.A.; DOS SANTOS, A.F.; Hidrogênio, o Combustível do Futuro, Diversitas Journal, vol. 4, nº 2, pg 356 – 366, 2019.

ANNAND, W.J.D. Heat transfer in the cylinders of reciprocating internal combustion engines, Proceedings of the Institution of Mechanical Engineers, 177 (36), 973-996, 1963.

ANTONIOSI, L; MAINTINGER, S. A Evolução do Etanol Brasileiro: do PROALCOOL aos dias atuais.,1º Congresso de Inovação, Ciência e Tecnologia do IFSP, São Paulo, 29 de novembro de 2016

BAECHTEL, J., Practical Engine Airflow: Performance Theory and Applications, ed. Cartech, Inc, 2015.

BISHOP, I. N.; Effect of Design Variables on Friction and Economy, SAE paper 640807, 1964

BRASIL. Ministério da Ciência, Tecnologia e Inovação. **Estimativas anuais das emissões de gases de efeito estufa no Brasil**. Brasília, 2020.

BROWN, W. L.; The Caterpiller, IMEP Meter and Engine Friction, SAE paper 730150, 1973

BRUNETTI, F.; **Motores de Combustão Interna: volume 1**, Ed. Blucher, São Paulo, 2012.

BRUNETTI, F.; **Motores de Combustão Interna: volume 2**, Ed. Blucher, São Paulo, 2012.

BUCKLEY, F.T.; ABCD – An Improved Coast Down Test and Analysis Method, SAE Transactions, SAE paper no. 950626, SAE International Congress and Exposition, Michigan, 1995.

BUKOVNIK, S.; OFFNER, G.; CAIKA V.; PRIEBSCH H.H; BARTZ W.J; Thermo-elasto-hydrodynamic lubrication model for journal bearing including shear rate-dependent viscosity, Lubrication Science 2007; 19: 231–245, 2007.

CANDIDO, A.C.A.F, **Análise das Eficiências Volumétrica, Global, Mecânica e Térmica de um Veículo Flex Operando com Etanol Hidratado e Gasolina em Diferentes Situações de carga**, Trabalho de Conclusão de Curso, Universidade Federal do Rio de Janeiro, 2016.

CARVALHO, R.N.; VILLELA, A.C.S; BARBOSA, R. A.; MELLO, E.S; E85 Performance, Emissions and Fuel Consumption in Brazilian Flex Fuel Light Duty Vehicles, 21th SAE BRASIL International Congress and Exhibition, São Paulo, 2012.

CATON, J.A. **An Introduction to Thermodynamic Cycle Simulations for Internal Combustion Engines**, John Wiley & Sons Ltd, United Kingdom, 2015.

CHAPIN, C.E.; Road Load Measurement and Dynamometer Simulation Using Coastdown Techniques, SAE Transactions, SAE paper no. 810828, Michigan, 1981.

CIBSE. Guide C. Reference Data 07, Ed.Chartered Institution of Building Services Engineers (CIBSE), 2007.

EHSANI, M.; GAO, Y.; EMADI, A., **Modern Electric, Hybrid Electric, and Fuel Cells Vehicles**, 2nd ed., Florida, EUA: CRC Press Taylor and Francis Group, 2009.

EIA, **U.S. Energy Information Administration**., 2021, disponível em < https://www.eia.gov/energyexplained/biofuels/use-of-ethanol.php>

ENGINEERING TOOLBOX: https://www.engineeringtoolbox.com/rolling-friction-resistance-d_1303.html, Último acesso em 15/06/2021.

FERGUSSON, C.; KIRKPATRICK, A, **Internal Combustion Engines: Applied Thermosciences**, 3rd Ed., John Wiley & Sons Ltd, 2015.

FIGUEIREDO, O. Treinamento em métodos estatísticos e suas aplicações – análise de regressão. Instituto de Matemática, UFRJ.

FINOL C.A.; ROBINSON, K Thermal Modeling of modern engines: a review of empirical correlations to estimate the in-cylinder heat transfer coefficient, Proceedings of the Institution of Mechanical Engineers – Part D – Journal of Automotive Engineering, 220 (12) 1765-81, 2006.

GILLESPIE, T.D, **Fundamentals of Vehicle Dynamics**, Society of Automotive Engineers Inc, Warrendale, 1992

GÜLDER, O.L., Burning Velocities of Ethanol-Isooctane Blends, Combustion and Flame, vol. 56, pp. 261-268, 1984.

GUZZELA, L.; SCIARETTA, A.; **Vehicle Propulsion Systems: Introduction to Modeling and Optimization**, 3rd edition, Springer, ISBN 978-3-549-25195, 2005.

HAN, B. S., CHUNG, Y. J., KWON, Y. J., LEE, S. Empirical formula for instantaneous heat transfer coefficient in spark ignition engines. SAE paper 972995, 1997

HEYWOOD, J.B**, Internal Combustion Engines Fundamentals**, 2 Ed., McGraw-Hill Book Company, New York, 2018.

HINKLE D. E., WIERSMA W., JURS S. G. **Applied Statistics for the Behavioral Sciences**. Houghton Mifflin, 2003.

HOHENBERG, G.F, .Advanced Approaches for Heat Transfer Calculations, SAE paper 790825, 1979.

HUCHO, W., **The Aerodynamics of Road Vehicles**, Butterworths Publishers, London, 1965.

IMPARATO, L,. Brasil será o fiel depositário do motor a combustão no mundo automotivo elétrico?, **Automotive Business**, out. 2019. Seção disponível em: < https://www.automotivebusiness.com.br/artigo/1806/brasil-sera-o-fiel-depositario-do-motor-a-combustao-no-mundo-automotivo-eletrico.>

KADIJK, G; LIGTERING, N.; Road load determination of passenger cars, TNO, 2012

KAMMIL, M.; RAHMAN, M.M; BAKAR, R.A.; An Integrated Model for Predicting Engine Friction Losses in Internal Combustion Engine, International Conference on Mechanical Engineering Research (ICMER2013), July, 2013.

KATZ, J.; **Race Car Aerodynamics: Designing for Speed**, Bentley Publishers, 2nd edition, USA, 1995

KIM, C., LEE, H., MYUNG, C, Study on the Criteria for the Determination of the Road Load Correlation for Automobiles and an Analysis of Key Factors**,** Energies 9” 7-9, 2016.

KLINE, S. J.; MCCLINTOCK, F. A. Describing uncertainties in single-sample experiments. **Mechanical Engineering**, v. 75, p. 3-8, jan. 1953.

KUHLWEIN, J.; The Impact of Official Versus Real-World Road Loads On CO_2 Emissions and Fuel Consumption of European Passenger Cars.

MACHADO, G. B. **Metodologias para desenvolvimento de combustíveis e determinação da velocidade de propagação de chama em motores de ignição por centelha**. 2012. 297 p. Doutorado (D.Sc.) – Departamento de Engenharia Mecânica, Pontifícia Universidade Católica do Rio de Janeiro/PUC-RJ, Rio de Janeiro, 2012.

MASHADI, B.; CROLLA, D., **Vehicle Powertrain Systems**, John Wiley & Sons, Ltd, United Kingdom, 2012

MCBEATH, S., **Competition Car Downforce**, Haynes Publishers, Somerset, 1998

MELO, T. C. C. Incerteza de medição em ensaios de emissões veiculares - Proposta de metodologia de cálculo. In: INMETRO – Fórum De Discussão De Ensaios De Proficiência, Rio de Janeiro, Mai. 2006. Disponível em: <www.inmetro.gov.br>.

MELLO, T.C.C; MACHADO, G.B,.; MACHADO JUNIOR, R.T; BELCHIOR, C.R.P.; PEREIRA, P.P. Thermodynamic Modeling of Compression, Combustion and Expansion Processes of Gasoline, Ethanol and Natural Gas with Experimental Validation on a Flexible Fuel Engine. In: International Conference For Engines For Automobile. Napoli, Italy, 2007, SAE paper 2007-24-0035. Warrendale: SAE 2007.

MOCK, P. The Future of Vehicle Emissions Testing and Compliance, The International Council of Clear Transportation, 2016

NAJAFI, G.; GHOBADIAN, B.; TAVAKOLI, T.; BUTTSWORTH, D.R.; YUSAF, T.F.; FAIZOLLAHNEJAD, M., Performance and exhaust emissions of a gasoline engine with ethanol blended gasoline fuels using artificial neural network, **Applied Energy**, v.86, p. 630-639. Amsterdam: Elsevier, 2009.

PATTON, K. J., R. G. NITSCHKE, HEYWOOD, J.B, Development and Evaluation of a Friction Model for Spark Ignition Engines, SAE paper 890836, 1989.

PEUGEOT. **Peugeot 207: Guia de Utilização**., 2011.

PRADELLE, F. **Use of Biofuels in compression ignition engines – Potentials of diesel-biodiesel-ethanol blends**, Doutorado (D.Sc.) – Departamento de Engenharia Mecânica, Pontifícia Universidade Católica do Rio de Janeiro/PUC-RJ, Rio de Janeiro, 2017.

SAE RECOMMENDED PRACTICE J1263, “Road Load Measurement and Dynamometer Simulation Using Coastdown Techniques,” 39, SAE International, Warrendale, PA, 2010.

SAE RECOMMENDED PRACTICE J1491-06, Vehicle Acceleration Measurement. USA: SAE, 2006.

SAE RECOMMENDED PRACTICE J2263, “Road Load Measurement Using Onboard Anemometer and Coastdown Techniques,” 12, SAE International, Warrendale, PA, 2008.

SANDOVAL, D., HEYWOOD, J. B., An Improved Friction Model for Spark Ignition Engines, SAE paper 2003-01-0725, 2003.

SHAYLER, P., D. LEONG; M.MURPHY, Contributions to Engine Friction During Cold, Low Speed Running and the Dependence on Oil Viscosity, SAE paper 2005-01-1654, 2005.

SOARES, S.M.C; SODRÉ, J.R.; Effects of Atmospheric Temperature and Pressure on the Performance of a Vehicle, Proceedings of the Institution of Mechanical Engineers, Part D, page 473-477, 2002.

SONNTAG, R. E., BORGNAKKE, C., WYLEN, V.G. J**. Fundamentals of Thermodynamics**, 6th edition, Ed. Wiley, 2003.

TAYLOR, C., **Internal Combustion Engine in Theory and Practice: Thermodynamics, Fluid Flow, Performance: Volume 1**, Mit Press, 2nd edition, 1985

VARGAS R.A.; CHIBA R.; FRANCO, E.G.; SEO, E.S.M.; Hidrogênio: O Vetor Energético do Futuro?, Centro de Ciências e Tecnologia de Materiais (CCTM). Instituto de Pesquisas Energéticas e Nucleares (IPEN). Universidade de São Paulo (USP), 2014.

VILANOVA, C.; Detalhes do TU3JP, **Revista O Mecânico**, 22 de Junho de 2015. Seção disponível em: <https://omecanico.com.br/detalhes-do-tu3jp/>

VILLELA, A.C.S.; MACHADO, G.B., Multifuel Engine Performance, Emissions and Combustion using Anhydrous and Hydrous Ethanol, 21th SAE BRASIL International Congress and Exhibition, São Paulo, 2012.

VILLELA, A.S.C.; BOTERO, S.; CARVALHO, R.N**,** Vehicle Speed Recovery Test Methodologies on Chassis Dynamometer and Their Correlation with Track Test Results, 24th SAE BRASIL International Congress and Display, 2015-36-0196, São Paulo, September, 2015.

VILLELA, A.S.C.; BOTERO, S.W.; MACHADO, G.B.; Vehicle Efficiency on Chassis Dynamometer, 23rd SAE BRASIL International Congress and Display, 2014-36-0263, São Paulo, October, 2014.

VILLELA, A.S.C.; CARVALHO, R.N.; Fuel Consumption Technical and Economical Study for Flexible Fuel Vehicles, 18º Congresso e Exposição Internacionais da Tecnologia da Mobilidade, São Paulo, 2009.

VILLELA, A.S.C.; Coast Down Curve Computational Modeling and Its Influence on Urban and Highway Autonomy Results, 26th SAE BRASIL International Congress and Display, SAE paper no. 2017-39-0319, São Paulo, Novembre, 2017.

VILLELA, A.S.C.; Vehicle Coastdown Coefficients Determination In Chassis Dynamometer – An Alternative to Track Tests, 25th SAE BRASIL International Congress and Display, São Paulo, October, 2016.

VONBUM, C**.,** Impactos Ambientais e Econômicos dos Veículos Elétricos e Híbridos Plug-In: Uma Revisão da Literatura, Brasília, agosto de 2015.

WHITE, R.A; KORST, H.H.; The Determination of Vehicle Drag Contributions from Coast-Down Tests, SAE Transactions, SAE paper no. 720099, 1972.

WIEBE,I .**Halbemprirische Formel fur die Verbrennungsgeschwiwindigkeit**, Moscow: Verlag der Akademie der Wissenschaften der UdSSR, 1967
WILLIAMS, J.A. **Engineering Tribology**, Oxford University Press, New York, pg. 241, 1994.

WONG. J.Y, **Theory of Ground Vehicles**, John Wiley and Sons: Ontario, Canada, 2000.

WOSCHNI, G. A universally applicable equation for the instantaneous heat transfer coefficient in the internal combustion engine, SAE Transactions, SAE paper no. 67093176, 3065-83, 1968.

YASIN, T.P. The Analytical Basis of Automobile Coastdown Testing, SAE Paper 780334, 1978.

Appendix I: Friction Modeling for Engines (Sandoval, 2003)

The internal combustion engines friction fall into three main categories: those that are speed-independent, proportional to speed (hydrodynamic friction), or those proportional to squared speed (turbulence dissipation). There are still parts whose friction is a combination of these three factors.

According to Williams (2005), the components found in the hydrodynamic lubrication regime must be modified to compensate for temperature differences from lubricating oil. The author suggests that this change should be made by multiplying these terms by a scale factor related to the viscosity of the oil:

$$\mu_{\text{scaling}} = \sqrt{\frac{\mu(\mathrm{T})}{\mu_{\mathrm{o}}(\mathrm{T_o})}} \tag{I.1}$$

where $\mu(\mathrm{T})$ is the viscosity of the oil in the enginefor which friction predictions are being made, and it is the reference viscosity $\mu_{\mathrm{o}}(\mathrm{T_o})$ that was used to calibrate the model when it was first developed. Considering the oil density as constant, we have in relation to kinematic viscosity:

$$\mu_{\text{scaling}} = \sqrt{\frac{v(\mathrm{T})}{v_o(\mathrm{T_o})}} \tag{I.2}$$

The reference kinematic viscosity $v_0$can be calculated using vogel's equation (Sandoval, 2003; Williams, 2005):

$$v_0 = \mathrm{k}\exp\left(\frac{\theta_1}{\theta_2 + \mathrm{T}}\right) \tag{I.3}$$

where v_0 is the kinematic viscosity of low shear rate oil in cSt, and k (cSt), θ_1(°C) and (θ_2°C) are constant correlation for a given lubricant and T is the temperature of the oil in °C.

To convert the kinematic viscosity of low shear rate to high shear rate, it is necessary to multiply for a reason μ_{inf}/μ_{the}:

$$v = v_o\left(\frac{\mu_{\mathrm{inf}}}{\mu_{\mathrm{o}}}\right) \tag{I.4}$$

From this, all data can be found in table II.1, taken from Sandoval (2003), for several different lubricating oils. The value of μ_{inf}/μ_o for SAE 10W-40 oil, used in the vehicle of this work, was taken from Bukovnik et al. (2007), as equal to 0.7.

Oil Grade	k(cSt)	θ1(°C)	θ2(°C)	μ∞/μ	c1	c2
0W 40	0.01341	1986.4	189.7	0.67	2.5	0.026
5W 20	0.04576	1224	134.1	0.94	2.5	0.029
5W 40	0.15	1018.74	125.91	0.8	2.3	0.0225
10W 30	0.1403	869.72	104.4	0.76	2.3	0.0225
10W 50A	0.0352	1658.88	163.54	0.49	2.43	0.0218
10W 50B	0.0507	1362.4	129.8	0.52	2.28	0.0269
15W 40A	0.1223	933.46	103.89	0.9	2.3	0.0225
15W 40B	0.03435	1424.3	137.2	0.79	2.5	0.026
20W 50	0.0639	1225.46	117.7	0.84	2.3	0.0225
SAE 10	0.0258	1345.42	144.58	1	2.3	0.0225
SAE 30	0.0246	1432.29	132.94	1	2.3	0.0225
SAE 50	0.0384	1349.94	115.16	1	2.3	0.0225

Table II.1: Viscosity data for different lubricating oils

In view of this information, the following are the correlations of the Sandoval model (2003) for each engine component responsible for generating friction:

- Friction in piston and connecting rod assembly:

The loss of energy from this set is composed of the friction of the piston and its rings with the cylinder walls and the contact between the bearings of the connecting rod with the crankshaft.

$$\mathrm{fmep_{skirt}} = \mathrm{c_{ps}}\frac{\overline{\mathrm{S_p}}}{\mathrm{B}}\left(\frac{\mu}{\mu_o}\right)^{\frac{1}{2}} \tag{I.5}$$

$$\mathrm{fmep_{rings}} = \mathrm{c_{pr}}\left(1+\frac{1000}{\mathrm{N}}\right)\frac{1}{\mathrm{B}^2} \tag{I.6}$$

$$\mathrm{fmep_{crod}} = \mathrm{c_b}\left(\frac{\mathrm{ND_b^3 L_b n_b}}{\mathrm{B^2 Sn_c}}\right)\left(\frac{\mu}{\mu_o}\right)^{0.5} \tag{I.7}$$

With the values of c_{ps} = 294 kPa-mm-s/m, c_b = 3.03x10^{-4} and c_{pr} = 4.06x10^4 kPa-mm².

Sandoval (2003) uses the model proposed by Bishop (1969) to increase friction between the piston and the cylinder from the engine load:

$$\mathrm{fmep_{gas}} = \mathrm{c_g}\frac{\mathrm{p_{intake}}}{\mathrm{p_{atm}}}\left(0.088\mathrm{r_c}\left(\frac{\mu}{\mu_o}\right)^{0.5} + 0.182^{1.33-\mathrm{K}\overline{\mathrm{S_p}}}\right) \quad \text{(I.8)}$$

with K = 2.38x10^{-2} s/m and c_g = 6.89. P_{intake} is the pression in the intake system and p_{atm} is atmospheric pressure.

- Friction in crankshaft assembly:

For the crankshaft to rotate, a bearing housing is required to attach the engine assembly. This junction is made through the use of bearings, which reduce friction from movement between these parts, and sealed, which prevent the leakage of lubricating oil.

Therefore, we can say that the portion of power lost by friction is due to the bearings of the crankshaft, as well as the seals that compose them. There is also turbulence dissipation that occurs to transport lubricating oil to the bearings. The friction from the main bearings can be calculated similarly to the connecting rod bearings, as the two are equals:

$$\mathrm{fmep_{bearings}} = \mathrm{c_b}\left(\frac{\mathrm{ND_b^3L_bn_b}}{\mathrm{B^2Sn_c}}\right)\left(\frac{\mu}{\mu_o}\right)^{0.5} \quad \text{(I.9)}$$

$$\mathrm{fmep_{seals}} = \mathrm{c_s}\frac{\mathrm{D_b}}{\mathrm{n_cB^2S}} \quad \text{(I.10)}$$

$$\mathrm{fmep_{turbulence}} = \mathrm{c_t}\left(\frac{\mathrm{D_bN^2n_b}}{\mathrm{n_c}}\right) \quad \text{(I.11)}$$

With c_s = 1.22x10^5 kPa-mm² and c_t=1.35x10^{-10}.

- Valve train friction:

According to Heywood (2018), the friction in the valve train comes mainly from three areas: camshaft with bearings coupled, camshaft with tappets and the fulcrum with the rockers.

Friction in the camshaft bearings operates under the hydrodynamic lubrication regime and is given by:

$$\mathrm{fmep_{cam}} = \mathrm{c_c}\frac{\mathrm{Nn_{cs}}}{\mathrm{n_c B^2 S}} \tag{I.12}$$

where n_{cs} is the number of bearings on the camshaft. Sandoval (2003) proposes that c_c = 244 kPa-min/rev-mm³, adding a value of 4,12 kPa to rely on camshaft seals.

The friction from the contact between the camshaft and the follower depends on the geometry. The cam follower can have rolling or flatface.

$$\mathrm{fmep_{flat}} = \mathrm{C_{ff}}\left(1 + \frac{1000}{\mathrm{N}}\right)\frac{\mathrm{n_v}}{\mathrm{Sn_c}} \tag{I.13}$$

$$\mathrm{fmep_{roll}} = \mathrm{C_{rf}}\left(\frac{\mathrm{Nn_v}}{\mathrm{n_c S}}\right) \tag{I.14}$$

The other terms are related to valve train components that are under full or partial hydrodynamic lubrication regime, such as valves and their guides:

$$\mathrm{fmep_{valve}} = \mathrm{C_{oh}}\left(\frac{\mathrm{L_v N^{0.5} n_v}}{\mathrm{BSn_c}}\right) + \mathrm{C_{om}}\left(1 + \frac{1000}{\mathrm{N}}\right)\frac{\mathrm{L_v n_v}}{\mathrm{Sn_c}} \tag{I.15}$$

The values of C_{ff}, C_{rf}, C_{oh} and C_{om} depend on the type of cam shaft configuration (SOHC or DOHC). These values can be seen in Table I.3:

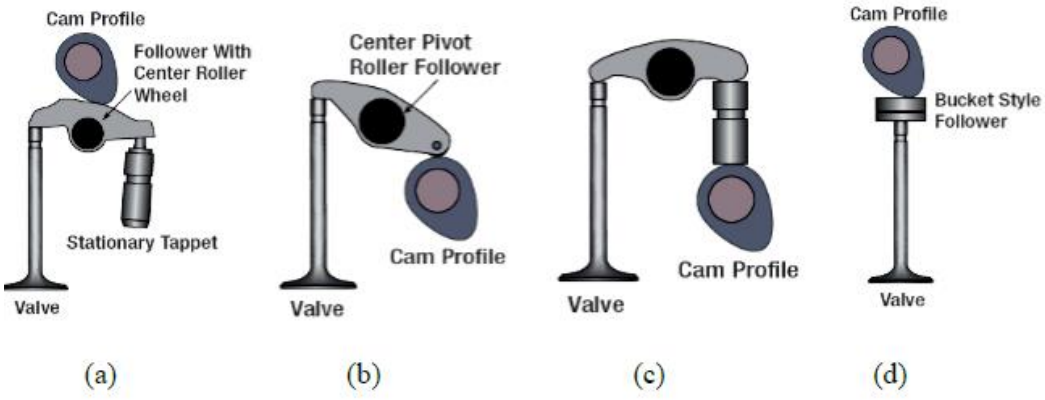

Figure II.0.1: Valve train settings (Kammil, 2013)

Type I	OHC	Overhead cam; direct acing/ flat or roller follower
Type II	OHC	Overhead cam; End pivot rocker/ flat or roller follower
Type III	OHC	Overhead cam; Center pivot rocker/flat or roller follower
Type IV	CIB	Cam-in-block; rocker arm/flat or roller follower

Table II.0.2: Different configurations of train valves. (Kammil, 2013)

Configuration	Type	Flat Follower C_{ff} (KPa-mm)	Roller Follower C_{rf} (KPa-mm-min/rev)	Oscillating Hydrodynamic C_{oh} (KPa-mm-min/rev)$^{1/2}$	Oscillating Mixed C_{om} (KPa)
Single overhead cam (SOHC)	I	200	0.0076	0.5	107
Double overhead cam (DOHC)	I	133	0.0050	0.5	10.7
Single overhead cam (SOHC)	II	600	0.0227	0.2	42.8
Single overhead cam (SOHC)	III	400	0.0151	0.5	21.4
Cam in block (CIB)	IV	400	0.0151	0.5	32.1

Table I. 0.3: Constants for the different types of valve train for the Sandoval model. (Kammil, 2013)

- Activation of accessories:

The correctaction used by Sandoval (2003) for the prediction of losses by the activation of engine accessories is given as:

$$\text{afmep} = 6.23 + 5.22 \times 10^{-3}\text{N} - 1.79 \times 10^{-7}\text{N}^2 \qquad \text{(II.16)}$$

- Total friction:

From the correlations found in the work of Sandoval (2003), the total friction of the internal combustion engine, considering camshaft with roller face, is given by:

$$\begin{aligned}\text{tfmep} = {} & \text{fmep}_{\text{skirt}} + \text{fmep}_{\text{rings}} + \text{fmep}_{\text{crod}} + \text{fmep}_{\text{gas}} + \text{fmep}_{\text{bearings}} + \text{fmep}_{\text{cam}} \\ & + \text{fmep}_{\text{seals}} + \text{fmep}_{\text{turbulence}} + \text{fmep}_{\text{roll}} + \text{fmep}_{\text{valve}} + \text{afmep} \\ & + \text{pmep}\end{aligned}$$

In this work, the pumping losses were calculated by the integral of the pressure curves of the fuel tests.

Appendix II - Coastdown Tests Simulations (Kadijk, 2012)

In Kadijk (2012) publication, 8 road vehicles were tested. In this study, the results were compared with the correlations found in the literature. Table II.1 shows the parameters of each vehicle and the conditions of the environment in which the experiments were carried out.

	Vehicle Parameters				Ambient Conditions			
	Type	Mass (kg)	Tire Pressure(bar)	Tire Size	Air velocity (m/s)	Pressure (bar)	Temperature (K)	Af (m²)
Vehicle 1	Sedan	1465	2,3	R16 215/55	4,6	1,01	289,65	1,992
Vehicle 2	SW	1566	2,2	R16 205/55	5,51	1,01	279,44	2,04856
Vehicle 3	Hatchback	1329	2,4	R15 185/65	3	1,025	289,25	1,91584
Vehicle 4	Hatchback	1325	2,3	R16 195/55	3,2	1,023	276,05	1,9136
Vehicle 5	Hatchback	1026	unknown	R15 185/55	< 5m/s (unk. Value)	1	278,65	1,74616
Vehicle 6	Sedan	1962	2,7	unknown	< 5m/s (unk. Value)	1,016	293,15	2,27032
Vehicle 7	MPV	1640	2,3	R16 205/60	< 5m/s (unk. Value)	1,05	278,65	2,09
Vehicle 8	Sedan	1724	2,5	R17 215/55	1	1,013	285,95	2,13704

Table II.0.1: Parameters of the vehicles tested by Kadijk (2012)

Before performing the speed recovery tests with the Peugeot 207 SW on the VULCAN chassis dynamometer, it is necessary to determine the respective road loads coefficients of the vehicle, so these can be simulated by braking forces in the dyno rollers. Therefore, this section aims to demonstrate the methodology used to find the coefficients. The choice of these parameters was based on a comparison of the results obtained by the correlations found in the literature for road loads and the experimental results of coastdown tests found in Kadijk (2012) for eight different vehicles (the autor did not mention witch vehicles were used in the work).

Kadijk (2012) published the results of coastdown tests that were performed in two places and with eight different vehicles. With the aid of the VBOX II equipment, installed inside the cars, the author obtained the speed values as a function of time.

On the left side of equation II.1, there is the acceleration force that is calculated by equation II.2.

$$-m_v \varepsilon \frac{dv}{dt} = m_v g f_r \cos(\alpha) + \frac{1}{2} \rho_{amb} C_d A_f V_r^2 \tag{II.1}$$

$$F_{ac} = m_v \varepsilon \left[\frac{v_{i+1} - v_i}{t_{i+1} - t_i} \right] \tag{II.2}$$

where ε represents the inertia of the drivetrain rotational components and it is given by Ehsani (2009) and Gillespie (1992) as equation 4.59:

$$\varepsilon = 1 + 0{,}04 + 0{,}0025 i_c^2 i_D^2 \tag{II.3}$$

In equation II.2 the "i" is the instant of the acquisition of each speed and time term acquired by VBOX II. By obtaining the values of the acceleration force, it's possible to obtain the values of the coefficients of the curve F_0, F_1 and F_2 by linear regression.

According to the literature review, it was considered that the parabolic term F_2 is related to aerodynamic drag, as given by equation II.4.

$$F_D(v_v) = F_2 v_v^2 \tag{II.4}$$

The Kadijk (2012) experiments were carried out in two opposite directions in order to nullify the effects of wind on aerodynamic drag and, therefore, an average of the results was taken. As a result, equation II.4 is not function of the wind speed. The mean velocity is also provided in the Kadijk (2012) work.

Kadijk (2012) did not mention the values of the drag coefficients of the vehicles and also did not mention which models were used, making it impossible to obtain this information by manufacturers' data. Therefore, the drag coefficient was calculated according to equation II.5.

$$C_{d_{exp}} = \frac{2F_2}{\rho_{air,amb} A_f} \tag{II.5}$$

where $\rho_{air,amb}$ is the atmospheric air density of the tests in kg/m³, obtained by the ideal gases law with the pressure and temperature of the environment that can be found in Kadijk (2012) and can be seen in Appendix IX. A_f is the frontal area of the vehicle in m² and was calculated by equation II.6, found in Wong (2000):

$$A_f = 1{,}6 + 0{,}00056(m_v - 765) \tag{II.6}$$

where m_v is the mass of the vehicle in kg, which can be seen in Table II.1.

Once the parameters related to the aerodynamic drag coefficient are obtained, the data related to the rolling resistance are still missing. Thus, all the correlations mentioned in the literature review for the rolling resistance coefficient (chapter 2 of this work) were used, witch was:

$$f_r = f_o + 3.24 f_s \left(\frac{v_v}{161}\right)^{2.5} \quad \text{(II.7)}$$

$$f_r = 0.01\left(1 + \frac{v_v}{100}\right) \quad \text{(II.8)}$$

$$f_r = \left(0.014\frac{2}{p_{tire}}\right)\left(1 + \left(0{,}6214\frac{v_v}{100}\right)^2\right) \quad \text{(II.9)}$$

$$f_r = s(0.0116 + 0.0000142 v_v) \quad \text{(II.10)}$$

The simulated values of the rolling resistance coefficients were multiplied by the mass of the vehicle and the gravity acceleration so that the force was calculated.

A From this, the correlation used in this work was the proposed by Villela (2017), since this was made to be in accordance with the ABNT NBR 10132 (2014) standard. From the vehicle data, the results of the coefficients are:

$$F_{0_{SIM}}' = 0.2615\left(\frac{m_v}{p_{tire}}\right) + 22.153 \quad \text{(II.11)}$$

$$F_{2_{SIM}}' = 0.0656(C_d A_f) - 0.0055 \quad \text{(II.12)}$$

Based on these results, it is shown the coefficient of determination (R^2) of each simulation that represents the distance in relation the experimental result of the track test found in Kadijk (2012), in Table II.2, using equations II.7 to II.12.

Road Load Correlation	R^2								
	Vehicle 1	Vehicle 2	Vehicle 3	Vehicle 4	Vehicle 5	Vehicle 6	Vehicle 7	Vehicle 8	Average
II.7	0,8028	0,9556	0,9665	0,8287	0,9850	0,5262	0,9045	0,8130	0,8478
II.8	0,9723	0,9463	0,9933	0,9706	0,9830	0,8564	0,9994	0,9669	0,9610
II.9	0,9931	0,9004	0,9041	0,9516	0,9273	0,9888	0,9427	0,9735	0,9477
II.10	0,9553	0,9768	0,9938	0,9403	0,9913	0,9444	0,9946	0,9852	0,9727
II.11 / II.12	0,9907	0,9018	0,9364	0,9987	0,8898	0,9078	0,9915	0,9827	0,9499

Table II.0.2: Coefficient of determination from the rolling resistance coefficients in relation to the coastdown tests made by Kadijk (2012).

With the results obtained, it is noted that the correlations obtained a good approximation with the results on track performed by Kadijk (2012). However, the correlation seen in Gillespie (1992) and Brunetti (2012), represented by equation 5.2, did not present good results, obtaining a general average in the tests of 0.8478 for the coefficient of determination.

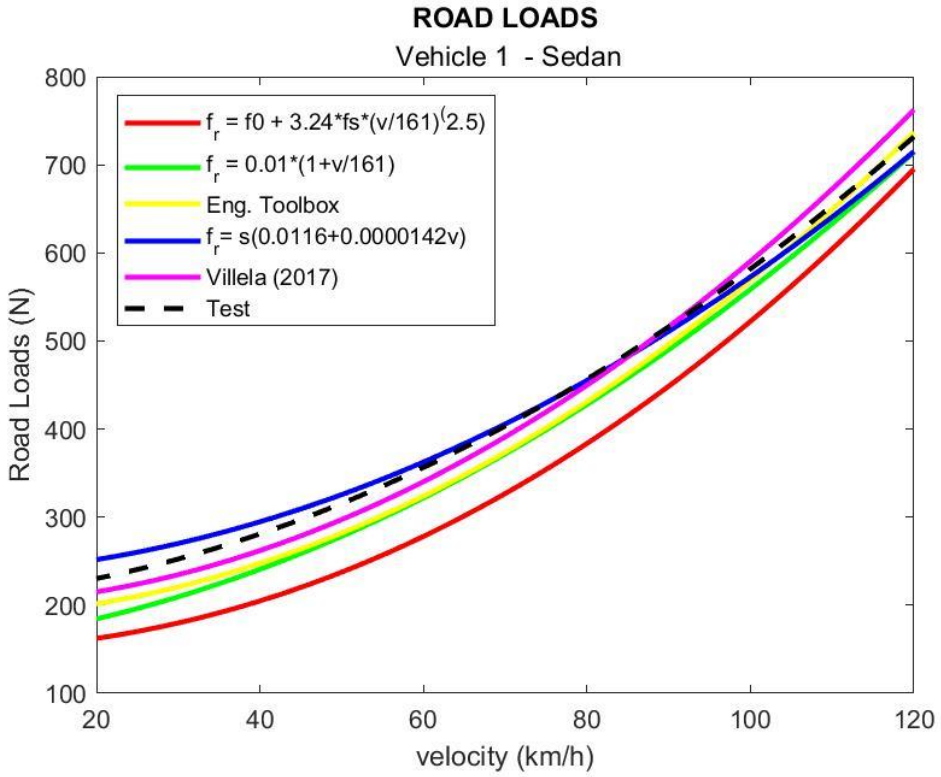

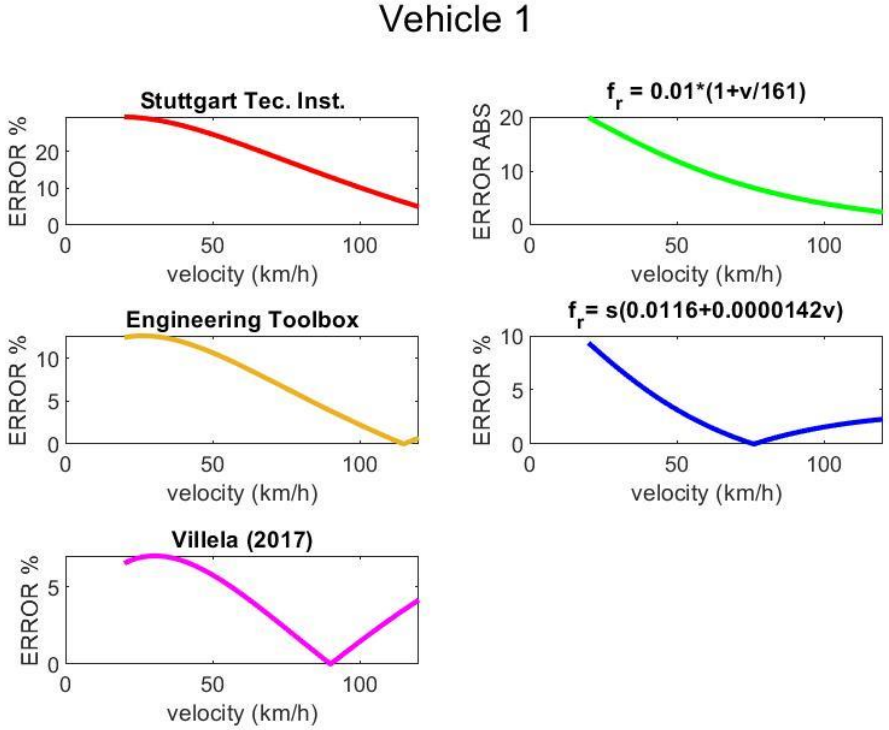

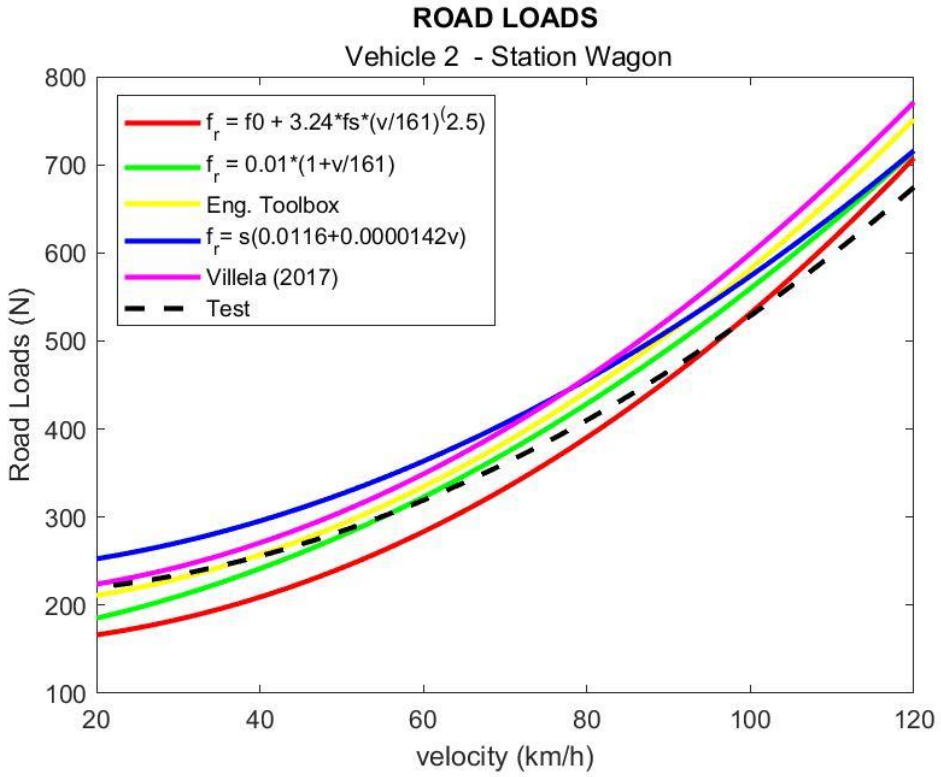

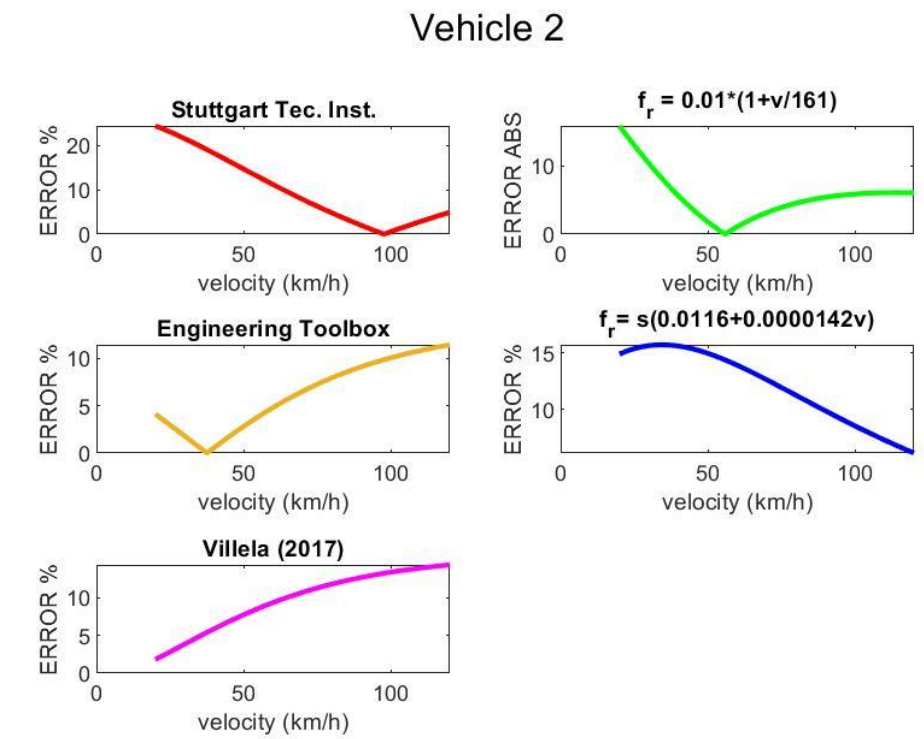

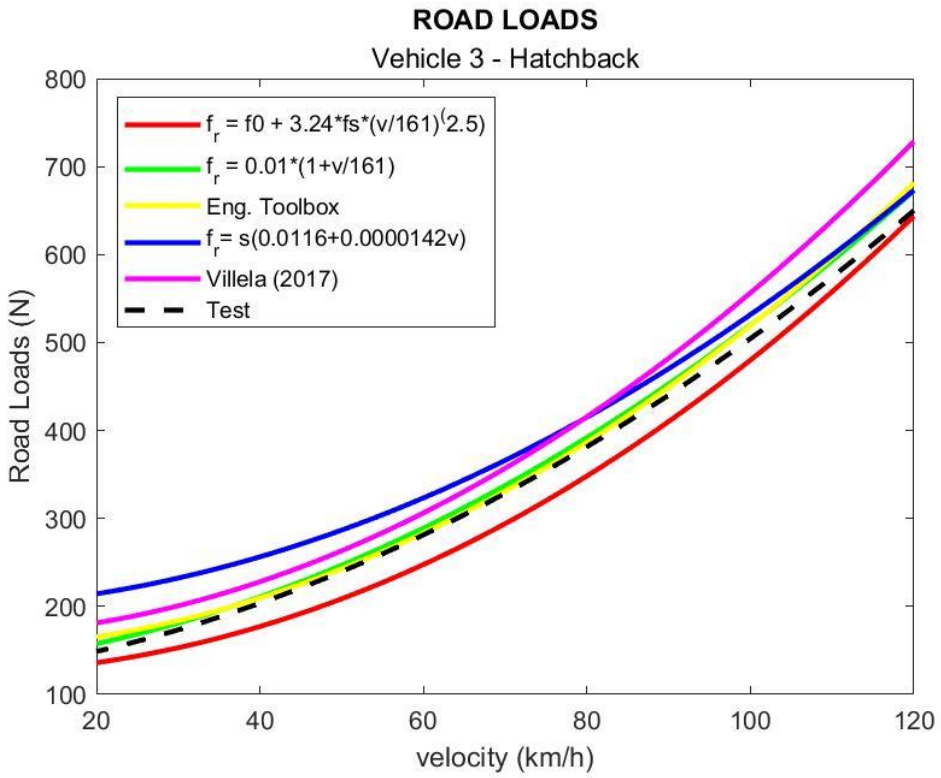

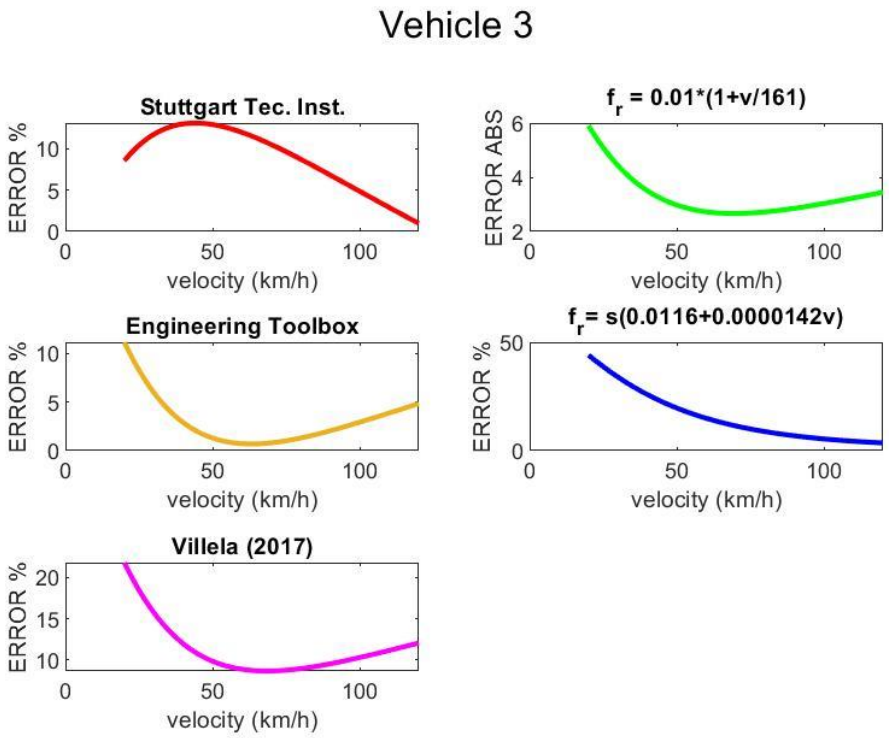

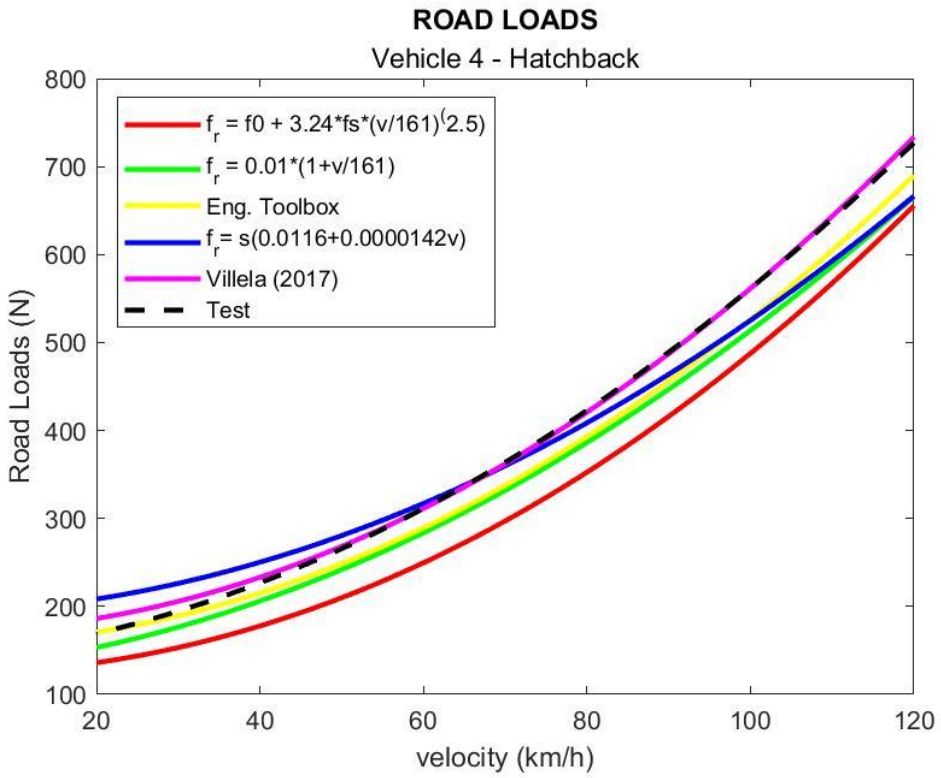

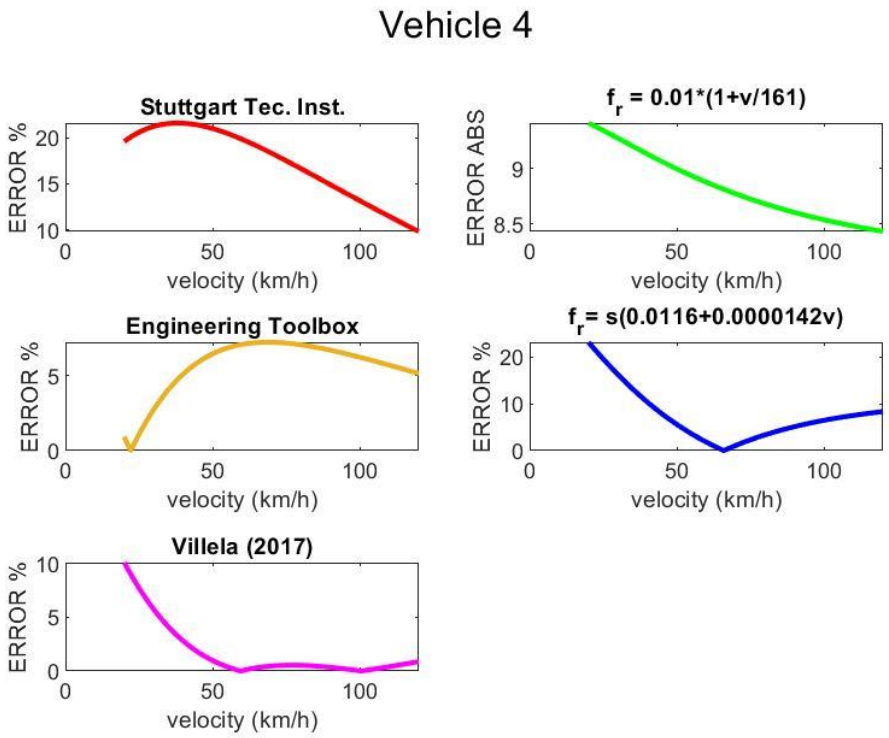

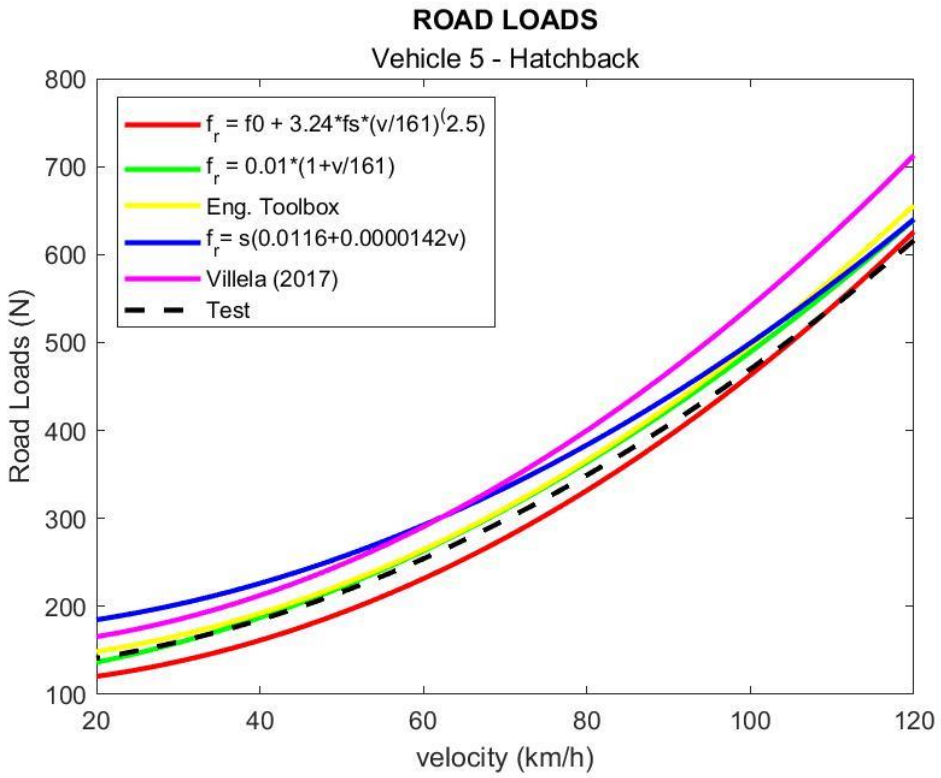

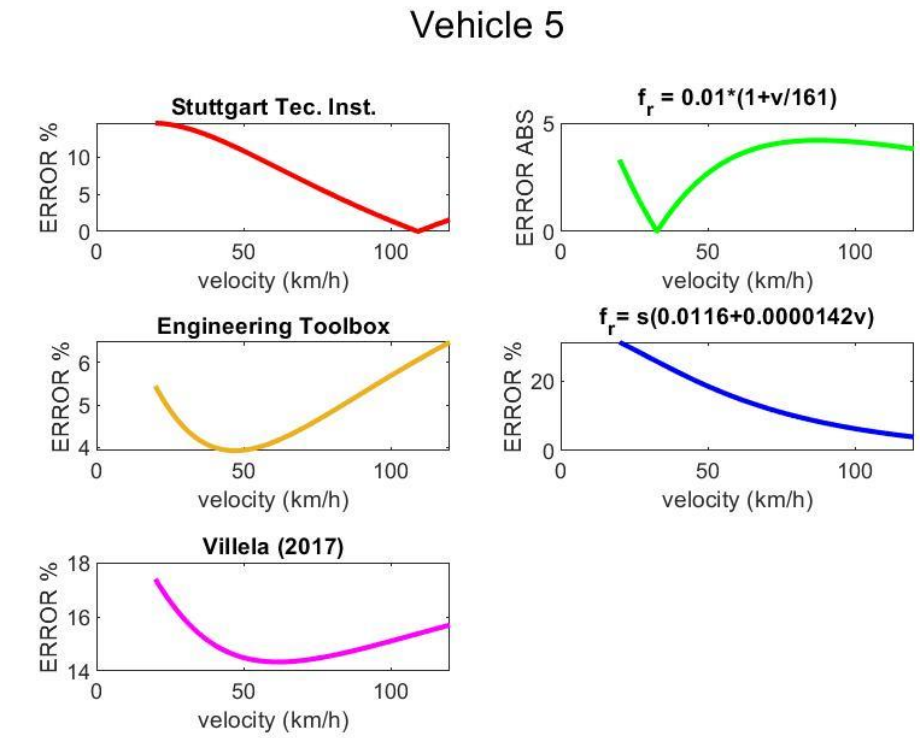

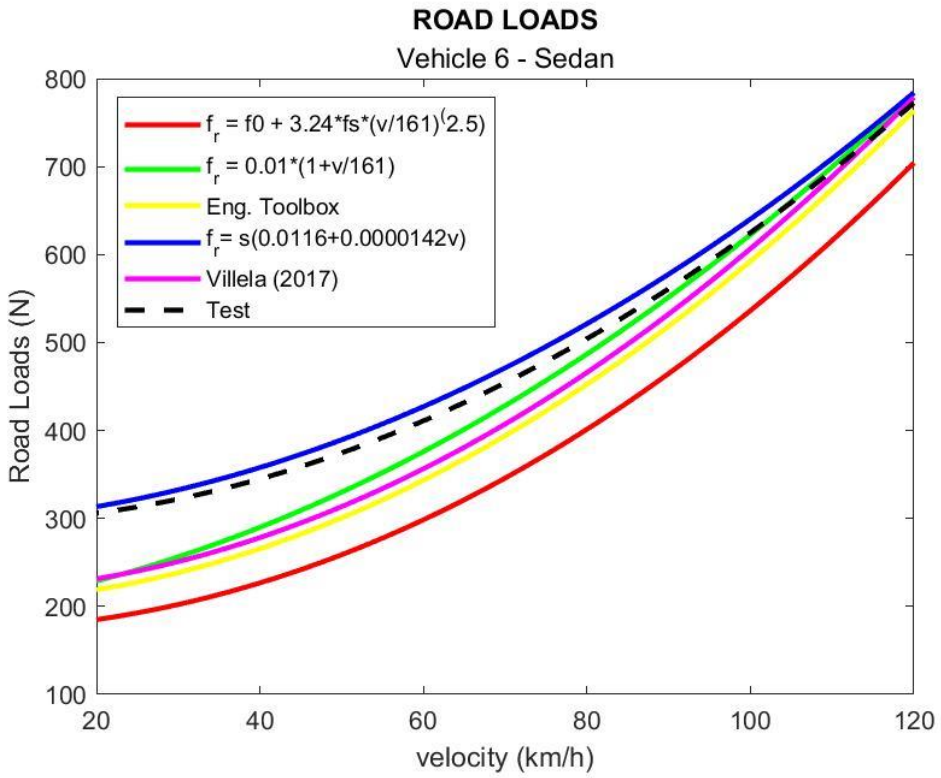

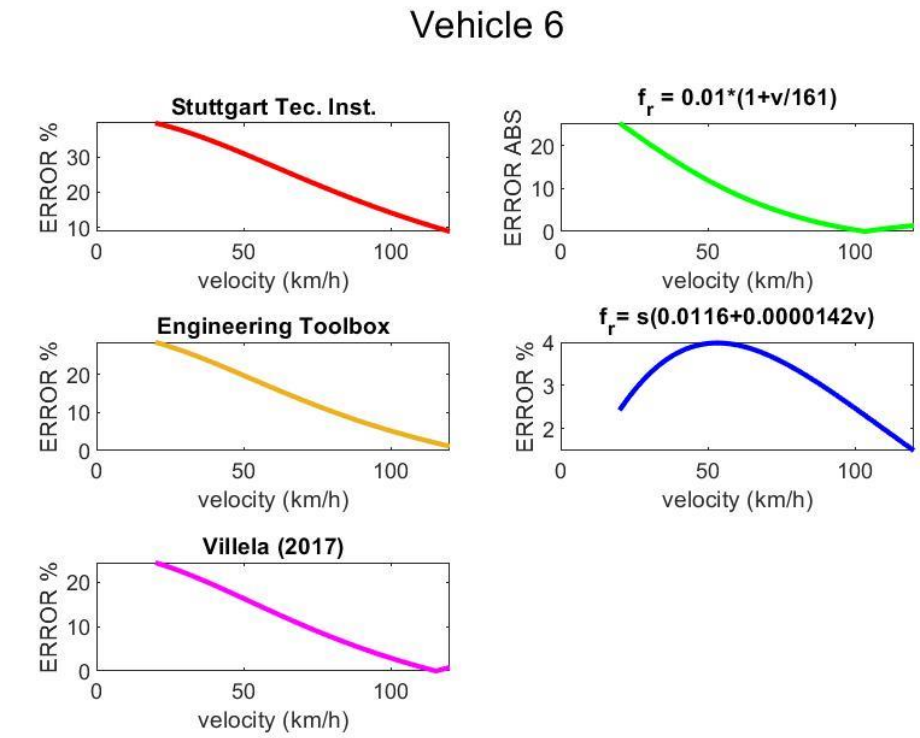

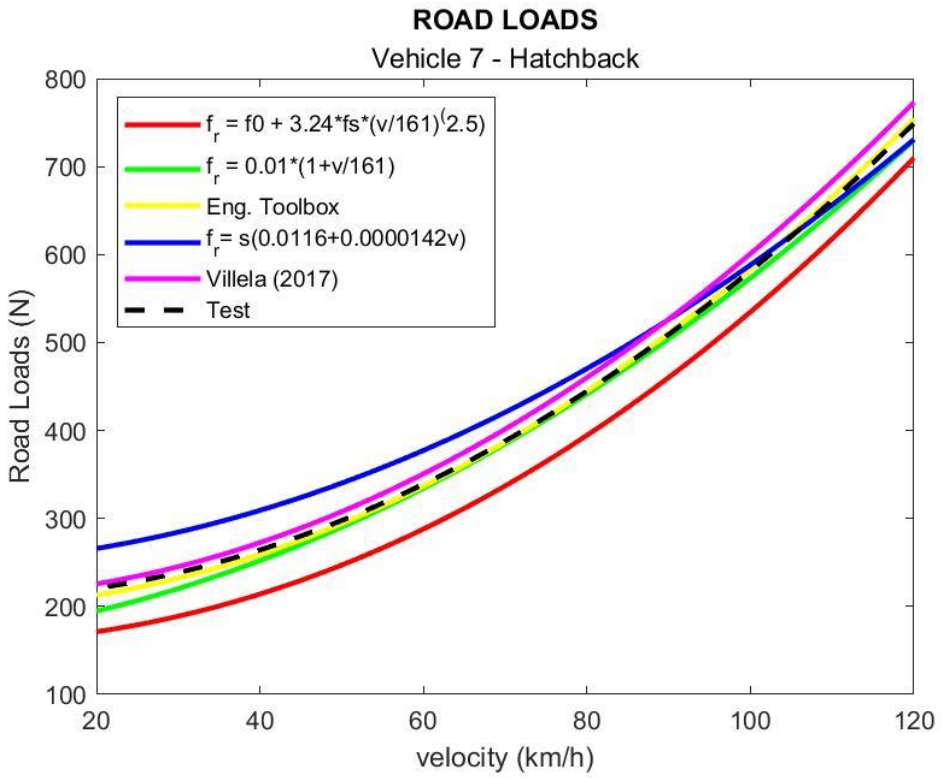

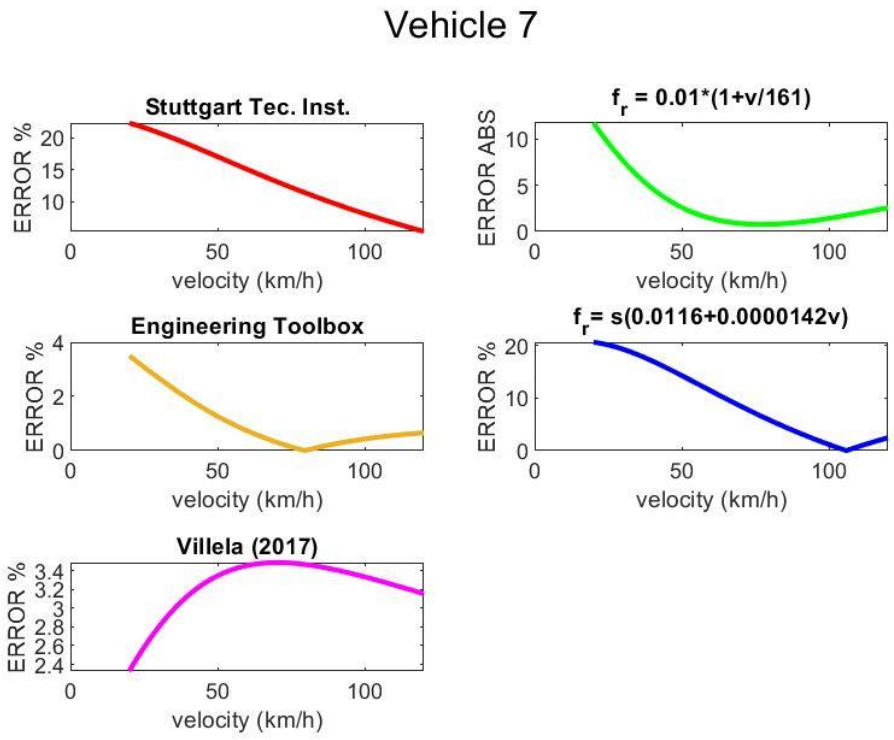

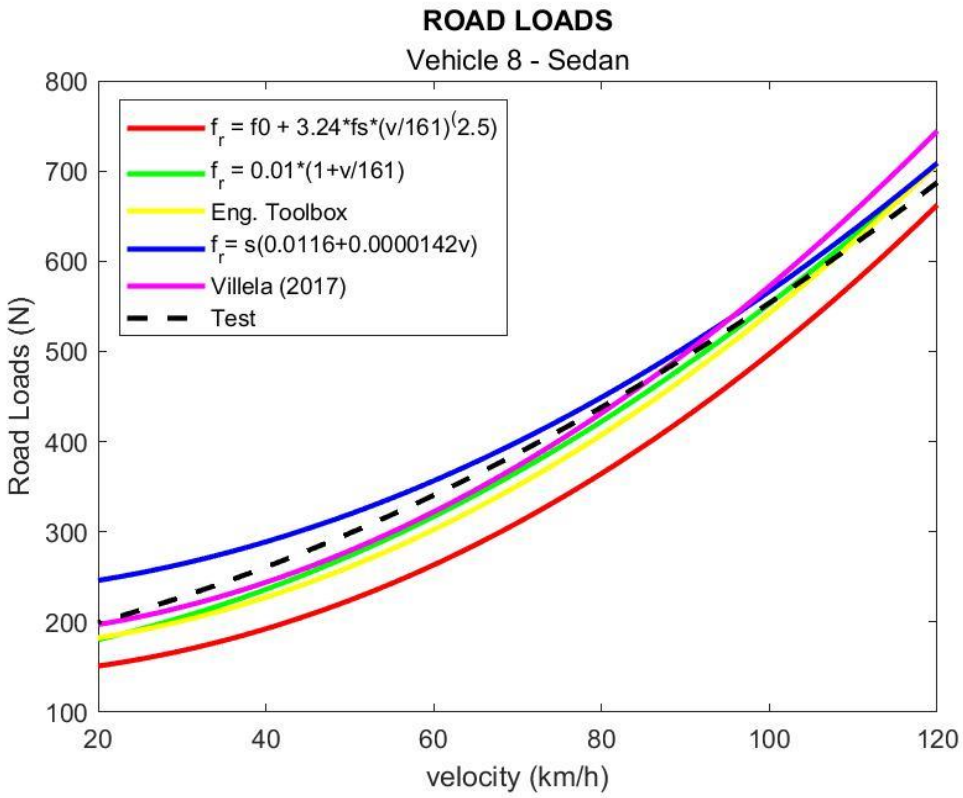

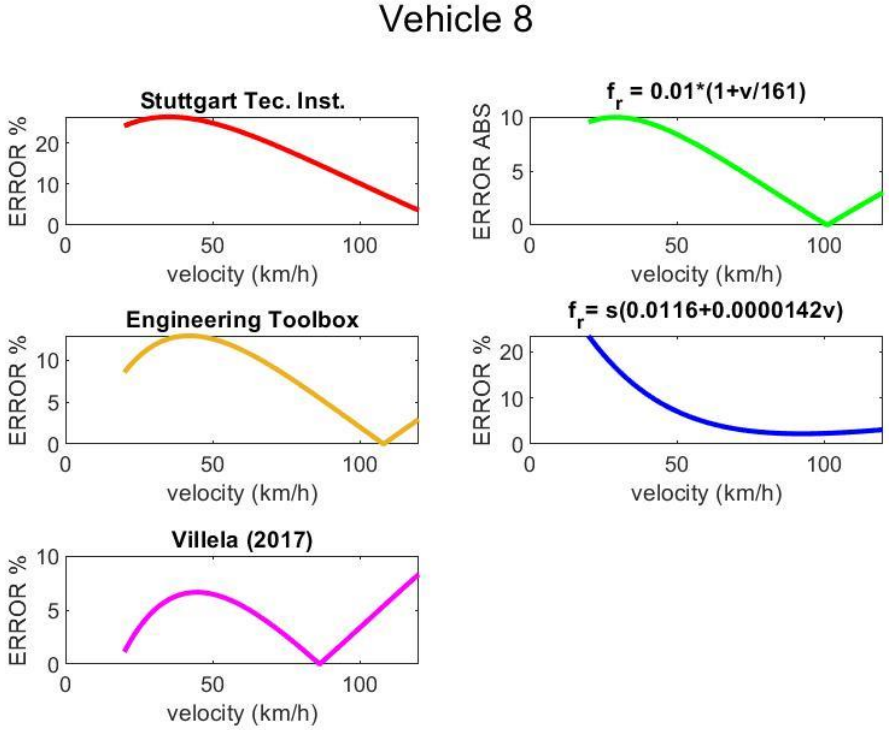

Appendix III - Uncertainties

1300 RPM	E22	E50	E85	E100	H36	H81	H100	
Ia	0	0	0	0	0	0	0	Engine Speed (RPM)
Ib	1	1	1	1	1	1	1	
Ic	1	1	1	1	1	1	1	
Ie	2	2	2	2	2	2	2	
Ia	0,2625	0,1247	0,1414	0,0471	0,1247	0,1633	0,0816	Torque (N.m)
Ib	0,1923	0,1949	0,1948	0,1923	0,1981	0,1938	0,1924	
Ic	0,3254	0,2314	0,2407	0,198	0,2341	0,2534	0,209	
Ie	0,6507	0,4628	0,4814	0,3959	0,4681	0,5069	0,418	
Ia	0,0047	0,017	0	0,0047	0,0094	0,0047	0,0125	Fuel Consumption(kg/h)
Ib	0,0221	0,0259	0,0323	0,0319	0,0253	0,0306	0,0329	
Ic	0,0226	0,031	0,0323	0,0322	0,027	0,0309	0,0352	
Ie	0,0453	0,062	0,0645	0,0645	0,054	0,0618	0,0704	
Ia	0,0047	0	0,0047	0	0,0094	0,0125	0,0047	λ
Ib	0,0058	0,0058	0,0053	0,0056	0,0058	0,0059	0,0058	
Ic	0,0075	0,0058	0,0071	0,0056	0,0110	0,0138	0,0075	
Ie	0,0149	0,0117	0,0142	0,0112	0,0221	0,0276	0,0149	
Ia	0,1063	0,0156	0,0118	0,0543	0,0107	0,0188	0,012	TFMEP (bar)
Ib	0,0187	0,019	0,019	0,0188	0,0193	0,0189	0,0188	
Ic	0,1079	0,0246	0,0224	0,0574	0,0221	0,0267	0,0223	
Ie	0,2158	0,0492	0,0448	0,1149	0,0442	0,0533	0,0445	
Ia	0,0356	0,0216	0,0216	0,0094	0,0216	0,0163	0,0125	Brake Power (kW)
Ib	0,028	0,0284	0,0284	0,028	0,0289	0,0283	0,028	
Ic	0,0453	0,0357	0,0357	0,0296	0,0361	0,0326	0,0307	
Ie	0,0906	0,0714	0,0714	0,0591	0,0721	0,0653	0,0614	
Ia	0,0041	0,0014	0,0008	0,0019	0,0011	0,0005	0,0002	Thermal Efficiency
Ib	0,0027	0,0026	0,0027	0,003	0,0028	0,0029	0,003	
Ic	0,0049	0,003	0,0028	0,0036	0,003	0,0029	0,003	
Ie	0,0099	0,0059	0,0056	0,0072	0,006	0,0059	0,006	
Ia	0,0084	0,001	0,0007	0,0042	0,0007	0,0016	0,0008	Mechanical Efficiency
Ib	0,0054	0,0055	0,0055	0,0054	0,0055	0,0054	0,0054	
Ic	0,01	0,0056	0,0055	0,0068	0,0056	0,0057	0,0055	
Ie	0,02	0,0111	0,011	0,0136	0,0112	0,0113	0,0109	
Ia	0,0005	0,001	0,0005	0,0004	0,0007	0,0002	0,0004	Global Efficiency
Ib	0,003	0,0029	0,0029	0,0032	0,0031	0,0032	0,0033	
Ic	0,0031	0,0031	0,003	0,0033	0,0032	0,0032	0,0033	
Ie	0,0061	0,0062	0,0059	0,0066	0,0064	0,0063	0,0066	

2500 RPM	E22	E50	E85	E100	H36	H81	H100	
Ia	0,0000	0,2222	0,2222	0,0000	0,2222	0,2222	0,0000	Engine Speed (RPM)
Ib	1,0000	1,0000	1,0000	1,0000	1,0000	1,0000	1,0000	
Ic	1,0000	1,0244	1,0244	1,0000	1,0244	1,0244	1,0000	
Ie	2,0000	2,0488	2,0488	2,0000	2,0488	2,0488	2,0000	
Ia	0,0816	0,0816	0,0471	0,1247	0,0471	0,0816	0,0000	Torque (N.m)
Ib	0,2192	0,2204	0,2217	0,2213	0,2207	0,2180	0,2204	
Ic	0,2339	0,2350	0,2267	0,2540	0,2257	0,2328	0,2204	
Ie	0,4678	0,4701	0,4534	0,5080	0,4514	0,4656	0,4408	
Ia	0,0082	0,0170	0,0205	0,0330	0,0000	0,0082	0,0094	Fuel Consumption(kg/h)
Ib	0,0469	0,0527	0,0669	0,0658	0,0520	0,0640	0,0692	
Ic	0,0476	0,0554	0,0700	0,0736	0,0520	0,0645	0,0699	
Ie	0,0952	0,1108	0,1399	0,1472	0,1040	0,1291	0,1398	
Ia	0,0000	0,0000	0,0000	0,0047	0,0047	0,0000	0,0094	λ
Ib	0,0056	0,0058	0,0053	0,0056	0,0058	0,0058	0,0058	
Ic	0,0056	0,0058	0,0053	0,0073	0,0075	0,0058	0,0110	
Ie	,0112	0,0117	0,0106	0,0147	0,0149	0,0115	0,0220	
Ia	,0202	0,0143	0,0407	0,0084	0,0193	0,0215	0,0097	TFMEP (bar)
Ib	,0213	0,0215	0,0216	0,0216	0,0215	0,0212	0,0215	
Ic	,0294	0,0258	0,0461	0,0231	0,0289	0,0302	0,0236	
Ie	,0588	0,0516	0,0922	0,0463	0,0578	0,0604	0,0471	
Ia	,0245	0,0294	0,0094	0,0262	0,0082	0,0249	0,0094	Brake Power (kW)
Ib	,0585	0,0588	0,0592	0,059	0,0589	0,0582	0,0588	
Ic	,0634	0,0658	0,0599	0,0646	0,0595	0,0633	0,0596	
Ie	,1268	0,1316	0,1199	0,1292	0,119	0,1266	0,1191	
Ia	,0001	0,001	0,0017	0,0011	0,0005	0,0004	0,0002	Thermal Efficiency
Ib	,0029	0,003	0,003	0,0034	0,003	0,0031	0,0033	
Ic	0,0029	0,0032	0,0034	0,0035	0,0031	0,0031	0,0033	
Ie	0,0059	0,0063	0,0068	0,0071	0,0061	0,0062	0,0066	
Ia	0,0016	0,0009	0,0029	0,0007	0,0014	0,0016	0,0007	Mechanical Efficiency
Ib	0,0061	0,0061	0,0062	0,0061	0,0061	0,0061	0,0061	
Ic	0,0063	0,0062	0,0068	0,0062	0,0063	0,0063	0,0062	
Ie	0,0126	0,0124	0,0136	0,0124	0,0126	0,0126	0,0123	
Ia	0,0005	0,0005	0,0005	0,0007	0,0001	0,0003	0,0004	Global Efficiency
Ib	0,0034	0,0034	0,0034	0,0038	0,0035	0,0035	0,0037	
Ic	0,0034	0,0035	0,0034	0,0038	0,0035	0,0035	0,0037	
Ie	0,0069	0,0069	0,0068	0,0077	0,007	0,007	0,0075	

3500 RPM	E22	E50	E85	E100	H36	H81	H100	
Ia	0	0,6667	0	0	0,6667	0,6667	0	Engine Speed (RPM)
Ib	1	1	1	1	1	1	1	
Ic	1	1,2019	1	1	1,2019	1,2019	1	
Ie	2	2,4037	2	2	2,4037	2,4037	2	
Ia	0,0816	0,0471	0,3742	0,0816	0,0943	0,1247	0,0471	Torque (N.m)
Ib	0,215	0,2173	0,2192	0,218	0,2157	0,2151	0,2177	
Ic	0,23	0,2223	0,4336	0,2328	0,2354	0,2487	0,2227	
Ie	0,46	0,4446	0,8673	0,4656	0,4709	0,4973	0,4454	
Ia	0,0082	0,0125	0,0125	0,0163	0,0141	0,0236	0,0205	Fuel Consumption(kg/h)
Ib	0,0667	0,0748	0,1017	0,1019	0,0749	0,0932	0,1038	
Ic	0,0672	0,0759	0,1025	0,1032	0,0763	0,0962	0,1059	
Ie	0,1344	0,1518	0,205	0,2064	0,1525	0,1923	0,2117	
Ia	0,0047	0	0	0	0	0	0	λ
Ib	0,0054	0,0054	0,0049	0,0051	0,0054	0,0054	0,0054	
Ic	0,0071	0,0054	0,0049	0,0051	0,0054	0,0054	0,0054	
Ie	0,0142	0,0109	0,0098	0,0102	0,0109	0,0107	0,0107	
Ia	0,0028	0,0053	0,0813	0,0054	0,0089	0,0535	0,0113	TFMEP (bar)
Ib	0,021	0,0212	0,0214	0,0213	0,021	0,021	0,0213	
Ic	0,0211	0,0218	0,0841	0,022	0,0228	0,0575	0,0241	
Ie	0,0423	0,0436	0,1682	0,0439	0,0456	0,115	0,0481	
Ia	0,0411	0,0216	0,1283	0,0262	0,0216	0,0499	0,0189	Brake Power (kW)
Ib	0,0796	0,0804	0,0811	0,0807	0,0798	0,0796	0,0805	
Ic	0,0895	0,0833	0,1518	0,0848	0,0827	0,094	0,0827	
Ie	0,1791	0,1665	0,3036	0,1697	0,1654	0,1879	0,1655	
Ia	0,0002	0,0003	0,002	0,0005	0,0001	0,0016	0,0002	Thermal Efficiency
Ib	0,0029	0,0029	0,0027	0,003	0,0029	0,003	0,0031	
Ic	0,0029	0,0029	0,0034	0,0031	0,0029	0,0034	0,0031	
Ie	0,0058	0,0058	0,0068	0,0061	0,0057	0,0067	0,0063	
Ia	0,0002	0,0004	0,0059	0,0004	0,0006	0,004	0,0008	Mechanical Efficiency
Ib	0,006	0,006	0,0061	0,006	0,006	0,006	0,006	
Ic	0,006	0,0061	0,0085	0,0061	0,006	0,0072	0,0061	
Ie	0,012	0,0121	0,017	0,0121	0,0121	0,0144	0,0122	
Ia	0,0003	0,0003	0,0007	0,0005	0,0003	0,0003	0,0005	Global Efficiency
Ib	0,0033	0,0033	0,003	0,0034	0,0033	0,0033	0,0034	
Ic	0,0033	0,0033	0,0031	0,0034	0,0033	0,0033	0,0035	
Ie	0,0066	0,0066	0,0062	0,0068	0,0066	0,0067	0,007	

Appendix IV - TU3 Tests Parameters

Fuel	RPM	Throttle Open Area (%)	T_{amb} (H)	p_{amb} (Pa)	ρ_{amb} (kg/m³)	UR(%)	W	p_v (Pa)	p_d (Pa)
E22	1300	100	30,50	99491,35	1,1430	50,60	0,014	2207,56	97283,79
	2500	100	33,00	99422,40	1,1343	46,90	0,015	2357,44	97064,96
	3500	100	37,50	99353,45	1,1233	40,70	0,017	2622,65	96730,80
E50	1300	100	22,10	100184,35	1,1649	55,50	0,009	1474,70	98709,65
	2500	100	24,10	100115,40	1,1566	48,30	0,009	1448,39	98667,01
	3500	100	25,50	99977,50	1,1510	40,50	0,008	1320,35	98657,15
E85	1300	100	29,60	99563,80	1,1244	45,10	0,012	1868,59	97695,21
	2500	100	32,90	99563,80	1,1100	41,40	0,013	2069,33	97494,47
	3500	100	25,00	99701,70	1,1444	56,10	0,011	1775,33	97926,37
E100	1300	100	31,70	99353,45	1,1317	62,20	0,019	2905,48	96447,97
	2500	100	34,80	99284,51	1,1233	51,20	0,018	2845,25	96439,26
	3500	100	38,10	99146,61	1,1121	51,30	0,022	3414,92	95731,69
H36	1300	100	30,80	99839,60	1,1449	54,70	0,016	2427,68	97411,92
	2500	100	32,50	99839,60	1,1389	50,80	0,016	2482,69	97356,91
	3500	100	39,30	99701,70	1,1250	43,40	0,020	3081,76	96619,94
H81	1300	100	24,20	99908,55	1,1522	52,40	0,010	1580,80	98327,75
	2500	100	26,90	99839,60	1,1405	46,00	0,010	1628,93	98210,67
	3500	100	27,20	99632,75	1,1371	44,70	0,010	1611,01	98021,74
H100	1300	100	24,10	99563,80	1,1482	53,60	0,010	1607,33	97956,47
	2500	100	25,40	99563,80	1,1433	49,30	0,010	1597,72	97966,08
	3500	100	27,00	99632,75	1,1362	49,30	0,011	1756,07	97876,68

Fuel	m_{total} (kg/h)	$m_{air,wet}$ (kg/h)	$m_{air,dry}$ (kg/h)	m_{vapor} (kg/h)	m_{fuel} (kg/h)	m_{total} (kg)	$m_{air,wet}$ (kg)	$m_{air,dry}$ (kg)	m_{vapor} (kg)	m_{fuel} (kg)	λ
E22	57,927	54,097	53,344	0,753	3,830	4,33E-04	4,05E-04	3,99E-04	5,63E-06	2,86E-05	1
	119,480	111,360	109,702	1,657	8,120	4,65E-04	4,33E-04	4,27E-04	6,44E-06	3,16E-05	0,97
	161,905	150,365	147,871	2,494	11,540	4,50E-04	4,18E-04	4,11E-04	6,93E-06	3,21E-05	0,92
E50	62,662	58,182	57,646	0,536	4,480	4,69E-04	4,35E-04	4,31E-04	4,01E-06	3,35E-05	1,01
	127,402	118,292	117,222	1,070	9,110	4,95E-04	4,60E-04	4,56E-04	4,16E-06	3,54E-05	1,01
	169,325	156,375	155,084	1,291	12,950	4,70E-04	4,34E-04	4,31E-04	3,59E-06	3,60E-05	0,94
E85	59,303	53,713	53,082	0,632	5,590	4,44E-04	4,02E-04	3,97E-04	4,72E-06	4,18E-05	0,91
	124,003	112,443	110,978	1,465	11,560	4,82E-04	4,37E-04	4,32E-04	5,70E-06	4,50E-05	0,92
	175,568	157,958	156,196	1,761	17,610	4,88E-04	4,39E-04	4,34E-04	4,89E-06	4,89E-05	0,85
E100	54,258	48,738	47,842	0,896	5,520	4,06E-04	3,64E-04	3,58E-04	6,70E-06	4,13E-05	0,97
	112,756	101,386	99,559	1,827	11,370	4,38E-04	3,94E-04	3,87E-04	7,10E-06	4,42E-05	0,98
	159,508	141,858	138,778	3,079	17,650	4,43E-04	3,94E-04	3,85E-04	8,55E-06	4,90E-05	0,88
H36	55,990	51,600	50,812	0,788	4,390	4,19E-04	3,86E-04	3,80E-04	5,89E-06	3,28E-05	1,01
	114,951	105,941	104,287	1,654	9,010	4,47E-04	4,12E-04	4,06E-04	6,43E-06	3,50E-05	1,01
	155,340	142,380	139,610	2,770	12,960	4,32E-04	3,96E-04	3,88E-04	7,69E-06	3,60E-05	0,94
H81	60,723	55,433	54,884	0,549	5,290	4,54E-04	4,15E-04	4,10E-04	4,10E-06	3,96E-05	1
	127,336	116,246	115,059	1,187	11,090	4,95E-04	4,52E-04	4,47E-04	4,62E-06	4,31E-05	1
	173,893	157,713	156,117	1,596	16,180	4,83E-04	4,38E-04	4,34E-04	4,43E-06	4,49E-05	0,93
H100	56,390	50,690	50,178	0,512	5,700	4,22E-04	3,79E-04	3,75E-04	3,83E-06	4,26E-05	1,01
	116,402	104,422	103,374	1,049	11,980	4,53E-04	4,06E-04	4,02E-04	4,08E-06	4,66E-05	0,99
	165,166	147,206	145,582	1,625	17,960	4,59E-04	4,09E-04	4,04E-04	4,51E-06	4,99E-05	0,93

Fuel	imep (bar)	bmep (bar)	tfmep (bar)	amep+rbmep(bar)	pmep (bar)	pmáx (bar)/ Crankshaft Angle (º)
E22	10,017	8,866	1,152	1,094	0,057	38,732 30º
	11,762	10,113	1,650	1,424	0,226	50,936 22º
	11,756	9,928	1,828	1,449	0,379	53,759/ 22º
E50	10,434	8,986	1,449	1,434	0,014	51,129 21º
	11,815	10,177	1,637	1,468	0,170	52,579 20º
	12,024	10,029	1,994	1,496	0,498	58,158 19º
E85	10,529	8,977	1,552	1,526	0,026	56,266 18º
	11,980	10,233	1,748	1,534	0,214	55,396 21º
	12,141	10,085	2,056	1,561	0,495	58,508 19º
E100	10,520	8,884	1,636	1,622	0,014	50,511 22º
	11,892	10,205	1,687	1,462	0,225	57,317 19º
	12,012	10,066	1,946	1,573	0,373	56,209 19º
H36	10,553	9,161	1,392	1,362	0,030	55,77 18º
	11,764	10,196	1,568	1,376	0,193	53,115 21º
	11,876	9,956	1,920	1,450	0,471	53,185 23º
H81	10,422	8,930	1,492	1,460	0,031	52,297 19º
	11,739	10,076	1,663	1,426	0,237	50,581 22º
	11,975	9,946	2,029	1,531	0,497	55,545 20º
H100	10,197	8,884	1,312	1,271	0,041	47,577 22º
	11,604	10,177	1,427	1,203	0,225	50,528 22º
	12,086	10,057	2,029	1,582	0,447	55,657 20º

Fuel	$\dot{Q}_{inj}$ (kW)	P_i (kW)	P_b (kW)	P_f (kW)	$P_{rf} + P_{ac}$ (kW)	P_p (kW)	$\dot{Q}_{ht}$ (kW)	$\dot{Q}_{inc}$ (kW)	$\dot{Q}_{ex}$ (kW)
E22	41,757	14,766	13,497	1,697	1,613	0,085	6,040	9,237	11,714
	88,528	33,343	29,833	4,676	4,036	0,640	11,348	17,734	26,103
	125,815	46,654	41,536	7,254	5,750	1,503	15,501	28,165	35,494
E50	44,374	15,381	13,219	2,135	2,114	0,021	5,425	14,185	9,383
	90,233	33,492	28,923	4,642	4,161	0,481	10,495	18,065	28,182
	128,268	47,718	40,022	7,914	5,939	1,975	15,614	27,860	37,076
E85	45,746	15,520	13,573	2,288	2,249	0,039	6,223	15,616	8,387
	94,602	33,961	30,022	4,954	4,347	0,607	10,741	28,382	21,518
	144,112	48,184	40,563	8,160	6,196	1,964	14,437	48,509	32,982
E100	41,101	15,507	13,699	2,411	2,390	0,021	7,138	7,821	10,635
	84,659	33,712	30,447	4,784	4,146	0,638	12,706	10,499	27,741
	131,419	47,672	42,693	7,722	6,242	1,480	16,732	29,344	37,671
H36	42,994	15,556	13,934	2,052	2,007	0,045	6,945	6,902	13,591
	88,241	33,349	29,941	4,446	3,899	0,547	11,871	15,548	27,473
	126,926	47,132	41,854	7,621	5,753	1,869	16,492	24,236	39,067
H81	42,010	15,363	13,255	2,199	2,153	0,046	5,905	10,466	10,276
	88,070	33,276	28,957	4,714	4,044	0,671	10,077	20,095	24,621
	128,492	47,526	40,136	8,051	6,077	1,974	14,194	33,425	33,347
H100	40,744	15,031	13,244	1,934	1,874	0,061	6,714	7,104	11,895
	85,633	32,896	29,248	4,045	3,409	0,636	11,540	13,996	27,202
	128,378	47,967	40,639	8,053	6,277	1,776	16,238	26,450	37,723

Fuel	Q_{inj} (J)	W_i (J)	W_b (J)	W_f (J)	W_{rf} + W_{ac} (J)	W_p (J)	Q_{ht} (J)	Q_{inc} (J)	Q_{ex} (J)
E22	1124,215	340,76	301,593	39,172	37,216	1,956	139,381	213,153	430,918
	1239,396	400,12	344,004	56,117	48,437	7,680	136,178	212,803	490,294
	1258,148	399,89	337,721	62,173	49,288	12,886	132,866	241,418	483,971
E50	1194,679	354,95	305,677	49,274	48,793	0,482	125,194	327,340	387,193
	1263,266	401,90	346,204	55,698	49,932	5,767	125,942	216,775	518,647
	1282,680	409,01	341,177	67,834	50,906	16,928	133,838	238,797	501,035
E85	1231,623	358,17	305,363	52,802	51,901	0,901	143,597	360,377	369,484
	1324,424	407,53	348,088	59,446	52,168	7,278	128,895	340,580	447,415
	1441,122	413,00	343,062	69,940	53,106	16,834	123,750	415,792	488,578
E100	1106,565	357,86	302,221	55,639	55,163	0,476	164,717	180,481	403,506
	1185,228	404,55	347,146	57,403	49,750	7,653	152,473	125,991	502,215
	1314,190	408,62	342,434	66,188	53,505	12,683	143,413	251,521	510,634
H36	1157,541	358,99	311,646	47,346	46,318	1,029	160,264	159,282	479,002
	1235,378	400,18	346,832	53,353	46,793	6,559	142,457	186,579	506,158
	1269,264	403,99	338,664	65,326	49,309	16,017	141,360	207,734	516,181
H81	1131,036	354,53	303,792	50,737	49,678	1,059	136,263	241,524	398,720
	1232,979	399,32	342,748	56,569	48,522	8,047	120,926	241,138	471,597
	1284,915	407,36	338,350	69,012	52,092	16,920	121,666	286,496	469,392
H100	1096,943	346,86	302,221	44,640	43,242	1,397	154,940	163,937	431,206
	1198,863	394,75	346,204	48,544	40,907	7,637	138,478	167,947	497,690
	1283,781	411,14	342,119	69,023	53,803	15,220	139,181	226,718	506,739

Fuel	sfc (g/kWh))	ηv	ηc	ηth	ηm	ηglobal	Torque (N)	Corrected Torque (N)	K (ABNT NBR ISO 1585)
E22	293,06	87,943	81,040	30,311	88,50	26,827	96,0	99,15	1,033
	283,25	94,765	82,830	32,284	85,98	27,756	109,5	113,95	1,041
	292,89	92,138	80,812	31,784	84,45	26,843	107,5	113,33	1,054
E50	338,22	93,251	72,600	29,711	86,12	25,587	97,3	97,10	0,998
	315,77	99,315	82,840	31,815	86,14	27,405	110,2	110,48	1,003
	325,34	94,304	81,383	31,887	83,42	26,599	108,6	109,20	1,005
E85	422,45	88,963	70,740	29,081	85,26	24,794	97,2	99,70	1,026
	398,52	97,973	74,285	30,771	85,41	26,282	110,8	114,68	1,035
	439,99	95,529	71,148	28,658	83,07	23,805	109,2	110,67	1,013
E100	421,49	79,662	83,690	32,340	84,45	27,312	96,2	100,63	1,046
	393,03	86,851	89,370	34,133	85,81	29,289	110,5	116,30	1,052
	441,80	87,346	80,861	31,093	83,80	26,057	109,0	116,48	1,069
H36	325,07	83,630	86,240	31,013	86,81	26,923	99,2	102,35	1,032
	311,74	89,726	84,897	32,394	86,67	28,075	110,4	114,37	1,036
	328,01	86,859	83,634	31,829	83,83	26,682	107,8	114,19	1,059
H81	401,84	89,761	78,646	31,346	85,69	26,860	96,7	97,37	1,007
	388,27	98,858	80,443	32,386	85,83	27,798	109,1	110,61	1,014
	409,89	96,091	77,703	31,703	83,06	26,332	107,7	109,51	1,017
H100	435,24	82,349	85,055	31,621	87,13	27,551	96,2	97,28	1,011
	415,25	88,595	85,991	32,927	87,70	28,878	110,2	111,72	1,014
	449,97	89,680	82,340	32,026	83,21	26,649	108,9	110,88	1,018

Fuel	CA10	CA50	CA90	CA90 - CA10 (º)	ΔΘd (º)	ΔΘr ()	ΔΘo (º)
E22	12	24	43	31	17,25	31	48,25
	7	18	34	27	19,55	27	46,55
	5	16	32	27	21,19	27	48,19
E50	6	15	33	27	18,00	27	45,00
	6	16	32	26	21,75	26	47,75
	3	13	28	25	19,94	25	44,94
E85	3	12	31	28	15,76	28	43,76
	5	15	29	24	20,76	24	44,76
	2	13	27	25	18,10	25	43,10
E100	6	16	39	33	14,05	33	47,05
	2	13	30	28	18,50	28	46,50
	4	15	31	27	20,10	27	47,10
H36	2	12	41	39	13,97	39	52,97
	5	16	33	28	20,75	28	48,75
	3	16	34	31	20,02	31	51,02
H81	4	14	31	27	16,75	27	43,75
	5	17	32	27	20,75	27	47,75
	3	14	28	25	19,50	25	44,50
H100	5	16	37	32	14,36	32	46,36
	6	17	35	29	22,50	29	51,50
	3	14	33	30	19,19	30	49,19

Sandoval Model (2003)

Fuel	Mechanical Efficiency								
	1300 RPM			2500 RPM			3500 RPM		
	Model	Experimental	Error %	Model	Experimental	Error %	Model	Experimental	Error %
E22	89,424	88,505	1,038	87,730	85,975	2,041	84,266	84,453	0,220
E50	90,200	86,118	4,740	88,226	86,141	2,420	83,598	83,415	0,219
E85	90,203	85,258	5,800	88,036	85,413	3,071	83,796	83,065	0,879
E100	90,342	84,452	6,975	87,863	85,811	2,392	84,646	83,802	1,007
H36	90,200	86,811	3,903	87,995	86,668	1,532	83,638	83,830	0,229
H81	90,019	85,689	5,053	87,572	85,833	2,026	83,533	83,059	0,571
H100	89,759	87,130	3,016	87,574	87,703	0,147	84,123	83,212	1,095

Fuel	tfmep (bar)								
	1300 RPM			2500 RPM			3500 RPM		
	Model	Experimental	Error %	Model	Experimental	Error %	Model	Experimental	Error %
E22	1,059	1,152	7,994	1,443	1,650	12,515	1,850	1,828	1,197
E50	1,023	1,449	29,402	1,391	1,637	15,044	1,972	1,994	1,104
E85	1,032	1,552	33,543	1,433	1,748	17,982	1,967	2,056	4,313
E100	1,016	1,636	37,885	1,443	1,687	14,464	1,844	1,946	5,208
H36	1,034	1,392	25,691	1,412	1,568	9,956	1,943	1,920	1,187
H81	1,040	1,492	30,256	1,459	1,663	12,273	1,972	2,029	2,800
H100	1,044	1,312	20,422	1,442	1,427	1,045	1,919	2,029	5,426

Heywood Model (1988)

uel	Mechanical Efficiency								
	1300 RPM			2500 RPM			3500 RPM		
	Model	experimental	Error %	Model	experimental	Error %	Model	experimental	Error %
22	87,527	88,505	1,105	85,908	85,975	0,078	82,072	84,453	2,818
50	88,025	86,118	2,215	85,971	86,141	0,198	82,472	83,415	1,131
85	88,133	85,258	3,372	86,165	85,413	0,880	82,641	83,065	0,511
100	88,122	84,452	4,346	86,062	85,811	0,293	82,455	83,802	1,607
36	88,160	86,811	1,553	85,910	86,668	0,874	82,254	83,830	1,880
81	88,011	85,689	2,710	85,880	85,833	0,054	82,401	83,059	0,792
100	87,746	87,130	0,706	85,716	87,703	2,265	82,563	83,212	0,780

Fuel	tfmep(bar)								
	1300 RPM			2500 RPM			3500 RPM		
	Model	experimental	Error %	Model	experimental	Error %	Model	experimental	Error %
E22	1,25	1,15	8,51	1,66	1,65	0,48	2,11	1,83	15,31
E50	1,25	1,45	13,74	1,66	1,64	1,23	2,11	1,99	5,69
E85	1,25	1,55	19,50	1,66	1,75	5,15	2,11	2,06	2,51
E100	1,25	1,64	23,61	1,66	1,69	1,77	2,11	1,95	8,32
H36	1,25	1,39	10,23	1,66	1,57	5,68	2,11	1,92	9,74
H81	1,25	1,49	16,23	1,66	1,66	0,33	2,11	2,03	3,88
H100	1,25	1,31	4,78	1,66	1,43	16,15	2,11	2,03	3,87

Appendix V - Vehicle's speed recovery time: Experimental and Simulated.

2	Test No.	SPARC Vehicle Data			Experimental Torque Model					Sandoval Friction Model (2003)					Heywood Friction Model (1988)				
		v0 (km/h)	vf(km/h)	t_{dyno} (s)	t_{sim}(s)	Error (%)	R^2	EQM%	EQM	t_{sim}(s)	Error (%)	R^2	EQM%	EQM	t_{sim}(s)	Error (%)	R^2	EQM%	EQM
3 ear	Test 1	38,4	78	7,1	7,53	6,12	0,9899	0,0588	0,209	7,86	0,11	0,9717	0,0986	0,350	8,07	0,14	0,9509	0,1297	0,460
	Test 2	38,7	77,5	6,9	7,31	6,00	0,9892	0,0610	0,210	7,62	0,10	0,9707	0,1003	0,346	7,83	0,13	0,9495	0,1316	0,454
	Test 3	38,3	77,9	7,1	7,58	6,83	0,9866	0,0678	0,241	7,91	0,11	0,9662	0,1076	0,382	8,12	0,14	0,9436	0,1390	0,494
	Test 4	57,2	95,4	7,3	8,41	15,21	0,9079	0,1776	0,648	9,44	0,29	0,7380	0,2995	1,093	9,84	0,35	0,6375	0,3523	1,286
	Test 5	57,9	95	7	8,10	15,75	0,9033	0,1821	0,637	9,09	0,30	0,7293	0,3046	1,066	9,47	0,35	0,6270	0,3576	1,252
	Test 6	57,7	95,9	7,3	8,47	15,98	0,9027	0,1826	0,666	9,54	0,31	0,7222	0,3085	1,126	9,95	0,36	0,6167	0,3623	1,323
4 ear	Test 7	37,7	77,4	10	10,57	5,65	0,9891	0,0609	0,304	10,80	0,08	0,9790	0,0846	0,423	11,06	0,11	0,9617	0,1142	0,571
	Test 8	37,0	78,2	10,4	10,94	5,16	0,9908	0,0559	0,291	11,18	0,08	0,9813	0,0797	0,415	11,46	0,10	0,9649	0,1092	0,568
	Test 9	37,2	79,3	10,5	11,10	5,67	0,9866	0,0676	0,355	11,35	0,08	0,9753	0,0916	0,481	11,63	0,11	0,9566	0,1214	0,637
	Test 10	56,9	95,2	9,6	10,21	6,32	0,9912	0,0547	0,262	10,65	0,11	0,9727	0,0963	0,462	10,96	0,14	0,9504	0,1300	0,624
	Test 11	56,6	94,2	9,4	9,96	5,96	0,9909	0,0555	0,261	10,38	0,10	0,9730	0,0959	0,4507	10,68	0,14	0,9509	0,1292	0,607
	Test 12	56,9	93,7	9,3	9,77	5,09	0,9956	0,0386	0,180	10,18	0,09	0,9823	0,0777	0,361	10,47	0,13	0,9642	0,1104	0,513

E50	Test No.	SPARC Vehicle Data			Experimental Torque Model					Sandoval Friction Model (2003)					Heywood Friction Model (1988)				
		v0 (km/h)	vf(km/h)	t_{dyno} (s)	t_{sim}(s)	Error (%)	R^2	EQM%	EQM	t_{sim}(s)	Error (%)	R^2	EQM%	EQM	t_{sim}(s)	Error (%)	R^2	EQM%	EQM
3rd Gear	Test 1	37,9	77,9	7,1	7,57	6,57	0,9882	0,0637	0,226	7,48	5,39	0,9932	0,0482	0,171	7,65	7,72	0,9844	0,0731	0,260
	Test 2	38,0	78,8	7,2	7,72	7,23	0,9848	0,0722	0,260	7,64	6,13	0,9917	0,0532	0,191	7,81	8,43	0,9804	0,0819	0,295
	Test 3	38,4	78,1	7	7,48	6,82	0,9876	0,0652	0,228	7,40	5,69	0,9927	0,0499	0,175	7,56	8,00	0,9836	0,0750	0,263
	Test 4	57,6	95,4	7,1	8,23	15,96	0,9174	0,1683	0,597	8,43	18,75	0,8988	0,1863	0,661	8,43	18,67	0,8877	0,1962	0,697
	Test 5	58,3	94,7	6,8	7,87	15,69	0,9025	0,1829	0,622	8,05	18,40	0,8833	0,2001	0,680	8,05	18,39	0,8701	0,2111	0,718
	Test 6	57,7	95,6	7,1	8,23	15,94	0,9074	0,1782	0,633	8,43	18,77	0,8879	0,1960	0,696	8,42	18,65	0,8758	0,2063	0,733
4th Gear	Test 7	37,3	76,5	9,9	10,39	4,91	0,9924	0,0508	0,252	10,06	1,57	0,9997	0,0103	0,051	10,36	4,66	0,9945	0,0434	0,215
	Test 8	37,3	76,7	9,9	10,42	5,30	0,9900	0,0584	0,289	10,09	1,96	0,9993	0,0156	0,077	10,40	5,06	0,9924	0,0508	0,251
	Test 9	37,3	77	9,9	10,47	5,75	0,9885	0,0625	0,309	10,14	2,41	0,9987	0,0207	0,103	10,45	5,52	0,9912	0,0547	0,271
	Test 10	56,7	95,6	9,7	10,25	5,71	0,9924	0,0508	0,246	10,13	4,40	0,9961	0,0363	0,176	10,38	7,06	0,9885	0,0625	0,303
	Test 11	56,4	94,8	9,6	10,07	4,91	0,9946	0,0430	0,206	9,94	3,54	0,9969	0,0325	0,1561	10,20	6,21	0,9915	0,0538	0,2583
	Test 12	56,6	95,2	9,8	10,12	3,27	0,9978	0,0273	0,134	9,99	1,96	0,9983	0,0240	0,118	10,25	4,57	0,9958	0,0377	0,185

5	Test No.	SPARC Vehicle Data			Experimental Torque Model					Sandoval Friction Model (2003)					Heywood Friction Model (1988)				
		v0 (km/h)	vf(km/h)	t_{dyno} (s)	t_{sim}(s)	Error (%)	R^2	EQM%	EQM	t_{sim}(s)	Error (%)	R^2	EQM%	EQM	t_{sim}(s)	Error (%)	R^2	EQM%	EQM
3 ear	Test 1	38,3	77,7	7	7,43	6,12	0,9912	0,0549	0,192	7,46	6,51	0,9897	0,0593	0,208	7,60	8,64	0,9800	0,0829	0,290
	Test 2	38,0	78,1	7,1	7,59	6,89	0,9898	0,0592	0,210	7,62	7,26	0,9882	0,0635	0,225	7,77	9,39	0,9778	0,0872	0,309
	Test 3	38,2	78,1	7	7,50	7,21	0,9883	0,0633	0,222	7,53	7,59	0,9866	0,0677	0,237	7,68	9,73	0,9746	0,0933	0,327
	Test 4	56,5	95,5	7,3	8,81	20,72	0,8807	0,2021	0,738	8,72	19,44	0,8848	0,1986	0,725	8,78	20,34	0,8650	0,2150	0,785
	Test 5	57,1	95,1	7,1	8,57	20,73	0,8810	0,2020	0,717	8,48	19,50	0,8850	0,1985	0,705	8,55	20,42	0,8653	0,2148	0,763
	Test 6	57,1	95,9	7,3	8,87	21,45	0,8721	0,2093	0,764	8,76	20,06	0,8777	0,2047	0,747	8,83	20,90	0,8581	0,2204	0,805
4 ear	Test 7	36,9	77	10,1	10,54	4,31	0,9939	0,0455	0,230	10,49	3,90	0,9963	0,0357	0,180	10,77	6,58	0,9869	0,0668	0,337
	Test 8	37,1	77,4	10,1	10,58	4,80	0,9936	0,0467	0,236	10,55	4,41	0,9958	0,0376	0,190	10,82	7,11	0,9862	0,0686	0,346
	Test 9	37,2	76,8	10	10,35	3,48	0,9963	0,0356	0,178	10,31	3,09	0,9980	0,0262	0,131	10,57	5,75	0,9906	0,0566	0,283
	Test 10	57,3	94,7	9,3	9,75	4,86	0,9955	0,0393	0,183	9,81	5,53	0,9940	0,0453	0,211	10,04	7,92	0,9858	0,0695	0,323
	Test 11	56,0	96,2	10	10,50	5,01	0,9950	0,0413	0,206369	10,56	5,64	0,9933	0,0476	0,2379	10,80	8,01	0,9842	0,0732	0,3662
	Test 12	55,9	95,7	9,9	10,36	4,60	0,9960	0,0368	0,182	10,42	5,23	0,9948	0,0420	0,208	10,65	7,60	0,9878	0,0645	0,319

E100	Test No.	SPARC Vehicle Data			Experimental Torque Model					Sandoval Friction Model (2003)					Heywood Friction Model (1988)				
		v0 (km/h)	vf(km/h)	t_{dyno} (s)	t_{sim}(s)	Error (%)	R^2	EQM%	EQM	t_{sim}(s)	Error (%)	R^2	EQM%	EQM	t_{sim}(s)	Error (%)	R^2	EQM%	EQM
3rd Gear	Test 1	38,1	80,3	7,5	8,08	7,73	0,9833	0,0756	0,284	8,47	12,93	0,9552	0,1238	0,464	8,70	16,06	0,9291	0,1557	0,584
	Test 2	38,8	80,2	7,3	7,85	7,48	0,9805	0,0816	0,298	8,23	12,73	0,9498	0,1311	0,479	8,46	15,85	0,9217	0,1637	0,598
	Test 3	38,5	77,3	6,8	7,27	6,96	0,9868	0,0673	0,229	7,60	11,83	0,9633	0,1122	0,382	7,81	14,81	0,9407	0,1427	0,485
	Test 4	57,4	96	7,2	8,30	15,25	0,9229	0,1626	0,585	9,01	25,12	0,8005	0,2614	0,941	9,39	30,42	0,7145	0,3128	1,126
	Test 5	58,2	95,8	7	8,08	15,41	0,9121	0,1736	0,607	8,77	25,34	0,7803	0,2744	0,961	9,15	30,66	0,6886	0,3267	1,144
	Test 6	57,9	94,2	6,7	7,65	14,14	0,9261	0,1593	0,534	8,28	23,65	0,8084	0,2565	0,859	8,62	28,68	0,7262	0,3066	1,027
4th Gear	Test 7	37,2	77,4	10,1	10,71	6,05	0,9878	0,0643	0,325	10,91	8,05	0,9823	0,0775	0,391	11,19	10,77	0,9657	0,1080	0,546
	Test 8	37,8	78,4	10,2	10,78	5,69	0,9893	0,0602	0,307	11,00	7,84	0,9836	0,0747	0,381	11,28	10,55	0,9674	0,1053	0,537
	Test 9	36,9	76,9	10	10,65	6,50	0,9861	0,0688	0,344	10,84	8,44	0,9811	0,0802	0,401	11,12	11,17	0,9639	0,1108	0,554
	Test 10	55,9	95,2	9,7	10,29	6,07	0,9907	0,0562	0,273	10,81	11,41	0,9664	0,1070	0,519	11,12	14,60	0,9423	0,1401	0,679
	Test 11	55,9	95,1	9,7	10,25	5,70	0,9931	0,0484	0,23475	10,77	11,01	0,9717	0,0981	0,4759	11,08	14,18	0,9498	0,1307	0,6340
	Test 12	56,0	95,5	9,8	10,32	5,26	0,9922	0,0516	0,253	10,84	10,59	0,9689	0,1028	0,504	11,15	13,76	0,9456	0,1360	0,666

H36	Test No.	SPARC Vehicle Data			Experimental Torque Model					Sandoval Friction Model (2003)					Heywood Friction Model (1988)				
		v0 (km/h)	vf(km/h)	t_{dyno} (s)	t_{sim}(s)	Error (%)	R^2	EQM%	EQM	t_{sim}(s)	Error (%)	R^2	EQM%	EQM	t_{sim}(s)	Error (%)	R^2	EQM%	EQM
3 ear	Test 1	38,2	77,3	7,1	7,50	5,59	0,9908	0,0562	0,200	7,83	10,22	0,9731	0,0961	0,341	8,01	12,76	0,9534	0,1264	0,449
	Test 2	38,3	77	6,9	7,44	7,79	0,9816	0,0794	0,274	7,76	12,48	0,9581	0,1199	0,414	7,94	15,09	0,9338	0,1507	0,520
	Test 3	37,9	76,1	6,8	7,26	6,77	0,9841	0,0738	0,251	7,56	11,22	0,9634	0,1120	0,381	7,74	13,82	0,9400	0,1435	0,488
	Test 4	57,3	94,2	7,1	7,88	11,03	0,9464	0,1355	0,481	8,75	23,29	0,8193	0,2489	0,884	8,85	24,65	0,7860	0,2708	0,961
	Test 5	57,3	95	7,2	8,16	13,31	0,9206	0,1649	0,594	9,09	26,19	0,7656	0,2834	1,020	9,18	27,50	0,7279	0,3053	1,099
	Test 6	57,2	94,9	7,1	8,08	13,75	0,9186	0,1671	0,593	8,99	26,59	0,7628	0,2851	1,012	9,08	27,91	0,7246	0,3072	1,091
4 ear	Test 7	37,7	76,2	9,7	10,28	5,98	0,9871	0,0663	0,321	10,43	7,56	0,9827	0,0768	0,372	10,73	10,59	0,9635	0,1115	0,541
	Test 8	37,7	77,9	10,1	10,73	6,20	0,9886	0,0622	0,314	10,90	7,91	0,9837	0,0744	0,376	11,21	10,96	0,9651	0,1089	0,550
	Test 9	37,5	76,9	9,9	10,54	6,50	0,9867	0,0672	0,333	10,70	8,12	0,9818	0,0786	0,389	11,01	11,17	0,9623	0,1133	0,561
	Test 10	55,8	93,5	9,5	9,98	5,03	0,9937	0,0465	0,221	10,42	9,64	0,9771	0,0883	0,420	10,69	12,55	0,9564	0,1218	0,578
	Test 11	56,0	94,9	9,8	10,36	5,76	0,9909	0,0557	0,273	10,84	10,62	0,9707	0,0998	0,4888	11,13	13,53	0,9476	0,1336	0,6545
	Test 12	56,3	94,2	9,5	10,12	6,49	0,9869	0,0667	0,317	10,57	11,31	0,9640	0,1107	0,526	10,85	14,25	0,9383	0,1449	0,688

1	Test No.	SPARC Vehicle Data			Experimental Torque Model					Sandoval Friction Model (2003)					Heywood Friction Model (1988)				
		v0 (km/h)	vf(km/h)	t_{dyno} (s)	t_{sim}(s)	Error (%)	R^2	EQM%	EQM	t_{sim}(s)	Error (%)	R^2	EQM%	EQM	t_{sim}(s)	Error (%)	R^2	EQM%	EQM
3rd Gear	Test 1	38,4	78,1	7,1	7,60	7,07	0,9871	0,0665	0,236	7,61	7,23	0,9877	0,0649	0,231	7,76	9,23	0,9779	0,0869	0,309
	Test 2	38,1	76,7	6,9	7,28	5,46	0,9929	0,0493	0,170	7,28	5,52	0,9936	0,0469	0,162	7,42	7,52	0,9862	0,0687	0,237
	Test 3	38,1	77,3	6,9	7,39	7,13	0,9839	0,0743	0,256	7,40	7,23	0,9856	0,0702	0,242	7,54	9,25	0,9739	0,0946	0,326
	Test 4	56,7	95,2	7,2	8,29	15,08	0,9282	0,1568	0,564	8,44	17,20	0,9095	0,1761	0,634	8,53	18,45	0,8901	0,1940	0,699
	Test 5	56,9	95,9	7,3	8,51	16,60	0,9006	0,1845	0,673	8,67	18,80	0,8776	0,2047	0,747	8,76	20,02	0,8551	0,2228	0,813
	Test 6	57,0	94,9	7,1	8,16	14,87	0,9335	0,1509	0,536	8,31	16,99	0,9156	0,1701	0,604	8,40	18,24	0,8968	0,1881	0,668
4th Gear	Test 7	37,7	77,6	10,1	10,60	4,97	0,9937	0,0463	0,234	10,43	3,28	0,9983	0,0240	0,121	10,68	5,73	0,9927	0,0500	0,252
	Test 8	38,2	76,8	9,7	10,23	5,48	0,9937	0,0462	0,224	10,07	3,78	0,9983	0,0237	0,115	10,31	6,25	0,9927	0,0497	0,241
	Test 9	37,5	77,2	10	10,55	5,47	0,9917	0,0532	0,266	10,37	3,75	0,9978	0,0274	0,137	10,62	6,21	0,9910	0,0554	0,277
	Test 10	56,5	94,7	9,5	10,10	6,31	0,9911	0,0552	0,262	10,12	6,49	0,9913	0,0545	0,259	10,33	8,74	0,9819	0,0784	0,372
	Test 11	56,1	95,8	9,9	10,45	5,57	0,9939	0,0456	0,226	10,47	5,78	0,9938	0,0459	0,2272	10,69	8,00	0,9864	0,0680	0,3365
	Test 12	55,4	94,7	9,7	10,27	5,91	0,9931	0,0483	0,234	10,29	6,04	0,9936	0,0466	0,226	10,50	8,28	0,9852	0,0710	0,344

H100	Test No.	SPARC Vehicle Data			Experimental Torque Model					Sandoval Friction Model (2003)					Heywood Friction Model (1988)				
		v0 (km/h)	vf(km/h)	t_{dyno} (s)	t_{sim}(s)	Error (%)	R^2	EQM%	EQM	t_{sim}(s)	Error (%)	R^2	EQM%	EQM	t_{sim}(s)	Error (%)	R^2	EQM%	EQM
3 ear	Test 1	38,1	77,8	7	7,58	8,28	0,9859	0,0696	0,244	7,67	9,51	0,9788	0,0853	0,298	7,84	12,00	0,9626	0,1133	0,396
	Test 2	38,4	76,9	6,8	7,26	6,78	0,9870	0,0667	0,227	7,35	8,04	0,9799	0,0831	0,283	7,51	10,50	0,9636	0,1117	0,380
	Test 3	38,0	77,6	7,1	7,48	5,36	0,9921	0,0521	0,185	7,57	6,57	0,9866	0,0679	0,241	7,74	8,99	0,9732	0,0958	0,340
	Test 4	58,0	95,5	7,1	8,07	13,67	0,9354	0,1488	0,528	7,95	11,97	0,9384	0,1452	0,516	8,11	14,19	0,9133	0,1723	0,612
	Test 5	58,4	94,7	6,9	7,81	13,12	0,9389	0,1448	0,500	7,70	11,58	0,9412	0,1420	0,490	7,85	13,80	0,9166	0,1691	0,583
	Test 6	57,9	93,9	6,7	7,72	15,19	0,9143	0,1715	0,575	7,63	13,84	0,9157	0,1702	0,570	7,78	16,12	0,8858	0,1980	0,663
4 ear	Test 7	37,4	76,6	9,8	10,43	6,38	0,9886	0,0623	0,305	10,53	7,41	0,9856	0,0701	0,343	10,80	10,16	0,9699	0,1012	0,496
	Test 8	37,5	77,2	10	10,55	5,50	0,9908	0,0560	0,280	10,65	6,54	0,9880	0,0638	0,319	10,93	9,27	0,9735	0,0949	0,474
	Test 9	37,6	76,2	9,8	10,17	3,76	0,9952	0,0405	0,198	10,27	4,77	0,9934	0,0475	0,233	10,53	7,44	0,9821	0,0781	0,383
	Test 10	55,1	94,3	9,8	10,25	4,64	0,9948	0,0420	0,206	10,41	6,27	0,9891	0,0608	0,298	10,68	8,94	0,9758	0,0908	0,445
	Test 11	56,7	94,3	9,4	9,81	4,35	0,9956	0,0386	0,181	9,96	5,98	0,9903	0,0574	0,2698	10,21	8,65	0,9776	0,0873	0,4101
	Test 12	56,4	93,6	9,3	9,76	4,97	0,9945	0,0433	0,201	9,92	6,64	0,9886	0,0623	0,289	10,17	9,32	0,9751	0,0922	0,429

Appendix VI – Acceleration Performance of the Peugeot 207 SW

uel	No. Test	3rd Gear								4th Gear							
		40 to 80 km/h				60 to 100 km/h				40 to 80 km/h				60 to 100 km/h			
		ax (m/s²)	R²	ax (m/s²) average	SD	ax (m/s²)	R²	ax (m/s²) average	SD	ax (m/s²)	R²	ax (m/s²) average	SD	ax (m/s²)	R²	ax (m/s²) average	SD
22	Test 1	1.567	0.9996	1,568	0,002027	1.457	0.9954	1,458	0,013668	1.098	0.9993	1,1	0,005147	1.114	0.9998	1,113	0,009297
	Test 2	1.571	0.9986			1.476	0.9959			1.095	0.9986			1.123	0.9997		
	Test 3	1.566	0.9994			1.442	0.9976			1.107	0.9997			1.101	0.9998		
50	Test 1	1.598	0.9985	1,599	0,003498	1.488	0.9970	1,489	0,00098	1.102	0.9997	1,105	0,003196	1.488	0.9970	1,489	0,009982
	Test 2	1.596	0.9999			1.489	0.9941			1.110	0.9999			1.489	0.9941		
	Test 3	1.604	0.9989			1.490	0.9974			1.104	0.9996			1.490	0.9974		
85	Test 1	1.595	0.9995	1,6	0,003996	1.496	0.9968	1,491	0,00572	1.103	0.9998	1,102	0,003496	1.496	0.9968	1,491	0,001643
	Test 2	1.600	0.9988			1.494	0.9981			1.106	0.9999			1.494	0.9981		
	Test 3	1.604	0.9994			1.483	0.9983			1.098	0.9998			1.483	0.9983		
E100	Test 1	1.592	0.9971	1,601	0,011286	1.483	0.9962	1,495	0,011722	1.105	0.9997	1,103	0,002682	1.483	0.9962	1,495	0,002387
	Test 2	1.593	0.9974			1.492	0.9971			1.104	0.9983			1.492	0.9971		
	Test 3	1.617	0.9990			1.511	0.9987			1.099	0.9989			1.511	0.9987		
H36	Test 1	1.546	0.9994	1,567	0,014972	1.444	0.9976	1,462	0,014981	1.097	0.9998	1,103	0,003989	1.444	0.9976	1,462	0,006117
	Test 2	1.581	0.9993			1.459	0.9972			1.106	0.9999			1.459	0.9972		
	Test 3	1.574	0.9999			1.481	0.9973			1.106	0.9997			1.481	0.9973		
H81	Test 1	1.579	0.9995	1,581	0,007083	1.487	0.9985	1,485	0,004487	1.098	0.9995	1,095	0,002433	1.487	0.9985	1,485	0,002274
	Test 2	1.574	0.9992			1.489	0.9977			1.095	0.9985			1.489	0.9977		
	Test 3	1.591	0.9993			1.479	0.9986			1.092	0.9996			1.479	0.9986		
H100	Test 1	1.589	0.9995	1,583	0,008736	1.466	0.9979	1,477	0,017825	1.109	0.9996	1,099	0,008459	1.466	0.9979	1,477	0,000406
	Test 2	1.589	0.9984			1.463	0.9979			1.100	0.9999			1.463	0.9979		
	Test 3	1.571	0.9992			1.502	0.9979			1.088	0.9998			1.502	0.9979		

Tests	Fuel	Dyno			Bench Tests			Sandoval (2003)			Heywood (1988)		
		ax (m/s²)	EQM (km/h)	EQMp	ax (m/s²)	EQM (km/h)	EQMp	ax (m/s²)	EQM (km/h)	EQMp	ax (m/s²)	EQM (km/h)	EQMp
7	**E22**	1,0977	0,1040	0,0018	1,0502	0,0626	0,0011	1,0290	0,0620	0,0011	1,0046	0,0632	0,0011
	E50	1,1020	0,1021	0,0018	1,0545	0,0550	0,0010	1,0893	0,0527	0,0009	1,0567	0,0488	0,0009
	E85	1,1031	0,0828	0,0015	1,0652	0,0677	0,0012	1,0683	0,0565	0,0010	1,0412	0,0534	0,0009
	E100	1,1049	0,1240	0,0022	1,0490	0,0771	0,0014	1,0292	0,0647	0,0011	1,0044	0,0682	0,0012
	H36	1,0973	0,0927	0,0016	1,0452	0,0372	0,0007	1,0308	0,0753	0,0013	1,0022	0,0753	0,0013
	H81	1,0980	0,1784	0,0031	1,0516	0,0513	0,0009	1,0684	0,0654	0,0011	1,0435	0,0609	0,0011
	H100	1,1088	0,1900	0,0034	1,0508	0,0647	0,0011	1,0393	0,0367	0,0006	1,0134	0,0365	0,0006
8	**E22**	1,0954	0,0696	0,0012	1,0534	0,0689	0,0012	1,0319	0,0690	0,0012	1,0074	0,0704	0,0012
	E50	1,1096	0,0942	0,0017	1,0561	0,0548	0,0010	1,0908	0,0543	0,0010	1,0581	0,0503	0,0009
	E85	1,1061	0,0922	0,0016	1,0656	0,0665	0,0012	1,0684	0,0594	0,0010	1,0413	0,0560	0,0010
	E100	1,1042	0,0803	0,0014	1,0527	0,0705	0,0012	1,0315	0,0739	0,0013	1,0066	0,0779	0,0013
	H36	1,1057	0,1267	0,0022	1,0465	0,0422	0,0007	1,0308	0,0933	0,0016	1,0023	0,0928	0,0016
	H81	1,0945	0,1968	0,0034	1,0538	0,0471	0,0008	1,0707	0,0584	0,0010	1,0458	0,0543	0,0009
	H100	1,0998	0,1063	0,0019	1,0518	0,0632	0,0011	1,0401	0,0389	0,0007	1,0141	0,0387	0,0007
9	**E22**	1,1073	0,0908	0,0016	1,0613	0,0674	0,0012	1,0392	0,0723	0,0012	1,0145	0,0753	0,0013
	E50	1,1040	0,1533	0,0027	1,0598	0,0544	0,0010	1,0944	0,0560	0,0010	1,0616	0,0518	0,0009
	E85	1,0977	0,1113	0,0020	1,0707	0,0651	0,0011	1,0737	0,0544	0,0010	1,0465	0,0513	0,0009
	E100	1,0989	0,1702	0,0030	1,0495	0,0814	0,0014	1,0306	0,0604	0,0011	1,0057	0,0636	0,0011
	H36	1,1058	0,1184	0,0021	1,0433	0,0398	0,0007	1,0284	0,0826	0,0014	0,9999	0,0825	0,0014
	H81	1,0921	0,1155	0,0020	1,0518	0,0518	0,0009	1,0690	0,0606	0,0011	1,0690	0,0606	0,0011
	H100	1,0882	0,1005	0,0018	1,0607	0,0631	0,0011	1,0491	0,0350	0,0006	1,0229	0,0348	0,0006

Appendix VII – MATLAB CODE

- INPUTS

```
function [ic,id,Cd,Af,m,r,p] = car_parameters

%Transmission
ic = [41/12,38/21,41/32,39/40,33/43];   %transmission gear ratios
id = 60/14;                             %differencial gear ratio

Cd = 0.31;      % Drag coefficient

Af = 2.01;      % Frontal area of the vehicle (m²)

m = 1113+70;       % vehicle mass (kg)

p = 33;         % tire pressure (psi)

aro = 14;       % wheel size (inches)

Lb = 185;       % Tire width (mm)

sb = 65;        % Tire height/width

Cp = 3.05;      % radial tire coefficient (Brunneti)

r = (aro/(2*39.37) + Lb*sb*10^(-5))*Cp/pi;

end
```

```
function [ncs,Lv_ad,Lv_ex,dv_ad,dv_ex,nv_ad,nv_ex,Cff,Crf,Com,Coh] =
valve_train_geometry

%Parâmetros do trem de válvulas

ncs = 5;                        %Number of camshaft bearings

type = 2;                       %type of the valve train
config = 'SOHC';                %Configuration of the camshaft
follower = 'roller follower';   %type of the camshaft follower

Lv_ad = 8.8;                    %Maximum valve lift - intake valve (mm)
Lv_ex = 8.75;                   %Maximum valve lift - exhaust valve (mm)

dv_ad = 35;                     %Intake valve diameter (mm)
dv_ex = 27.5;                   %Exhaust valve diameter (mm)

nv_ad = 4;                      %total of intake valves of the ICE
nv_ex = 4;                      %total of exhaust valves of the ICE
```

```
if type==1
    if strcmp('SOHC',config)==1
        Coh = 0.5; %(kPa-mm-min/rev)^1/2
        Com = 107; %kPa
        if strcmp ('roller follower',follower)==1
            Cff =0;
            Crf = 0.0076;    %kPa-mm-min/rev
        else
            Crf = 0;
            Cff = 200;       %kPa-mm
        end
    else
        Coh = 0.5; %(kPa-mm-min/rev)^1/2
        Com = 107; %kPa
        if strcmp('roller follower',follower)==1
            Cff = 0;
            Crf = 0.0050;    %kPa-mm-min/rev
        else
            Crf = 0;
            Cff = 133;       %kPa-mm
        end
    end
elseif type == 2
    Coh = 0.2;
    Com = 42.8;
    if strcmp ('roller follower',follower)==1
        Cff = 0;
        Crf = 0.0227;
    else
        Crf = 0;
        Cff = 600;
    end
elseif type == 3
    Coh = 0.5;
    Com = 21.4;
    if strcmp ('roller follower',follower)==1
        Cff = 0;
        Crf = 0.0151;
    else
        Crf = 0;
        Cff = 400;
    end
else
    Coh = 0.5;
    Com = 32.1;
    if strcmp ('roller follower',follower)==1
        Cff = 0;
        Crf = 0.0151;
    else
        Crf = 0;
        Cff = 400;
    end
end

end
```

```
function [B,S,L,a,Db,nb,Lb,rc,nc,ncr,Lcr,Dcr] = engine_geometry

%Principal parameters

B = 75;          %Bore (mm)
S = 77;          %Stroke (mm)
L = 126.8;       %Connecting rod size (mm)
rc = 10.5;       %Compression Ratio
nc = 4;          %Number of cylinders of the ICE

%crankshaft

a = 38.5;        %Radius of the crankshaft
Db = 2*38.5;     %Diameter of the main bearings(mm)
Lb = 17.29;      %Width of the main bearings (mm)
nb = 5;          %number of main bearings

%Connecting rod

ncr = 4;         %number of bearings
Lcr = 19.75;      %Width of the bearings (mm)
Dcr = Db;        %Diameter of the bearings (mm)

end
```

- MAIN FUNCTION

```
clc
clear all
%% INPUTS

% Engine Geometry

[B,S,L,a,Db,nb,Lb,rc,nc,ncr,Lcr,Dcr] = engine_geometry;     %(mm)

% Valve Train Parameters

[ncs,Lv_ad,Lv_ex,dv_ad,dv_ex,nv_ad,nv_ex,Cff,Crf,Com,Coh] =
valve_train_geometry;

%Valve timing

teta_open_ad = 2;    %open ATDC
teta_close_ad = 33;  %close ABTC
teta_open_ex = 35;   %open BBDC
teta_close_ex = 2;   %close BTDC

% Vehicle Parameters
```

```
[ic,id,Cd,Af,m,r_w,p_tire] = car_parameters;

% Engine Tested Speeds (RPM)

qtd_tests = 3;          %number of tests made in dyno
gear = 4;               %gear tested
sp_range = 60100;       %speed range SR tests

qtd_rot = 3;          %number of engine speeds tested in the bench
delta_teta = 1;       %sensor resolution for the crankshaft angle
N_eng = [1300,2500,3500];

correlation = 3; % 2: Sandoval (2003) / 3: Heywood (1988)

mu_sc = 0.7; %low shear-high shear oil viscosity ratio (for Sandoval
Friction Model)

% FUEL

fuel_names =  ["E22","E50","E85","E100","H36","H81","H100"];
AF =        [13.928, 12.74, 10.435, 8.935, 11.46, 10.375, 8.716];
%AF ration
LHV = [39249, 35657.5, 29460.75, 26805, 35257.344, 28588.97, 25732.8]*10^3;
%Lower Heating Value (J/kg)

% ROAD LOAD COEFFICIENTS

F0 = 102.12;     %N
F1 = -0.5767;    %N/(km/h)
F2 = 0.03562;    %N/(km/h²)

%%
%Engine Geometry and Kinematics

[V,A,Vd,Vc,s,dt,Sp,v_Sp,teta,teta_rad,x] =
Engine_Kinematics(delta_teta,S,B,rc,a,L,N_eng,qtd_rot);
v_precision = x;
N_RPM = linspace(N_eng(1,1),N_eng(1,qtd_rot),v_precision)';

[~,qtd_fuels] = size(fuel_names);    %Total of fuels testing
[~,qtd_gears] = size(ic);           %number of gears

trans_eff = zeros(1,qtd_tests);

% Friction Losses - Simulation
if correlation == 2
    sim_name = 'Sandoval(2003)';
else
    sim_name = 'Heywood(1988)';
end

%Open files
```

```
bench_file_name = sprintf('Testes de
Retomada/Results/SRTests_bench_%d_%d.txt',gear,sp_range);
sim_file_name = sprintf('Testes de
Retomada/Results/SRTests_%s_%d_%d.txt',sim_name,gear,sp_range);

benchID = fopen(bench_file_name,'w');
simID = fopen(sim_file_name,'w');

trans_eff_ID = fopen(sprintf('Testes de Retomada/Results/Average
Transmission Efficiency/Trans_eff_%d_%d.txt',gear,sp_range),'w');

%Write in  first line - title

fprintf(benchID,'Simulation Method: Bench Torque\n\n');
fprintf(simID,sprintf('Simulation Method: Pressure curves + %s friction
model for SI Engines\n\n',sim_name));
fprintf(trans_eff_ID,sprintf('Average Transmission Efficiency\n %d Gear ,
Speed Range: %d km/h\n\n',gear,sp_range));

for i = 1:qtd_fuels

    %Pressure curves x crankshaft angle
    [p_cyl,p_intake] = read_data_pressure (fuel_names(1,i),qtd_rot,x);

    %Massic flow rates, Exp. Torque, lambda and Room Conditions
    [Tb,lambda,p_amb,T_amb,P_intake,T_intake,T_room,m_f_dot,adv_ig,UR] =
get_experimental_data(i,qtd_rot);

    %Engine parameters analysis - Experimental Torque
    [Tb,imep,bmep,tfmep,pmep] = engine_analysis_exp
(V,A,Vd,Vc,dt,Sp,fuel_names(1,i),nc,p_cyl,teta,x,N_eng,...

LHV(1,i),AF(1,i),teta_open_ad,teta_close_ad,teta_open_ex,Tb,lambda,p_amb,T_a
mb,T_room,m_f_dot,adv_ig,UR,qtd_rot);

    %Engine Friction Models - Simulated Torque
    [Tb_sim,tfmep_sim,bmep_sim] = simulated_tfmep
(correlation,imep,qtd_rot,N_eng,Sp,mu_sc,Vd,B,S,Db,nb,Lb,rc,nc,ncr,Lcr,Dcr,n
cs,dv_ad,dv_ex,Lv_ad,Lv_ex,nv_ad,nv_ex,Cff,Crf,Com,Coh,P_intake,p_amb);
    if correlation == 2
        tfmep_sim = tfmep_sim + pmep; %consider the pmep from pressure
curves for Sandoval(2003) model
    end

    %Generate polynomials
    W_brake_dot = bmep.*N_eng*nc*Vd/(120);
    [y_Wb_dot,Wb_dot_pol] = generate_pol
(W_brake_dot,N_RPM,N_eng,1,v_precision);  %in function of the RPM
    [y_Tb,Tb_pol] = generate_pol (Tb,N_RPM,N_eng,2,v_precision);
%experimental torque and friction
    [y_tfmep,tfmep_pol] = generate_pol
(tfmep/1000,N_RPM,N_eng,2,v_precision);
    [y_Tb_sim,Tb_pol_sim] = generate_pol (Tb_sim,N_RPM,N_eng,2,v_precision);
%simulated torque and friction
```

```
    [y_tfmep_sim,tfmep_pol_sim] = generate_pol
(tfmep_sim/1000,N_RPM,N_eng,2,v_precision);

    %comparing simulation with experimental:

    %Friction mep
    figure
    plot(N_RPM,y_tfmep,'b',N_RPM,y_tfmep_sim,'r')
    hold all
    for j =1:qtd_rot
        plot(N_eng(j),tfmep(j)/1000,'bo',N_eng(j),tfmep_sim(j)/1000,'ro')
    end
    legend({'Bench','Simulation'},'Location','Southeast')
    xlabel('RPM')
    ylabel('TFMEP (kPa)')
    title(sprintf('%s\nFriction MEP',fuel_names(i)))
    subtitle(sprintf('%s',sim_name))

    %Engine Torque
    figure
    plot(N_RPM,y_Tb,'b',N_RPM,y_Tb_sim,'r')
    hold all
    for j =1:qtd_rot
        plot(N_eng(j),Tb(j),'bo',N_eng(j),Tb_sim(j),'ro')
    end
    legend({'Bench','Simulation'},'Location','Southeast')
    xlabel('RPM')
    ylabel('Brake Torque (N)')
    title(sprintf('%s\nEngine Torque (N)',fuel_names(i)))
    subtitle(sprintf('%s',sim_name))

    %Write .txt
    fprintf(benchID,fuel_names(1,i));
    fprintf(simID,fuel_names(1,i));
    fprintf(benchID,'\n\n');
    fprintf(simID,'\n\n');

    fprintf(benchID,'vo(km/h)  vf(km/h)  tf_dyno(s)  tf_sim   R²   EQM
EQMp\n');
    fprintf(simID,'vo(km/h)  vf(km/h)  tf_dyno(s)  tf_sim   R²   EQM
EQMp\n');

    fprintf(trans_eff_ID,'%s',fuel_names(i));

    %% CHASSIS DYNAMOMETER TESTS

    for no_test = 1:qtd_tests

        sr_benchID = fopen(sprintf('Testes de
retomada/Results/BENCH_%s_%d_%d_%d.txt',fuel_names(i),gear,sp_range,no_test)
,'w');
        sr_simID = fopen(sprintf('Testes de
retomada/Results/%s_%s_%d_%d_%d.txt',sim_name,fuel_names(i),gear,sp_range,no
_test),'w');
        fprintf(sr_benchID,'v(km/h) tdyno(s) tsim (s)\n\n');
```

```
        fprintf(sr_simID,'v(km/h) tdyno(s) tsim (s)\n\n');

        %get data from files (car speed and wheel power)
        str = sprintf('%s_%d_%d_%d',fuel_names(i),gear,sp_range,no_test);
        DATA = readmatrix(sprintf('Testes de Retomada/%s',str));
        v_v  = DATA(:,1);                                   %car speed in
function of the time in dyno (km/h)
        Pw   = DATA(:,2)*10^3;                              %Power on wheels
measured on the dyno (kW)
        [size_t,~] = size(v_v);
        t    = transpose(0:0.1:(size_t-1)/10);              %time of the SR
tests in dyno(s)
        N_SR    =  v_v*60*ic(gear)*id/(3.6*2*pi*r_w);      %engine-vehicle
relation during the SR test
        Pb   = polyval(Wb_dot_pol(1,:),N_SR);

        %transmission efficiency

        eff  = (Pw./Pb);
        figure
        plot(v_v,Pb/1000,v_v,Pw/1000)
        title(sprintf('%s',fuel_names(i)))
        subtitle(sprintf('Test %d',no_test))
        xlabel('v (km/h)')
        ylabel('Power(kW)')
        legend('Engine Power','Wheel Power')
        name_plot = sprintf('Testes de Retomada/Results/Average Transmission
Efficiency/TRANS_EFF_%s_%d_%d_%d',fuel_names(i),gear,sp_range,no_test);
        print(name_plot,'-djpeg')
        trans_eff =  mean(eff);              %get the average transmission
efficiency

        fprintf(trans_eff_ID,'  %0.4f',trans_eff);

        %Speed recovery time simulation

        %experimental torque:
        [tf_bench,t_bench,R_2_bench,EQM_bench,EQMp_bench] =
speed_recovery_simulation(gear,t,v_v,trans_eff,ic,id,m,r_w,Tb_pol,F0,F1,F2);
        %simulated torque:
        [tf_sim,t_sim,R_2_sim,EQM_sim,EQMp_sim] =
speed_recovery_simulation(gear,t,v_v,trans_eff,ic,id,m,r_w,Tb_pol_sim,F0,F1,
F2);

        %writing results in the txt file

        fprintf(benchID,'%0.2f  %0.2f  %0.3f  %0.3f  %0.4f  %0.4f
%0.4f\n',v_v(1,1),v_v(length(v_v)),t(length(t)),tf_bench,R_2_bench,EQM_bench
,EQMp_bench);
        fprintf(simID,'%0.2f  %0.2f  %0.3f  %0.3f  %0.4f  %0.4f
%0.4f\n',v_v(1,1),v_v(length(v_v)),t(length(t)),tf_sim,R_2_sim,EQM_sim,EQMp_
sim);

        fprintf(sr_benchID,'%0.2f %0.2f %0.2f\n',[v_v;t;t_bench]);
        fprintf(sr_simID,'%0.2f %0.2f %0.2f\n',[v_v;t;t_sim]);
```

```
        %plot speed recovery tests

        plot(t,v_v,'--',t_bench,v_v,t_sim,v_v)
        legend({'Dyno','Bench',sim_name},'Location','Southeast');
        title ('Speed Recovery Tests')
        subtitle(sprintf('%s, Test %d, Gear %d',fuel_names(i),no_test,
gear))
        xlabel('Car Speed (km/h)')
        ylabel('Time (s)')
        name_plot = sprintf('Testes de
Retomada/Results/Images/%s_%d_%d_%d',fuel_names(i),gear,sp_range,no_test);
        print(name_plot,'-djpeg')

    end

    fprintf(trans_eff_ID,'\n');
    fprintf(benchID,'\n');
    fprintf(simID,'\n');

end

fclose('all');


function [p_cyl,p_intake] = read_data_pressure (fuel_name,qtd_rot,x)

p_cyl = zeros(x,qtd_rot);           % Cylinder pressure(Pa)
p_intake = zeros(x(1,1),qtd_rot);   % Intake Manifold Pressure(Pa)

for i=1:qtd_rot

    data_fuel = readmatrix('Motor
Bancada/Data_Engine.xlsx','Sheet',fuel_name); %Leitura da tabela com as
propriedades

    p_cyl(:,i) = abs(data_fuel(:,3+2*(i-1)))*10^5;
    p_intake(:,i) = abs(data_fuel(:,2+2*(i-1)))*10^5;

end

end


function
[m_tot,m_tot_dot,m_aw_dot,m_ad_dot,m_aw,m_ad,m_v,m_f,P_dry,Pv,R_aw,w] =
colect_data (UR,P,T,AF,m_f_dot,lambda,dt)

R_ad = 289.03;      %dry air constant(J/(kg.K))
R_v = 461.5;        %vapor of water constant(J/(kg.K))

% Vazão mássica de ar seco (kg/h)
```

```
m_ad_dot = m_f_dot*(AF*lambda); %vazão de ar seco (kg/h)

%Vapor saturation pressure (kPa)

Pv_sat  = 10^(30.59051-8.2*log10(T+273.15)+0.0024804*(T+273.15)-
3142.31/(T+273.15));

Pv = UR*Pv_sat*10^3/100;          %Vapor pressure (Pa)

P_dry = P-Pv;                     %dry air pressure (Pa)

w = 0.622*Pv/(P-Pv);         %absolute umidity

R_aw= (R_ad + R_v*w)/(1+w);      %wet air constant (J/(kgK))

m_aw_dot = m_ad_dot*(1+w);           %wet air massic flow rate(kg/h)

m_tot_dot = m_aw_dot + m_f_dot;      %total massic flow rate(kg/h)

% masses inside the cylinder (kg)

m_tot = 0; m_f=0; m_ad = 0; m_aw = 0; m_v = 0;

for j=1:180+30

    m_tot = m_tot_dot*dt/3600 + m_tot;

    m_f = m_f_dot*dt/3600 + m_f;

    m_ad = m_ad_dot*dt/3600 + m_ad;

    m_aw = m_aw_dot*dt/3600 + m_aw;

    m_v = m_aw - m_ad;

end

end

function [T,lambda,Pamb,Tamb,Pad,Tad,T_room,mf_dot,adv_ig,UR] =
get_experimental_data(fuel_line,qtd_rot)

T = zeros(1,qtd_rot);lambda = zeros(1,qtd_rot);Pamb = zeros(1,qtd_rot);
Tad = zeros(1,qtd_rot);adv_ig = zeros(1,qtd_rot);UR = zeros(1,qtd_rot);
mf_dot = zeros(1,qtd_rot);Tamb = zeros(1,qtd_rot);Pad = zeros(1,qtd_rot);
T_room = zeros(1,qtd_rot);

for i=1:qtd_rot

    exp_data = readmatrix('Motor Bancada/Data_Engine','Sheet','Experimental
Parameters');
```

```
    T(1,i) = exp_data(fuel_line,8+10*(i-1));                % Experimental
Torque

    lambda(1,i) = exp_data(fuel_line,11+10*(i-1));          % lambda

    Pamb(1,i) = exp_data(fuel_line,3+10*(i-1));             % Ambient
Pressure (Pa)

    Pad(1,i) = exp_data(fuel_line,7+10*(i-1));              % Intake
Pressure (Pa)

    T_room(1,i) = exp_data(fuel_line,5+10*(i-1));           % Room
Temperature(C)

    Tad(1,i) = exp_data(fuel_line,6+10*(i-1));              % Intake
Temperature(C)

    Tamb(1,i) = exp_data(fuel_line,2+10*(i-1));             % Ambient
Temperature (C)

    mf_dot(1,i) = exp_data(fuel_line,10+10*(i-1));              % fuel
massic flow rate(kg/h)

    adv_ig(1,i) = exp_data(fuel_line,9+10*(i-1));           % Avanço de
ignição (graus)

    UR(1,i) = exp_data(fuel_line,4+10*(i-1));               % Umidity (%)

end


end
```

- ENGINE ANALYSIS FUNCTION

```
function [Tb,imep,bmep,tfmep,pmep] = engine_analysis_exp
(V,A,Vd,Vc,dt,Sp,fuel_name,nc,p_cyl,teta,x,N_eng,...

LHV,AF,teta_open_ad,teta_close_ad,teta_open_ex,Tb,lambda,P_amb,T_amb,T_room,
m_fuel_dot,adv_ig,UR,qtd_rot)
%% Obtenção dos dados experimentais

save = 2; % if = 1, save images on the folder

tam_vector = [x,qtd_rot];
tam_file = [1,qtd_rot];

max_p = zeros(tam_file);teta_max_p = zeros(tam_file);m_ad_dot =
zeros(tam_file);m_ad = zeros(tam_file);m_fuel = zeros(tam_file);
```

```
m_tot = zeros(tam_file); m_tot_dot = zeros(tam_file);pv = zeros(tam_file);w
= zeros(tam_file); m_aw = zeros(tam_file);
m_v = zeros(tam_file);p_air_d = zeros(tam_file);R_aw = zeros
(tam_file);W_ind_dot = zeros(tam_file);W_ind = zeros(tam_file); C_F = zeros
(tam_file);
W_pump = zeros(tam_file); W = zeros(tam_vector);m_aw_dot =
zeros(tam_file);W_brake_dot = zeros(tam_file);tfmep = zeros(tam_file);
W_tf_dot = zeros(tam_file);W_tf = zeros(tam_file);bmep =
zeros(tam_file);rfmep = zeros(tam_file);mec_ef = zeros(tam_file);W_rf_dot =
zeros(tam_file);
W_brake = zeros(tam_file);W_rf = zeros(tam_file);sfc = zeros(tam_file);y_exp
= zeros(tam_file);y_comp = zeros(tam_file);delta_teta_o = zeros(tam_file);
R_2_comp = zeros(tam_file);R_2_exp = zeros(tam_file);T_cyl = zeros
(tam_vector);Q_INJ = zeros(tam_file);Q_INJ_dot = zeros(tam_file);
h = zeros (tam_vector);Qht = zeros (tam_file); dQht = zeros
(tam_vector);dQht_dt = zeros(tam_vector); Qht_dot = zeros(tam_file);
dQn = zeros (tam_vector);dQn_dt = zeros (tam_vector);H_inc_comb =
zeros(tam_file);HR = zeros (tam_file);dHR = zeros (tam_vector);dHR_dt =
zeros (tam_vector);
xb = zeros(tam_vector); CA10 = zeros(tam_file);CA50 = zeros(tam_file);CA90 =
zeros(tam_file);delta_teta_d = zeros (tam_file);delta_teta_b =
zeros(tam_file);
H_inc_comb_dot = zeros (tam_file);H_exh = zeros(tam_file); H_exh_dot = zeros
(tam_file);comb_eff = zeros (tam_file);  comb_eff_2= zeros
(tam_file);rho_amb = zeros (tam_file);
vol_eff = zeros (tam_file); thermal_eff = zeros (tam_file); global_eff=
zeros (tam_file);imep = zeros(tam_file);W_pump_dot = zeros(tam_file);pmep =
zeros(tam_file);

for i=1:qtd_rot

    [max_p(i),teta_max_p(i)] = max(p_cyl(:,i));
    teta_max_p(i) = teta_max_p(i) - 360;    %ajustment of the angles (-360
to 360 degrees)
    [dp,dV] = diff_pressure_volume(x,p_cyl(:,i),V);

    % Mass (kg) and Mass flow rate (kg/h)


[m_tot(i),m_tot_dot(i),m_aw_dot(i),m_ad_dot(i),m_aw(i),m_ad(i),m_v(i),m_fuel
(i),p_air_d(i),pv(i),R_aw(i),w(i)] ...
    = colect_data
(UR(i),P_amb(i),T_amb(i),AF,m_fuel_dot(i),lambda(i),dt(i));

    [W(:,i),W_ind(i),W_pump(i),W_ind_dot(i),W_pump_dot(i),imep(i),pmep(i)] =
indicated_data (p_cyl(:,i),Vd,dV,teta,N_eng(i),nc,x);

    % Brake (Watts,Joules,Pascal)

[bmep(i),W_brake(i),W_brake_dot(i),tfmep(i),W_tf(i),W_tf_dot(i),rfmep(i),W_r
f(i),W_rf_dot(i),mec_ef(i)] =
brake_experimental(imep(i),W_ind(i),W_ind_dot(i),pmep(i),W_pump(i),W_pump_do
t(i),Tb(i),N_eng(i),Vd,nc);

    % Specific Fuel Consumption (g/kW.h)
```

```
    sfc(i) = (1000*m_fuel_dot(i))/(W_brake_dot(i)*10^-3); %(g/kWh)

    %Polytropic coefficient

    log_p_cyl = log(p_cyl(:,i));
    log_V = log(V);

    [y_comp(i),y_exp(i),R_2_comp(i),R_2_exp(i)] = polytropic_coefficient ...
(save,fuel_name,N_eng(i),log_p_cyl,log_V,teta_max_p(i),adv_ig(i),teta_close_
ad,teta_open_ex);

    %Cylinder Temperature (K)

    T_cyl(:,i) = temperature_cylinder (p_cyl(:,i),V,m_tot(i),R_aw(i),x);

    %Injected Heat

    Q_INJ(i) = m_fuel(i)*LHV; % by cylinder (J)
    Q_INJ_dot(i) = m_fuel_dot(i)*LHV/3600; % Power injected (W)

    %Convective coefficient - Hohenberg(W/(m².K))

    h(:,i) = hohenberg (p_cyl(:,i),T_cyl(:,i),V,Sp(i),x);

    %Heat Rejected to the Walls

    [Qht(i),dQht(:,i),dQht_dt(:,i)] = heat_rejected_walls
(h(:,i),T_cyl(:,i),A,teta,dt(i),x);

    %Net Heat

    [dQn(:,i),dQn_dt(:,i)] = heat_net
(p_cyl(:,i),dp,dV,y_comp(i),y_exp(i),dt(i),V,teta,x);

    %Heat Released

    [HR(i),dHR(:,i),dHR_dt(:,i)] = heat_released
(dQn(:,i),dQht(:,i),dQn_dt(:,i),dQht_dt(:,i));

    %Mass fraction burned

    [xb(:,i),CA10(i),CA50(i),CA90(i)] =
mass_fraction_burned(HR(:,i),dHR(:,i),teta,x);

    %Combustion duratio n

    delta_teta_d(i) = CA10(i) - (adv_ig(i)*(-1));           %flame
development angle
    delta_teta_b(i) = CA90(i) - CA10(i);                    %rapid-burning
angle
```

```
    delta_teta_o(i) = delta_teta_d(i) + delta_teta_b(i);     %overal burning
angle

    %Energy lost due to incomplete combustion

    H_inc_comb(i) = Q_INJ(i) - HR(i);
    H_inc_comb_dot(i) = H_inc_comb(i)*nc*N_eng(i)/120;

    % Exhaust Heat Loss (J)

    H_exh(i) = Q_INJ(i) - W_ind(i) - H_inc_comb(i) - Qht(i);
    H_exh_dot(i) = Q_INJ_dot(i) - W_ind_dot(i) - H_inc_comb_dot(i) -
Qht_dot(i);

   % Mechanical, Thermal and Combustion efficiencies

    comb_eff(i) = HR(i)/Q_INJ(i);
    comb_eff_2(i) = 0.9*(4.6509*lambda(i)-2.0764*lambda(i)^2-1.6082);
    [rho_amb(i),vol_eff(i)] =
volumetric_efficiency(m_ad_dot(i),p_air_d(i),T_room(i),Vd,N_eng(i));
    thermal_eff(i) = W_ind(i)/Q_INJ(i);
    global_eff(i) = W_brake(i)/Q_INJ(i);

    % Correction Factor

    C_F(i) = correction_factor (p_air_d(i),T_amb(i));
    Tb(i) = Tb(i)*C_F(i);
    bmep(i) = bmep(i)*C_F(i);
    W_brake_dot(i) = W_brake_dot(i)*C_F(i);

    %write to txt data
    M_file =
[teta';p_cyl(:,i)'/10^5;W(:,i)';T_cyl(:,i)';h(:,i)';dHR(:,i)';dQn(:,i)';dQht
(:,i)';xb(:,i)'];
    file_name = sprintf('Motor
Bancada/Results/%s_%d.txt',fuel_name,N_eng(i));
    fileID = fopen(file_name,'w');

    fprintf(fileID, ' teta  p_cyl(bar) dW_cyle(J)   T_cyl(K)  h(W/(m².k))
HR(J)   HT(J)  H_net(J)  xb \n\n');
    fprintf(fileID,' %d   %0.2f        %0.2f        %0.2f      %0.2f
%0.2f    %0.2f    %0.2f      %0.2f\n' ,M_file);
    fclose(fileID);

end

%Write datas to txt files
file_name = sprintf('Motor Bancada/Results/DATA_%s.txt',fuel_name);
fileID = fopen(file_name,'wt');
parameters = ['RPM','Tb (N)','pmax(bar)',' Wi_dot(W)',' Wi(J)','
imep(bar)','  Wb_dot(W)','  Wb(J)','  bmep(bar)','  tfmep(bar)','
pmep(bar)','  sfc(g/kWh)','  nv','   nc','   nth','   nmec','   ng'];
```

```
M_file = [N_eng; Tb; max_p/10^5;
W_ind_dot/1000;W_ind;imep/10^5;W_brake_dot/1000;W_brake;bmep/10^5;tfmep/10^5
;pmep/10^5;sfc;vol_eff;comb_eff;thermal_eff;mec_ef;global_eff];
fprintf(fileID,'%s\n\n',parameters);
fprintf(fileID,'%d  %0.2f   %0.2f   %0.3f   %0.3f   %0.3f   %0.3f   %0.3f
%0.3f   %0.3f    %0.3f     %0.4f    %0.4f   %0.4f    %0.4f    %0.4f   %0.4f
\r\n', M_file);
fclose(fileID);



for i=1:qtd_rot

    figure
    plot(teta,dHR(:,i),teta,dQn(:,i),teta,dQht(:,i))
    axis ([-30 180 -inf inf])
    title('Effects of  Heat Transfer')
    subtitle(sprintf('%s, %d RPM', fuel_name,N_eng(i)))
    xlabel('Crankshaft Angle (^\circ)')
    ylabel('Q(J)')
    legend({'Heat Released','Net Heat','Heat Loss'},'Location','southeast')
    if (save==1)
        name_fig = sprintf('%s_%s_%d','Heats',fuel_name,N_eng(i));
        print(name_fig,'-djpeg')
    end
end

plot_heatrates
('HeatRates',save,dQn_dt/10^6,dHR_dt/10^6,dQht_dt,N_eng,teta,qtd_rot,fuel_na
me,'b')

% Fraction of mass burn

figure
for i=1:qtd_rot
    plot(teta,xb(:,i)*100)
    hold on
    title ('Mass Fraction Burned')
    subtitle(sprintf('Fuel: %s',fuel_name))
    legend({sprintf('%d RPM',N_eng(i))})
    xlabel('Crankshaft Angle(degrees)')
    ylabel('x_b (%)')
end


function [dp,dV] = diff_pressure_volume(x,p,V)

dV = zeros(x,1);
dp = zeros(x,1);

for pos = 2:x

    dV(pos,1) = V(pos,1)-V(pos-1,1);
```

```
end

for pos = 2:x

    dp(pos,1) = p(pos,1)-p(pos-1,1);

end

end


function [W_tot,W_gross,W_pump,Wi_dot,W_pump_dot,imep,pmep] = indicated_data
(p,Vd,dV,teta,N,n_cil,x)

W_gross = 0;
W_pump = 0;
W_cycle = zeros (x,1);

for i=1:x(1,1)-1

    W_cycle(i+1,1) = (p(i+1,1)+p(i,1))*dV(i,1)/2;

    if((teta(i+1,1)>=-180)&&(teta(i+1,1)<=180))

        W_gross = W_gross + W_cycle(i+1,1); %gross indicated work (J)

    else

        W_pump = W_pump + W_cycle(i+1,1);  %pumping work (J)

    end
end

W_tot = W_cycle;

W_pump_dot = n_cil*W_pump*N/(120) ;      % pumping power (W)

Wi_dot = n_cil*W_gross*N/(120) ;         % indicated power(W)

imep = Wi_dot*120/(n_cil*Vd*N);          % indicated mean effective
pressure(Pa)

pmep = W_pump_dot*120/(n_cil*Vd*N);      % pumping mean effective
pressure(Pa)

pmep = abs(pmep);
W_pump = abs(W_pump);
W_pump_dot = abs(W_pump_dot);


end
```

```
function [xb,CA10,CA50,CA90] = mass_fraction_burned(HR,dHR,teta,x)

%contadores
cont_xb_CA10 = 1;cont_xb_CA50 = 1;cont_xb_CA90 = 1;

for i=1:x

    xb(i,1) = dHR(i,1)/HR;

    if ((xb(i,1)>=0.1) && (cont_xb_CA10 ==1))
        CA10(1,1) = teta(i,1);
        cont_xb_CA10 = 2;
        if(teta(i)<-5)
            cont_xb_CA10 = 1;
        end
    end

    if ((xb(i,1)>=0.5) && (cont_xb_CA50 ==1))
        CA50(1,1) = teta(i,1);
        cont_xb_CA50 = 2;
    end

    if ((xb(i,1)>=0.9) && (cont_xb_CA90 ==1))
        CA90(1,1) = teta(i,1);
        cont_xb_CA90 = 2;
    end

end

end


function
[bmep,W_brake,W_brake_dot,tfmep,W_tf,W_tf_dot,rfmep,W_rf,W_rf_dot,mec_ef] =
brake_experimental(imep_g,W_ind,W_ind_dot,pmep,W_pump,W_pump_dot,T,N,Vd,n_ci
l)

bmep = pi*T/Vd;

W_brake_dot = 2*pi*N*T/60;

W_brake = 120*W_brake_dot/(n_cil*N);

tfmep = (imep_g - bmep);

W_tf_dot=  W_ind_dot - W_brake_dot;

W_tf =  W_ind - W_brake;

W_rf_dot = W_tf_dot - W_pump_dot;

W_rf = W_tf - W_pump;
```

```
rfmep = (tfmep - pmep);

% Mechanical efficiency

mec_ef = bmep/(imep_g);


end

function [gama_comp,gama_exp,R_2_comp,R_2_exp] = polytropic_coefficient
(salva_imagem,filename,N,log_p,log_V,teta_max_p,adv_ig,teta_close_ad,teta_op
en_ex)

% Expoente da Compressão

R_2_comp = 0;
R_2_exp = 0;

ad = 60;

while(R_2_comp<0.9984)

    duracao_compressao = 180 - 5 - teta_close_ad - ad;

    x_comp = zeros(duracao_compressao,1);
    y_comp = zeros(duracao_compressao,1);

    for i=1:duracao_compressao

        x_comp(i,1) = log_V(i + 179 + teta_close_ad + ad,1);
        y_comp(i,1) = log_p(i + 179 + teta_close_ad + ad);

    end

    pol_gama_comp = polyfit(x_comp',y_comp',1);

    y_reta_comp = polyval(pol_gama_comp,x_comp);

    R_2_comp = R_2_coefficient (y_reta_comp,y_comp);

    ad = ad + 2;

end

ad = 60;

while(R_2_exp<0.999)

    duracao_expansao = 180 - teta_max_p-teta_open_ex - ad;

    y_exp = zeros(duracao_expansao,1);
```

```
    x_exp = zeros(duracao_expansao,1);

    for i=1:duracao_expansao

        x_exp(i,1) = log_V(i+359+teta_max_p+12,1);
        y_exp(i,1) = log_p(i+359+teta_max_p+12);

    end

    pol_gama_exp = polyfit(x_exp',y_exp',1);
    y_reta_exp = polyval(pol_gama_exp,x_exp);

    R_2_exp = R_2_coefficient (y_reta_exp,y_exp);

    ad = ad + 2;

end

gama_comp = -pol_gama_comp(1);
gama_exp = - pol_gama_exp(1);

figure
plot(log_V,log_p)
hold on
plot(x_comp,y_reta_comp',x_exp,y_reta_exp','Linewidth',2)
title(sprintf('LOG P X LOG V'))
subtitle(sprintf('Fuel: %s (%d RPM)',filename,N))
xlabel('LOG V')
ylabel ('LOG P')
text(-10.4,12.5,sprintf('y(x) = %d x +
%d',pol_gama_comp(1),pol_gama_comp(2)),'fontweight','bold','Fontsize',10);
text(-9.3,15.3,sprintf('y(x) = %d x +
%d',pol_gama_exp(1),pol_gama_exp(2)),'fontweight','bold','Fontsize',10);
grid on

if salva_imagem==1
    name_fig = sprintf('LOGPV_%d_%s',N,filename);
    print(name_fig,'-djpeg')
% end


end


function h = hohenberg (p,T,V,Sp,x)

h1 = zeros(x,1);

C1 = 130;
C2 = 1.4;

for pos=1:x
```

```
    h1(pos,1) = C1*(p(pos,1)/10^5)^(0.8)*T(pos,1)^(-
0.4)*(Sp+C2)^(0.8)*V(pos,1)^(-0.06);

end

h = h1;

end



function [dQn,dQn_dt] = heat_net (p,dp,dV,y_comp,y_exp,dt,V,teta,x)

dQn = zeros(x,1);     %Heat rejected to the walls vector (J)
dQn_dt = zeros(x,1); %Heat Rejected to the walls rate (J/s)

for pos=2:x

    if(teta(pos)<0)
        y = y_comp;
    else
        y = y_exp;
    end

    dQn_dt(pos,1) = (1/(y-1))*(y*(p(pos,1)+p(pos-1,1))*dV(pos,1)/(2*dt) +
(V(pos,1)+V(pos-1,1))*dp(pos,1)/(2*dt));

    if (teta(pos,1)>=-150)

        dQn(pos,1) = dQn_dt(pos,1)*dt(1,1)+dQn(pos-1,1);

    end

end

end


function [Qht,dQht,dQht_dt] = heat_rejected_walls (h,T,A,teta,dt,x)

Tw = 375; % Wall Temperature (K)

dQht = zeros(x,1);     %Heat rejected to the walls vector (J)
dQht_dt = zeros(x,1); %Heat Rejected to the walls rate (J/s)

for pos = 2:x

    if(teta(pos,1)<=-45) % Correction Factor (Melo et al, 2006)
        fw = 1.77;
    elseif ((teta(pos,1)>-45)&&(teta(pos,1)<-36))
        fw = 1.67;
    elseif ((teta(pos,1)>-36)&&(teta(pos,1)<-27))
        fw = 1.68;
```

```
    else
        fw = 1.45;
    end

    dQht_dt(pos,1) = fw*A(pos,1)*h(pos,1)*(T(pos,1)-Tw);

    dQht(pos,1) = (dQht_dt(pos,1)*dt +dQht(pos-1,1));
end

Qht = dQht(pos,1); %Heat Rejected to the walls (J)

end

function [HR,dHR,dHR_dt] = heat_released (dQn,dQht,dQn_dt,dQht_dt)

dHR = dQn + dQht; dHR_dt = dQn_dt + dQht_dt;

HR= max(dHR);

end

function [rho,vol_eff] = volumetric_efficiency(ma_dot,p,T,Vd,N)

R = 287; %constante do ar
rho = p/((273.15+T)*R);
vol_eff= 120*ma_dot/(4*Vd*N*rho*3600);

end

function C_F = correction_factor (p_air_dry,T_amb)

alpha = 1.2;
beta = 0.6;
C_F = ((99000/p_air_dry)^alpha)*(((273.15 + T_amb)/298)^beta);

end

function R_2 = R_2_coefficient (y_reta,y_experimental)

erro_y = (y_experimental-y_reta).^2;
soma_erro_y = sum(erro_y);

media_y = mean(y_experimental);

erro_med = (y_experimental - media_y).^2;
soma_erro_med = sum(erro_med);

R_2 = 1 - soma_erro_y/soma_erro_med;

end
```

```
function plot_heatrates
(name,salva_imagem,net,hr,ht,N,teta,qtd_rot,fuel_name,c)

for i=1:qtd_rot

    figure
    plot(teta,net(:,i),'color',c)
    axis([-20 45 -inf inf])
    title(sprintf('%s\n %d RPM',fuel_name,N(i)));
    xlabel('Crankshaft Angle (^\circ)')
    ylabel('Net Heat Rate (MJ/s)')
    if (salva_imagem==1)
        name_fig = sprintf('%s_%s_%d',name,fuel_name,N(i));
        print(name_fig,'-djpeg')
    end

    figure
    plot(teta,hr(:,i),'color',c)
    axis([-20 45 -inf inf])
    title(sprintf('%s\n %d RPM',fuel_name,N(i)));
    xlabel('Crankshaft Angle (^\circ)')
    ylabel('Heat Released Rate(MJ/s)')
    if (salva_imagem==1)
        name_fig = sprintf('%s_%s_%d',name,fuel_name,N(i));
        print(name_fig,'-djpeg')
    end

    figure
    plot(teta,ht(:,i),'color',c)
    axis([-150 +150 -inf +inf])
    title(sprintf('%s\n %d RPM',fuel_name,N(i)));
    xlabel(' Crankshaft Angle (^\circ)')
    ylabel('Heat Transfer Rate - Hohenberg (J/s)')
    if (salva_imagem==1)
        name_fig = sprintf('%s_%s_%d',name,fuel_name,N(i));
        print(name_fig,'-djpeg')
    end

end

end

function [y,pol] = generate_pol (M,x,N_eng,tam,precisao)

tam_file = size(M);

y = zeros(precisao,tam_file(1,1));

for i=1:tam_file(1,1)

    pol = polyfit (N_eng,M,tam);
    y(:,i) = polyval(pol,x);

end
```

```
end
```

- ERROR CALCULATIONS: FUNCTIONS

```
function [EQM,EQMp] = error_calculation (y_exp,y_sim)

delta_y = abs(y_exp-y_sim);

delta_y_2 = delta_y.^2;

[n,~] = size(y_exp);

y_med = mean (y_exp);

EQM = (sum(delta_y_2)/n)^(1/2);

EQMp = EQM/y_med;

end

function R_2 = R_2_coefficient (y_reta,y_experimental)

erro_y = (y_experimental-y_reta).^2;
soma_erro_y = sum(erro_y);

media_y = mean(y_experimental);

erro_med = (y_experimental - media_y).^2;
soma_erro_med = sum(erro_med);

R_2 = 1 - soma_erro_y/soma_erro_med;

end
```

- TFMEP SIMULATION FUNCTION

```
function [Tb,tfmep,bmep] = simulated_tfmep
(sheet,imep,qtd_rot,N,Sp,mu_sc,Vd,B,S,Db,nb,Lb,rc,nc,ncr,Lcr,Dcr,ncs,dv_ad,d
v_ex,Lv_ad,Lv_ex,nv_ad,nv_ex,Cff,Crf,Com,Coh,p_intake,p_amb)

tfmep = zeros(1,qtd_rot);

if sheet ==2 % Sandoval (2003)

    [fmep,pmep] = friction_losses_sandoval...
```

```
(qtd_rot,N,Sp,B,S,rc,p_intake,p_amb,Db,Lb,nb,nc,nv_ad,dv_ad,dv_ex,Lv_ad,nv_e
x,Lv_ex,Cff,Crf,Coh,Com,Lcr,ncr,Dcr,ncs,mu_sc);

    tfmep = fmep+pmep; %considering the pmep from the pressure curves

else  % Heywood 2018

    for i=1:qtd_rot

        tfmep(i) = (0.97 + 0.15*(N(i)/1000) + 0.05*(N(i)/1000)^2)*10^5;

    end
end

bmep = imep-tfmep;
Wb_dot = bmep.*N*nc*Vd/(120);
Tb = (60/(2*pi))*(Wb_dot./N);

end


function [fmep,pmep] =
friction_losses_sandoval(qtd_rot,N,Sp,B,S,rc,p_intake,p_amb,Db,Lb,nb,nc,nv_a
d,dv_ad,dv_ex,Lv_ad,nv_ex,Lv_ex,Cff,Crf,Coh,Com,Lcr,ncr,Dcr,ncs,mu_sc)

tam_file = [1,qtd_rot];

%Inicializando os vetores

fmep = zeros (tam_file);int_valve_mep = zeros (tam_file); exh_valve_mep=
zeros(tam_file);
rcmep_gas = zeros(tam_file);afmep = zeros(tam_file); cfmep =
zeros(tam_file);
cammep = zeros(tam_file); vtmep = zeros(tam_file);
rcmep = zeros(tam_file);turb_diss_mep = zeros(tam_file);fmep_skirt =
zeros(tam_file);
seals_mep = zeros (tam_file);main_bearing_mep = zeros(tam_file);pmep = zeros
(tam_file);
fmep_rings = zeros(tam_file);fmep_cr_bearings = zeros(tam_file);

for i=1:qtd_rot

    %Auxiliary Friction
    afmep(i) = auxiliary_friction(N(i));

    %Crankshaft Friction
    [cfmep(i),seals_mep(i),main_bearing_mep(i),turb_diss_mep(i)] =
crankshaft_friction(Db,Lb,B,S,nc,nb,N(i),mu_sc);

    %Camshaft Friction
    cammep(i) = camshaft_bearings_friction (N(i),S,B,ncs,nc,mu_sc);
```

```
    %Valvetrain Friction

    int_valve_mep(i) =
valve_friction(N(i),B,S,nc,nv_ad,Lv_ad,mu_sc,Cff,Crf,Coh,Com); %intake valve

    exh_valve_mep(i) = valve_friction
(N(i),B,S,nc,nv_ex,Lv_ex,mu_sc,Cff,Crf,Coh,Com);

    % Valve Train Friction(kPa)

    vtmep(i) = int_valve_mep(i)+exh_valve_mep(i)+cammep(i);

    % Reciprocating friction (kPa)

    [rcmep(i),fmep_skirt(i),fmep_rings(i),fmep_cr_bearings(i)] =...
        reciprocating_friction (Sp(i),B,S,N(i),Lcr,ncr,Dcr,nc,mu_sc);

    rcmep_gas(i) =
gas_pressure_sandoval(Sp(i),rc,p_intake(i),p_amb(i),mu_sc);

    [pmep(i),~,~] =
pumping_mep_friction(p_amb(i),p_intake(i),Sp(i),dv_ad/B,dv_ex/B,nv_ad,nv_ex)
;

    fmep(i) = (rcmep_gas(i) + rcmep(i) + vtmep(i) + cfmep(i) +
afmep(i))*10^3; %total friction (p_amb)

end

pmep = pmep*10^3; %p_amb
function csmep = camshaft_bearings_friction (N,S,B,nb,nc,mu_sc)

%atrito nos rolamentos do eixo de cames

csmep = 244*mu_sc*N*nb/(S*nc*B^2) + 4.12;

end



function [cfmep,seals_mep,main_bearing_mep,turb_dissipation] =
crankshaft_friction (Db,Lb,B,S,nc,nb,N,mu_sc)

C1 = 1.22*10^5;
C2 = 3.03*10^-4;
C3 = 1.35*10^(-10);

seals_mep = C1*(Db/(B^2*S*nc));
main_bearing_mep = C2*mu_sc*(N*Lb*nb*Db^3/(S*nc*B^2));
turb_dissipation = C3*(Db^2*N^2*nb/nc);

cfmep = seals_mep + main_bearing_mep + turb_dissipation;
```

```
end

function vmep = valve_friction(N,B,S,nc,nv,Lv,mu_sc,Cff,Crf,Coh,Com)

vmep = Cff*(1+500/N)*nv/(S*nc) + Crf*(N*nv/(S*nc)) + ...
    Coh*mu_sc*(nv*Lv^(1.5)*N^(0.5)/(B*S*nc)) + Com*(1+500/N)*Lv*nv/(S*nc);

end

function rf_mep_gas = gas_pressure_sandoval(Sp,rc,pi,pa,mu_sc)

K = 2.38*10^-2; %Recomendado por Sandoval e Heywood

rf_mep_gas =  6.89*(pi/pa)*(0.088*rc*mu_sc+0.182*rc^(1.33-2*K*Sp));

end



function csmep = camshaft_bearings_friction (N,S,B,nb,nc,mu_sc)

%atrito nos rolamentos do eixo de cames

csmep = 244*mu_sc*N*nb/(S*nc*B^2) + 4.12;

end

function tfmep = total_friction_heywood_1988 (N)

tfmep(i) = (0.97 + 0.15*(N(i)/1000) + 0.05*(N(i)/1000)^2)*10^5;

end
```


- SPEED RECOVERY TESTS SIMULATION

```
function [tf,t_sim,R_2,EQM,EQMp] =
speed_recovery_simulation(gear,t,v_v,eff_trans,ic,id,m,r_w,T_RPM_pol,F0,F1,F
2)

t_sim   = zeros(size(v_v));

beta =  60*ic(gear)*id/(2*pi*r_w);

A = T_RPM_pol(1,1)*beta^2; %engine speed (RPM) to vehicle speed (km/h)
B = T_RPM_pol(1,2)*beta;
C = T_RPM_pol(1,3);
```

```
F1 = F1*3.6; %km/h to m/s
F2 = F2*(3.6)^2;

%% Solution
%also transform km/h to m/s

a = A(1,1); b = B(1,1); c = C(1,1); U = (ic(gear)*id/(r_w))*eff_trans(1,1);
t1 = (2*m*atanh((F1 - U*b + (v_v(1,1)/3.6)*(2*F2 - 2*U*a))/(F1^2 + U^2*b^2 -
4*F0*F2 + 4*F0*U*a - 2*F1*U*b + 4*F2*U*c - 4*U^2*a*c)^(1/2)))/(F1^2 +
U^2*b^2 - 4*F0*F2 + 4*F0*U*a - 2*F1*U*b + 4*F2*U*c - 4*U^2*a*c)^(1/2);
for i=2:length(v_v)
    t2 = (2*m*atanh((F1 - U*b + (v_v(i,1)/3.6)*(2*F2 - 2*U*a))/(F1^2 +
U^2*b^2 - 4*F0*F2 + 4*F0*U*a - 2*F1*U*b + 4*F2*U*c -
4*U^2*a*c)^(1/2)))/(F1^2 + U^2*b^2 - 4*F0*F2 + 4*F0*U*a - 2*F1*U*b +
4*F2*U*c - 4*U^2*a*c)^(1/2);
    t_sim(i,1) = t2 - t1;
end
tf(1,1) = t_sim(i,1);

R_2(1,1) = R_2_coefficient (t_sim,t);

[EQM(1,1),EQMp(1,1)] = error_calculation (t,t_sim);


end
```

- DYNO ACCELERATION PERFORMANCE MAIN FUNCTION

```
%% DYNO ACCELERATION PERFORMANCE

clc
clear all

qtd_tests = 3;
gear = 3 ;
sp_range = 4080;
fuel_names =  ["E22","E50","E85","E100","H36","H81","H100"];

tam = [1,qtd_tests]; %size of the vectors
[~,qtd_fuels] = size(fuel_names);
legend_name = strings(1,qtd_tests+1);

for i = 1:qtd_tests

    legend_name(i) = sprintf('Test %d',i);

end
legend_name(i+1) = "Linear Model";

for j=1:qtd_fuels
```

```
    a = zeros(tam);
    v_v_f = zeros(tam);
    v_v_0 = zeros(tam);
    tf = zeros(tam);
    EQM = zeros(tam);
    EQMp = zeros(tam);
    a_av = 0;
    v_v_0_av = 0;
    R_2 = zeros(tam);

    %first line of the .txt file
    title_file = 'a_x(m/s²)  dif(/100)  R²  a_med(m/s²)';

    %open file to write on it
    file_name = sprintf('acceleration
results/DYNO_SRtest_%s_%d.txt',fuel_names(j),sp_range);
    fileID = fopen(file_name,'wt');
    fprintf(fileID,title_file); %put the first line
    fprintf(fileID,'\n\n');

    figure
    for i=1:qtd_tests

        %get data from files (car speed and wheel power)

        str = sprintf('%s_%d_%d_%d',fuel_names(j),gear,sp_range,i);
        DATA = readmatrix(sprintf('Testes de Retomada/SPARC V/%s',str));
        v_v  = DATA(:,1);   %car speed in function of the time in dyno
(km/h)
        [size_t,~] = size(v_v);
        t  = transpose(0:0.1:(size_t-1)/10);    %time of the SR tests in
dyno(s)

        %Linear fitting

        f = polyfit(t,v_v,1);
        a(i) = f(1,1);
        v_v_sim = polyval(f,t);
        [EQM(i),EQMp(i)] = error_calculation (v_v,v_v_sim);
        v_v_0(i) = f(1,2);
        v_v_f(i) = v_v(length(v_v));
        tf(i) = t(length(t));
        a_av = a_av + a(i);
        v_v_0_av = v_v_0_av + v_v_0(i);

        plot(t,v_v,'--','LineWidth',2)
        hold all
    end

    a_av = a_av/qtd_tests; v_v_0_av = v_v_0_av/qtd_tests;
    f_AV(1,1) = a_av; f_AV(1,2) = v_v_0_av;

    v_v_sim_av = polyval(f_AV,t);
```

```
    plot(t,v_v_sim_av,'k','LineWidth',2)

    for i=1:qtd_tests

        str = sprintf('%s_%d_%d_%d',fuel_names(j),gear,sp_range,i);
        DATA = readmatrix(sprintf('Testes de Retomada/SPARC V/%s',str));
        v_v  = DATA(:,1);
        [size_t,~] = size(v_v);
        t  = transpose(0:0.1:(size_t-1)/10);

        R_2(i) = R_2_coefficient (polyval (f_AV,t,1),v_v);
        dif =(a(i)-a_av)/a_av;

        fprintf(fileID,'%0.3f  %0.4f   %0.4f   %0.3f\n',a(i)/3.6, dif ,
R_2(i), a_av/3.6);

        str = {sprintf('v(km/h) = %f*t(s) + %f',a_av,v_v_0_av)};
        text(0.5,75,str,'color','k','fontweight','bold','Fontsize',10);
        text(6,60+2*i,sprintf('R² =
%f',R_2(i)),'fontweight','bold','color','r','Fontsize',10);
        name_fig = sprintf('%s_%dgear_60100',fuel_names(j),gear);
        legend(legend_name,'Location','Southeast')

    end

    fclose('all');

    xlabel ('speed recovery time(s)')
    ylabel ('v_v (km/h)')
    title('Dyno Acceleration Performance')
    subtitle(sprintf('%s',fuel_names(j)));
    name_plot = sprintf('acceleration
results/%s_%d_%d',fuel_names(j),gear,sp_range);
    print(name_plot,'-djpeg')

end
```


- ROAD LOADS SIMULATIONS (KADIJK, 2012)

```
%% FUNÇÃO PRINCIPAL
% LEONARDO PEDREIRA PEREIRA - DEPARTAMENTO DE ENGENHARIA MECÂNICA DA PUC RIO

%%
_____________________________________________________________________________
_____________________________________________
clc
clear all

%% VALORES INICIAIS
```

```
qtd_carros = 8;                         %quantidade de veículos para teste
v = [120 100 80 60 40 20];              %vetor de velocidades
delta_v = 10/3.6;                       %diferença de velocidades medidas
c = 1000;                               %tamanho do vetor dos valores empíricos
v_emp = linspace(120,20,c);             %vetor de velocidades para os cálculos
empíricos

R_2 = zeros(5,8);
F1 = zeros(qtd_carros,3);
F2 = zeros(qtd_carros,3);
F3 = zeros(qtd_carros,3);
F4 = zeros(qtd_carros,3);
F5 = zeros(qtd_carros,3);
pol_ap = zeros(qtd_carros,3);
pol_test = zeros(qtd_carros,3);
erro_rel_1 = zeros(qtd_carros,c);
erro_rel_2 = zeros(qtd_carros,c);
erro_rel_3 = zeros(qtd_carros,c);
erro_rel_4 = zeros(qtd_carros,c);
erro_rel_5 = zeros(qtd_carros,c);

g = 9.81;   %aceleração da gravidade
R_ar = 287; %Constante do ar
P = 101325; %Pressão atmosférica
T = 298.15; %Temperatura ambiente
rho = P/(R_ar*T);   %densidade

for i=1:qtd_carros

    [M,P_Pneu,t_ap,t,K,~,~,Af,v_ar,v_x,alpha,title_name] =
vehicle_parameters_TNO(i);

    %%
    % Coastdown test

    [pol_test(i,:),Pot_test,F_test,v_test] = NEDC_COASTDOWN
(M,v,t,delta_v,c,K);
    Cd = 2*pol_test(1)*3.6^2/(Af*rho); %Coeficiente de Arrasto Aerodinâmico

    [pol_ap(i,:),~,~,~] = NEDC_COASTDOWN (M,v,t_ap,delta_v,c,K);

    %Pega os coeficientes das curvas de força

    [F1(i,3),F1(i,2),F1(i,1)] = roadload_coefficients
(M,g,Af,Cd,rho,P_Pneu,2); %linear ehsani
    [F2(i,3),F2(i,2),F2(i,1)] = roadload_coefficients
(M,g,Af,Cd,rho,P_Pneu,3); %eng.toolbox
    [F3(i,3),F3(i,2),F3(i,1)] = roadload_coefficients
(M,g,Af,Cd,rho,P_Pneu,4); %linear brunetti
    [F4(i,3),F4(i,2),F4(i,1)] = roadload_coefficients
(M,g,Af,Cd,rho,P_Pneu,5); %Villela

    % Cálculo pelas correlações
```

```
    [Pot_emp_1,F_emp_1,Farr_1,Fr_1,Fg_1] = ROAD_LOAD
(v_emp/3.6,v_ar,alpha,...
        Cd,Af,P_Pneu,M,rho,g,1);
    [Pot_emp_2,F_emp_2,Farr_2,Fr_2,Fg_2] = ROAD_LOAD
(v_emp/3.6,v_ar,alpha,...
        Cd,Af,P_Pneu/14.504,M,rho,g,2);
    [Pot_emp_3,F_emp_3,Farr_3,Fr_3,Fg_3] = ROAD_LOAD
(v_emp/3.6,v_ar,alpha,...
        Cd,Af,P_Pneu/14.504,M,rho,g,3);
    [Pot_emp_4,F_emp_4,Farr_4,Fr_4,Fg_4] = ROAD_LOAD
(v_emp/3.6,v_ar,alpha,...
        Cd,Af,P_Pneu/14.504,M,rho,g,4);
    [Pot_emp_5,F_emp_5,Farr_5,Fr_5,Fg_5] = ROAD_LOAD
(v_emp/3.6,v_ar,alpha,...
        Cd,Af,P_Pneu/14.504,M,rho,g,5);

    %Coeficiente de determinação - R²

    R_2(1,i) = R_2_coefficient (F_test,F_emp_1);
    R_2(2,i) = R_2_coefficient (F_test,F_emp_2);
    R_2(3,i) = R_2_coefficient (F_test,F_emp_3);
    R_2(4,i) = R_2_coefficient (F_test,F_emp_4);
    R_2(5,i) = R_2_coefficient (F_test,F_emp_5);

    %Cálculo do erro relativo

    [erro_rel_1(i,:),~] = calculate_error(F_test,F_emp_1,c);
    [erro_rel_2(i,:),~] = calculate_error(F_test,F_emp_2,c);
    [erro_rel_3(i,:),~] = calculate_error(F_test,F_emp_3,c);
    [erro_rel_4(i,:),~] = calculate_error(F_test,F_emp_4,c);
    [erro_rel_5(i,:),~] = calculate_error(F_test,F_emp_5,c);

    %% PLOTAGEM DOS GRÁFICOS

    figure


plot(v_emp,F_emp_1,'r',v_emp,F_emp_2,'g',v_emp,F_emp_3,'y',v_emp,F_emp_4,'b'
,v_emp,F_emp_5,'m',v_test,F_test,'--k','LineWidth',2)
    title('ROAD LOADS')
    subtitle(sprintf('%s',title_name))
    xlabel('velocity (km/h)')
    ylabel('Road Loads (N)')
    legend({'f_r = f0 + 3.24*fs*(v/161)^(2.5)','f_r = 0.01*(1+v/161)','Eng.
Toolbox','f_r= s(0.0116+0.0000142v)','Villela
(2017)','Test'},'Location','northwest')
    name_fig = sprintf('RLoad_Vehicle_%d',i);
    print(name_fig,'-djpeg')

    figure

    subplot(3,2,1)
    plot(v_emp,erro_rel_1(i,:),'r','LineWidth',2)
```

```
    title('Stuttgart Tec. Inst.')
    xlabel('velocity (km/h)')
    ylabel('ERROR %')

    subplot(3,2,2)
    plot(v_emp,erro_rel_2(i,:),'g','LineWidth',2)
    title('f_r = 0.01*(1+v/161)')
    xlabel('velocity (km/h)')
    ylabel('ERROR ABS')

    subplot(3,2,3)
    plot(v_emp,erro_rel_3(i,:),'color',[0.9290 0.6940 0.1250],'LineWidth',2)
    title('Engineering Toolbox')
    xlabel('velocity (km/h)')
    ylabel('ERROR %')

    subplot(3,2,4)
    plot(v_emp,erro_rel_4(i,:),'b','LineWidth',2)
    title('f_r= s(0.0116+0.0000142v)')
    xlabel('velocity (km/h)')
    ylabel('ERROR %')

    subplot(3,2,5)
    plot(v_emp,erro_rel_5(i,:),'m','LineWidth',2)
    title('Villela (2017)')
    xlabel('velocity (km/h)')
    ylabel('ERROR %')

    sgtitle (sprintf('Vehicle %d',i))

    name_fig = sprintf('Error_Vehicle_%d',i);
    print(name_fig,'-djpeg')
end

figure
for i=1:qtd_carros

    subplot(2,4,i)
    plot(v_emp,erro_rel_1(i,:),'r','LineWidth',2)
    title (sprintf('Vehicle %d',i))
    xlabel('velocity (km/h)')
    ylabel('ERROR %')

end
sgtitle (sprintf('Relative Error - Stuttgart Tec. Inst.'))
name_fig = sprintf('Error_StutTec');
print(name_fig,'-djpeg')

figure
for i=1:qtd_carros

    subplot(2,4,i)
    plot(v_emp,erro_rel_2(i,:),'g','LineWidth',2)
    title (sprintf('Vehicle %d',i))
```

```
    xlabel('velocity (km/h)')
    ylabel('ERROR %')

end
sgtitle (sprintf('Relative Error - f_r = 0.01*(1+v/161)'))
name_fig = sprintf('Linear');
print(name_fig,'-djpeg')

figure
for i=1:qtd_carros

    subplot(2,4,i)
    plot(v_emp,erro_rel_3(i,:),'color',[0.9290 0.6940 0.1250],'LineWidth',2)
    title (sprintf('Vehicle %d',i))
    xlabel('velocity (km/h)')
    ylabel('ERROR %')

end
sgtitle (sprintf('Relative Error - Eng. Toolbox'))
name_fig = sprintf('Error_EngToolbox');
print(name_fig,'-djpeg')

figure
for i=1:qtd_carros

    subplot(2,4,i)
    plot(v_emp,erro_rel_4(i,:),'b','LineWidth',2)
    title (sprintf('Vehicle %d',i))
    xlabel('velocity (km/h)')
    ylabel('ERROR %')

end
sgtitle (sprintf('Relative Error - Brunetti'))
name_fig = sprintf('Error Brunetti');
print(name_fig,'-djpeg')

figure
for i=1:qtd_carros

    subplot(2,4,i)
    plot(v_emp,erro_rel_5(i,:),'m','LineWidth',2)
    title (sprintf('Vehicle %d',i))
    xlabel('velocity (km/h)')
    ylabel('ERROR %')

end
sgtitle (sprintf('Relative Error - Villela (2017)'))
name_fig = sprintf('Error_Villela');
print(name_fig,'-djpeg')


function [p,Pot_real_plot,F_real_plot,v_real_plot] = NEDC_COASTDOWN
(M,v_real,t_real,delta_v,c,K)
```

```
[~,colum_number] = size(v_real) ;

%% COASTDOWN TESTS

%Cálculo da ROAD LOAD

RT = zeros(1,colum_number);
F_real = zeros(1,colum_number);
for i=1:colum_number
    RT(1,i) = (1/t_real(i))*M*delta_v;
    F_real (1,i) = RT(1,i)*K(i);
end

p = polyfit(v_real,F_real,2);
%coeficientes do polinômio de 2 grau

%Criação dos vetores para plotagem

v_real_plot = linspace(v_real(1),v_real(colum_number),c);
%inicializandovetor de velocidade para plotagem
F_real_plot = polyval(p,v_real_plot);
%inicializando vetor de Força para plotagem

[~,colum_number_plot] = size(F_real_plot);
Pot_real_plot = zeros(1,colum_number_plot);

for i=1:colum_number_plot
    Pot_real_plot(i) = (F_real_plot(i)*(v_real_plot(i))/3.6);        %criação
do vetor potência
end

end


function [F0,F1,F2] = roadload_coefficients (M,g,Af,Cd,rho,p,n)

if n == 2
    F0 = 0.001*M*g;
    F1 = 0.001*M*g/161;
    F2 = (1/2)*rho*Cd*Af;
elseif n==3
    F0 = M*g*0.014*2/p;
    F1=0;
    F2 = (M*g*0.014*2/p)*(0.6214/100)^2;
elseif n==4
    s = 1.316;
    F0 = M*g*s*0.0116;
    F1 = 0.0000142*M*g*s;
    F2 = (1/2)*rho*Cd*Af;
else
    F0 = 0.2615*(M/p)+22.153;
    F1 = 0;
    F2 = 0.0656*(Cd*Af)-0.0055;
end
```

```
end


function [Pot_emp,F_emp,Farr,Fr,Fg] = ROAD_LOAD
(v_emp,v_ar,alpha,Cd,Af,p,M,rho,g,n_fr)

tam = size(v_emp);                                  %tamanho do vetor
velocidade

%% Inicializando a matriz para coeficiente de rolagem do Inst. Politec. de
Stuttgart
if n_fr==1
    if p < 20
        M_f0 = readmatrix ('f0_1.xlsx');
        M_fs = readmatrix ('fs_1.xlsx');
    else
        M_f0 = readmatrix ('f0_2.xlsx');
        M_fs = readmatrix ('fs_2.xlsx');
    end
    j=1;
    while(1)
        if(p<M_f0(j,1))
            break
        end
        j=j+1;
    end
    x_f0 = [0,M_f0(j,1),M_f0(j+1,1)];
    y_f0 = [0,M_f0(j,2),M_f0(j+1,2)];
    f0 = interp1(x_f0,y_f0,p);
    j=1;
    while(1)
        if(p<=M_fs(j,1))
            break
        end
        j=j+1;
    end
    x_fs = [0,M_fs(j,1),M_fs(j+1,1)];
    y_fs = [0,M_fs(j,2),M_fs(j+1,2)];
    fs = interp1(x_fs,y_fs,p);
end

%% inicialização de vetor

v_w = zeros(tam);
f = zeros(tam);
Farr = zeros(tam);
Fr = zeros(tam);
F_emp = zeros(tam);
Pot_emp = zeros(tam);

%Força de rampa
Fg = M*g*sin(alpha);

for i=1:tam(2)
```

```
    v_w(i) = v_emp(i);
%     v_w (i) = (((v_emp(i) + v_ar)+(v_emp(i) - v_ar))/2);
    % FORÇA DE ROLAGEM
    % COEFICIENTE DE ROLAGEM
    if n_fr ==1 %Stuttgart Tec.

        Farr(i) = (1/2)*rho*Cd*Af*(v_w(i))^2;
        f(i) = f0 + 3.24*fs*(v_emp(i)*3.6/161)^(2.5);
        Fr(i) = M*g*f(i)*cos(alpha);

    elseif n_fr==2 %Gillespie

        Farr(i) = (1/2)*rho*Cd*Af*(v_w(i))^2;
        f(i) = 0.01*(1+v_emp(i)*3.6/161);
        Fr(i) = M*g*f(i)*cos(alpha);

    elseif n_fr==3 %Eng. Toolbox

        Farr(i) = (1/2)*rho*Cd*Af*(v_w(i))^2;
        Fr(i) = (0.014*2/p)*(1+(0.6214*v_emp(i)*3.6/(100))^2)*(M*g);

    elseif n_fr==4 %Brunetti

        Farr(i) = (1/2)*rho*Cd*Af*(v_w(i))^2;
        s = 1.316;
        f(i) = s*(0.0116+0.0000142*v_emp(i)*3.6);
        Fr(i) = M*g*f(i)*cos(alpha);

    else %Villela

        Fr(i) = 0.2615*(M/p)+22.153;
        Farr(i) = (0.0656*(Cd*Af)-0.0055)*(v_w(i)*3.6)^2;

    end

    %Resultante de todas as forças EMPÍRICAS
    F_emp(i) = Fr(i) + Fg + Farr(i);

    %Potência absorvida
    Pot_emp(i) = F_emp(i)*(v_emp(i))/3.6;
end
end
```